Titre: Title:	Transformer Modeling for Low-And Mid-Frequency Electromagnetic Transients Simulation
Auteur: Author:	Mathieu Lambert
Date:	2014
Type:	Mémoire ou thèse / Dissertation or Thesis
Référence: Citation:	Lambert, M. (2014). Transformer Modeling for Low-And Mid-Frequency Electromagnetic Transients Simulation [Ph.D. thesis, École Polytechnique de Montréal]. PolyPublie. https://publications.polymtl.ca/1455/

UNIVERSITÉ DE MONTRÉAL

TRANSFORMER MODELING FOR LOW- AND MID-FREQUENCY ELECTROMAGNETIC TRANSIENTS SIMULATION

MATHIEU LAMBERT
DÉPARTEMENT DE GÉNIE ÉLECTRIQUE
ÉCOLE POLYTECHNIQUE DE MONTRÉAL

THÈSE PRÉSENTÉE EN VUE DE L'OBTENTION
DU DIPLÔME DE PHILOSOPHIÆ DOCTOR
(GÉNIE ÉLECTRIQUE)
MAI 2014

UNIVERSITÉ DE MONTRÉAL

ÉCOLE POLYTECHNIQUE DE MONTRÉAL

Cette thèse intitulée :

TRANSFORMER MODELING FOR LOW- AND MID-FREQUENCY ELECTROMAGNETIC TRANSIENTS SIMULATION

présentée par : LAMBERT Mathieu
en vue de l'obtention du diplôme de : Philosophiæ Doctor
a été dûment acceptée par le jury d'examen constitué de :

M. KOCAR Ilhan, Ph.D., président
M. MAHSEREDJIAN Jean, Ph.D., membre et directeur de recherche
M. SIROIS Frédéric, Ph.D., membre et codirecteur de recherche
M. MARTÍNEZ DURÓ Manuel, Ph.D., membre et codirecteur de recherche
M. KARIMI Houshang, Ph.D., membre
M. REZAEI-ZARE Afshin, Ph.D., membre

Myths are persistent because they are not questioned;
they are persuasive because they offer a simplistic view of a complex reality;
and they are unrealistic because they disguise the truth.
– Barbara Flores

By ignoring the very alive phenomena underlying the lifeless symbols
it is still possible to get correct numerical answers,
but it is not possible to form a correct physical picture,
much less to build a physical model that corresponds term by term to the equations.
– Gabriel Kron

ACKNOWLEDGEMENTS

First and foremost, I would like to thank my dissertation supervisor, Dr. Jean Mahseredjian, for his patience and support during this project. Most of the contributions of this work would not have been possible without the freedom of research that I had the privilege to have during the course of this work.

I also wish to express my gratitude to one of my co-supervisor, Dr. Frédéric Sirois, for his help in unveiling the mysteries of electromagnetic fields. Most (if not all) the physical intuition I developped during these years can be attributed to him.

I am thankful to my other co-supervisor, Dr. Manuel Martínez Duró, for his precious guidance. I wish to thank him for his knowledge and expertise in transformer modeling for EMTP, but also for his intellectual rigor and insightful debates that we have had. It is to him I owe my passion for reading and my hunger for knowledge.

I would like also to thank Andy Wan for our fruitful discussions, as well as many other graduate students of the group.

Finally, I wish to acknowledge the financial support from EDF R&D and École Polytechnique de Montréal.

RÉSUMÉ

Dans cette thèse, de nouveaux modèles de transformateurs pour les transitoires électromagnétiques à basse fréquence ont été développés pour les appareils cuirassés. Ces modèles utilisent l'approche des inductances de fuite couplées, qui a l'avantage de ne pas nécessiter l'emploi d'enroulements fictifs pour connecter le modèle de fuite à un modèle topologique du noyau, tout en arrivant au même résultat en court-circuit que le modèle BCTRAN (matrice d'admittance indéfinie).

Afin d'accroître le raffinement des modèles, il est proposé de partitionner les enroulements en *bobines* (agencement d'un ou de plusieurs tours de l'enroulement complet). Cependant, les mesures en court-circuit entre les bobines ne sont jamais disponibles, car on ne peut pas avoir accès à chaque bobine séparément en pratique. Pour combler cette lacune, une nouvelle méthode analytique basée sur la méthode des images a été développée, ce qui permet le calcul des inductances de court-circuit en 2-D entre des conducteurs de section rectangulaire. Les résultats de la nouvelle méthode convergent vers ceux obtenus par la méthode des éléments finis en 2-D. De plus, l'hypothèse que le champ de fuite est approximativement 2-D pour les transformateurs cuirassés a été validée à l'aide d'une simulation en 3-D avec un modèle plus complet de transformateur, incluant la cuve et les écrans magnétiques.

Le produit de cette nouvelle méthode pour calculer les inductances de court-circuit entre les bobines a été utilisé pour calculer les inductances propres et mutuelles du modèle d'inductances de fuite couplées. Les résultats montrent, d'une part, que l'inductance de court-circuit totale des enroulements correspond bien aux mesures expérimentales et d'autre part, que le modèle d'inductances de fuite couplées donne des résultats identiques en court-circuit au modèle BCTRAN.

En général, les inductances de fuite dans les modèles de transformateurs sont calculées à partir des essais en court-circuit et la branche de magnétisation est calculée à partir des essais à vide. De plus, on suppose généralement que les fuites sont négligeables pour le transformateur à vide et que le courant de magnétisation est infime pendant un court-circuit. Bien que l'hypothèse de perméabilité infinie soit valable pendant un court-circuit, car la force magnétomotrice dans le noyau est négligeable, on ne peut en dire autant de l'hypothèse selon laquelle les fuites sont négligeables à vide. En fait, le noyau ferromagnétique du transformateur commence à saturer à vide et une partie du flux magnétique fuit à l'extérieur du noyau. Pour prendre cela en compte, une méthode analytique novatrice est proposée dans cette thèse, qui permet d'enlever la contribution des flux de fuite lors des essais à vide afin de calculer correctement les branches de magnétisation des modèles proposés.

Cependant, il doit être souligné que les courants de Foucault ont été négligés lors du développement de la nouvelle méthode analytique pour calculer les inductances de court-circuit (comme pour les autres méthodes analytiques). De façon similaire, les pertes d'enroulements ont été omises du modèle d'inductances de fuite couplées, ainsi que dans la méthode précédente pour enlever la contribution des flux de fuite des mesures à vide. L'inclusion de ces pertes sera étudiée dans un travail ultérieur.

Les deux modèles de transformateurs présentés dans cette thèse sont basés sur l'hypothèse classique que le flux magnétique du transformateur peut être contenu (voir discrétisé) à l'intérieur de tubes de flux. C'est aussi la supposition que l'on fait généralement pour les modèles de transformateurs dits « topologiques ». Malgré le fait que ces modèles soient soi-disant basés sur le comportement physique du flux, il existe plusieurs modèles topologiques pour un même transformateur. Dans cet ouvrage, il est démontré que ces différences peuvent s'expliquer en partie à l'aide des concepts de flux *divisé* et flux *intégral* et il est expliqué que l'approche à flux divisé est le résultat de manipulations mathématiques, alors que l'approche à flux intégral est plus physiquement acceptable. Qui plus est, il est montré que dans le cas d'un transformateur monophasé à deux enroulements, les inductances de fuite du modèle à flux divisé doivent être non linéaires pour que les deux approches soient mathématiquement équivalentes.

Même au sein des modèles à flux intégral ou parmi ceux à flux divisé, il existe des différences, qui proviennent essentiellement de la définition des « trajectoires de flux » dans le modèle. En fait, le côté arbitraire de ce choix provient de l'hypothèse classique que le flux magnétique peut être confiné à l'intérieur de tubes de flux et qu'il ne peut pas fuir des parois de ces tubes, d'où découle la théorie des circuits magnétiques. Ainsi, dépendamment des conditions d'opération du transformateur (degré de saturation du noyau, court-circuit, etc.), cela peut engendrer différents choix pour les trajectoires du flux (tubes) et par le fait même différents modèles. Dans cette thèse, un nouveau cadre théorique est développé pour permettre au flux magnétique de fuir des parois de ces tubes, où l'ensemble de ceux-ci dans l'espace forme un maillage. De plus, une généralisation est proposée dans cet ouvrage pour inclure les pertes, ainsi que les capacités parasites, engendrant ce qui pourrait s'appeler la *théorie sur les circuits électromagnétiques*. Il est aussi expliqué que cette théorie est en fait équivalente à ce qui est appelé les formulations finies (telle que la méthode des éléments finis), aboutissant à la réunion entre les théories de circuit et l'électromagnétisme discret. Non seulement ce cadre théorique permettra de développer ultérieurement des modèles réellement topologiques de transformateurs, où les circuits électrique et magnétique sont définis sur des maillages duaux, mais aussi des modèles de machines et de lignes électriques (on peut même prendre en compte la propagation de l'onde).

ABSTRACT

In this work, new models are developed for single-phase and three-phase shell-type transformers for the simulation of low-frequency transients, with the use of the coupled leakage model. This approach has the advantage that it avoids the use of fictitious windings to connect the leakage model to a topological core model, while giving the same response in short-circuit as the indefinite admittance matrix (BCTRAN) model.

To further increase the model sophistication, it is proposed to divide windings into coils in the new models. However, short-circuit measurements between coils are never available. Therefore, a novel analytical method is elaborated for this purpose, which allows the calculation in 2-D of short-circuit inductances between coils of rectangular cross-section. The results of this new method are in agreement with the results obtained from the finite element method in 2-D. Furthermore, the assumption that the leakage field is approximately 2-D in shell-type transformers is validated with a 3-D simulation.

The outcome of this method is used to calculate the self and mutual inductances between the coils of the coupled leakage model and the results are showing good correspondence with terminal short-circuit measurements.

Typically, leakage inductances in transformers are calculated from short-circuit measurements and the magnetizing branch is calculated from no-load measurements, assuming that leakages are unimportant for the unloaded transformer and that magnetizing current is negligible during a short-circuit. While the core is assumed to have an infinite permeability to calculate short-circuit inductances, and it is a reasonable assumption since the core's magnetomotive force is negligible during a short-circuit, the same reasoning does not necessarily hold true for leakage fluxes in no-load conditions. This is because the core starts to saturate when the transformer is unloaded. To take this into account, a new analytical method is developed in this dissertation, which removes the contributions of leakage fluxes to properly calculate the magnetizing branches of the new models.

However, in the new analytical method for calculating short-circuit inductances (as with other analytical methods), eddy-current losses are neglected. Similarly, winding losses are omitted in the coupled leakage model and in the new analytical method to remove leakage fluxes to calculate core parameters from no-load tests. These losses will be taken into account in future work.

Both transformer models presented in this dissertation are based on the classical hypothesis that flux can be discretized into flux tubes, which is also the assumption used in a category of models called *topological models*. Even though these models are physically-based,

there exist many topological models for a given transformer geometry. It is shown in this work that these differences can be explained in part through the concepts of *divided* and *integral* fluxes, and it is explained that divided approach is the result of mathematical manipulations, while the integral approach is more "physically-accurate". Furthermore, it is demonstrated, for the special case of a two-winding single-phase transformer, that the divided leakage inductances have to be nonlinear for both approaches to be equivalent.

Even between models of the divided or integral approach models, there are differences, which arise from the particular choice of so-called "flux paths" (tubes). This arbitrariness comes from the fact that with the classical hypothesis that magnetic flux can be confined into predefined flux tubes (leading to classical magnetic circuit theory), it is assumed that flux cannot leak from the sides of flux tubes. Therefore, depending on the transformer's operation conditions (degree of saturation, short-circuit, etc.), this can lead to different choices of flux tubes and different models. In this work, a new theoretical framework is developed to allow flux to leak from the sides of the tube, and generalized to include resistances and capacitances in what is called *electromagnetic circuit theory*. Also, it is explained that this theory is actually equivalent to what is called finite formulations (such as the finite element method), which bridges the gap between circuit theory and discrete electromagnetism. Therefore, this enables not only to develop topologically-correct transformer models, where electric and magnetic circuits are defined on dual meshes, but also rotating machine and transmission lines models (wave propagation can be taken into account).

TABLE OF CONTENTS

DEDICATION iii

ACKNOWLEDGEMENTS iv

RÉSUMÉ v

ABSTRACT vii

TABLE OF CONTENTS ix

LIST OF TABLES xii

LIST OF FIGURES xiii

LIST OF ACRONYMS AND ABBREVIATIONS xviii

CHAPTER 1 INTRODUCTION 1
1.1 Basic concepts 2
1.1.1 Maxwell's equations 2
1.1.2 Integral quantities 4
1.1.3 Flux tubes 4
1.1.4 Magnetic and electric circuits 5
1.1.5 Analogies between magnetic and electric circuits 6
1.1.6 Electric and magnetic potentials 8
1.1.7 Sources in magnetic circuits 9
1.1.8 Connection between magnetic and electric circuits 13
1.1.9 Inductances and duality 16
1.2 Literature review 20
1.3 Dissertation statement 24
1.4 Objectives 26
1.5 Dissertation outline 26

CHAPTER 2 ANALYTICAL CALCULATION OF LEAKAGE INDUCTANCES . . 28
2.1 Definition of the problem 29
2.2 Classical approach 33

2.3 Space harmonics . . . 36
2.3.1 Double Fourier series . . . 37
2.4 Method of images . . . 42
2.5 New approach . . . 46
2.6 Application examples and validation . . . 57
2.7 Results . . . 61
2.7.1 Results for the 360 MVA transformer . . . 61
2.7.2 Results for the 570 MVA transformer . . . 67
2.7.3 Results for the 96 MVA transformer . . . 67
2.8 Discussion . . . 68
2.9 Conclusion . . . 71

CHAPTER 3 COUPLED LEAKAGE MODEL . . . 73
3.1 Integral and divided fluxes . . . 76
3.2 Star-delta transformation . . . 78
3.3 Coupled leakage approach . . . 83
3.4 Methods . . . 86
3.5 Results . . . 88
3.6 Discussion . . . 88
3.7 Conclusion . . . 89

CHAPTER 4 SHELL-TYPE TRANSFORMER CORE MODELING . . . 91
4.1 Air-core inductance versus saturation inductance . . . 91
4.2 Parameter estimation from typical no-load tests . . . 92
4.2.1 From RMS to peak values . . . 93
4.2.2 Extension of the saturation curve beyond and between no-load points . 98
4.3 Calculation of magnetizing branches for single-phase transformers . . . 99
4.3.1 Simple example . . . 102
4.3.2 Application example and validation . . . 103
4.4 Calculation of magnetizing branches for three-phase transformers . . . 106
4.5 Conclusion . . . 111

CHAPTER 5 DISCRETE ELECTROMAGNETISM . . . 112
5.1 Magnetostatics . . . 113
5.2 Magnetoquasistatics . . . 116
5.3 Dynamics . . . 119
5.4 Resistance, reluctance and capacitance . . . 122

5.5 Boundary conditions 125
5.6 Conclusion 127

CHAPTER 6 CONCLUSION 129
6.1 Summary 129
6.2 Limitations of the new methods 130
6.3 Future work 131

REFERENCES 133

LIST OF TABLES

Table 2.1 Performance comparison to calculate the 484 inductances 63
Table 3.1 Short-circuit inductance for the 360 MVA transformer seen from the HV side, ©2014 IEEE 89
Table 3.2 Positive-sequence short-circuit inductance windings 1 and 2 for the 96 MVA transformer seen from the HV side, ©2014 IEEE 89
Table 3.3 Positive-sequence short-circuit inductance windings 1 and 3 for the 96 MVA transformer seen from the HV side, ©2014 IEEE 89
Table 3.4 Positive-sequence short-circuit inductance windings 1 and 4 for the 96 MVA transformer seen from the HV side, ©2014 IEEE 89
Table 4.1 No-load measurements (RMS) for the LV winding of the 360 MVA transformer 105

LIST OF FIGURES

Figure 1.1 Flux tube. 5
Figure 1.2 Toroidal inductor. 10
Figure 1.3 Equivalent toroidal inductor. 11
Figure 1.4 Example of magnetic circuit with nine conductors and cuts. 12
Figure 1.5 A conducting torus wound around a core canalizing a time-varying magnetic flux. 13
Figure 1.6 A conducting torus wound around a magnetic torus forming dual loops. 14
Figure 1.7 Dual loops with Hopkinsons' analogy. 15
Figure 1.8 Dual loops with Buntenbach's analogy. 15
Figure 1.9 Example of a magnetic circuit with two windings coupled with two electric circuits. 18
Figure 1.10 Graphical derivation of the dual circuit. 18
Figure 1.11 Dual circuit coupled with the two electric circuits. 18
Figure 1.12 Dual circuit simplified with ideal with ideal transformers. 19
Figure 1.13 Single-phase N-winding Saturable Transformer Component. 20
Figure 1.14 Magnetic circuit of the UMEC model for the two-winding three-legged transformer. 22
Figure 1.15 Magnetic circuit of the Hybrid transformer model for the two-winding three-legged transformer. 22
Figure 1.16 Magnetic circuit of the TOPMAG model for the two-winding three-legged transformer. 22
Figure 2.1 Typical 2-D domain boundaries. 31
Figure 2.2 Neumann boundary value problem in 2-D to calculate the short-circuit inductance between two rectangular cross-section coils. 32
Figure 2.3 Geometry considered in the classical approach. 34
Figure 2.4 Fringing flux for different winding geometries. 35
Figure 2.5 Magnetic flux during short-circuit in the presence of a trapezoidal cross-section high-voltage winding. 36
Figure 2.6 Current-carrying conductor in front of a semi-infinite slab and its image (Lambert *et al.*, 2013, Fig. 1), ©2013 IEEE. 43
Figure 2.7 Method of images with an infinitely-permeable boundary ($k = 1$). . . . 43
Figure 2.8 Method of images with a flux line boundary ($k = -1$). 44

Figure 2.9 Current-carrying conductor between two parallel semi-infinite slabs and its images. 45
Figure 2.10 Current-carrying conductor inside a rectangular cavity and its images. . 46
Figure 2.11 Method of images in cylindrical coordinates. 46
Figure 2.12 Pair of rectangular conductors inside a rectangular cavity and their doubly-periodic images. 47
Figure 2.13 Dimensions of the rectangular conductor within the core window (Lambert *et al.*, 2013, Fig. 3), ©2013 IEEE. 48
Figure 2.14 The 360 MVA shell-type single-phase two-winding transformer (Lambert *et al.*, 2013, Fig. 4), ©2013 IEEE. 58
Figure 2.15 The 360 MVA transformer's window with pancake coils numbered from 1 to 44 (Lambert *et al.*, 2013, Fig. 5), ©2013 IEEE. 59
Figure 2.16 The 570 MVA shell-type single-phase two-winding transformer. 59
Figure 2.17 The 96 MVA transformer's window with pancake coils numbered from 1 to 26. 60
Figure 2.18 Coarse mesh for the calculation of $L_{sc}(1, 44)$ for the 360 MVA transformer with the 2-D FEM. 62
Figure 2.19 Convergence of the short-circuit inductance value with the 2-D FEM with mesh refinement. 62
Figure 2.20 Relative error between the short-circuit inductance $L_{sc}(1, 44)$ of the 360 MVA transformer calculated with (2.80) (without and with substitutions) and the FEM in 2-D. 64
Figure 2.21 Relative error between the short-circuit inductance $L_{sc}(1, 44)$ of the 360 MVA transformer calculated with Roth's method and the FEM in 2-D. 64
Figure 2.22 Error in the calculation of the short-circuit inductances $L_{sc}(i, j)$ of the 360 MVA transformer of the method of images (4 layers) with respect to the FEM in 2-D (Lambert *et al.*, 2013, Fig. 7), ©2013 IEEE. 65
Figure 2.23 Error in the calculation of the short-circuit inductances $L_{sc}(i, j)$ of the 360 MVA transformer of the method of images (4 layers), with the substitutions, and with respect to the FEM in 2-D. 65
Figure 2.24 Error in the calculation of the short-circuit inductances $L_{sc}(i, j)$ of the 360 MVA transformer of Roth's method (110 harmonics) with respect to the FEM in 2-D. 66

Figure 2.25 Error in the calculation of the short-circuit inductances $L_{sc}(i,j)$ of the 360 MVA transformer of the classical approach with respect to the FEM in 2-D (Lambert *et al.*, 2013, Fig. 8), ©2013 IEEE. 66
Figure 2.26 Leakage flux in the 570 MVA transformer during the short-circuit between coils 1 and 44, and flux density along the middle plane. 67
Figure 2.27 Error in the calculation of the short-circuit inductances $L_{sc}(i,j)$ of the 96 MVA transformer of the method of images (4 layers) with respect to the FEM in 2-D. 68
Figure 2.28 Error in the calculation of the short-circuit inductances $L_{sc}(i,j)$ of the 96 MVA transformer of the method of images (4 layers), with the substitutions, and with respect to the FEM in 2-D. 68
Figure 2.29 Error in the calculation of the short-circuit inductances $L_{sc}(i,j)$ of the 96 MVA transformer of Roth's method (110 harmonics) with respect to the FEM in 2-D. 69
Figure 2.30 Error in the calculation of the short-circuit inductances $L_{sc}(i,j)$ of the 96 MVA transformer of the classical approach with respect to the FEM in 2-D. 69
Figure 3.1 Equivalent magnetic circuits of a three-phase two-winding three-legged transformer, with divided leakage flux. 75
Figure 3.2 Equivalent magnetic circuits of a three-phase two-winding three-legged transformer, with integral leakage flux. 75
Figure 3.3 Magnetic flux paths of a single-phase two-winding shell-type transformer, ©2014 IEEE. 77
Figure 3.4 Equivalent magnetic circuits of a single-phase two-winding shell-type transformer, ©2014 IEEE. 78
Figure 3.5 Dual electric circuits of a single-phase two-winding shell-type transformer, ©2014 IEEE. 78
Figure 3.6 Equivalent magnetic circuits for the three-winding single-phase shell-type transformer, ©2014 IEEE. 79
Figure 3.7 Dual electric circuits for the three-winding single-phase shell-type transformer, ©2014 IEEE. 79
Figure 3.8 Two-slope piecewise-linear magnetizing curve for L_{c_1} and L_{c_2} of the Π equivalent, ©2014 IEEE. 82
Figure 3.9 Resulting piecewise-linear leakage curve for L_{l_1} and L_{l_2} of the T equivalent, ©2014 IEEE. 82

Figure 3.10 Resulting piecewise-linear magnetizing curve for L_c of the T equivalent, ©2014 IEEE. . . . 82
Figure 3.11 Star equivalent circuit for the single-phase four-winding transformer (core inductances not shown), ©2014 IEEE. . . . 84
Figure 3.12 Simplified star equivalent circuit for the single-phase N-winding transformer (core inductances not shown), ©2014 IEEE. . . . 85
Figure 3.13 Coupled leakage model for the single-phase N-winding shell-type transformer with cylindrical windings (reciprocal mutual inductances $\mathscr{L}_{ji}$ are not shown), ©2014 IEEE. . . . 85
Figure 3.14 Magnetic flux paths for the three-phase N-winding shell-type transformer with pancake windings, ©2014 IEEE. . . . 87
Figure 3.15 Equivalent magnetic circuit for the three-phase N-winding shell-type transformer with sandwiched windings (mutual reluctances $\mathscr{R}_{ij}$ are not shown, except for $\mathscr{R}_{A_{12}}$), ©2014 IEEE. . . . 87
Figure 3.16 Coupled leakage model for the three-phase N-winding shell-type transformer with sandwiched windings (mutual inductances $\mathscr{L}_{ij}$ are not shown, except for $\mathscr{L}_{A_{12}}$), ©2014 IEEE. . . . 87
Figure 4.1 Piecewise linear magnetizing branch seen from a terminal. . . . 93
Figure 4.2 Degrees of freedom for the single-phase coupled leakage model without winding losses. . . . 99
Figure 4.3 Length of each magnetizing branch for a single-phase shell-type transformer with N coils. . . . 100
Figure 4.4 Simple example of a 4-coil transformer. . . . 103
Figure 4.5 Resulting curves calculated from RMS no-load measurements. . . . 104
Figure 4.6 Modified Frölich equation fitted to the piecewise-linear inductance. . . . 104
Figure 4.7 Type-96 hysteresis loop with constant width. . . . 105
Figure 4.8 Flux linkages across the low-voltage terminals of the 360 MVA transformer. . . . 106
Figure 4.9 Currents in the low-voltage terminal of the 360 MVA transformer. . . . 107
Figure 4.10 Length of each magnetizing branch for a Three-phase shell-type transformer with N coils. . . . 108
Figure 5.1 Magnetostatic cell without magnetomotive force sources. . . . 114
Figure 5.2 A loop of reluctances surrounding a current. . . . 115
Figure 5.3 A loop of reluctances including couplings to the electric circuit. . . . 117
Figure 5.4 Resistive cell without electromotive force sources. . . . 118
Figure 5.5 A loop of resistances surrounding a time-varying flux. . . . 119

Figure 5.6 Resistive and capacitive cell without electromotive force sources. 120
Figure 5.7 Equivalent branches for electric and magnetic circuits. 121
Figure 5.8 Lengthwise average for the calculation of (self) permeance. 124
Figure 5.9 Areawise average for the calculation of (self) capacitance and (self) conductance. 126
Figure 5.10 Two conductors in air with Perfect Electric Conductor boundary conditions. 128

LIST OF ACRONYMS AND ABBREVIATIONS

dc	Direct Current
DoF	Degree of Freedom
EMF	Electromotive Force
EMT	Electromagnetic Transients
EMTP	ElectroMagnetic Transients Program
EQS	ElectroQuasiStatics
ES	ElectroStatics
FDTD	Finite Difference Time Domain
FEM	Finite Element Method
FIT	Finite Integration Technique
HV	High Voltage
IEEE	Institute of Electrical and Electronics Engineers
KCL	Kirchhoff's Current Law
KVL	Kirchhoff's Voltage Law
LV	Low Voltage
MMF	Magnetomotive Force
MQS	MagnetoQuasiStatics
MS	MagnetoStatics
PEEC	Partial Element Equivalent Circuit
RNM	Reluctance Network Method
RMS	Root Mean Square
SFO	Slow-Front Overvoltage
STC	Saturable Transformer Component
TOV	Temporary OverVoltages
UMEC	Unified Magnetic Equivalent Circuit

CHAPTER 1

INTRODUCTION

Transformers have been around for more than a century (almost two), and date back to the discovery of electromagnetic induction by Faraday in 1831, with its rudimentary transformer made of two coils wound over an iron ring (Uppenborn, 1889). Even though the practical application of this apparatus to early alternating current grids (for lighting) dates back to Jablochkoff (Uppenborn, 1889), the invention of the transformer is often attributed to Gaulard and Gibbs, or to Zipernowski, Blathý and Déri. Transformers are an important (if not critical) element of distribution and transmission systems, because without them it would have been impossible to distribute power over long distances. Transformers were a decisive factor in the victory of alternating currents in the *War of the Electric Currents*, along with Tesla's induction motor (Jonnes, 2004).

Today, transformers are ubiquitous in transmission and distribution grids, and because of their nonlinear and frequency-dependent behaviors, they can have a significant impact on power system transients. As such, adequate transformer models are necessary to properly assess system vulnerabilities and network optimization.

In the field of transformer modeling applied to electromagnetic transient studies, it is common to divide the studied phenomena into two categories, depending on the frequency of the concerned transient. The first concerns the transients in the low- and mid-frequency ranges, and the second deals with the high-frequency range. The main reason for this separation in transformer modeling comes from the importance or not to include the transformer's ferromagnetic core representation in the calculations. Physically, the penetration depth of an electromagnetic wave decreases as the frequency increases, which means that the magnetic flux gets confined on the core's surface. Hence, at high frequencies, the core nonlinearities are essentially unimportant, while the transformer capacitances become increasingly important. The converse is also true: at low frequencies, the ferromagnetic core is important (for transients that allow the circulation of magnetic flux in the core, i.e. not in short-circuit conditions), while the capacitances are usually negligible. Also, the penetration depth in conductors decreases as the frequency increases, which leads to an increase of the effective resistance by confining current density toward the outer surfaces of the conductors, thus diminishing the cross section through which the current can flow.

According to (IEC, 2004) and (CIGRÉ, 1997), the electromagnetic transients in the low- and mid- frequency ranges are the temporary overvoltages (TOV) and the slow-front over-

voltages (SFO). The frequencies of interest in these transients are below the first winding resonance, which is typically a few kilohertz (Martinez-Velasco *et al.*, 2005, § 1). Examples of studies in these categories include ferroresonance, transformer energization and geomagnetically induced currents.

As we delve deeper into each topic of this dissertation, specific concepts need to be introduced, but before that, a presentation of the general concepts on the subject of transformer modeling is necessary.

1.1 Basic concepts

Before discussing about transformer modeling, the definition of basic concepts that will be used in this dissertation is in order. These definitions are necessary in order to understand the problems associated with current models.

Since we are mostly interested in circuit models, we will be dealing with *lumped* or *discretized* models, as opposed to *distributed* or *continuous* models (in the space and time sense). Therefore, we are interested in average (integral) quantities, such as *electromotive force*, *magnetomotive force*, *magnetic flux* and *electric current*, and the relations existing between them. A more rigorous development on discrete electromagnetism will be made in Chapter 5, in order to explain the generalization of *magnetic circuit theory* into *electromagnetic circuit theory*, but before, let us review how electric and magnetic circuit theory is generally taught in Electrical Engineering, as seen for instance in (Dept. Elect. Eng., Massachusetts Inst. Technology, 1943; Slemon, 1992).

1.1.1 Maxwell's equations

Let us start with Maxwell's partial differential equations

$$\vec{\nabla} \times \vec{E} = -\frac{\mathrm{d}\vec{B}}{\mathrm{d}t} \tag{1.1}$$

$$\vec{\nabla} \times \vec{H} = \vec{J} + \frac{\mathrm{d}\vec{D}}{\mathrm{d}t} \tag{1.2}$$

$$\vec{\nabla} \cdot \vec{B} = 0 \tag{1.3}$$

$$\vec{\nabla} \cdot \vec{D} = \rho \tag{1.4}$$

along with the constitutive equations

$$\vec{B} = \mu\vec{H} \tag{1.5}$$

$$\vec{D} = \varepsilon\vec{E} \tag{1.6}$$

$$\vec{J} = \sigma\vec{E} \tag{1.7}$$

in the linear homogeneous and isotropic materials, where $\vec{E}$ is the electric field, $\vec{D}$ is the electric displacement field, $\vec{B}$ is the induction field, $\vec{H}$ is the magnetic field, $\vec{J}$ is the current density, ρ is the charge density, μ is the permeability, ε is the permittivity and σ is the conductivity.

With the identity

$$\vec{\nabla} \cdot \left(\vec{\nabla} \times \vec{X}\right) = 0 \tag{1.8}$$

for a given vector field $\vec{X}$, we can also deduce the charge conservation law from (1.2) by applying the divergence on both sides, along with (1.4)

$$\begin{aligned} \vec{\nabla} \cdot \left(\vec{\nabla} \times \vec{H}\right) &= \vec{\nabla} \cdot \left(\vec{J} + \frac{\mathrm{d}\vec{D}}{\mathrm{d}t}\right) \\ 0 &= \vec{\nabla} \cdot \vec{J} + \frac{\mathrm{d}}{\mathrm{d}t}\vec{\nabla} \cdot \vec{D} \\ \vec{\nabla} \cdot \vec{J} &= -\frac{\mathrm{d}\rho}{\mathrm{d}t} \end{aligned} \tag{1.9}$$

When defining electromagnetic problems, it is common to simplify (1.1)–(1.4) using the *static* or *quasistatic* approximations. In static approximations, namely magnetostatic (MS) and electrostatic (ES), the time dependence of fields is neglected, which means that $\frac{\mathrm{d}\vec{B}}{\mathrm{d}t} = 0$ in (1.1) and $\frac{\mathrm{d}\vec{D}}{\mathrm{d}t} = 0$ in (1.2) (implying that $\frac{\mathrm{d}\rho}{\mathrm{d}t} = 0$ in (1.9)). In comparison, with the quasistatic approximations, namely magnetoquasistatic (MQS) and electroquasistatic (EQS), only one of the time dependence is neglected.

Since we are interested by low-frequency transients, the *displacement currents* $\frac{\mathrm{d}\vec{D}}{\mathrm{d}t}$ will be small in comparison to $\vec{J}$ in (1.2) and can safely be neglected, which results in the magnetostatic or magnetoquasistatic approximation, depending if the magnetic induction $\frac{\mathrm{d}\vec{B}}{\mathrm{d}t}$ is considered (i.e. with eddy currents or induced voltage in conductors) or not. Hence, according to (1.9), we also have $\vec{\nabla} \cdot \vec{J} = 0$. For more details on the limits of validity of each approximation, see for instance (Benderskaya, 2007, § 2.2.4).

1.1.2 Integral quantities

In order to discretize (lump in space) the partial differential equations (1.1)–(1.4) into differential algebraic equations (magnetic or electric circuits, differentiated with respect to time), we need to define (oriented) integral quantities in space (R^3).

The electric or conduction current I is the quantity of current density $\vec{J}$ through a surface S. In other words, it is the surface integral of the component of $\vec{J}$ normal to the surface, which is given by

$$I = \iint_S \vec{J} \cdot \mathrm{d}\vec{s} \tag{1.10}$$

where $\mathrm{d}\vec{s}$ is the surface's normal vector.

The magnetic flux ϕ is the flux of induction $\vec{B}$ embraced by a surface S, which is

$$\phi = \iint_S \vec{B} \cdot \mathrm{d}\vec{s} \tag{1.11}$$

Similarly, the electric flux ψ is the flux of electric displacement $\vec{D}$ embraced by a surface S, which is

$$\psi = \iint_S \vec{D} \cdot \mathrm{d}\vec{s} \tag{1.12}$$

The electromotive force e is the path integral of the electric field $\vec{E}$ along a curve L, given by

$$e = \int_L \vec{E} \cdot \mathrm{d}\vec{l} \tag{1.13}$$

where $\mathrm{d}\vec{l}$ is the path's tangent vector.

In a similar fashion, the magnetomotive force $\mathscr{F}$ is the path integral of the magnetic field $\vec{H}$ along a curve L

$$\mathscr{F} = \int_L \vec{H} \cdot \mathrm{d}\vec{l} \tag{1.14}$$

1.1.3 Flux tubes

If we choose a curve L so that $\mathrm{d}\vec{l}$ along this curve is tangent to $\vec{H}$, has the same orientation, and that the magnitude of the magnetic field H is constant along this curve, then (1.14) becomes

$$\mathscr{F} = Hl \tag{1.15}$$

where l is the length of this curve.

Similarly, if we choose a surface S so that $\mathrm{d}\vec{s}$ is tangent to $\vec{B}$, has the same orientation,

and that the magnitude of the induction field B is constant along this curve, then (1.11) becomes

$$\phi = Bs \tag{1.16}$$

where s is the area of this surface.

The previous two definitions lead to the concept of *flux tube*, as depicted in Fig. 1.1 (where $\mathscr{R}$ is the reluctance). Assuming that the permeability μ inside the flux tube is homogeneous and isotropic, the induction field $\vec{B}$ is collinear with the magnetic field $\vec{H}$, so that using (1.5), (1.15) becomes

$$\mathscr{F} = \frac{lB}{\mu} \tag{1.17}$$

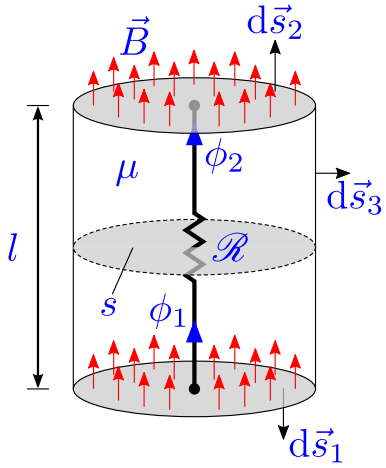

Figure 1.1 Flux tube.

1.1.4 Magnetic and electric circuits

According to Gauss's theorem

$$\oiint_S \vec{B} \cdot \mathrm{d}\vec{s} = \iiint_V \left(\vec{\nabla} \cdot \vec{B}\right) \mathrm{d}v \tag{1.18}$$

with (1.16) in (1.3), the sum of magnetic fluxes across the flux tube is zero

$$\iint_S \vec{B} \cdot \mathrm{d}\vec{s}_1 + \iint_S \vec{B} \cdot \mathrm{d}\vec{s}_2 + \iint_S \vec{B} \cdot \mathrm{d}\vec{s}_3 = 0$$

$$-\phi_1 + \phi_2 + \phi_3 = 0 \tag{1.19}$$

Since $\mathrm{d}\vec{s}_3$ of the flux tube is normal to $\vec{B}$ (and thus $\vec{H}$), the magnetic flux ϕ_3 across this surface is zero. Therefore, the magnetic flux $\phi_1 = \phi_2 = \phi$ for any cross-section of the flux tube, and using (1.16) in (1.17), we obtain

$$\mathscr{F} = \mathscr{R}\phi \tag{1.20}$$

where

$$\mathscr{R} = \frac{l}{\mu s} \tag{1.21}$$

is called the *reluctance*. Equation (1.20) is sometimes called *Hopkinsons' law*[1], in honor to the contribution to magnetic circuit theory by the Hopkinson brothers (Hopkinson, 1885; Hopkinson and Hopkinson, 1886).

Similarly, we can derive Ohm's law for resistive circuits, using (1.7), (1.10) and (1.13), for a *current tube*, which is

$$e = RI \tag{1.22}$$

where

$$R = \frac{l}{\sigma s} \tag{1.23}$$

is called the *resistance*.

1.1.5 Analogies between magnetic and electric circuits

An analogy between reluctance and resistance can be seen from (1.21) and (1.23), along with (1.20) and (1.22). With this analogy, which is sometimes called *Hopkinsons' analogy*[2], magnetic circuits can be studied as resistive circuits, where the magnetomotive force $\mathscr{F}$ is analogous to the electromotive force e, and the magnetic flux ϕ is analogous to conduction current I.

One of the shortcomings of Hopkinsons' analogy with respect to resistive circuits is that the product of electromotive force and conduction current gives power, while the product of their analog counterpart, namely the magnetomotive force and the magnetic flux, gives energy. This can be a problem in circuit simulators if a magnetic circuit is modeled with resistors and if (standard electric circuit) meters are used to measure power or energy in this circuit, for instance.

Another shortcoming is that resistors are dissipative elements. As such, when performing thermal noise analysis, circuit simulators will insert current sources in parallel with resistors (Blanken, 2001, p. 446), where reluctances in this analogy will be mistaken for resistances.

1. See for instance (Blanken, 2001, p. 446).
2. See for instance (Roguin and Ranjamina, 1984; Mork, 1999).

To alleviate these problems, it was proposed by Buntenbach in (Buntenbach, 1968) and concurrently by Carpenter in (Carpenter, 1968) to use capacitors instead of resistors for this analogy with electric circuits. In this analogy, which will be called *Buntenbach's analogy*, the time derivative of magnetic flux $\frac{\mathrm{d}\phi}{\mathrm{d}t}$ is chosen as the analog of electric current I, while maintaining the analogy of magnetomotive force $\mathscr{F}$ with electromotive force e. Rewriting (1.20) in terms of the inverse of reluctance, called permeance $\mathscr{P}$, we get

$$\phi = \mathscr{P}\mathscr{F} \tag{1.24}$$

By comparing the previous equation with the definition of capacitance

$$\psi = Ce \tag{1.25}$$

it can be seen that in Buntenbach's analogy, permeance $\mathscr{P}$ is analog to capacitance C, magnetomotive force $\mathscr{F}$ is analog to electromotive force e and magnetic flux ϕ is analog to electric flux ψ. Therefore, the choice of the time-derivative of magnetic flux $\frac{\mathrm{d}\phi}{\mathrm{d}t}$ as analog to electric current I comes from the fact that the time-derivative of electric flux ψ is the electric current.

With this analogy, the product of the time-derivative of magnetic flux $\frac{\mathrm{d}\phi}{\mathrm{d}t}$ and the magnetomotive force $\mathscr{F}$ now gives power rather than energy.

Several applications of Buntenbach's analogy can be found in the literature [3], but Hopkinsons' analogy is still mostly used (and taught). For this reason, reluctances will be represented by resistances in this dissertation, but remembering that we ought to be careful if we have to calculate power or energy in magnetic circuits.

Another difference with Hopkinsons' analogy is that an initial condition on magnetomotive force cannot be imposed in a resistor in circuit simulators, whereas with Buntenbach's analogy, it can be imposed through an initial voltage condition in a capacitor, as seen in (Haydock, 1985, § 2.8.1). In order to take this initial condition into account in Hopkinsons' analogy, a dc voltage source must be added in series with the reluctance, corresponding to the initial condition on magnetomotive force (analog to electromotive force).

Finally, magnetic losses (hysteresis) [4] are treated differently with Hopkinsons' analogy. As an approximation, because hysteresis is a nonlinear phenomenon, they can be accounted for *linearly* by what is called a *magnetic loss element* in (Cherry, 1949; Magdziarz and Żagań,

3. See for instance (Haydock, 1985; Blanken and Van Vlerken, 1991; Haydock and Holland, 1994; Hamill, 1993, 1994; Eaton, 1994, 1998; Cheng *et al.*, 2000; Blanken, 2001; Yan and Lehman, 2005; Zhalefar and Sanaye-Pasand, 2006).

4. Note that it is assumed that the material of the flux tube is non conducting (no eddy currents). More on this subject later.

1986) or *transferance* in (Laithwaite, 1967; Carpenter, 1968), which is analog to inductance according to Hopkinsons' analogy. In contrast, with Buntenbach's analogy, magnetic losses are represented simply by resistors.

1.1.6 Electric and magnetic potentials

Using the identity (1.8), it can be seen that a divergence-free field can be expressed as the curl of another vector field, called *vector potential*, since the divergence of a curl is zero. Therefore, according to (1.3), the induction field $\vec{B}$ can be expressed as

$$\vec{B} = \vec{\nabla} \times \vec{A} \tag{1.26}$$

where $\vec{A}$ is called the *magnetic vector potential*.

Also, with the identity

$$\vec{\nabla} \times \left(\vec{\nabla} X \right) = \vec{0} \tag{1.27}$$

the curl of a gradient field is zero. In other words, if a vector field is *conservative*, i.e. it is irrotational, and assuming that the domain is simply-connected (more about this later), it can be expressed as a gradient of a *scalar potential*. Therefore, using (1.27) and (1.26) in (1.1), we get

$$\begin{aligned} \vec{\nabla} \times \vec{E} &= -\frac{\mathrm{d}\left(\vec{\nabla} \times \vec{A} \right)}{\mathrm{d}t} \\ \vec{\nabla} \times \left(\vec{E} + \frac{\mathrm{d}\vec{A}}{\mathrm{d}t} \right) &= \vec{0} \\ \vec{E} + \frac{\mathrm{d}\vec{A}}{\mathrm{d}t} &= -\vec{\nabla}\varphi \end{aligned} \tag{1.28}$$

where φ is called the *electric scalar potential*.

Similarly, a divergence-free current density $\vec{J}$ (charge conservation) can be expressed as the curl of another vector field $\vec{T}$, called the *electric vector potential*

$$\vec{J} = \vec{\nabla} \times \vec{T} \tag{1.29}$$

With the magnetoquasistatic (MQS) approximation, using (1.29) and (1.27) in (1.2) results

in

$$\begin{aligned} \vec{\nabla} \times \vec{H} &= \vec{\nabla} \times \vec{T} \\ \vec{\nabla} \times \left(\vec{H} - \vec{T} \right) &= \vec{0} \\ \vec{H} - \vec{T} &= -\vec{\nabla}\Omega \end{aligned} \tag{1.30}$$

where Ω is called the *magnetic scalar potential*.

1.1.7 Sources in magnetic circuits

Then comes the matter of where to insert sources in magnetic circuits.

Using Stokes' theorem

$$\iint_S \left(\vec{\nabla} \times \vec{H} \right) \cdot \mathrm{d}\vec{s} = \oint_L \vec{H} \cdot \mathrm{d}\vec{l} \tag{1.31}$$

and integrating on both sides of (1.2) (using the magnetoquasistatic approximation) on a surface S, along with the definition of conduction current (1.10), we get

$$\begin{aligned} \oint_L \vec{H} \cdot \mathrm{d}\vec{l} &= \iint_S \vec{J} \cdot \mathrm{d}\vec{s} \\ &= I \end{aligned} \tag{1.32}$$

where I is the *total* conduction current flowing through the surface S, and L is the surface's boundary. Therefore, in the case where the surface S crosses a coil made of N turns, and if we say that the current in the coil is I, the total current crossing through S will be NI.

Let us consider a simple inductor, made of a coil of N turns wound on a toroidal core with a very high permeability μ (linear, homogeneous and isotropic), so that $\vec{H}$ and $\vec{B}$ are essentially in the toroidal direction $\hat{\theta}$, as shown in Fig. 1.2. Therefore, if we choose the circular path L with the same orientation as $\vec{H}$, (1.32) becomes

$$\begin{aligned} \oint_L \vec{H} \cdot \mathrm{d}\vec{l} &= \iint_S \vec{J} \cdot \mathrm{d}\vec{s} \\ Hl &= NI \end{aligned} \tag{1.33}$$

where S is the surface bounded by L. According to the definition of a flux tube made in § 1.1.3, we could choose a toroidal flux tube whose start and end surfaces meet (reluctance looped onto itself). Furthermore, as shown in § 1.1.6, if there is no current density $\vec{J}$ in the flux tube, the magnetic field $\vec{H}$ can be expressed as the gradient of magnetic scalar potentials

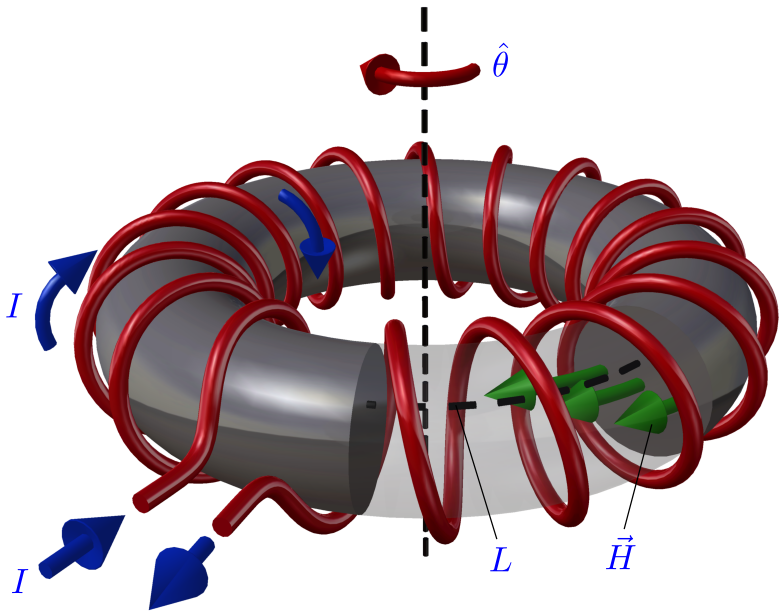

Figure 1.2 Toroidal inductor.

Ω. Therefore, it can be anticipated that magnetic scalar potential is diminished as we travel along L in this flux tube. However, the potential across the starting face of the tube will be different than that of the end face, even though both faces meet to close the tube. Hence, if the flux tube is closed on itself (looped reluctance), where is the source of magnetomotive force in this circuit?

The answer lies in *topology*. By separatating space into conducting and non-conducting domains, there will be "holes" in the non-conducting domain, i.e. this domain is not *simply connected*. Therefore, $\vec{H}$ is no longer conservative, even though it is irrotational inside non-conducting space. In order for $\vec{H}$ to be conservative in the non-conducting domain, it is necessary to make *cuts*, so that the domain becomes simply connected.

In the previous example, since there is approximately no flux outside the core (we assumed that μ was very high inside the core, much higher than outside), the problem at hand is essentially the same as the one presented in Fig. 1.3 (because there is no flux between each turn), where the current in the wire is NI. Hence, the non-conducting domain is doubly connected (there is one hole) and we need to create one cut in the torus, so it becomes simply connected (the choice of the cut is arbitrary). The source of magnetomotive force is inserted into this cut and its value, according to (1.33), will be equal to NI. Note that because magnetomotive force is analog to electromotive force in Hopkinsons' analogy, it is represented by a voltage source in the magnetic circuit, and this voltage source is controlled by a current in the electric circuit (wire).

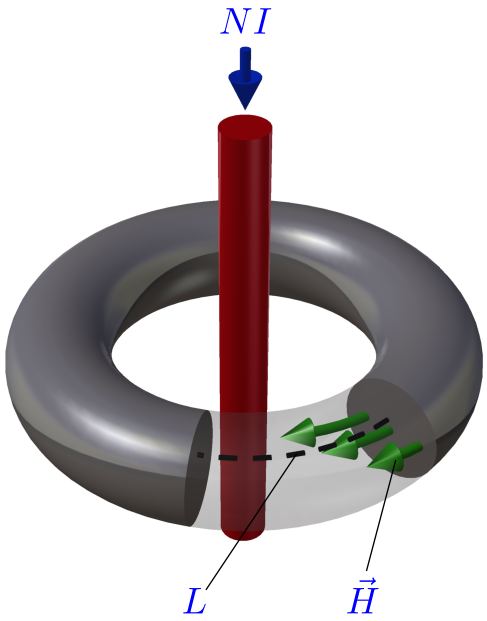

Figure 1.3 Equivalent toroidal inductor.

Let us now consider a more complex example, where flux can now flow between wires, as shown in the 2-D problem of Fig. 1.4. Again, it is assumed that magnetic flux is confined within the core (in grey). It can be seen that the non-conducting domain is 10-connected, i.e. there are nine holes. To make the domain simply connected (1-connected), it is necessary to create nine cuts. These cuts can be seen in Fig. 1.4, numbered from 1 to 9. This example is useful to show how to deal with touching cuts (cuts 4 and 5). By inserting a MMF source for wire 4 inside cut 4 and one for wire 5 inside cut 5, it can be seen that a loop around wire 4 only will also incorrectly include the MMF source from wire 5, since the loop passes through cut 5. Therefore, when dealing with touching cuts, the MMF source of an inner cut needs to be "propagated" to all other cuts leading to the boundary, so that it cancels for any loop not including wire 5. This principle is similar to the way sources are included in the Reluctance Network Method (Turowski, 1995, pp. 152–154). More details regarding this method will be given in Chapter 5.

In a similar fashion to the insertion of *electric sources* in *magnetic circuits*, the insertion of *magnetic sources* in *electric circuits* can be made following the same reasoning.

Analogously to the example shown in Fig. 1.3, let us consider the example presented in Fig. 1.5, where a conducting torus is wound around a highly permeable core. Assuming that magnetic flux is essentially constrained inside the core (more on this assumption later), then according to (1.1), the electric field $\vec{E}$ is irrotational inside the conducting torus. Therefore, the same topology problem arises, where $\vec{E}$ is not conservative because of the "hole" created

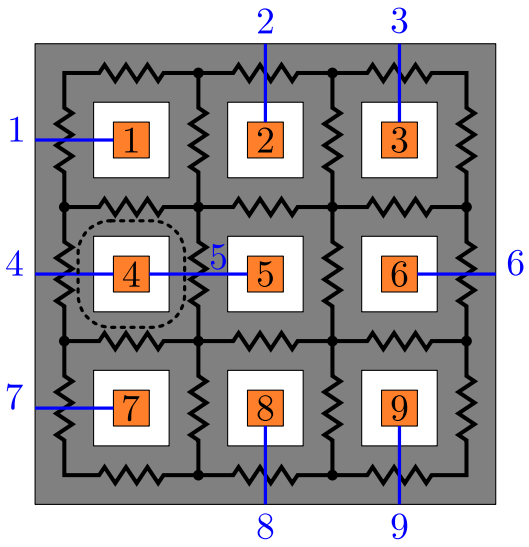

Figure 1.4 Example of magnetic circuit with nine conductors and cuts.

by the flux tube (core) passing through the conducting "loop", and we have to perform a cut so that the doubly connected torus becomes simply connected. Again, the choice of the cut is arbitrary (as long as the torus becomes simply connected), but a simple choice is to cut the torus along its cross section.

Integrating on both sides of (1.1) on a surface S and using Stokes' theorem (1.31) along with the definition of magnetic flux (1.11), we get

$$\begin{aligned} \oint_L \vec{E} \cdot \mathrm{d}\vec{l} &= -\iint_S \frac{\mathrm{d}\vec{B}}{\mathrm{d}t} \cdot \mathrm{d}\vec{s} \\ &= -\frac{\mathrm{d}\phi}{\mathrm{d}t} \end{aligned} \tag{1.34}$$

where ϕ is the *total* magnetic flux crossing through the surface S, and L is the surface's boundary. It is often approximated that if a coil of N turns is sufficiently stranded (so that the eddy currents in the strands are negligible), it can be represented by an equivalent torus, like the one shown in Fig. 1.5. Then, remembering that we assumed that the magnetic flux was confined inside the core (and negligible outside), we can express (1.34) as the total flux linked by the coil, by choosing a path L that is tangential to $\vec{E}$

$$\begin{aligned} \oint_L \vec{E} \cdot \mathrm{d}\vec{l} &= -\iint_S \frac{\mathrm{d}\vec{B}}{\mathrm{d}t} \cdot \mathrm{d}\vec{s} \\ El &= -N\frac{\mathrm{d}\phi}{\mathrm{d}t} \end{aligned} \tag{1.35}$$

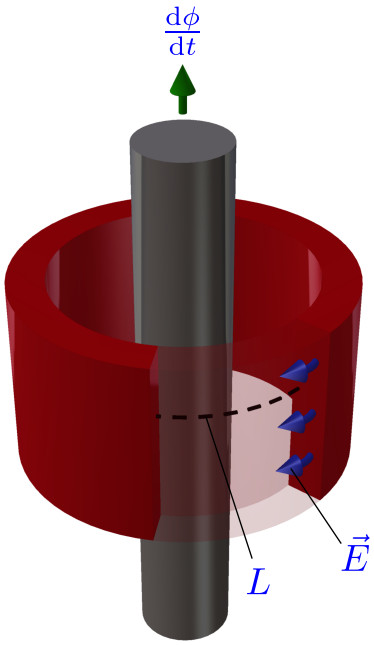

Figure 1.5 A conducting torus wound around a core canalizing a time-varying magnetic flux.

Again, El represents the electric scalar potential drop (or simply voltage drop) across the torus and according to (1.13), $-N\frac{d\phi}{dt}$ is the induced electromotive force (or rather counter electromotive force, to emphasize that the direction of the induced EMF is opposite to the direction of the time derivative of magnetic flux, as illustrated in Fig. 1.5). As demonstrated previously for magnetic circuits, the induced EMF (source) in electric circuits is inserted in the cut. From an electric circuit standpoint, the source is a voltage source, controlled by the time-derivative of magnetic flux of the magnetic circuit.

The total magnetic flux linked by a coil of N turns is often called *flux linkage*, which is given by

$$\lambda = N\phi \tag{1.36}$$

The idea of inserting the source in the cut is similar to the idea of *reference layer* discussed in (Benderskaya, 2007, § 3.3).

1.1.8 Connection between magnetic and electric circuits

The remaining question is on how to connect magnetic circuits to electric circuits. By combining the previous two examples, we get two interlocking loops, electric (conducting) and magnetic (permeable), as illustrated in Fig. 1.6.

According to Hopkinsons' analogy, the equivalent circuit for these loops is shown in

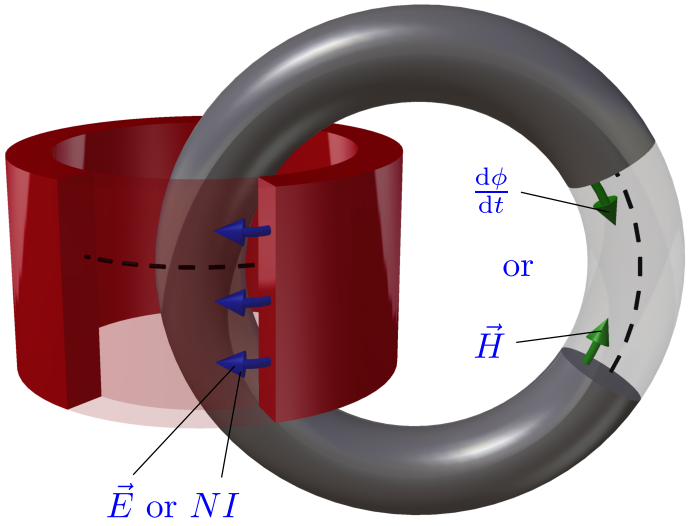

Figure 1.6 A conducting torus wound around a magnetic torus forming dual loops.

Fig. 1.7a. Of course, since there are no sources in this circuit, the solution is the trivial one (unless there is an initial condition). However, the purpose of this example is to show the link between electric and magnetic circuits, regardless of where the sources are located. Since magnetic flux is the analog of current in Hopkinsons' analogy, and magnetomotive force is the analog of electromotive force, we can rewrite (1.33) and (1.35) in terms of voltages (v_1, v_2) and currents (i_1, i_2) of the two controlled voltage source in Fig. 1.7a

$$v_1 = -N\frac{\mathrm{d}i_2}{\mathrm{d}t} \tag{1.37}$$

$$v_2 = Ni_1 \tag{1.38}$$

It turns out that these are the equations of a two-port circuit element called *Type 2 L-R mutator*, which is a particular type of *mutator*, as defined in (Chua, 1968, 1971) [5]. With this type of mutator, the resistance (which is the analog of reluctance in Hopkinsons' analogy) placed across the second port (magnetic port) in Fig. 1.7b is seen as *inductance* from the first port (electric port).

Similarly, according to Buntenbach's analogy, the equivalent circuit for the loops of Fig. 1.6 is depicted in Fig. 1.8a, where permeances are analog to capacitances. Since the time-derivative of magnetic flux is analog to current, and the magnetomotive force is analog to

5. Strickly speaking, the factor N is missing from the equations in (Chua, 1968, Table 1), but it can be considered as the *gain* of the mutator.

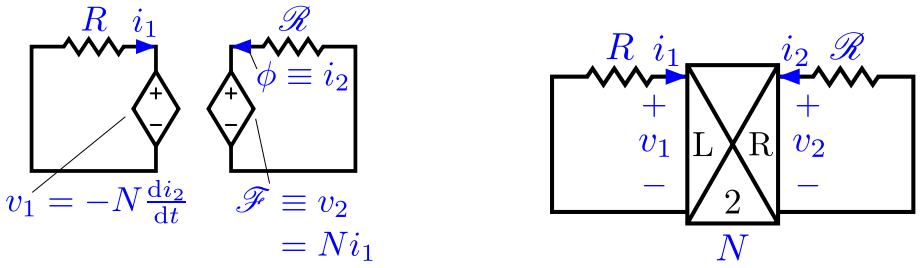

(a) Equivalent electric and magnetic circuits

(b) Type 2 L-R mutator

Figure 1.7 Dual loops with Hopkinsons' analogy.

electromotive force with this analogy, the two-port equations become

$$v_1 = -Ni_2 \tag{1.39}$$

$$v_2 = Ni_1 \tag{1.40}$$

These are the equations of a particular mutator called *Type 1 L-C mutator* (again with a gain N), also known as *gyrator* (Tellegen, 1948), where a capacitance across the second port (magnetic port) in Fig. 1.8b is seen as an inductance from the first port (electric port).

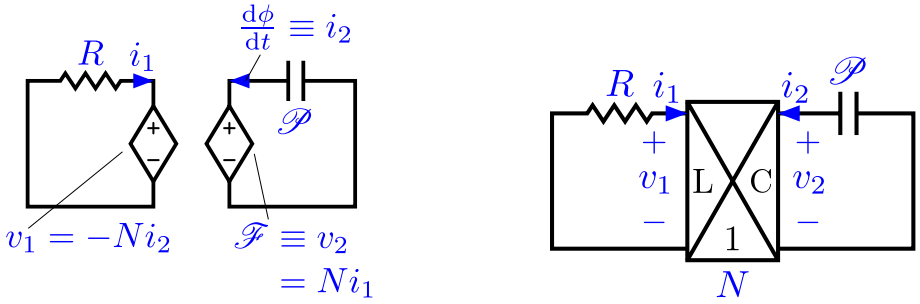

(a) Equivalent electric and magnetic circuits

(b) Type 1 L-C mutator

Figure 1.8 Dual loops with Buntenbach's analogy.

As it can be seen, the resistances from Hopkinsons' analogy and the capacitances from Buntenbach's analogy are both viewed as inductances from the electric circuit. Therefore, the statement in (Turowski, 1995, p. 174) that

> "Ohm's law for magnetic circuits $V_\mu = \Phi R_\mu$ can only be applied to static or quasi-static magnetic fields at a constant frequency f. For such fields magnetic flux becomes a full analogue of electric current. In the case of transient fields, however, it is better to associate the magnetic flux $\Phi = \int \mathbf{B} \cdot \mathrm{ds}$ with the electric

> flux $\Psi = \int \mathbf{D} \cdot \mathrm{ds}$ rather than with the electric current $i = \int \mathbf{J} \cdot \mathrm{ds}$. The electric flux corresponds to an electric charge $Q = Cu = \Psi$."

is incorrect. A similar assertion was made in (Haydock and Holland, 1994, p. 2996). The analogy used (Hopkinsons' or Buntenbach's) is not related with the transient or static nature of the electromagnetic problem at hand. As mentioned before, both analogies are seen as inductances from the electric circuit and will draw the same current from an electrical source (the inductor's initial condition on current can be accounted for with a dc voltage source in series with the reluctance), as demonstrated in (Lambert *et al.*, 2014a).

The implementation of these mutators in circuit simulators is straightforward using commonly available coupled resistances and inductances, as shown in (Lambert *et al.*, 2014a). Other names are also used in the literature to describe these two-port elements, for instance *linkage element* in (Haydock, 1985; Haydock and Holland, 1994), or *magnetic interface* in (El-Hamamsy and Chang, 1989).

Instead of using either analogies, some authors prefer to directly interface the magnetic equations to electric circuits. See for instance (Chen, 1996; Enright, 1996).

1.1.9 Inductances and duality

Inductance (or self-inductance) L is defined as the ratio of a coil's flux linkage λ and its current i

$$L = \frac{\lambda}{i} = \frac{N\phi}{i} \tag{1.41}$$

Combining the relationship (1.33) between a coil's current and magnetomotive force, and of the relationship (1.36) between its flux linkage and magnetic flux with (1.20), we get the relationship between inductance and reluctance [6]

$$L = \frac{N^2}{\mathscr{R}} \tag{1.42}$$

Therefore, in electric circuit theory, there is a passive (two-pole) element, inductance, which corresponds to its magnetic circuit counterpart, reluctance. The problem remains to convert a magnetic circuit into its equivalent electric circuit.

In a key paper (Cherry, 1949), Cherry introduced the principle of *duality* for magnetic circuits, in order to deduce an equivalent electric (dual) circuit. This principle can be explained as follows. As illustrated in Figs. 1.9–1.12, reluctances are converted to inductances using (1.42). However, what number of turns N do we choose in the case where there are more than one coil (with a different number of turns)? The case where there are multiple

6. In the case where a nonlinear reluctance curve $\mathscr{F} - \phi$ needs to be converted into a nonlinear inductance curve $\lambda - i$, one needs to use (1.14), (1.33) and (1.36).

coils in the magnetic circuit with different number of turns was treated in (Cherry, 1949, § 7), where an arbitrary common number of turns N_c may be used as N in (1.42) (in that paper, the highest common factor amongst the number of turns for each coil was used). We can choose this number of turn to be unity ($N_c = 1$), to simplify. In that case, (1.42) simplifies to

$$L = \frac{1}{\mathscr{R}} = \mathscr{P} \tag{1.43}$$

Furthermore, magnetomotive forces in the magnetic circuit are dual to currents in the electric circuit, and according to (1.33), we will have

$$\mathscr{F} = N_c i \tag{1.44}$$

Similarly, from (1.35), the time-derivative of magnetic fluxes in the magnetic circuit are dual to electromotive forces in the electric circuit, given by

$$v = -N_c \frac{\mathrm{d}\phi}{\mathrm{d}t} \tag{1.45}$$

Therefore, it can be seen with (1.10)–(1.14) that the duality principle is a transformation between line and surface integral quantities. In other words, loops in the magnetic circuit become nodes in the electric circuit (and vice versa), as illustrated in Fig. 1.10. Finally, the equations of each two-port element of Fig. 1.11 are

$$v_1 = \frac{N_1}{N_c} v_a \tag{1.46}$$

$$i_a = -\frac{N_1}{N_c} i_1 \tag{1.47}$$

and

$$v_2 = \frac{N_2}{N_c} v_c \tag{1.48}$$

$$i_c = -\frac{N_2}{N_c} i_2 \tag{1.49}$$

which are the equations of ideal transformers of ratios $N_1 : N_c$ and $N_c : N_2$, respectively, as illustrated in Fig. 1.12. Note that because of the arbitrariness of N_c, we could choose $N_c = N_1$ or $N_c = N_2$. In that case, the ideal transformers will be of ratios $N_1 : N_2$ and $1 : 1$ (which is equivalent to $N_1 : N_1$ or $N_2 : N_2$), which is the approach chosen in (Cho, 2002, Fig. 2.6), (Martinez-Velasco and Mork, 2005, Fig. 3) or (Mork *et al.*, 2007a, Fig. 4), for instance.

The principle of duality is extended to nonlinear magnetic circuits in (Slemon, 1953),

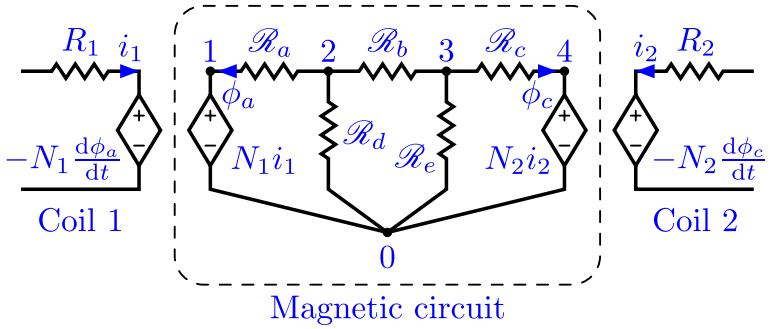

Figure 1.9 Example of a magnetic circuit with two windings coupled with two electric circuits.

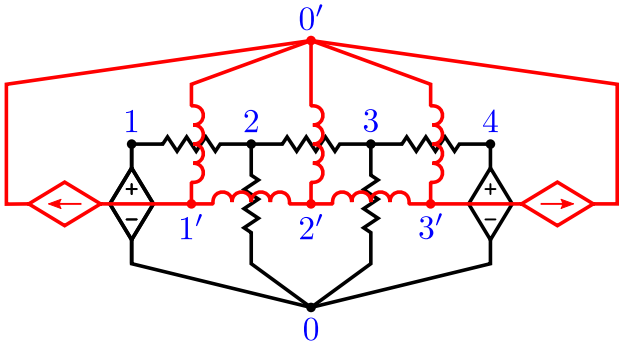

Figure 1.10 Graphical derivation of the dual circuit.

where duality is also explained using the circuit loop matrix and *mesh fluxes*. Unfortunately, the demonstration is not as rigorous as the author presumes, because a different set of *loops* can be found from the magnetic circuit of (Slemon, 1953, Fig. 1b) (out of a possible total of 6 loops for this circuit). However, as mentioned in (Chua and Lin, 1975, § 3-3), not all the loop equations are necessary to describe Kirchhoff's Voltage Law (KVL) for this circuit, because some equations will be dependent. Only a set containing the maximum number of independent equations is necessary. In the case of a *planar* network, i.e. a network that can be drawn on a plane without any crossing branches, such as the one presented in (Slemon,

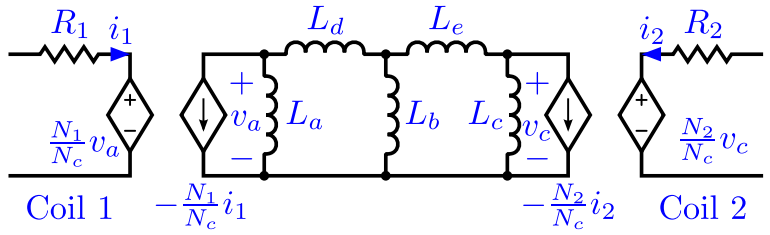

Figure 1.11 Dual circuit coupled with the two electric circuits.

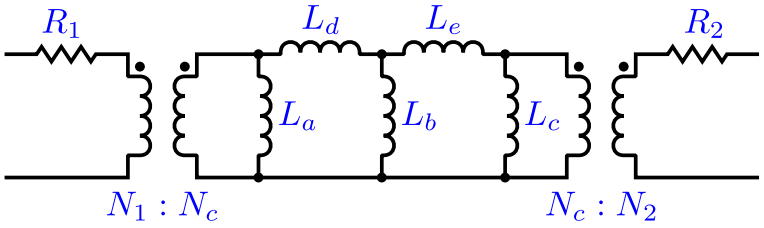

Figure 1.12 Dual circuit simplified with ideal with ideal transformers.

1953, Fig. 1b), an independent set of loops can easily be constructed by choosing each *mesh* of the circuit (Chua and Lin, 1975, p. 138). This brings an important point about the mathematical description of duality discussed in (Slemon, 1953), but also for the preceding graphical procedure seen in Fig. 1.10: the magnetic circuit has to be planar for the dual circuit to exist, as demonstrated in (Whitney, 1932, pp. 357–358) in terms of graph theory.

In the particular case of a transformer, it is mentioned in (Cherry, 1949, § 6) that the dual circuit does not exist for a transformer with more than three windings, because it is said that the magnetic circuit is non-planar [7]. Fortunately, different means were developed to transform a non-planar circuit into a planar one. On one hand, (Julia, 1939) and later generalized in (Bloch, 1946), transformations of non-planar circuits into planar circuits were proposed that use ideal transformers. On the other hand, it was proposed in (Erdei, 1962) to use mutual inductances to transform a non-planar circuit into a planar one. Therefore, it can be seen that this transformation is not unique. As such, one might argue that the resulting planar network loses its physical meaning, as what is meant in (Bloch, 1946, p. 677) by "geometrical properties".

In the case of more complex 3-D magnetic circuits, which will be discussed in Chapter 5, the application of these transformations (followed by duality) is less straightforward. In that case, possible dual circuits will be similar to that proposed in the Partial Element Equivalent Circuit (PEEC) method (Ruehli, 1972, 1974; Ekman, 2003) (with mutual inductances), or to the one developed earlier in (Kron, 1944) (with ideal transformers). Therefore, the dual circuit is not unique and it also loses its "geometrical properties", as seen for instance by comparing (Kron, 1944, Fig. 1) and (Ekman, 2003, Fig. 3.8), with (Turowski *et al.*, 1990, Fig. 5). Additional details about 3-D electromagnetic circuits are given in Chapter 5.

7. In fact, this is not necessarily the case, as it will be shown for a model of a shell-type transformer in Chapter 3.

1.2 Literature review

The literature review presented in this section is intended to complement the specific literature reviews of each chapter, but also serves to introduce the problems associated with present transformer models. It is not intended to be exhaustive, but rather to provide an introduction to transformer models available in EMT-type programs, such as EMTP-RV (Mahseredjian *et al.*, 2007; Mahseredjian, 2008). A few literature reviews on low- and mid-frequency transformer modeling already exist, see for instance (Martinez-Velasco and Mork, 2005) and (Amoiralis *et al.*, 2009, § 5). Also, for reviews more specifically applied to transformer modeling for GIC studies, see (Mahseredjian, 2012; Lambert and Mahseredjian, 2013).

The low-frequency transformer models still mostly used by engineers today in EMT-type programs are the *Saturable Transformer Component* (STC) and BCTRAN. See for instance (Gérin-Lajoie *et al.*, 2013; Salimi *et al.*, 2013) for recent articles that use the STC model, and (Martínez Duró *et al.*, 2013) for simulations made with BCTRAN.

The STC model is also known as the star equivalent circuit, where supposedly the integral of the voltage at the star point is the image of the magnetic flux inside the core. Therefore, the model of the core (magnetizing branch) is connected in parallel at this point, and the current drawn in this branch would be an image of the core's magnetomotive force. The resulting circuit for the single-phase transformer is shown in figure 1.13, where additional windings are accounted for by inserting their series impedance to the star point. Therefore, it is a single-phase model for N-winding transformers, although this representation is not valid for $N > 3$ (Blume *et al.*, 1951) [8]. This aspect will be discussed in Chapter 3.

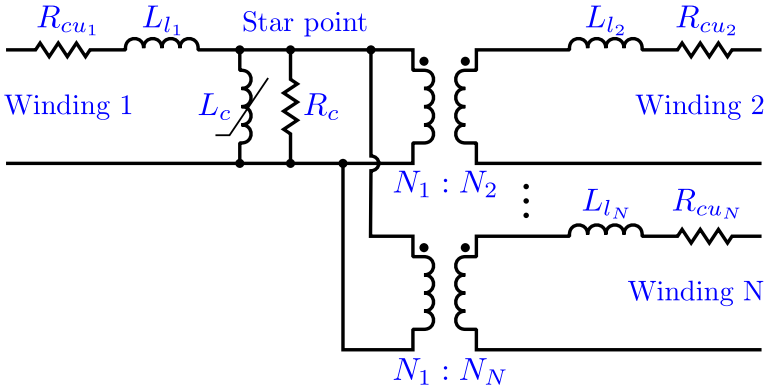

Figure 1.13 Single-phase N-winding Saturable Transformer Component.

The extention of the STC model for three-phase two-winding transformer can be done

8. Because the N-winding transformer has $N(N-1)/2$ independent series impedances; hence, a four-winding transformer can not be represented by four star-connected impedances, unlike the proposition made by Steinmetz for multi-secondary windings transformers (Steinmetz, 1897, Fig. 101).

by adding a fictious delta-connected winding to account for the zero-sequence reluctance paths (Dommel, 1992, § 6.5), if no delta connected winding is present. However, to do so, an additionnal short-circuit test would be necessary to characterize the fictious winding and in the case of a three-winding three-phase transformer, the addition of this fictious winding makes the model invalid, because $N > 3$ (Dommel, 1992, § 6.5).

It is shown in (Dick and Watson, 1981) that placing the magnetizing branch to the star point can lead to a large error. Instead, it is proposed to modify the STC model to place the magnetizing branch in parallel at the terminals of the innermost winding (which is usually the lowest voltage winding for cylindrical windings), and the zero-sequence impedance in parallel at the terminals of the outermost winding (which is usually the highest voltage winding for cylindrical windings). Physically, it also makes more sense, because with cylindrical windings there is little leakage flux between the innermost winding and the wound leg. Therefore, the integral of the voltage of the innermost winding is approximately equal to the flux linkage in the leg. Of course, this is neglecting possible yoke saturation, as mentioned in (Dommel, 1992, § 6.6.2).

The BCTRAN model is a short-circuit model valid for N-winding transformers (Brandwajn *et al.*, 1982). The model is made of N coupled R-L branches (per phase), calculated from short-circuit tests, based on the indefinite admittance matrix (Chua and Chen, 1976, pp. 765–769). To take into account the magnetizing current, magnetizing branches can be added in parallel at the terminals of the innermost winding, as similarly done with the modified STC model.

Another type of low-frequency transformer model is also used in EMT-type programs, called "topological", because it is based on the discretization of the transformer geometry into flux tubes (sometimes also called flux *paths*), as seen in § 1.1. The three currently available topological models in EMT-type programs are UMEC, TOPMAG and the Hybrid transformer model.

The Unified Magnetic Equivalent Circuit (UMEC) model was developped in 1996 by Enright (Enright, 1996; Enright *et al.*, 1997, 1998, 1999) and implemented in EMTDC (Woodford *et al.*, 1983) in an attempt to replace the classical modeling approach used in EMTDC with a topological model. Since the mutators are not available in EMTDC, the equations of the magnetic circuit are directly inserted into the admittance matrix through a multi-port Norton equivalent circuit. In order to appreciate the difference with this model and other topological models, the magnetic circuit considered for the derivation of the three-legged transformer model is shown in Fig. 1.14. Reluctances $\mathscr{R}_{Y_1}$ and $\mathscr{R}_{Y_2}$ represent the left and right yokes, respectively (note that bottom yokes are added to the length of top yokes, since they share the same magnetic flux in this circuit, so that the lengths of $\mathscr{R}_{Y_1}$ and $\mathscr{R}_{Y_2}$ are twice the

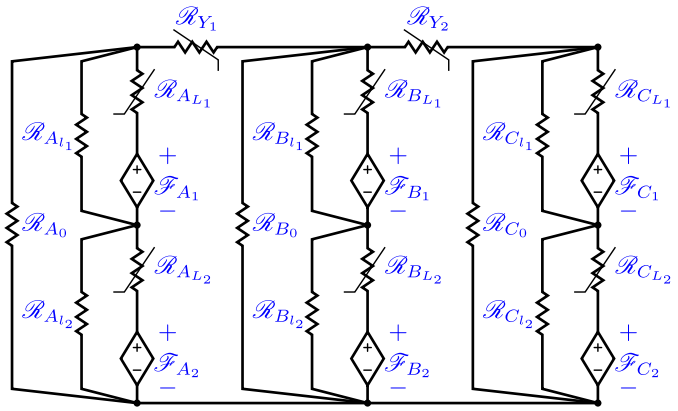

Figure 1.14 Magnetic circuit of the UMEC model for the two-winding three-legged transformer.

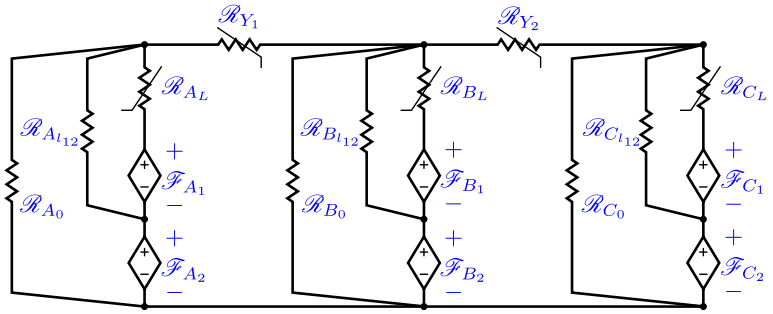

Figure 1.15 Magnetic circuit of the Hybrid transformer model for the two-winding three-legged transformer.

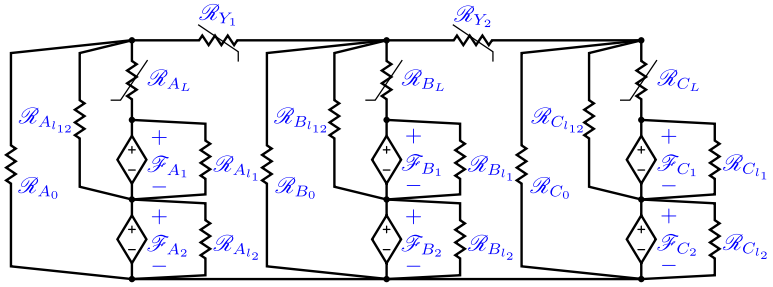

Figure 1.16 Magnetic circuit of the TOPMAG model for the two-winding three-legged transformer.

length of yokes). Reluctances $\mathscr{R}_{A_{L_1}}$, $\mathscr{R}_{B_{L_1}}$ and $\mathscr{R}_{C_{L_1}}$ represent half of the wound leg of each phase and reluctances $\mathscr{R}_{A_{L_2}}$, $\mathscr{R}_{B_{L_2}}$ and $\mathscr{R}_{C_{L_2}}$ represent the other half [9]. Similarly, reluctances with subscript l represent leakages for each winding. Reluctances $\mathscr{R}_{A_0}$, $\mathscr{R}_{B_0}$ and $\mathscr{R}_{C_0}$ are the zero-sequence shunting air paths [10].

The Hybrid transformer model was introduced in 2002 by Gonzalez-Molina and others (Gonzalez-Molina and Mork, 2002; Gonzalez-Molina *et al.*, 2003b,a, 2004; Mitra, 2002; Mitra *et al.*, 2003; Mitra, 2003; Cho, 2002), following their earlier work on the subject (Stuehm, 1993; Martinez-Velasco *et al.*, 1999; Mork, 1999). The synthesis of their work is presented in (Mork *et al.*, 2007a,b). The objective was to combine the simplicity of the short-circuit model BCTRAN with a more topologically correct core model, hence the name *Hybrid* transformer model. This is done by inserting a fictitious "infinitely thin" winding on the core leg. The short-circuit inductance between this fictitious winding and the innermost winding is estimated from the short-circuit inductance between low- and high-voltage windings, assuming a certain proportionality factor K. This factor is assumed to be equal to 0.5 in (Høidalen *et al.*, 2009), 0.7 in (Gonzalez-Molina *et al.*, 2003a), and 0.33 in (Chiesa *et al.*, 2010). The difficulty in having a detailed transformer model relies in its parameters identification. The implementation of the Hybrid transformer model of ATP-EMTP innovates in this way, offering the user various choices as input data: typical values, test report or design information (Høidalen *et al.*, 2007, 2009). Recent enhancements to the model with respect to core modeling are presented in (Høidalen *et al.*, 2011). Initially, before simplifying the dual circuit into an hybrid model (connecting BCTRAN with a topological core model using a fictitious winding), the magnetic circuit considered for the three-legged transformer is presented in figure 1.15 [11]. Reluctances $\mathscr{R}_{A_L}$, $\mathscr{R}_{B_L}$ and $\mathscr{R}_{C_L}$ represent the leg reluctance of each phase. Reluctances $\mathscr{R}_{A_{l_{12}}}$, $\mathscr{R}_{B_{l_{12}}}$ and $\mathscr{R}_{C_{l_{12}}}$ represent the leakage reluctances between windings 1 and 2.

The TOPMAG model was developped in 1994 by Narang and Brierley and implemented in the DCG/EPRI EMTP version 3 (Narang and Brierley, 1994; Narang *et al.*, 1997) in an effort to supersede the BCTRAN model. It is also available in EMTP-RV. The objectives

9. This separation is made from the doubtful assumption in (Enright, 1996, p. 40) that: "Although single-phase transformer windings are not generally wound separately on different limbs, each winding can be separated in the UMEC".

10. Note that the zero-sequence return path includes magnetic shunts and tank, which should therefore be represented by nonlinear reluctances. However, it is usually assumed that these structural elements cannot saturate (linear). Not to mention that zero-sequence measurements to quantify these nonlinearities are never available.

11. Note that the air reluctances in parallel with each core reluctance in (Mork *et al.*, 2007a, Fig. 3) are not included here, since the volume of air (flux tube) they represent is unclear, and their effect are usually included in the model in the nonlinear reluctances themselves (these shunt paths mostly affects the slope in saturation). Furthermore, the bottom yokes reluctances in (Mork *et al.*, 2007a, Fig. 3) were included in $\mathscr{R}_{Y_1}$ and $\mathscr{R}_{Y_2}$, since they share the same magnetic flux, as mentioned previously.

were to improve the core-type transformer model with concentric windings to include the core nonlinearities in a more rigorous way (i.e. instead of lumping them at the terminals of the innermost winding), in order to be able to simulate the unbalance between the center leg and the outer legs (longer magnetic paths) of a three-legged (or five-legged) transformer. The initial magnetic circuit considered (before simplifications) in this model for the three-legged transformer is shown in Fig. 1.16 [12]. In this case, there are both leakage reluctances for each winding and leakage reluctances between windings.

There are actually a lot more topological transformer models in the literature. One of those model is that presented by de León in (de León and Semlyen, 1992b; de León, 1992; de León and Semlyen, 1992a, 1993, 1994), which is argued to be the most complete transformer model, according to (Martinez-Velasco and Mork, 2005, § 5). However, one of the problems of transformer modeling is the lack of measurements to determine the model parameters, which could explain why such models are not implemented today in EMT-type programs.

Other examples of topological transformer models in the SABER program are those of (Yacamini and Bronzeado, 1994; Oliveira *et al.*, 2003; Apolônio *et al.*, 2004; de Azevedo *et al.*, 2007), and in ATP-EMTP, the SEATTLE XFORMER model (Chen and Neudorfer, 1992, 1993; Chen, 1996). Also, classical papers on topological transformer models include (Dick and Watson, 1981; Arturi, 1991, 1994).

1.3 Dissertation statement

According to the previous description of existing transformer models, shown in Section 1.2, and to the surrounding classic theories described in Section 1.1, several problems and associated questions arise.

Problem 1: In order to calculate leakage inductances, short-circuit tests are used, since the magnetic flux in these tests is forced to leak between the windings. However, in the case where a winding is divided into several *coils* (fraction of a winding), for instance to simulate interturn winding faults (Bastard *et al.*, 1994; Palmer-Buckle *et al.*, 1999), short-circuit tests between coils are never available. Therefore, this is related to the problem highlighted in § 1.2 that there is a lack of measurements to improve model sophistication.

Furthermore, the classical formula [13] to calculate the leakage inductance between two

12. This magnetic circuit would be the reciprocal of the dual circuit of (Narang and Brierley, 1994, Fig. 1b), for a two-winding transformer. The nonlinear zero-sequence inductances were also assumed here to be linear, as mentioned previously.

13. More details on this formula will be given in Chapter 2.

coils (or windings) from geometrical data assumes that leakage flux is parallel to the coils themselves, which is not the case in practice because of the fringing effect (the normal component of magnetic flux between the coils is generally not zero).

Problem 2: As mentioned before, it is often argued that, in non-topological models (e.g. STC, BCTRAN), it is best to connect the core model in parallel with the innermost winding [14]. While it is obvious to identify which winding is the innermost one for transformers with concentric cylindrical windings, which winding is the innermost for transformers with pancake windings, such as presented in (Gonzalez-Molina *et al.*, 2004, § 5.2)? This question also arises for hybrid models, where the fictitious winding is connected to the innermost winding (Mork *et al.*, 2007a, pp. 250–251). Not to mention that the proportionality factor K in (Mork *et al.*, 2007a) to calculate the leakage inductance between the innermost winding and the core from short-circuit measurements is quite arbitrary. Furthermore, if some of the models presented in Section 1.2 are called "topological", therefore supposedly physically-based, why are there so many different transformer models for the same transformer type (e.g., three-legged transformer)?

Problem 3: There is another problem associated with the modeling of the core and its inclusion at the innermost winding, or the fictitious winding, which is the *reversibility* of the model in saturation (Zirka *et al.*, 2012; Jazebi *et al.*, 2013). In other words, with these models, the magnetizing branch is calculated to fit open-circuit measurements made on one winding and the calculated (or sometimes measured) air-core inductance, but the inductance in saturation viewed from other windings of the model will be incorrect. The final slope of the magnetizing branch can be adjusted to match measurements of the other winding, as in (Zirka *et al.*, 2012, § 8), but it will be still non-reversible so that measurements from both windings cannot be matched.

Problem 4: In the derivation of "topological" transformer models, introduced in Section 1.2, it was assumed that magnetic fluxes were contained inside predefined paths (flux tubes), and that there is no leakage of flux from the sides of the flux tubes. Since we are mostly interested in the nonlinear behavior of the core for low- and mid-frequency electromagnetic transients, what happens to the magnetic circuit when the core saturates? There is a fundamental problem with the discretization of a magnetic behavior into flux tubes, not only because ferromagnetic materials that constitute "magnetic conductors" can saturate (therefore leaking more and more flux), but also because the difference between the relative permeabilities of "magnetic conductors" versus "magnetic insulators" are in the order of 10^3–10^4, whereas the difference in

14. See for instance (Dick and Watson, 1981, § 4.3) and (Narang and Brierley, 1994, p. 1342).

conductivities between "electric conductors" versus "electric insulators" are in the order of 10^{22}–10^{28}. Not to mention that if the topological models presented in Section 1.2 were truly physically-based, then they would be related with finite element models made of a very coarse mesh. Therefore, one can ask what would be the error associated with such a coarse discretization, and if those topological models are really more sophisticated than previous models.

This problem was highlighted in (Saldaña and Calzolari, 1997):

> "It's important to note that the accuracy of the equivalent [dual] electric circuit is largely dependent on the manner in which the magnetic system is reduced to a magnetic circuit."

1.4 Objectives

The main goal of this dissertation is to develop and validate new shell-type transformer models for the simulation of low- and mid-frequency electromagnetic transients in EMT-type programs, such as EMTP-RV or EMTDC. In order to do so, another important and related objective is to provide means to calculate the new model parameters. Specific objectives are as follows:

- Derive a new analytical formula to calculate short-circuit inductances between coils and validate the results with the finite element method.
- Provide new models for single-phase and three-phase shell-type transformers, without the use of fictitious windings.
- Present methods to calculate the core parameters (magnetizing branches).
- Validate the new models with experimental measurements.
- Generalize the theory surrounding flux tubes, in order to derive in the future a more topologically-correct discretization of the transformer in 3-D.

1.5 Dissertation outline

In Chapter 2, a new analytical method is presented for the calculation of leakage inductances of a shell-type transformer in 2-D. It is compared against other analytical methods, but also to the finite element method (FEM). Furthermore, the 2-D approximation for the leakage field is validated with a 3-D finite element model for a shell-type transformer.

Chapter 3 presents new topological transformer models for single-phase and three-phase shell-type transformers, that properly takes into account leakage inductances through a "coupled" leakage model, without using any fictitious windings. The analytical method of the previous chapter is used to calculate leakage inductances from geometrical data. Moreover,

in this chapter, part of the differences between existing topological transformer models is explained through the concept of integral and divided fluxes. The new analytical method of Chapter 2, along with the coupled leakage model presented in this chapter, are validated with experimental short-circuit data.

Chapter 4 discusses about the calculation of magnetizing branches (core model) for the shell-type transformer models of the previous chapter. This new procedure allows to build a reversible model, by including leakage inductances in the calculations. For this purpose, open-circuit test reports are used.

In Chapter 5, instead of using flux tubes and current tubes to derive magnetic circuits and electric circuits, respectively, the discretization of Maxwell's equations is generalized to the case where magnetic flux and electric current can leak from the sides of the tubes. This is achieved with what is called *finite formulations* and leads to two (magnetic and electric) interlocked circuits. These developments are not only useful for the generalization of topological transformer models, which leads to more sophisticated 3-D models, but also for any electromagnetic apparatus (such as cables, machines, etc.). It also leads to the strong coupling of *finite formulations* models (such as that of the Finite Element Method) inside EMT-type programs.

Finally, the conclusions of this dissertation are presented in Chapter 6, along with recommended research topics to be further examined in upcoming work.

CHAPTER 2

ANALYTICAL CALCULATION OF LEAKAGE INDUCTANCES

One of the critical parameters in low-frequency transformer modeling is the leakage inductance. This inductance is due to leakage flux, also termed *stray flux*[1] (Del Vecchio *et al.*, 2010, p. 456), which is the flux generated by a winding that does not *link* another winding. It is defined as the difference between self and mutual fluxes (Barret, 1976, eq. 3).

Typically, leakage inductance is calculated with the classic simplified formula (Kulkarni and Khaparde, 2004, § 3.1), even though modern computers would enable to calculate leakage inductance very precisely using the finite element method (FEM) in 2-D, or even in 3-D, and taking into account the complexity of the transformer's structure. The finite element method in 2-D is used for instance in (Silvester and Konrad, 1973; Andersen, 1973). However, the goal of this work is to propose a leakage inductance calculation routine that can be easily implemented in electromagnetic transients (EMT)-type programs. Hence, because of the complexity of the finite element method, a simpler solution is needed.

Several solutions have been developed to calculate self and mutual inductances, see for instance (Grover, 2004). However, in order to calculate leakage inductances, one has to take into account the presence of the core, which changes the boundary conditions. For this, different approaches were proposed over the years. One approach is to use space harmonics, where the magnetic vector potential inside the core window, found with the method of separation of variables, is expressed as a single or a double Fourier series. Another approach is to use the method of images, where the boundaries are removed and replaced by image conductors.

This chapter is based on a previously published paper (Lambert *et al.*, 2013), with enhanced explations, corrections and additional results. The new approach proposed in that paper combines the method of images with the expression of the magnetic vector potential of a rectangular cross-section conductor in air, and its convergence is improved in this chapter.

With the analytical methods presented in this chapter, it is possible to discretize each winding into coils (fractions of the winding) or even turns. This can be useful to simulate internal winding faults (Bastard *et al.*, 1994; Palmer-Buckle *et al.*, 1999; Avendaño Ceceña, 2011) or for high-frequency modeling (Gómez and de León, 2011; Avendaño Ceceña, 2011). These analytical methods allow also for the calculation of the leakage inductances between coils in sophisticated topological models (short-circuit measurements between coils are never

1. Note that there is ambiguity in the literature about the equivalence of this terminology. It is assumed in this dissertation that both words are equivalent.

available). This is the subject of the next chapter.

In this chapter, the new method is compared against the double Fourier series method and the classical approach. These methods are used to calculate the leakage inductance between coils of two single-phase shell-type transformers and a three-phase shell-type transformer, and they are validated with the results of the finite element method. The first transformer is the 360 MVA transformer presented in (Lambert *et al.*, 2013). The second transformer is a 570 MVA transformer for which a 3-D detailed magnetic model was available, which is used to evaluate the validity of the 2-D approximation with respect to 3-D. The third transformer is a 96 MVA three-phase transformer.

It is shown in this chapter that the classical approach gives erroneous results for coils whose fringing flux is not negligible. Furthermore, the improvement made on the new method decreases the calculation time by a factor of two (compared to the version in (Lambert *et al.*, 2013)). Even then, it is demonstrated that the improved new approach is less performant than the double Fourier series, but it is more general. Finally, it is shown that the 2-D approximation is acceptable for shell-type transformers.

2.1 Definition of the problem

To measure the leakage inductance between two windings, one has to inject magnetomotive forces equal in magnitude but opposite in directions in the two windings. This way, there will be no flux linking the two windings and there will only be leakage flux. In practice, this is approximately realized when one winding of the transformer is energized while the other is short-circuited, since the exciting current (or magnetomotive force) required by the core will be very small compared to short-circuit currents (magnetomotive forces), because of the high permeability of the core. Hence, the flux inside the core will be negligible with respect to the leakage flux.

To calculate leakage inductance from geometrical information involves computation of the resulting magnetic field during short-circuit. As will be seen later in § 2.2, some assumptions regarding the distribution of magnetic field during short-circuits allow simplifying greatly this calculation. In a more general way, the magnetic field outside the core during short-circuits can be calculated using Maxwell's law (1.2) in vacuum (with the magnetostatic approximation), along with (1.5), which gives

$$\vec{\nabla} \times \vec{B} = \mu_0 \vec{J} \tag{2.1}$$

where μ_0 is the permeability of vacuum. Since the vector field $\vec{B}$ is solenoidal ($\vec{\nabla} \cdot \vec{B} = 0$), it can be expressed as the curl of another vector field $\vec{B} = \vec{\nabla} \times \vec{A}$, as explained in § 1.1.6.

Using the identity $\vec{\nabla} \times (\vec{\nabla} \times \vec{A}) = \vec{\nabla}(\vec{\nabla} \cdot \vec{A}) - \vec{\nabla}^2 \vec{A}$ and the Coulomb gauge ($\vec{\nabla} \cdot \vec{A} = 0$), the problem to solve is essentially that of Poisson's equation

$$\vec{\nabla}^2 \vec{A} = -\mu_0 \vec{J} \tag{2.2}$$

Because the windings are stranded and also because short-circuits are low-frequency transients, the current density $\vec{J}$ can be assumed uniform over the cross-section of each strand. Therefore, a simplificative assumption generally made for this type of calculation is that the coil is considered as solid (with only one equivalent turn) and its current density is uniform and calculated from the total magnetomotive force of the coil. Then, the conduction current I (and the magnetomotive force, since it is assumed that the conductor is made of a single solid turn), according to (1.10), is defined as

$$I = \iint_S \vec{J} \cdot \mathrm{d}\vec{s} = JS \tag{2.3}$$

where S is the cross-sectional area of the conducting surface which is normal to $\vec{J}$.

Furthermore, the complex geometry of the transformer complicates the calculation of the stray field, and therefore, of the leakage inductances. To simplify, it is often assumed that the problem is approximately 2-D [2], i.e. that the leakage flux along the third dimension is negligible (thus neglecting the effect of adjacent windings, tank walls, structure, etc.). In this regard, there is a distinction in the literature between the modeling of core-type and shell-type transformers, but there is no concensus. On the one hand, the modeling of core-type transformers is often done using an "open-slot" boundary, as seen in Fig. 2.1a, where one of the sides is opened and the yokes extend to infinity. See for instance (Rogowski, 1908; Rabins, 1956; Fergestad and Henriksen, 1974). On the other hand, the model used for shell-type transformers is typically that of the "closed-slot" boundary, where the windings are surrounded by iron, as illustrated in Fig. 2.1b. See for instance (Rogowski, 1908, § 3). It is mentioned in (Heiles, 1932, p. 884) that the closed-slot boundary is valid if there is a seamless transition between the core and other ferromagnetic parts of the transformer (including the tank), and that experimental results show that it is approximately true in practice. To complicate things even further, both cylindrical and Cartesian coordinates are used in the literature. However, as indicated in (Billig, 1951, p. 56), the analytical results are simpler with Cartesian coordinates, since the solution in cylindrical coordinates involves

2. As mentioned in (Rabins, 1956, p. 266): "The second important assumption is the neglect of adjacent windings and tank walls. These corrections which are usually negligible are probably best handled empirically, though some qualitative effect may be found by locating a highly permeable or highly conducting cylinder outside the windings and by determining the reactances for these cases."

Bessel functions. Sometimes, such as in (Eslamian and Vahidi, 2012; Margueron *et al.*, 2007; Doebbelin *et al.*, 2009) a combination of closed-slot and semi-infinite slab boundaries is used to represent the portions inside and outside the core window, respectively, for core-type transformers. Another approach proposed in (Wilcox *et al.*, 1988, §. 5) is to cut and stretch the closed core into an equivalent cylinder with the same length than that of the core.

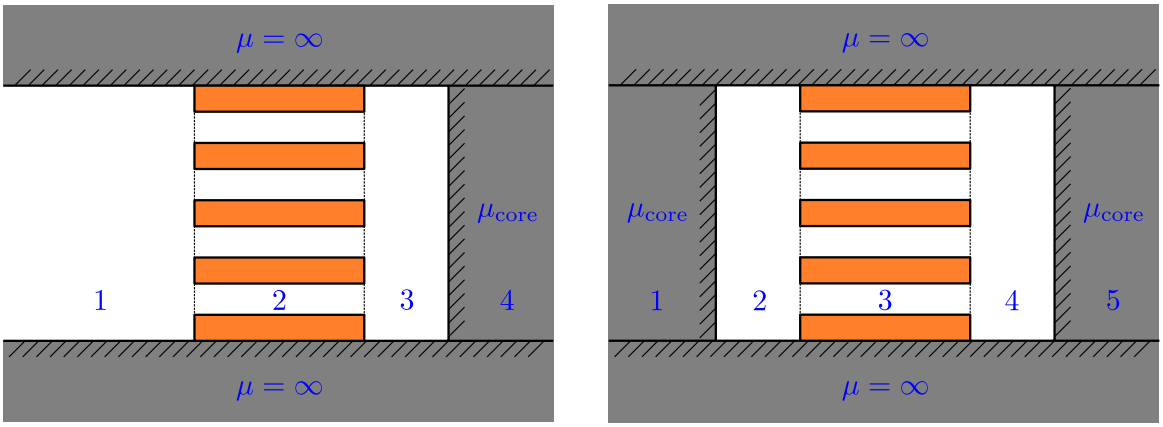

(a) Open-slot core-type transformer boundary (b) Closed-slot shell-type transformer boundary

Figure 2.1 Typical 2-D domain boundaries.

Finally, some authors consider a finite permeability for the core's legs (Rogowski, 1908; Roth, 1928a; Fergestad and Henriksen, 1974), while others assume that it is infinite (Roth, 1928b; Rabins, 1956). However, as mentioned earlier, the magnetomotive forces of two windings are approximately equal in magnitude and opposite in direction during a short-circuit in a transformer, which means that the magnetomotive force required to magnetize the core is negligible, as indicated in (Kulkarni and Khaparde, 2004, p. 92). In other words, the permeability of the core can be assumed infinite, which means that the tangential component of flux is zero and the normal component of the magnetic vector potential is also zero. Therefore, we have a homogeneous Neumann boundary condition with Poisson's equation (2.2), that is

$$\frac{\partial A_z}{\partial \vec{n}} = 0 \text{ on } B \tag{2.4}$$

where $\vec{n}$ is the normal vector of the boundary B. For this type of boundary value problem to have a solution, it is required that the compatibility condition

$$-\int_D \mu_0 \vec{J} \mathrm{d}D = 0 \tag{2.5}$$

be satisfied (Myint-U and Debnath, 2007, p. 352) [3]. In other words, the magnetomotive forces in the domain D (window) must cancel. This fact seems to have been overlooked in the demonstration of (Binns *et al.*, 1992, pp. 88–90).

With all the above considerations, the problem essentially becomes that of Fig. 2.2 for shell-type cores, where the first coil carries a positive magnetomotive force and the second coil carries a negative magnetomotive force. Hence, positive and negative superscripts are used in this chapter to denote variables and parameters of the first and second coils, respectively. In this problem, the current is directed along the z-axis and so will the Laplacian of $\vec{A}$. Subsequently, since the permeability is isotropic and uniform inside the rectangular cavity (vacuum), the magnetic vector potential will also be collinear with the z-axis. Since the two coils are represented by infinitely-long rectangular bars, a finite length needs to be considered to calculate the energy (and inductance) [4].

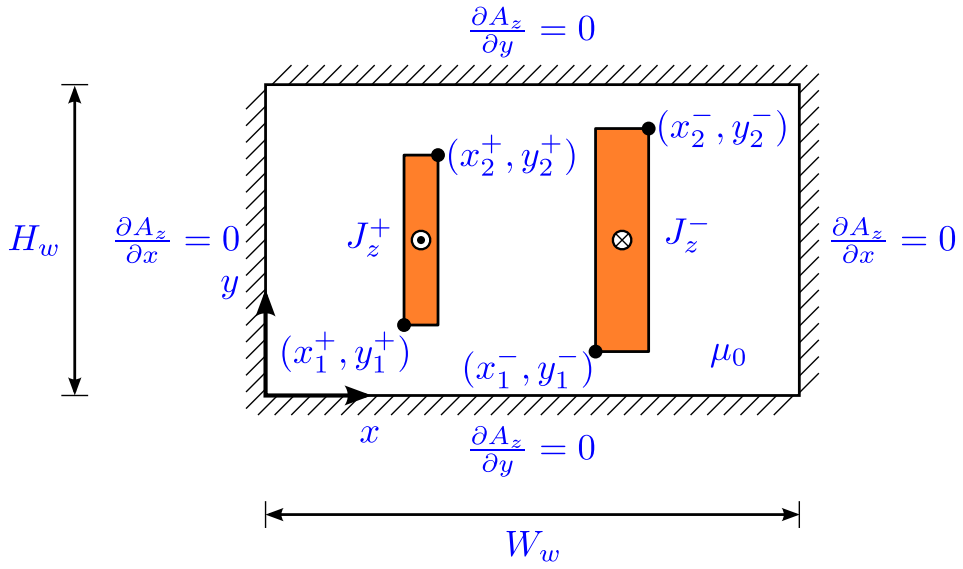

Figure 2.2 Neumann boundary value problem in 2-D to calculate the short-circuit inductance between two rectangular cross-section coils.

The magnetic energy is defined as

$$W = \frac{1}{2} \iiint_V \left(\vec{A} \cdot \vec{J} \right) \mathrm{d}V' \tag{2.6}$$

where V is the volume of the rectangular cavity. Since the current density is J_z inside the conductor and zero elsewhere, and also because $\vec{A}$ is collinear with $\vec{J}$, the magnetic energy

3. In this case, since the boundary conditions are homogeneous, the integral of the source term on the boundary (2.4) vanishes.

4. Otherwise, the energy is infinite.

becomes

$$W = \frac{J_z l_m}{2} \int_{x_1}^{x_2} \int_{y_1}^{y_2} A_z\left(x, y\right) \mathrm{d}y \, \mathrm{d}x \tag{2.7}$$

where l_m is the mean length of turn of the coil. Of course, the magnetic energy of an infinitely-long conductor is infinite; as such, it is needed to choose a representative extrusion length that approximates the energy of the real 3-D geometry. The validation of this approximation with respect to 3-D will be investigated in § 2.8.

With two coils, the total magnetic energy inside the core window is given by the sum of the energy in each coil, each given by (2.7). Using (2.3) in (2.7), the total magnetic energy becomes

$$W_{tot} = \frac{I l_m^+}{2S^+} \int_{x_1^+}^{x_2^+} \int_{y_1^+}^{y_2^+} A_z\left(x, y\right) \mathrm{d}y \, \mathrm{d}x - \frac{I l_m^-}{2S^-} \int_{x_1^-}^{x_2^-} \int_{y_1^-}^{y_2^-} A_z\left(x, y\right) \mathrm{d}y \, \mathrm{d}x \tag{2.8}$$

The short-circuit inductance between the two coils is given by

$$L_{sc} = \frac{2W_{tot}}{I^2} \tag{2.9}$$

Using (2.8) in (2.9), we obtain

$$L_{sc} = \frac{l_m^+}{IS^+} \int_{x_1^+}^{x_2^+} \int_{y_1^+}^{y_2^+} A_z\left(x, y\right) \mathrm{d}y \, \mathrm{d}x - \frac{l_m^-}{IS^-} \int_{x_1^-}^{x_2^-} \int_{y_1^-}^{y_2^-} A_z\left(x, y\right) \mathrm{d}y \, \mathrm{d}x \tag{2.10}$$

The analytical calculation of leakage inductance of the methods presented in 2.3 and 2.5 will rely upon the evaluation of the double integrals of (2.10), for which we have different expressions for the magnetic vector potential $A_z\left(x, y\right)$.

2.2 Classical approach

This first approximation for the calculation of leakage inductances was first proposed by Kapp in (Kapp, 1898) (see also (Kapp, 1908, ch. 9) and (Arnold and la Cour, 1904, ch. 3)) and is found in countless references throughout the literature [5], hence the name *classical approach*.

In order to obtain the classical formula for the leakage inductance, a few assumptions are necessary. From (Kapp, 1908, p. 177):

5. See for instance (Dept. Elect. Eng., Massachusetts Inst. Technology, 1943; Morris, 1951; Blume *et al.*, 1951; Karsai *et al.*, 1987; Slemon, 1992; Sawhney, 1997; Kulkarni and Khaparde, 2004; Del Vecchio *et al.*, 2010).

> "The ampere-turns in both coils being practically equal, the stray field of [the inner coil] will therefore be stronger than that of [the outer coil]. In order to be able to treat the problem mathematically we shall make the assumption that the two currents have a phase difference of 180° and that the ampere turns are equal. Both assumptions are very nearly correct. *We shall further assume that neither the yoke nor the other core has a material influence on the shape of the stray field, which we take to be distributed symmetrically round the axis of the coils.*"

The first two assumptions are typical for short-circuit calculations, as indicated in the previous section, and will be used in all other methods of this chapter as well. The simplifying assumption is the last one: by assuming that the magnetic field is everywhere parallel to the winding axis, the inductance can easily be calculated as the sum of the inductances of three fixed flux tubes. One tube for the volume of each winding (where the magnetomotive force $\mathscr{F}$ is linearly increasing or decreasing) and one tube for the volume of space in between (where the magnetomotive force $\mathscr{F}$ is constant), as illustrated in Fig. 2.3 for cylindrical windings.

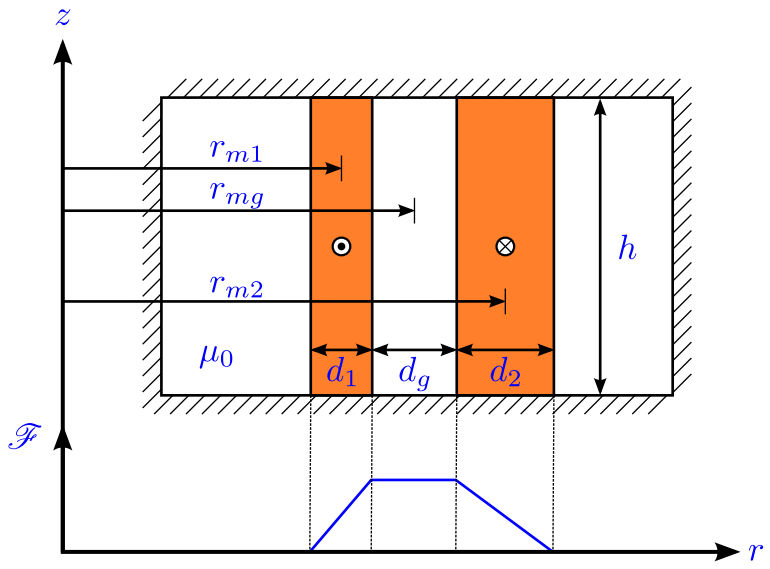

Figure 2.3 Geometry considered in the classical approach.

Using this assumption, the short-circuit inductance between windings 1 and 2 is found to be

$$L_{sc_{12}} = \frac{\mu_0 N^2}{h}\left[\frac{l_{m1}d_1}{3} + \frac{l_{m2}d_2}{3} + l_{mg}d_g\right] \tag{2.11}$$

where N is the number of turns of the winding at which this inductance is referred to (either seen from winding 1 or 2), h is the height, d_1 and d_2 are the thicknesses of windings 1 and 2, respectively, d_g is the thickness of the air gap between windings, l_{m1} and l_{m2} are the

mean length of turns of each winding, l_{mg} is the mean length of the air gap, and μ_0 is the permeability of vacuum (approximately equal to the permeability of air or mineral oil). For pancake windings, the principle is the same, but where h is the width of the pancake coils. In the case of cylindrical windings, we have $l_{m1} = 2\pi r_{m1}$, $l_{m2} = 2\pi r_{m2}$ and $l_{mg} = 2\pi r_{mg}$, where r_{m1}, r_{m2} and r_{mg} are the radial distances, as shown in Fig. 2.3.

The assumption that the magnetic flux is everywhere tangential to the winding axis means that the fringing effect of flux at winding ends (normal component of flux) is neglected. This is a good approximation if both windings have equal heights (or widths, in the case of pancake windings) and if the distances with the yokes are small, because the core's permeability is much higher than air (or oil) in the core window and flux will be almost perpendicular to the yokes. It is also assumed that current density is uniformly distributed in the windings. These assumptions are also stated in (de Kuijper, 1949, pp. 24–25). In practice, for high-voltage transformers, the magnetic flux is not everywhere tangential to the winding axis, as seen in (López-Fernández *et al.*, 2012, Fig. 6.17). The fringing effect can be seen in Fig. 2.4. The windings rectangular cross section is shown in white and the yokes are located at the top and at the bottom of each image. Flux lines are shown in black and the norm of flux density is illustrated on the shaded plot (blue being the smallest flux density and red being the highest). Fringing is small if both windings are close to the yokes (Fig. 2.4a), and where it is more important if windings are far from the yokes (Fig. 2.4b) or if the coils have unequal heights (Fig. 2.4c).

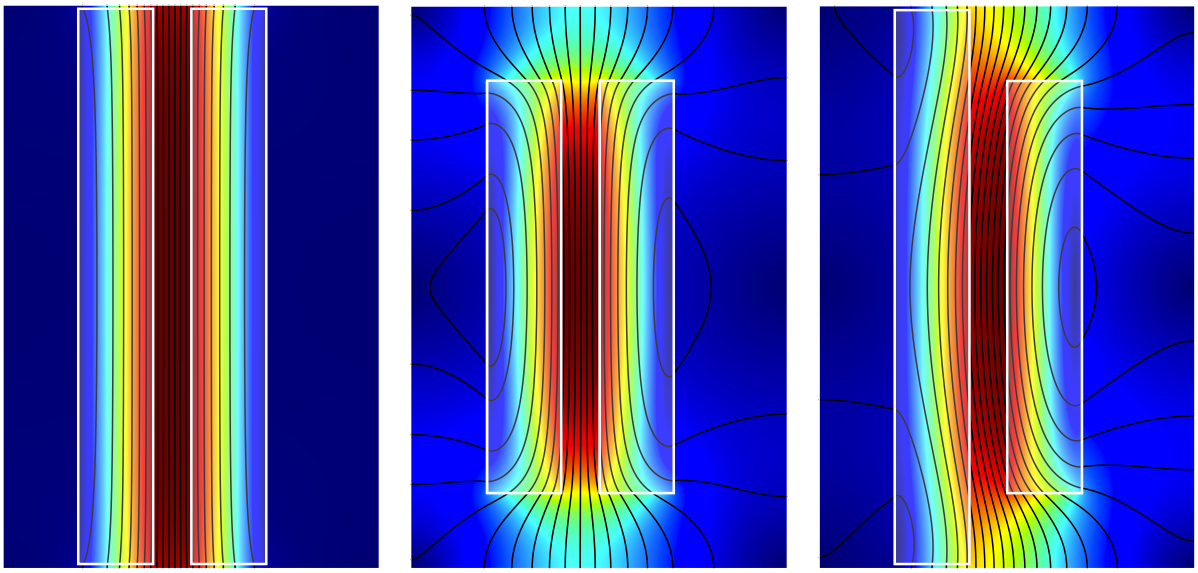

(a) Windings close to yokes (b) Windings far from yokes (c) Windings of unequal heights

Figure 2.4 Fringing flux for different winding geometries.

In the case of windings with unequal heights, on the one hand, it is proposed in (Del Vecchio *et al.*, 2010, p. 78) to use the average value of both heights $h = (h_1 + h_2)/2$. On the other hand, this average height is used as a measure of an equivalent air-gap height $h_g = (h_1 + h_2)/2$ in ATPDraw v5.7, where the three flux tubes have different heights and the short-circuit inductance becomes

$$L_{sc_{12}} = \mu_0 N^2 \left[\frac{l_{m1} d_1}{3h_1} + \frac{l_{m2} d_2}{3h_2} + \frac{l_{mg} d_g}{h_g} \right] \tag{2.12}$$

The classical approach was extended to take into account the tappered (trapezoidal) cross section of the high-voltage winding in Naderian-Jahromi *et al.* (2002), again assuming that magnetic flux is everywhere tangential to the winding axis. However, as it can be seen in Fig. 2.5, this is not the case.

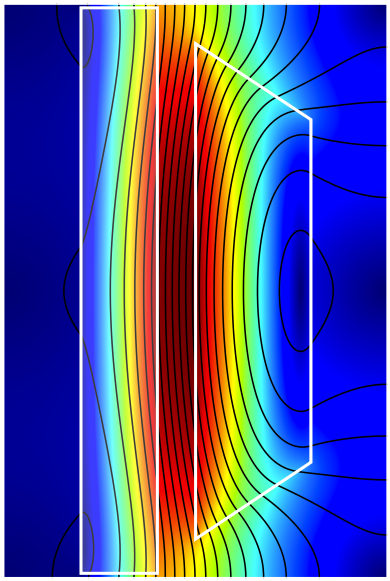

Figure 2.5 Magnetic flux during short-circuit in the presence of a trapezoidal cross-section high-voltage winding.

The effect of fringing flux over the accuracy of the classical approach (and its variants) is discussed in § 2.8.

2.3 Space harmonics

As seen in § 2.1, in order to calculate the short-circuit inductance without assuming that magnetic flux is everywhere tangential to the winding axis, the problem is essentially to solve Poisson's equation (2.2). The space harmonics methods are based on the use of Fourier series

to find a spatially periodic solution to Poisson's equation in different coordinate systems. The earliest attempt to find an analytical solution to the leakage field in transformers is given by Rogowski in his dissertation (Rogowski, 1908). An English summary of the method can be found in (Binns *et al.*, 1992, § 4.3.2). The method is also used in (Hammond, 1967, § 4) and (Robertson and Terry, 1929). He considered separately the problems of leakage in a core-type transformer and in a shell-type transformer, as shown in Fig. 2.1. In both cases, he assumed that the pancake windings had the same widths, and that the yokes extended to infinity and that their permeability was infinite. It was also assumed in both cases that the height of the wound leg located on the right was the same as the winding's height, that its permeability was finite, and that it was infinitely large. For the core-type transformer the effect of the return leg on the field distribution is neglected, while it is considered infinitely large for the shell-type transformer, with finite permeability. Dividing the problem into different regions, as illustrated in Fig. 2.1, and using the method of separation of variables, it is found that the magnetic vector potential is expressed as a single Fourier series. Note that he considered windings of equal widths, but it is not necessary if space is divided into more regions (at the expense of losing simplicity). Because of the complexity of this method, which is dependent on winding configuration and therefore difficult to generalize, it is not studied in this dissertation. Nevertheless, it is mentioned in (Eslamian and Vahidi, 2012, p. 2327) that both the single Fourier series and the double Fourier series (presented next) produce approximately the same results, within a precision of at least six digits.

2.3.1 Double Fourier series

Another solution to this elliptic partial differential equation (2.2) is given by means of a double Fourier series, as developped by Roth in a series of papers (Roth, 1927a,b, 1928b; Roth and Kouskoff, 1928; Roth, 1928a, 1932, 1936, 1938) [6]. An extension of Roth's method for conductors of any cross-section in 2-D is provided in (Pramanik, 1969) and an analog treatment using triple Fourier series is applied for 3-D (cartesian) in (Pramanik, 1975), including the effect of eddy currents. It is also used in (Boyajian, 1954) to calculate leakage reactances.

With the aid of the mathematical simplifications presented in (Roth and Kouskoff, 1928), it is shown in (Hammond, 1967) that the solution for the motor slot (or transformer with infinite yokes and no return legs, as considered by Rogowski) is equivalent to the solution obtained by Rogowski with the separation of variables, which is simply periodic [7]. For the

6. For an English summary of Roth's method, see (Langley Morris, 1940; Billig, 1951; Hammond, 1967), and for his complete bibliography, see (Bethenod, 1939).

7. By *simply* or *doubly* periodic, it is meant that the solution is spatially periodic along one or two directions, respectively.

rectangular cavity (or closed-slot, see Fig. 2.1b) problem, however, the solution is doubly periodic (assuming that the magnetomotive forces cancel out, otherwise there is no solution) and it can be demonstrated that Roth's double Fourier series for the magnetic vector potential is obtainable with the method of separation of variables, by substituting the source term with double Fourier series. This fact seems to have been overlooked in (Hammond, 1967, p. 1974) ("This accounts for the fact that Roth's method has slow convergence in comparison with the method of separation of variables"), where the separation of variables and Roth's method are presented as 2 different solutions, but in fact the separation of variables is a general method to solve partial differential equations and its results (given by Rogowski) are equivalent to Roth's solution (sometimes using mathematical simplifications, such as in (Roth and Kouskoff, 1928)). This was highlighted in the discussion in (Mullineux *et al.*, 1969). Of course, the method of separation of variables is more general in the sense that it can be applied to problems with boundary conditions different from Neumann or Dirichlet, as mentioned in (Hammond, 1967, p. 1973):

> "It follows that Roth's method cannot be applied to regions bounded by material of finite permeability or permittivity. Nor can it be applied to any physical problem in which the field has both normal and tangential components at a boundary."

Even in that case, a solution is proposed in (Roth, 1928a), where the permeability of the wound leg is considered finite, but where the permeability of the yokes and return leg are infinite. It would not be surprising if that result could be generalizable to all boundaries, through the use of the image coefficient (defined later in Section 2.4), but this is not studied here. One advantage of Roth's method over Rogowski's method is that the double Fourier series gives a single expression for the whole slot, while with single Fourier series the slot has to be divided into different regions in which the field is given by different expressions. However, the convergence is slower than with Rogowski's method, as indicated previously.

In order to explain this method adequately, the demonstration of the equations is presented next, which is not fully covered elsewhere for the closed-slot.

The general solution for the magnetic vector potential (oriented along the z-axis, as mentioned earlier) of Poisson's equation 2.2, using double Fourier series, takes the form

(Myint-U and Debnath, 2007, eq. 6.12.4)

$$A_z(x,y) = \frac{C_{0,0}}{4} + \frac{1}{2}\sum_{i=1}^{\infty}[C_{i,0}\cos m_i x + F_{i,0}\sin m_i x] + \frac{1}{2}\sum_{j=1}^{\infty}[C_{0,j}\cos n_j y + D_{0,j}\sin n_j y]$$
$$+\sum_{i=1}^{\infty}\sum_{j=1}^{\infty}[C_{i,j}\cos m_i x\cos n_j y + D_{i,j}\cos m_i x\sin n_j y$$
$$+F_{i,j}\sin m_i x\cos n_j y + G_{i,j}\sin m_i x\sin n_j y] \tag{2.13}$$

With the homogeneous Neumann boundary conditions [8]

$$\left.\frac{\partial A_z}{\partial x}\right|_{x=0} = 0 \tag{2.14}$$
$$\left.\frac{\partial A_z}{\partial x}\right|_{x=W_w} = 0 \tag{2.15}$$
$$\left.\frac{\partial A_z}{\partial y}\right|_{y=0} = 0 \tag{2.16}$$
$$\left.\frac{\partial A_z}{\partial y}\right|_{y=H_w} = 0 \tag{2.17}$$

and the partial differences of A_z with respect to x and y

$$\frac{\partial A_z}{\partial x} = -\frac{1}{2}\sum_{i=1}^{\infty}[C_{i,0}m_i\sin m_i x - F_{i,0}m_i\cos m_i x] - \sum_{i=1}^{\infty}\sum_{j=1}^{\infty}[C_{i,j}m_i\sin m_i x\cos n_j y$$
$$+D_{i,j}m_i\sin m_i x\sin n_j y - F_{i,j}m_i\cos m_i x\cos n_j y - G_{i,j}m_i\cos m_i x\sin n_j y] \tag{2.18}$$
$$\frac{\partial A_z}{\partial y} = -\frac{1}{2}\sum_{j=1}^{\infty}[C_{0,j}n_j\sin n_j y - D_{0,j}n_j\cos n_j y] - \sum_{i=1}^{\infty}\sum_{j=1}^{\infty}[C_{i,j}n_j\cos m_i x\sin n_j y$$
$$-D_{i,j}n_j\cos m_i x\cos n_j y + F_{i,j}n_j\sin m_i x\sin n_j y - G_{i,j}n_j\sin m_i x\cos n_j y] \tag{2.19}$$

It can be seen by combining (2.14) with (2.18) that $F_{i,0}$, $F_{i,j}$ and $G_{i,j}$ must be zero, and by combining (2.16) with (2.19) that $D_{0,j}$, $D_{i,j}$ and $G_{i,j}$ must be zero. Hence the magnetic vector potential for this problem is

$$A_z(x,y) = \frac{C_{0,0}}{4} + \frac{1}{2}\sum_{i=1}^{\infty}C_{i,0}\cos m_i x + \frac{1}{2}\sum_{j=1}^{\infty}C_{0,j}\cos n_j y + \sum_{i=1}^{\infty}\sum_{j=1}^{\infty}C_{i,j}\cos m_i x\cos n_j y \tag{2.20}$$

8. Again, it must be emphasized that with Neumann boundary conditions, the compatibility condition (2.5) must be satisfied (the magnetomotive forces inside the domain must cancel). Otherwise, there is no solution to this problem.

where it can be seen that the magnetic vector potential can be divided into four distinctive components $A_z = A_{0,0} + A_{i,0} + A_{0,j} + A_{i,j}$, as proposed in (Billig, 1951, p. 57) [9]. The first component $A_{0,0}$ is a constant, which can be set to zero, since the magnetic vector potential is defined up to a constant. The second component $A_{i,0}$ is called *main-field potential* in (Billig, 1951) or *axial component* in (Langley Morris, 1940), assuming of course that the winding's height (along the y-axis) is longer than the winding's width (along the x-axis), so that the main field is oriented along the y-axis. Since the induction $\vec{B}$ is given by the curl of $\vec{A}$, we have in 2-D

$$B_x = \frac{\partial A_z}{\partial y} \tag{2.21}$$

$$B_y = -\frac{\partial A_z}{\partial x} \tag{2.22}$$

Hence, the main-field component B_y is affected by a variation of A_z along x, which is why $A_{i,0}$ is the main-field component of the magnetic vector potential. The third component $A_{0,j}$ is termed the *cross-field potential* in (Billig, 1951) or *radial component* in (Langley Morris, 1940), because the cross-field component B_x is affected by a variation of A_z along y. The fourth component $A_{i,j}$ is called the *residual potential* in (Billig, 1951) and it is affected both by the variations of A_z along x and y.

By combining (2.15) with (2.18), it is necessary to have $\sin m_i W_w = 0$, for all i. This is the case if $m_i W_w$ is a multiple of π

$$m_i = \frac{i\pi}{W_w} \tag{2.23}$$

Also, by combining (2.17) with (2.19), it is necessary to have $\sin n_j H_w = 0$, for all j. This is the case if $n_j H_w$ is a multiple of π

$$n_j = \frac{j\pi}{H_w} \tag{2.24}$$

Differentiating (2.20) twice with respect to x and y, Poisson's equation becomes

$$-\frac{1}{2}\sum_{i=1}^{\infty} m_i^2 C_{i,0} \cos m_i x - \frac{1}{2}\sum_{j=1}^{\infty} n_j^2 C_{0,j} \cos n_j y - \sum_{i=1}^{\infty}\sum_{j=1}^{\infty} \left(m_i^2 + n_j^2\right) C_{i,j} \cos m_i x \cos n_j y = f(x,y) \tag{2.25}$$

9. A similar division is made in (Langley Morris, 1940, p. 486), but where the constant term is assumed to be zero.

where the source term $f(x, y)$ is given by

$$f(x,y) = \begin{cases} -\mu_0 J^+ & \text{if } x \in [x_1^+, x_2^+], y \in [y_1^+, y_2^+] \\ \mu_0 J^- & \text{if } x \in [x_1^-, x_2^-], y \in [y_1^-, y_2^-] \\ 0 & \text{elsewhere} \end{cases} \tag{2.26}$$

$$\tag{2.27}$$

The Fourier coefficients $C_{i,0}$, $C_{0,j}$ and $C_{i,j}$ of the double Fourier series can be found by multiplying $\cos m_i x \cos n_j y$ on both sides of (2.25) and integrating over the whole rectangular cavity. Using the definition of current (2.3) and remembering that the magnetomotive forces of each winding are equal and opposite, these coefficients are

$$C_{i,0} = \frac{2I\mu_0}{H_w W_w m_i^3} \left[\frac{(\sin m_i x_2^+ - \sin m_i x_1^+)(y_2^+ - y_1^+)}{S^+} - \frac{(\sin m_i x_2^- - \sin m_i x_1^-)(y_2^- - y_1^-)}{S^-} \right] \tag{2.28}$$

$$C_{0,j} = \frac{2I\mu_0}{H_w W_w n_j^3} \left[\frac{(x_2^+ - x_1^+)(\sin n_j y_2^+ - \sin n_j y_1^+)}{S^+} - \frac{(x_2^- - x_1^-)(\sin n_j y_2^- - \sin n_j y_1^-)}{S^-} \right] \tag{2.29}$$

$$C_{i,j} = \frac{4I\mu_0}{H_w W_w (m_i^2 + n_j^2) m_i n_j} \left[\frac{(\sin m_i x_2^+ - \sin m_i x_1^+)(\sin n_j y_2^+ - \sin n_j y_1^+)}{S^+} - \frac{(\sin m_i x_2^- - \sin m_i x_1^-)(\sin n_j y_2^- - \sin n_j y_1^-)}{S^-} \right] \tag{2.30}$$

At this point, it is useful to remember that $C_{i,0}$ contributes to $A_{i,0}$ (the main-field potential), $C_{0,j}$ contributes to $A_{0,j}$ (the cross-field potential), and $C_{i,j}$ contributes to $A_{i,j}$ (the residual potential). It is trivial to verify from (2.29) and (2.30) that if windings have equal heights and if it is equal to the window's height H_w, the cross-field potential coefficients $C_{0,j}$ and residual potential coefficients $C_{i,j}$ are zero, which means that flux lines are vertical [10]. This coincides with the assumptions of the classical approach and enables to calculate different correction factors, depending on the geometry, as presented in (Langley Morris, 1940).

10. The same reasoning can be applied to horizontal windings that have the same width than the window's width W_w. In that case, $C_{i,0} = 0$, $C_{i,j} = 0$, and the flux lines are horizontal.

Using (2.20) in (2.10), the short-circuit inductance becomes

$$L_{sc} = \frac{4\mu_0}{H_w W_w}\left[\frac{l_m^+}{S^+}\left(\sum_{i=1}^{\infty}\frac{2b^+g_i^+}{m_i^4}\left[\frac{b^+g_i^+}{S^+}-\frac{b^-g_i^-}{S^-}\right]+\sum_{j=1}^{\infty}\frac{2a^+g_j^+}{n_j^4}\left[\frac{a^+g_j^+}{S^+}-\frac{a^-g_j^-}{S^-}\right]\right.\right.$$
$$+\sum_{i=1}^{\infty}\sum_{j=1}^{\infty}\frac{g_i^+g_j^+}{m_i^2n_j^2(m_i^2+n_j^2)}\left[\frac{g_i^+g_j^+}{S^+}-\frac{g_i^-g_j^-}{S^-}\right]\Bigg)-\frac{l_m^-}{S^-}\Bigg(\sum_{i=1}^{\infty}\frac{2b^-g_i^-}{m_i^4}\left[\frac{b^+g_i^+}{S^+}-\frac{b^-g_i^-}{S^-}\right]$$
$$\left.\left.+\sum_{j=1}^{\infty}\frac{2a^-g_j^-}{n_j^4}\left[\frac{a^+g_j^+}{S^+}-\frac{a^-g_j^-}{S^-}\right]+\sum_{i=1}^{\infty}\sum_{j=1}^{\infty}\frac{g_i^-g_j^-}{m_i^2n_j^2(m_i^2+n_j^2)}\left[\frac{g_i^+g_j^+}{S^+}-\frac{g_i^-g_j^-}{S^-}\right]\Bigg)\right] \tag{2.31}$$

where g_i^+, g_j^+, g_i^- and g_j^- are given by

$$g_i^+ = \sin m_i x_2^+ - \sin m_i x_1^+ \tag{2.32}$$
$$g_j^+ = \sin n_j y_2^+ - \sin n_j y_1^+ \tag{2.33}$$
$$g_i^- = \sin m_i x_2^- - \sin m_i x_1^- \tag{2.34}$$
$$g_j^- = \sin n_j y_2^- - \sin n_j y_1^- \tag{2.35}$$

2.4 Method of images

The method of images was first introduced in (Thomson, 1845) as a mean for calculating the distribution of electricity on intersecting conductor planes. It was subsequently also used in the calculation of magnetic fields with the presence of iron, see for instance (Hammond, 1960; Carpenter, 1960; Lawrenson, 1962; Zisserman *et al.*, 1987; Roshen, 1990; Ishibashi and Sawado, 1990; Binns *et al.*, 1992; Okabe and Kikuchi, 1983).

The objective of the method of images is to find the same field that would result with the presence of interfaces or boundaries, but within a particular subset of the domain, by removing these interfaces or boundaries and considering image sources that mimics their behavior inside the subset domain of interest.

The simplest example is that of an infinitely-long conductor that carries a current density $\vec{J}$ in vacuum (of permeability μ_0), placed at a distance d in front of a semi-infinite slab of relative permeability μ_r, as illustrated in Fig. 2.6. To calculate the magnetic field on the right side of the boundary (where $x > 0$), the boundary can be removed by adding an image conductor at the image position $x = -d$ carrying a current density $k\vec{J}$, where k is the image coefficient. It must be emphasized here that this will correctly represent the magnetic field on the *right* of the boundary, but not on the left. In a similar fashion as in optics, where the reflected light depends on refractive indices of both materials, the image coefficient k takes the permeability of both materials into account. In the case considered here, where the

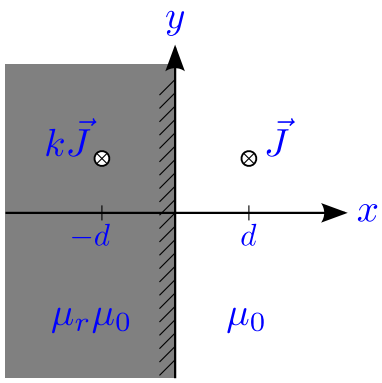

Figure 2.6 Current-carrying conductor in front of a semi-infinite slab and its image (Lambert *et al.*, 2013, Fig. 1), ©2013 IEEE.

conductor is located in vacuum, the image coefficient is given by [11]

$$k = \frac{\mu_r - 1}{\mu_r + 1} \tag{2.36}$$

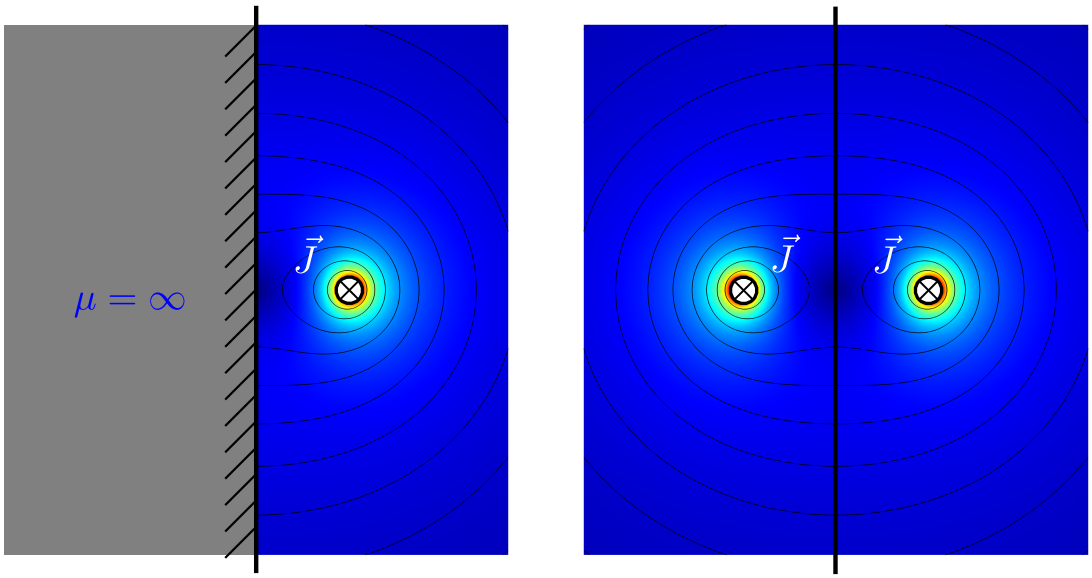

(a) With boundary (b) With the method of images

Figure 2.7 Method of images with an infinitely-permeable boundary ($k = 1$).

11. Otherwise, the image coefficient would be $k = \frac{\mu_{r2} - \mu_{r1}}{\mu_{r2} + \mu_{r1}}$, if the conductor is in Region 1 with relative permeability μ_{r1} (Binns *et al.*, 1992, p. 24).

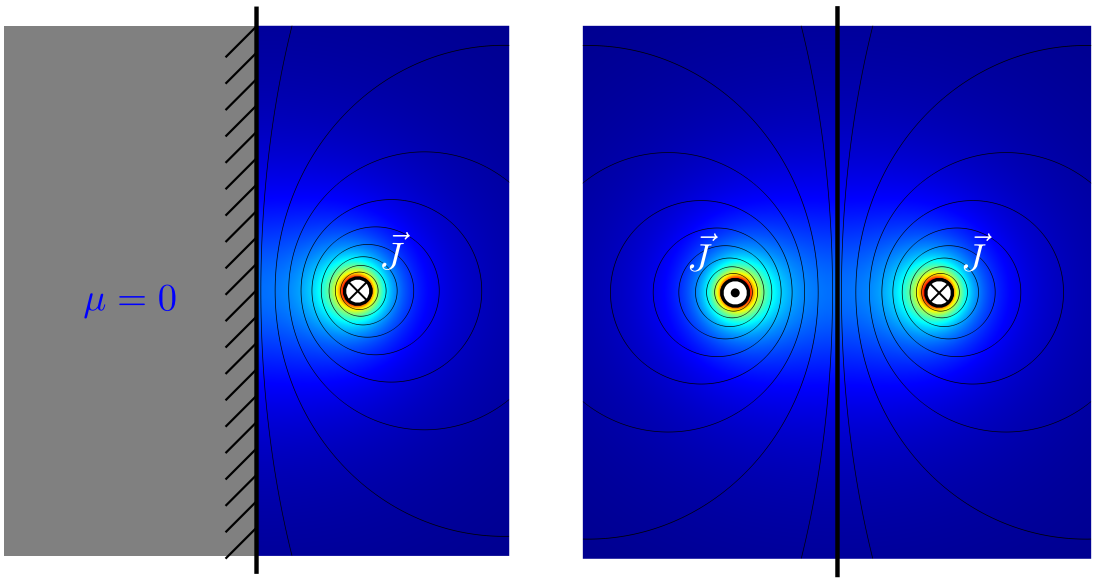

(a) With boundary (b) With the method of images

Figure 2.8 Method of images with a flux line boundary ($k = -1$).

Two extreme cases are of particular interest: when the permeability of the semi-infinite slab is infinite, $k = 1$, and when the permeability is zero, $k = -1$. These cases are illustrated in Figs. 2.7 and 2.8, respectively, where the equivalence of magnetic fields with the method of images can be observed. In the case where $k = 0$, it means that both materials have the same permeability (no magnetic boundary).

Another example of use of the method of images is that of the infinitely-long conductor carrying a current density $\vec{J}$ in vacuum, located between two semi-infinite parallel slabs of relative permeability μ_r, as shown in Fig. 2.9. In that case, as in optics with two parallel mirrors, there will be an infinite number of images (reflections), as shown in Fig. 2.9, to represent the resultant magnetic field between the parallel slabs. It can be seen that for each reflection, the current is multiplied by the image coefficient. Hence, for reflections of images, the power of k is increased for each subsequent reflection. Since the image coefficient k takes values between -1 and 1, it means that the contribution of images gradually diminishes after subsequent reflections. For the special case where $k = 1$ (infinitely permeable boundary), all the images carry the same current density $\vec{J}$, directed in the same way as the source. Otherwise, if $k = -1$, all the images carry the same current density, but the sign (direction) changes between even/odd reflections. This case is studied in (Roshen, 1990).

The method of images can also be applied to the case of an infinitely-long conductor carrying a current density $\vec{J}$ in vacuum, located inside a rectangular cavity of a material of relative permeability μ_r, as depicted in Fig. 2.10. One could conclude from the previous

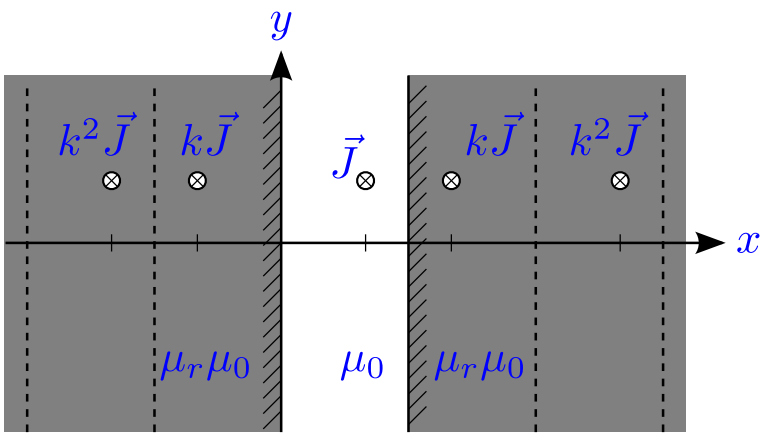

Figure 2.9 Current-carrying conductor between two parallel semi-infinite slabs and its images.

example that, in that case, there would be an infinite number of images along the x-axis and the y-axis, as seen in (Kulkarni and Khaparde, 2004, Fig. 3.6). However, the rectangular cavity is not a superposition of parallel semi-infinite slabs along the x-axis and the y-axis, since the corners also need to be taken into account. Hence, there are also images along the diagonals, as depicted in Fig. 2.10. Again, as in the previous case, if $k = 1$, all the images carry the same current density $\vec{J}$, in the same direction as the source, and if $k = -1$, the sign (direction) varies for even/odd reflections. These two extreme cases corresponds to the examples given in (Binns *et al.*, 1992, p. 29) for four intersecting boundaries.

Note that if the semi-finite slab of the first example had a finite thickness along the x-axis, in order to take into account the finite width of the yoke, there would also be an infinite number of images as described in (Zisserman *et al.*, 1987, § 3). However, since the permeability of the core is much higher than air, the currents of these internal reflections will be negligible.

The special case where $k = -1$, where the core is a flux line, is of particular interest to calculate the inductance with the presence of iron for high-frequency studies. See for instance (Gómez and de León, 2011).

In cylindrical coordinates, the method of images is more complicated, since the images must be compressed along the radial dimension $\vec{r}$, as seen in Fig. 2.11. Essentially, the space outside the core leg, where $a < r < \infty$, is mapped in the image space as $0 < r < a$. Hence, as the radius of the conductor goes to infinity, the radius of the image conductor goes to zero [12]. Furthermore, the solution for the magnetic vector potential in cylindrical coordinates gives

12. Note that this is different from (de León, 1992, eq. 3.12), where the radius of the image goes to $a/2$ if the radius of the conductor goes to infinity. This might explain why it was necessary to adjust the image current to an arbitrary value of 2.5 times the conductor current, even though it is assumed that the permeability of the core is infinite (de León, 1992, §3.1.2).

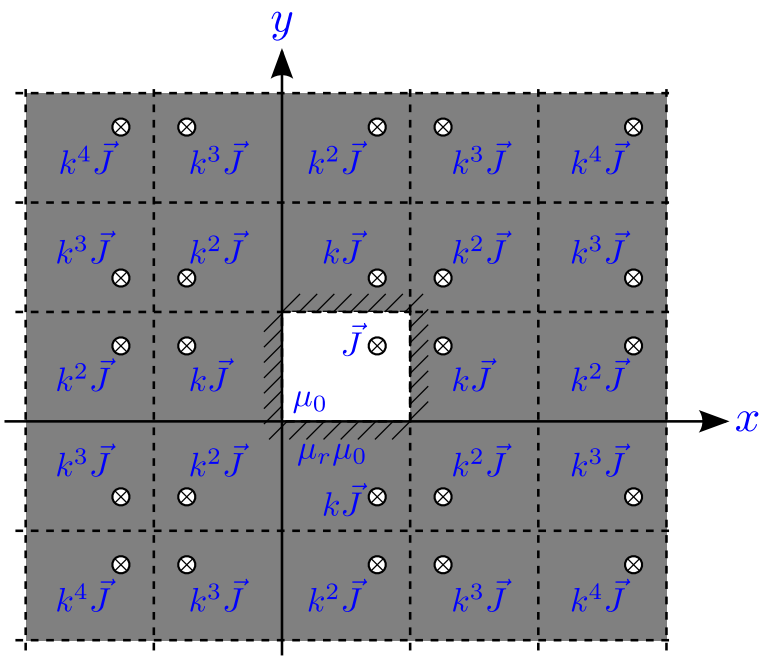

Figure 2.10 Current-carrying conductor inside a rectangular cavity and its images.

rise to Bessel functions (Smythe, 1950, §7.31), as indicated earlier. Hence, it is simpler to study this problem in 2-D Cartesian coordinates.

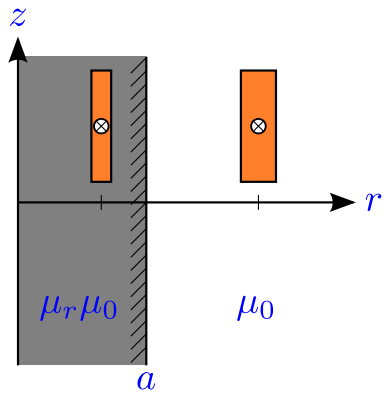

Figure 2.11 Method of images in cylindrical coordinates.

2.5 New approach

The goal is to take into account the effect of the core while calculating the short-circuit inductances. By applying the method of images to the case where two infinitely-long rectangular conductors (two coils of the transformer) are located inside a rectangular cavity (the

core window), and where the currents (magnetomotive forces) of each conductor are equal in magnitude and opposite in direction (i.e. to calculate the short-circuit inductance between pairs of coils), the problem of interest becomes that presented in Fig. 2.12 [13], for the magnetic field inside the rectangular cavity. Because the Laplacian is a linear operator, the magnetic vector potential $\vec{A}$ within the core window can be found as the superposition of the contribution of each images and conductors. Hence, the first step is to calculate the magnetic vector potential due to an infinitely-long rectangular conductor in vacuum.

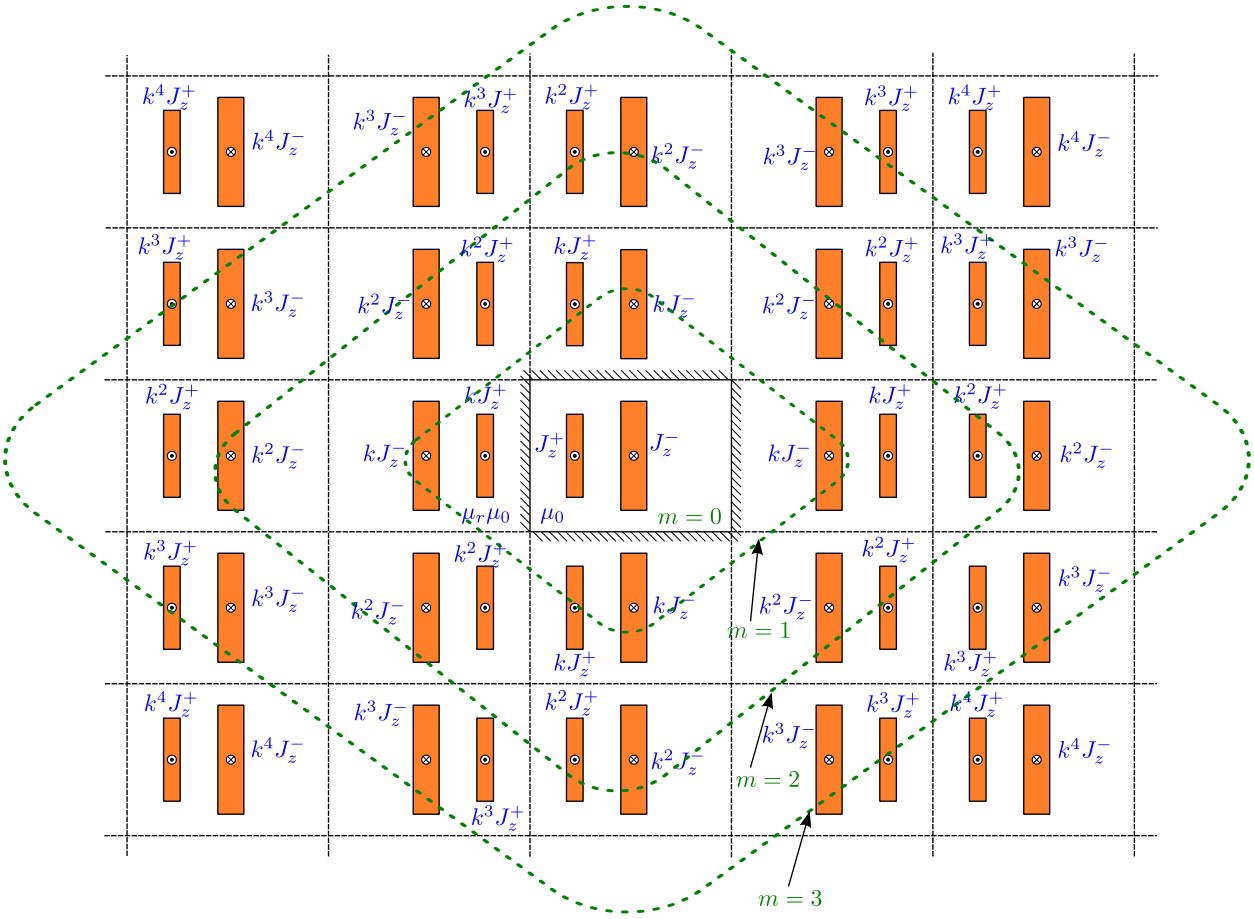

Figure 2.12 Pair of rectangular conductors inside a rectangular cavity and their doubly-periodic images.

Since each image and each conductor has its own position, it is useful to perform a change of coordinates to translate the origin in the center of each image/conductor (Sirois,

13. Note that there is an error in the powers of the image coefficient for the diagonal images in (Lambert *et al.*, 2013, Fig. 2). However, it does not change the results, since it is assumed that $k = 1$.

2002, pp. 88–90), as observed in Fig. 2.13. The local coordinates (u, v) are given by

$$u = x - \frac{x_1 + x_2}{2} \tag{2.37}$$

$$v = y - \frac{y_1 + y_2}{2} \tag{2.38}$$

where (x_1, y_1) is the position in global coordinates (x, y) of the lower-left corner and (x_2, y_2) is the position of the upper-right corner. Given that the width of the conductor is $2a$ and its height $2b$, we have

$$a = \frac{x_2 - x_1}{2} \tag{2.39}$$

$$b = \frac{y_2 - y_1}{2} \tag{2.40}$$

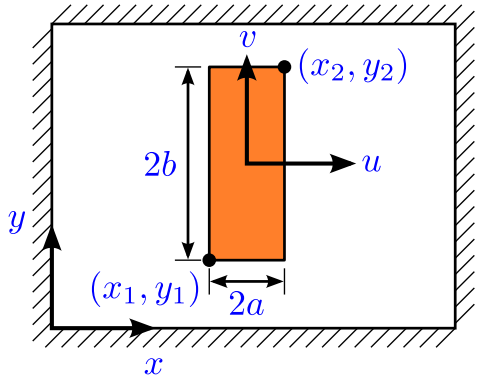

Figure 2.13 Dimensions of the rectangular conductor within the core window (Lambert *et al.*, 2013, Fig. 3), ©2013 IEEE.

The free-space Green's function $F(u, v; u', v')$ for the Laplacian in 2-D of (2.2) is given by (Myint-U and Debnath, 2007, § 11.4)

$$\begin{aligned} F(u, v; u', v') &= \frac{1}{2\pi} \log \left[\sqrt{(u - u')^2 + (v - v')^2} \right] \\ &= \frac{1}{4\pi} \log \left[(u - u')^2 + (v - v')^2 \right] \end{aligned} \tag{2.41}$$

It follows that the magnetic vector potential A_z at a point (u, v) in free-space is given by

$$A_z(u, v) = \iint F(u, v; u', v') h(u', v') \mathrm{d}v' \mathrm{d}u' \tag{2.42}$$

where u' and v' are the integration variables and $h(u', v') = -\mu_0 J_z(u', v')$ for positive im-

ages/conductor. The current density $J_z(u', v')$ is uniform and equal to J inside the rectangular image or conductor (i.e. for $-a < u < a, -b < v < b$) and is zero elsewhere. Combining (2.41) in (2.42) the magnetic vector potential is [14]

$$A_z(u,v) = -\frac{\mu_0 J}{4\pi} \int_{-a}^{a} \int_{-b}^{b} \log\left[(u-u')^2 + (v-v')^2\right] \mathrm{d}v' \mathrm{d}u' \tag{2.43}$$

Evaluating the double integral in (2.43) and combining (2.3) gives

$$A_z(u,v) = -\frac{I\mu_0}{16\pi ab} \sum_{n=1}^{9} A_n(u,v) \tag{2.44}$$

where the nine terms $A_n(u,v)$ are

$$\begin{aligned}
A_1(u,v) &= (a+u)(b+v)\log\left((a+u)^2 + (b+v)^2\right) \\
A_2(u,v) &= (a-u)(b+v)\log\left((a-u)^2 + (b+v)^2\right) \\
A_3(u,v) &= (a+u)(b-v)\log\left((a+u)^2 + (b-v)^2\right) \\
A_4(u,v) &= (a-u)(b-v)\log\left((a-u)^2 + (b-v)^2\right) \\
A_5(u,v) &= (a+u)^2\left[\arctan\left(\frac{b-v}{a+u}\right) + \arctan\left(\frac{b+v}{a+u}\right)\right] \\
A_6(u,v) &= (a-u)^2\left[\arctan\left(\frac{b-v}{a-u}\right) + \arctan\left(\frac{b+v}{a-u}\right)\right] \\
A_7(u,v) &= (b+v)^2\left[\arctan\left(\frac{a-u}{b+v}\right) + \arctan\left(\frac{a+u}{b+v}\right)\right] \\
A_8(u,v) &= (b-v)^2\left[\arctan\left(\frac{a-u}{b-v}\right) + \arctan\left(\frac{a+u}{b-v}\right)\right] \\
A_9 &= -12ab
\end{aligned}$$

This result is well known and is presented, for instance, in (Binns *et al.*, 1992, p. 71) [15]. See also (Strütt, 1926, p. 535), (Stevenson and Park, 1927, p. 130) and (Eslamian and Vahidi, 2012, p. 2327). Note that the constant term A_9 is often neglected, because it vanishes with the curl operator to calculate the induction $\vec{B} = \vec{\nabla} \times \vec{A}$. However, to calculate the energy with the magnetic vector potential, it is necessary to include this term.

As mentioned earlier, the magnetic vector potential inside the core window with two coils, each carrying equal and opposite magnetomotive forces, is given by the superposition of the

14. An alternative explanation is provided in (Doherty and Keller, 1936, pp. 228–231) for the appearance of the logarithm in 2-D for the infinitely-long wire.

15. In this reference, there is a typographic error for the first denominator in the A_7 term.

contributions of each conductor and its images. Hence, the total magnetic vector potential at coordinates (x, y) is given by

$$A_z(x,y) = \sum_{i=-M}^{M} \sum_{j=-M}^{M} k^m \left[A^+_{z,ij}(x,y) - A^-_{z,ij}(x,y) \right] \tag{2.45}$$

where the positive superscript represents the contribution of coil 1 and its images (where current is positive) and the negative superscript represents the contribution of coil 2 and its images (where current is negative, hence the substraction of each $A^-_{z,ij}$). In reality, the double sum should be infinite, since there is an infinite number of images. However, to evaluate numerically (2.45), it is needed to use a finite number of terms, or *layers* of images M, and where $m = |i| + |j|$ is the layer number [16]. For instance, the case where $i = 1$ and $j = 0$ represents the two images in the first rectangle at the right of the core window in Fig. 2.12, and the case $i = 0$ and $j = 0$ would represent the conductors themselves. Then, the position of the current image in (i, j) (or conductor), denoted by primed variables, is given by

$$x'_1 = \begin{cases} iW_w + x^+_1 & \text{if } i \text{ is even} \\ (i+1)W_w - x^+_2 & \text{if } i \text{ is odd} \end{cases} \tag{2.46}$$

$$x'_2 = \begin{cases} iW_w + x^+_2 & \text{if } i \text{ is even} \\ (i+1)W_w - x^+_1 & \text{if } i \text{ is odd} \end{cases} \tag{2.47}$$

$$y'_1 = \begin{cases} jH_w + y^+_1 & \text{if } j \text{ is even} \\ (j+1)H_w - y^+_2 & \text{if } j \text{ is odd} \end{cases} \tag{2.48}$$

$$y'_2 = \begin{cases} jH_w + y^+_2 & \text{if } j \text{ is even} \\ (j+1)H_w - y^+_1 & \text{if } j \text{ is odd} \end{cases} \tag{2.49}$$

for coil 1 and its images, where $(x^+_1, y^+_1; x^+_2, y^+_2)$ is the position of coil 1 (positive conductor) within the core window (of width W_w and height H_w, as illustrated in Fig. 2.2), as shown in

16. Note that since the powers of k in (Lambert *et al.*, 2013, Fig. 2) are incorrect, the definition of m is also different there. However, it does not change the results, since it is assumed that $k = 1$.

Fig. 2.13. For coil 2 and its images, their positions with respect to (i, j) are given by

$$x_1' = \begin{cases} iW_w + x_1^- & \text{if } i \text{ is even} \\ (i+1)W_w - x_2^- & \text{if } i \text{ is odd} \end{cases} \tag{2.50}$$

$$x_2' = \begin{cases} iW_w + x_2^- & \text{if } i \text{ is even} \\ (i+1)W_w - x_1^- & \text{if } i \text{ is odd} \end{cases} \tag{2.51}$$

$$y_1' = \begin{cases} jH_w + y_1^- & \text{if } j \text{ is even} \\ (j+1)H_w - y_2^- & \text{if } j \text{ is odd} \end{cases} \tag{2.52}$$

$$y_2' = \begin{cases} jH_w + y_2^1 & \text{if } j \text{ is even} \\ (j+1)H_w - y_1^- & \text{if } j \text{ is odd} \end{cases} \tag{2.53}$$

Let us go back to our core problem: the short-circuit inductance between two coils, calculated from (2.10). The magnetic vector potential $A_z(x, y)$ of each double integral of (2.10) is given by (2.45), where the contribution of each image (i, j) is given by (2.44), using the appropriate change of variables (2.37) and (2.38).

In order to calculate (2.10) analytically with the new approach, it is first needed to distribute the double integrals to each terms of (2.44). It can be seen that there are three different types of integrand. The double integrals of the first type are of the form

$$\begin{aligned} \Theta_1 &= \int_e^f \int_c^d s\, t \log\left[s^2 + t^2\right] \mathrm{d}t\, \mathrm{d}s \\ &= \frac{1}{8}\Big(-3(c-d)(c+d)(e-f)(e+f) \\ &+ \left(c^2+e^2\right)^2 \log\left[c^2+e^2\right] - \left(d^2+e^2\right)^2 \log\left[d^2+e^2\right] \\ &- \left(c^2+f^2\right)^2 \log\left[c^2+f^2\right] + \left(d^2+f^2\right)^2 \log\left[d^2+f^2\right]\Big) \end{aligned} \tag{2.54}$$

and corresponds to the integrals of A_1 to A_4 (with the appropriate substitutions for s, t, c,

d, e and f). The second type is of the form

$$\begin{aligned}\Theta_2 &= \int_e^f \int_c^d s^2 \arctan\left[\frac{t}{s}\right] \mathrm{d}t\, \mathrm{d}s \\ &= \frac{1}{24}\Bigg((c-d)(c+d)(e-f)(e+f) + 8ce^3 \arctan\left[\frac{c}{e}\right] \\ &- 8de^3 \arctan\left[\frac{d}{e}\right] - 8cf^3 \arctan\left[\frac{c}{f}\right] + 8df^3 \arctan\left[\frac{d}{f}\right] \\ &- \left(c^4 + 3e^4\right)\log\left[c^2+e^2\right] + \left(d^4+3e^4\right)\log\left[d^2+e^2\right] \\ &+ \left(c^4+3f^4\right)\log\left[c^2+f^2\right] - \left(d^4+3f^4\right)\log\left[d^2+f^2\right]\Bigg) \end{aligned} \tag{2.55}$$

which corresponds to the double integrals of A_5 to A_8 (note that there are two of these integrals in these terms, that is $A_5 = A_{5,1} + A_{5,2}$, where it is the integrals of $A_{5,1}$ and $A_{5,2}$ that are of the form Θ_2, again using the appropriate substitutions). The last type is the integration of the constant term A_9, which gives

$$\begin{aligned}\Theta_3^+ &= \int_{x_1^+ - \frac{x_1'+x_2'}{2}}^{x_2^+ - \frac{x_1'+x_2'}{2}} \int_{y_1^+ - \frac{y_1'+y_2'}{2}}^{y_2^+ - \frac{y_1'+y_2'}{2}} -12a'b' \,\mathrm{d}v\, \mathrm{d}u \\ &= -12a'b'(y_2^+ - y_1^+)(x_2^+ - x_1^+) = -3S'S^+ \end{aligned} \tag{2.56}$$

for the first term (integration over coil 1) of (2.10), and

$$\begin{aligned}\Theta_3^- &= \int_{x_1^- - \frac{x_1'+x_2'}{2}}^{x_2^- - \frac{x_1'+x_2'}{2}} \int_{y_1^- - \frac{y_1'+y_2'}{2}}^{y_2^- - \frac{y_1'+y_2'}{2}} -12a'b' \,\mathrm{d}v\, \mathrm{d}u \\ &= -12a'b'(y_2^- - y_1^-)(x_2^- - x_1^-) = -3S'S^- \end{aligned} \tag{2.57}$$

for the second term of (2.10).

By using the following change of variables for u and v, depending on the terms A_1 to A_8,

$$s = a \pm u \tag{2.58}$$
$$t = b \pm v \tag{2.59}$$
$$\mathrm{d}s = \pm \mathrm{d}u \tag{2.60}$$
$$\mathrm{d}t = \pm \mathrm{d}v \tag{2.61}$$

it can be seen that there are a total of eight different bounds for c, d, e and f, given by

$$h_1^+ = y_1^+ - y_1' \tag{2.62}$$
$$h_2^+ = y_2' - y_1^+ \tag{2.63}$$
$$h_3^+ = y_2^+ - y_1' \tag{2.64}$$
$$h_4^+ = y_2' - y_2^+ \tag{2.65}$$
$$h_5^+ = x_1^+ - x_1' \tag{2.66}$$
$$h_6^+ = x_2' - x_1^+ \tag{2.67}$$
$$h_7^+ = x_2^+ - x_1' \tag{2.68}$$
$$h_8^+ = x_2' - x_2^+ \tag{2.69}$$

for the positive conductor, and also eight for the negative conductor

$$h_1^- = y_1^- - y_1' \tag{2.70}$$
$$h_2^- = y_2' - y_1^- \tag{2.71}$$
$$h_3^- = y_2^- - y_1' \tag{2.72}$$
$$h_4^- = y_2' - y_2^- \tag{2.73}$$
$$h_5^- = x_1^- - x_1' \tag{2.74}$$
$$h_6^- = x_2' - x_1^- \tag{2.75}$$
$$h_7^- = x_2^- - x_1' \tag{2.76}$$
$$h_8^- = x_2' - x_2^- \tag{2.77}$$

Hence, after the change of variables for u and v given by (2.37) and (2.38), the integrals

of each term in (2.45) are of the form

$$\int_{x_1^+-\frac{x_1'+x_2'}{2}}^{x_2^+-\frac{x_1'+x_2'}{2}}\int_{y_1^+-\frac{y_1'+y_2'}{2}}^{y_2^+-\frac{y_1'+y_2'}{2}} A^+_{z,ij}(u,v)\,\mathrm{d}v\,\mathrm{d}u = -\frac{I\mu_0}{16\pi a'b'}\left(\Theta_1\Big|_{h_1^+}^{h_3^+}\Big|_{h_5^+}^{h_7^+} - \Theta_1\Big|_{h_1^+}^{h_3^+}\Big|_{h_6^+}^{h_8^+} - \Theta_1\Big|_{h_2^+}^{h_4^+}\Big|_{h_5^+}^{h_7^+} + \Theta_1\Big|_{h_2^+}^{h_4^+}\Big|_{h_6^+}^{h_8^+}\right.$$
$$- \Theta_2\Big|_{h_2^+}^{h_4^+}\Big|_{h_5^+}^{h_7^+} + \Theta_2\Big|_{h_1^+}^{h_3^+}\Big|_{h_5^+}^{h_7^+} + \Theta_2\Big|_{h_2^+}^{h_4^+}\Big|_{h_6^+}^{h_8^+} - \Theta_2\Big|_{h_1^+}^{h_3^+}\Big|_{h_6^+}^{h_8^+} - \Theta_2\Big|_{h_6^+}^{h_8^+}\Big|_{h_1^+}^{h_3^+}$$
$$\left.+\Theta_2\Big|_{h_5^+}^{h_7^+}\Big|_{h_1^+}^{h_3^+} + \Theta_2\Big|_{h_6^+}^{h_8^+}\Big|_{h_2^+}^{h_4^+} - \Theta_2\Big|_{h_5^+}^{h_7^+}\Big|_{h_2^+}^{h_4^+} + \Theta_3^+\right) \tag{2.78}$$

where the bounds of the innermost integral are replaced by the bounds of the left evaluation bars and the bounds of the outermost integral are replaced by the bounds of the right evaluation bars.

As seen in (2.10), the energy is evaluated over the two conductors (positive and negative), and where the magnetic vector potential is given by (2.45), itself divided from contributions from images of coil 1 (positive) and from images of coil 2 (negative). Hence, there are four different contributions (integrals) to consider: the contribution of the positive image on the magnetic vector potential of the positive conductor, the contribution of the positive image on the magnetic vector potential of the negative conductor, the contribution of the negative image on the magnetic vector potential of the positive conductor and the contribution of the negative image on the magnetic vector potential of the negative conductor. In other words, (2.10) is given by

$$\begin{aligned} L_{sc} = \frac{l_m^+}{IS^+} \sum_{i=-M}^{M} \sum_{j=-M}^{M} k^m \Bigg(& \int_{x_1^+ - \frac{x_1'+x_2'}{2}}^{x_2^+ - \frac{x_1'+x_2'}{2}} \int_{y_1^+ - \frac{y_1'+y_2'}{2}}^{y_2^+ - \frac{y_1'+y_2'}{2}} A_{z,ij}^+ (u,v)\, \mathrm{d}v\, \mathrm{d}u \\ & - \int_{x_1^+ - \frac{x_1'+x_2'}{2}}^{x_2^+ - \frac{x_1'+x_2'}{2}} \int_{y_1^+ - \frac{y_1'+y_2'}{2}}^{y_2^+ - \frac{y_1'+y_2'}{2}} A_{z,ij}^- (u,v)\, \mathrm{d}v\, \mathrm{d}u \Bigg) \\ & - \frac{l_m^-}{IS^-} \sum_{i=-M}^{M} \sum_{j=-M}^{M} k^m \Bigg(\int_{x_1^- - \frac{x_1'+x_2'}{2}}^{x_2^- - \frac{x_1'+x_2'}{2}} \int_{y_1^- - \frac{y_1'+y_2'}{2}}^{y_2^- - \frac{y_1'+y_2'}{2}} A_{z,ij}^+ (u,v)\, \mathrm{d}v\, \mathrm{d}u \\ & - \int_{x_1^- - \frac{x_1'+x_2'}{2}}^{x_2^- - \frac{x_1'+x_2'}{2}} \int_{y_1^- - \frac{y_1'+y_2'}{2}}^{y_2^- - \frac{y_1'+y_2'}{2}} A_{z,ij}^- (u,v)\, \mathrm{d}v\, \mathrm{d}u \Bigg) \end{aligned} \tag{2.79}$$

Finally, evaluating the three other contributions similarly to (2.78), the analytical result for the short-circuit inductance is given by

$$
\begin{aligned}
L_{sc} = \frac{\mu_0 l_m^+}{4\pi S^+} \sum_{i=-M}^{M} \sum_{j=-M}^{M} k^m \Bigg[-\frac{1}{S^+} \Bigg(& \Theta_1 \begin{vmatrix} h_3^+ & h_7^+ \\ h_1^+ & h_5^+ \end{vmatrix} - \Theta_1 \begin{vmatrix} h_3^+ & h_8^+ \\ h_1^+ & h_6^+ \end{vmatrix} - \Theta_1 \begin{vmatrix} h_4^+ & h_7^+ \\ h_2^+ & h_5^+ \end{vmatrix} + \Theta_1 \begin{vmatrix} h_4^+ & h_8^+ \\ h_2^+ & h_6^+ \end{vmatrix} - \Theta_2 \begin{vmatrix} h_4^+ & h_7^+ \\ h_2^+ & h_5^+ \end{vmatrix} \\
& + \Theta_2 \begin{vmatrix} h_3^+ & h_7^+ \\ h_1^+ & h_5^+ \end{vmatrix} + \Theta_2 \begin{vmatrix} h_4^+ & h_8^+ \\ h_2^+ & h_6^+ \end{vmatrix} - \Theta_2 \begin{vmatrix} h_3^+ & h_8^+ \\ h_1^+ & h_6^+ \end{vmatrix} - \Theta_2 \begin{vmatrix} h_8^+ & h_3^+ \\ h_6^+ & h_1^+ \end{vmatrix} + \Theta_2 \begin{vmatrix} h_7^+ & h_3^+ \\ h_5^+ & h_1^+ \end{vmatrix} \\
& + \Theta_2 \begin{vmatrix} h_8^+ & h_4^+ \\ h_6^+ & h_2^+ \end{vmatrix} - \Theta_2 \begin{vmatrix} h_7^+ & h_4^+ \\ h_5^+ & h_2^+ \end{vmatrix} - 3(S^+)^2 \Bigg) \\
& + \frac{1}{S^-} \Bigg(\Theta_1 \begin{vmatrix} h_3^+ & h_7^+ \\ h_1^+ & h_5^+ \end{vmatrix} - \Theta_1 \begin{vmatrix} h_3^+ & h_8^+ \\ h_1^+ & h_6^+ \end{vmatrix} - \Theta_1 \begin{vmatrix} h_4^+ & h_7^+ \\ h_2^+ & h_5^+ \end{vmatrix} + \Theta_1 \begin{vmatrix} h_4^+ & h_8^+ \\ h_2^+ & h_6^+ \end{vmatrix} - \Theta_2 \begin{vmatrix} h_4^+ & h_7^+ \\ h_2^+ & h_5^+ \end{vmatrix} + \Theta_2 \begin{vmatrix} h_3^+ & h_7^+ \\ h_1^+ & h_5^+ \end{vmatrix} \\
& + \Theta_2 \begin{vmatrix} h_4^+ & h_8^+ \\ h_2^+ & h_6^+ \end{vmatrix} - \Theta_2 \begin{vmatrix} h_3^+ & h_8^+ \\ h_1^+ & h_6^+ \end{vmatrix} - \Theta_2 \begin{vmatrix} h_8^+ & h_3^+ \\ h_6^+ & h_1^+ \end{vmatrix} + \Theta_2 \begin{vmatrix} h_7^+ & h_3^+ \\ h_5^+ & h_1^+ \end{vmatrix} + \Theta_2 \begin{vmatrix} h_8^+ & h_4^+ \\ h_6^+ & h_2^+ \end{vmatrix} - \Theta_2 \begin{vmatrix} h_7^+ & h_4^+ \\ h_5^+ & h_2^+ \end{vmatrix} - 3S^- S^+ \Bigg) \Bigg] \\
- \frac{\mu_0 l_m^-}{4\pi S^-} \sum_{i=-M}^{M} \sum_{j=-M}^{M} k^m \Bigg[-\frac{1}{S^+} \Bigg(& \Theta_1 \begin{vmatrix} h_3^- & h_7^- \\ h_1^- & h_5^- \end{vmatrix} - \Theta_1 \begin{vmatrix} h_3^- & h_8^- \\ h_1^- & h_6^- \end{vmatrix} - \Theta_1 \begin{vmatrix} h_4^- & h_7^- \\ h_2^- & h_5^- \end{vmatrix} + \Theta_1 \begin{vmatrix} h_4^- & h_8^- \\ h_2^- & h_6^- \end{vmatrix} - \Theta_2 \begin{vmatrix} h_4^- & h_7^- \\ h_2^- & h_5^- \end{vmatrix} \\
& + \Theta_2 \begin{vmatrix} h_3^- & h_7^- \\ h_1^- & h_5^- \end{vmatrix} + \Theta_2 \begin{vmatrix} h_4^- & h_8^- \\ h_2^- & h_6^- \end{vmatrix} - \Theta_2 \begin{vmatrix} h_3^- & h_8^- \\ h_1^- & h_6^- \end{vmatrix} - \Theta_2 \begin{vmatrix} h_8^- & h_3^- \\ h_6^- & h_1^- \end{vmatrix} + \Theta_2 \begin{vmatrix} h_7^- & h_3^- \\ h_5^- & h_1^- \end{vmatrix} \\
& + \Theta_2 \begin{vmatrix} h_8^- & h_4^- \\ h_6^- & h_2^- \end{vmatrix} - \Theta_2 \begin{vmatrix} h_7^- & h_4^- \\ h_5^- & h_2^- \end{vmatrix} - 3S^+ S^- \Bigg) \\
& + \frac{1}{S^-} \Bigg(\Theta_1 \begin{vmatrix} h_3^- & h_7^- \\ h_1^- & h_5^- \end{vmatrix} - \Theta_1 \begin{vmatrix} h_3^- & h_8^- \\ h_1^- & h_6^- \end{vmatrix} - \Theta_1 \begin{vmatrix} h_4^- & h_7^- \\ h_2^- & h_5^- \end{vmatrix} + \Theta_1 \begin{vmatrix} h_4^- & h_8^- \\ h_2^- & h_6^- \end{vmatrix} - \Theta_2 \begin{vmatrix} h_4^- & h_7^- \\ h_2^- & h_5^- \end{vmatrix} + \Theta_2 \begin{vmatrix} h_3^- & h_7^- \\ h_1^- & h_5^- \end{vmatrix} \\
& + \Theta_2 \begin{vmatrix} h_4^- & h_8^- \\ h_2^- & h_6^- \end{vmatrix} - \Theta_2 \begin{vmatrix} h_3^- & h_8^- \\ h_1^- & h_6^- \end{vmatrix} - \Theta_2 \begin{vmatrix} h_8^- & h_3^- \\ h_6^- & h_1^- \end{vmatrix} + \Theta_2 \begin{vmatrix} h_7^- & h_3^- \\ h_5^- & h_1^- \end{vmatrix} + \Theta_2 \begin{vmatrix} h_8^- & h_4^- \\ h_6^- & h_2^- \end{vmatrix} - \Theta_2 \begin{vmatrix} h_7^- & h_4^- \\ h_5^- & h_2^- \end{vmatrix} - 3(S^-)^2 \Bigg) \Bigg]
\end{aligned}
\tag{2.80}
$$

where the position of each image $(x_1', y_1'; x_2', y_2')$ as a function of (i, j) is given by (2.46)–(2.53).

It was found that by reorganizing the terms of the double sums in (2.80), a better convergence is obtained. Since the influence of images decreases with distance, it is better to start with the biggest contributions first, the conductors themselves, and then add the contributions of images in a decreasing fashion. This was not the case with the double sums from $-M$ to M. Instead, we can make a change of variables for i and j into "circular" variables m (layer of image or radius) and θ (angle), using *taxicab trigonometry* (Akça and Kaya, 1997).

The change of variables is given by

$$i = m\cos_T(\theta) \tag{2.81}$$

$$j = m\sin_T(\theta) \tag{2.82}$$

where $\sin_T$ and $\cos_T$ are the taxicab sine and cosine, respectively, defined as (Akça and Kaya, 1997)

$$\sin_T(\theta) = \begin{cases} \frac{\theta}{2} & \text{if } \theta \in [0,2] \\ 2 - \frac{\theta}{2} & \text{if } \theta \in [2,6] \\ -4 + \frac{\theta}{2} & \text{if } \theta \in [6,8] \end{cases} \tag{2.83}$$

$$\cos_T(\theta) = \begin{cases} 1 - \frac{\theta}{2} & \text{if } \theta \in [0,4] \\ -3 + \frac{\theta}{2} & \text{if } \theta \in [4,8] \end{cases} \tag{2.84}$$

The double sums are now defined for the variables $m = 1, 2, \cdots, M$ and $\theta = \frac{2}{m}, \frac{4}{m}, \cdots, 8$. Note that for $m = 0$ (the conductors themselves), the angle is undefined. Hence, this case is added first, before the double sums of (2.80). The effect of this change of variables is studied in § 2.7.

2.6 Application examples and validation

In order to validate the new method proposed in the previous section, this approach is used to calculate the leakage inductances between coils of three real shell-type transformers, and the results are compared against other methods presented in this chapter. The first transformer is a 360 MVA, $400/\sqrt{3}$ kV - 24 kV, 50 Hz, shell-type single-phase two-winding transformer with pancake coils. The core and the coils are presented in Fig. 2.14, where the cross-section of the transformer's window is illustrated in white. The 2-D problem is essentially that shown in Fig. 2.15. It can be seen that the two windings (low voltage and high voltage) are divided into 44 pancake coils, numbered from left to right. The high-voltage (HV) winding is represented in tones of red and the low-voltage (LV) winding is shown in tones of blue. Note that because the 2-D methods presented in this chapter are limited to rectangular cross-section conductors, it is not possible to simplify the coils into eight (solid) groups, because of the tapered profile of the high-voltage winding. Additionally, it would be possible to further divide each coil into individual (rectangular) turns, but this is not studied in this dissertation.

The second transformer is a 570 MVA, $405/\sqrt{3}$ kV - 20 kV, 50 Hz, shell-type single-phase two-winding transformer with a similar construction to the previous transformer (44 pancake

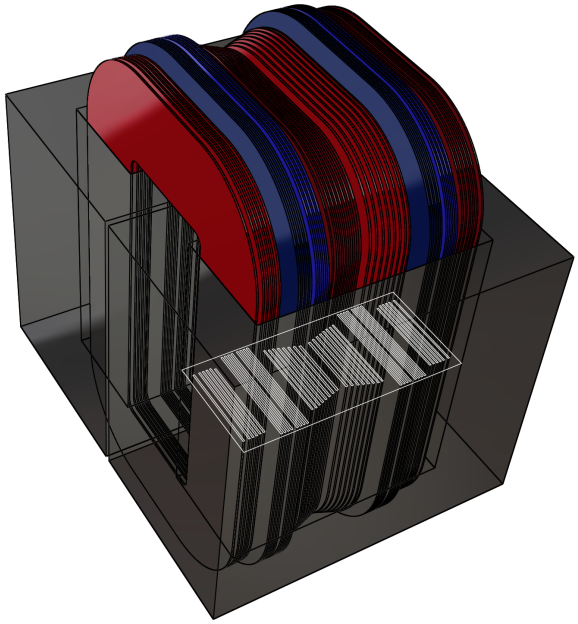

Figure 2.14 The 360 MVA shell-type single-phase two-winding transformer (Lambert *et al.*, 2013, Fig. 4), ©2013 IEEE.

coils). However, geometrical data about the tank, the magnetic shunts and the beams, was available for this transformer. Hence, it is used to validate the 2-D approximation with respect to a 3-D model closer to reality (from a magnetostatic point of view). This 3-D model is illustrated in Fig. 2.16, where only half of the transformer is modeled [17], because the other half is symmetrical. The tank is pictured in light grey, the core in dark grey, the magnetic shunts in yellow, the beams in green, the low-voltage coils in blue and the high-voltage coils in red. The left sides of the tank are hidden for clarity reasons.

The third transformer is a 96 MVA, 400 kV - 3 x 6.8 kV, 50 Hz, shell-type three-phase four-winding transformer. The four windings are divided into 26 pancake coils, numbered from left to right, as shown in Fig. 2.17. The high-voltage coils are illustrated in red, while the low-voltage coils of the three low-voltage windings are shown in blue.

Since the magnetic energy is mostly confined in air (or oil) between the short-circuited coils, it is usually assumed that the magnetomotive forces of each coil cancel one another (Kulkarni and Khaparde, 2004, p. 92), as indicated earlier. In other words, it means that the permeability of the core is considered infinite. This assumption is used for all 2-D calculations, in order to compare the different methods. The other typical assumption that was mentioned earlier is that the coils have only one (solid) turn, where the current density is distributed

17. To calculate the short-circuit inductance with $L_{sc} = 2W/I^2$, the energy W is twice the value calculated with this 3-D model.

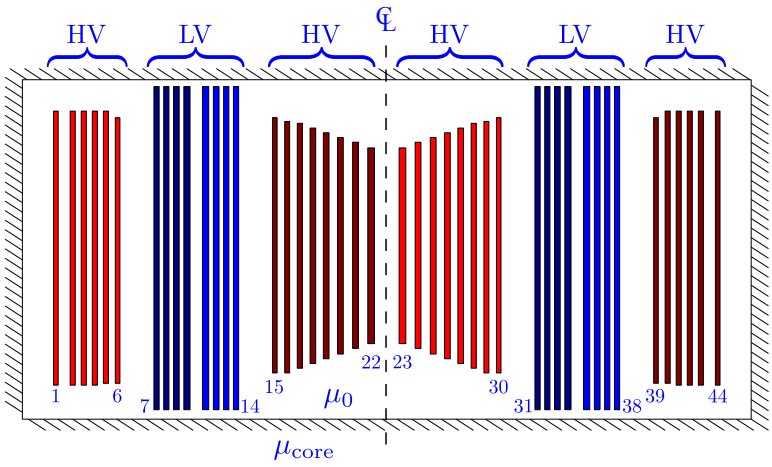

Figure 2.15 The 360 MVA transformer's window with pancake coils numbered from 1 to 44 (Lambert *et al.*, 2013, Fig. 5), ©2013 IEEE.

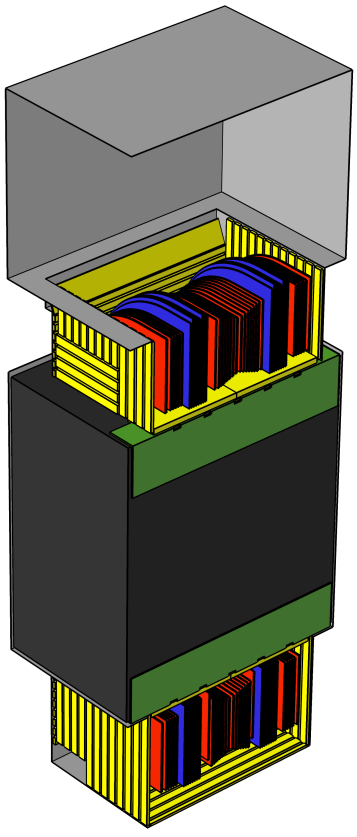

Figure 2.16 The 570 MVA shell-type single-phase two-winding transformer.

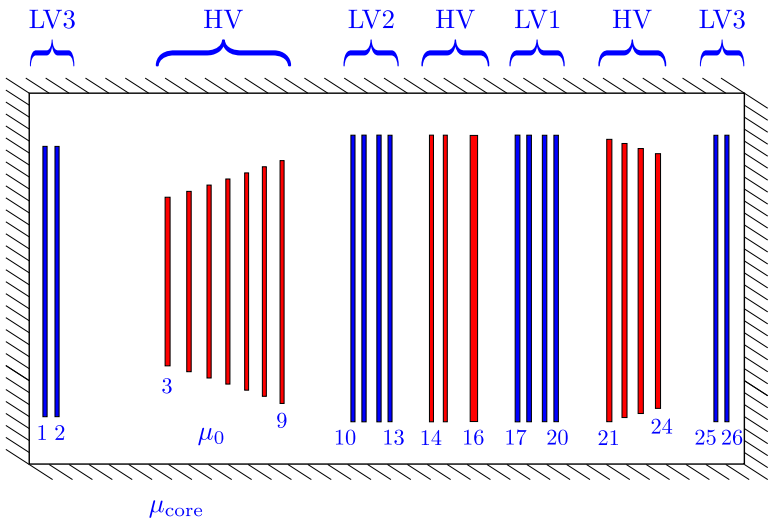

Figure 2.17 The 96 MVA transformer's window with pancake coils numbered from 1 to 26.

uniformly. In other words, the flux linkage is equal to the flux. To get the correct short-circuit inductances, one has to take into account the number of turns of each coil. This depends on the transformer model and is discussed in the next chapter.

The analytical methods presented in this chapter were simulated using MATLAB R2010a and the finite element models (in 2-D and 3-D) were computed with COMSOL 4.2a and 4.3, respectively. The calculations were made on a 2.4 GHz Intel Core i7 2760QM processor and 8 GB of RAM.

For the two single-phase transformers, the coils are distributed symmetrically within the core's window, as shown in Fig. 2.15. Hence, the short-circuit inductances will also be symmetrical. For instance, the short-circuit inductance $L_{sc}(1, 43)$ between coils 1 and 43 will be the same as the short-circuit inductance $L_{sc}(2, 44)$ between coils 2 and 44. As such, we can take advantage of this symmetry and need to calculate only a quarter of the short-circuit inductance matrix. For these transformers, the number of different short-circuit pairs is $N(N-1)/2 = 946$ (where $N = 44$ coils), but only 484 needs to be calculated. For the three-phase transformer, all short-circuit pairs ($N(N-1)/2 = 325$) need to be evaluated, since the distribution of coils within the window is not symmetrical, as seen in Fig. 2.17.

By computing the short-circuit inductance between each pair of coils, it is possible to construct the short-circuit inductance matrix as

$$[L_{sc}]_{N\times N} = \begin{bmatrix} 0 & L_{sc_{12}} & \cdots & L_{sc_{1N}} \\ L_{sc_{21}} & 0 & \cdots & L_{sc_{2N}} \\ \vdots & \vdots & \ddots & \vdots \\ L_{sc_{N1}} & L_{sc_{N2}} & \ldots & 0 \end{bmatrix} \tag{2.85}$$

where N is the number of coils. It can be seen that the diagonal of this matrix is zero, since the short-circuit inductance of a coil with itself is zero. This matrix is also symmetric, because the short-circuit inductance between coil a and b, $L_{sc}(a, b)$, is the same as the short-circuit inductance between coil b and a, $L_{sc}(b, a)$.

The short-circuit inductance matrix can be used afterwards to build the indefinite inductance matrix (Chua *et al.*, 1987, ch. 13, § 4.2), as presented in Brandwajn *et al.* (1982) (BCTRAN). This topic is studied in the next chapter.

2.7 Results

To validate the results obtained with the analytical methods presented in this chapter, the results are compared to the 2-D FEM, where the number of elements is taken as high as possible, in order for the approximation error to be very small.

2.7.1 Results for the 360 MVA transformer

First, let us examine the convergence for the calculation of the short-circuit inductance between coils 1 and 44 $L_{sc}(1, 44)$ of the 360 MVA transformer with the 2-D FEM, as a function of the number of degrees of freedom. The initial coarse mesh is shown in Fig. 2.18, with linear triangular elements, and it is successively refined to verify the calculated inductance value and the calculation time. The result is illustrated in Fig. 2.19, where the blue curve (square marks) shows the short-circuit inductance value as a function of the number of degrees of freedom, and the red graph (circle marks) corresponds to the calculation time with respect to the number of degrees of freedom. It can be seen that at around 20,000 degrees of freedom (or even at 10,000), the difference in the result becomes quite small for this particular case. However, to make sure it is also the case for all short-circuit pairs, and also because the calculation time is not much of a burden (even for extremely small elements), the highest number of degrees of freedom is used in subsequent calculations. Another reason to use such a high number of degrees of freedom is that the results of other methods presented in this chapter will be compared to the values calculated with the 2-D FEM, taken as the reference.

Using the previous short-circuit inductance value as a reference, the convergence of the new approach (2.80) as a function of the number of layers of images is illustrated in blue in Fig. 2.20 for the calculation of the short-circuit inductance between coils 1 and 44 of the 360 MVA transformer. The number of layers of images M is gradually increased from 0 to 14. The relative error is expressed in percentage.

As mentioned earlier, the convergence of (2.80) is improved by reorganizing the terms of the sums using taxicab trigonometry. The results of the substitutions (2.81) and (2.82) is

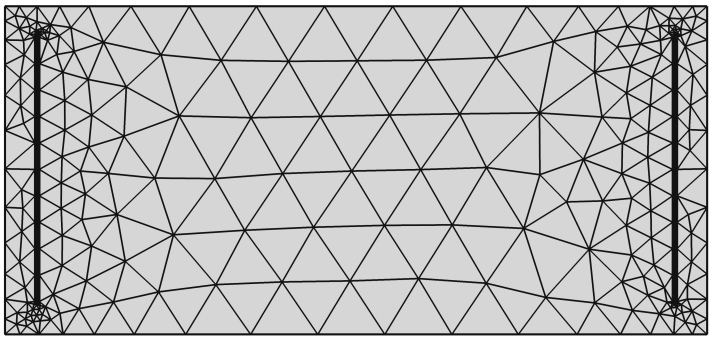

Figure 2.18 Coarse mesh for the calculation of $L_{sc}(1, 44)$ for the 360 MVA transformer with the 2-D FEM.

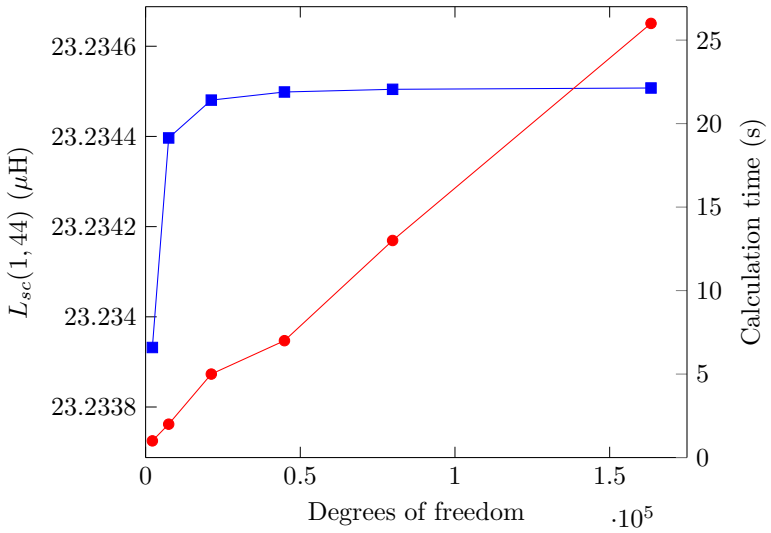

Figure 2.19 Convergence of the short-circuit inductance value with the 2-D FEM with mesh refinement.

shown in Fig. 2.20, in red.

Of course, increasing the number of layers of images will increase the computational time of the new method. For the calculation of the 484 short-circuit inductances of the 360 MVA transformer (as mentioned in the previous section, only a quarter of the matrix needs to be calculated, because of symmetry), the performance of the new method as a function of M is shown in Table 2.1. In comparison, the calculation of the 484 inductances with the 2-D FEM took about 4 hours, but again remembering that the number of degrees of freedom is not optimal.

The next step is to evaluate the convergence of Roth's method using double Fourier series. In this case, it is the number of space harmonics that is increased from 0 to 14. The result

Table 2.1 Performance comparison to calculate the 484 inductances

Method	**Total time [s]**
Method of images, 1 layer	1.6
Method of images, 3 layers	8.8
Method of images, 4 layers	14.5
Method of images, 14 layers	151.1
Method of images with substitutions, 1 layer	0.9
Method of images with substitutions, 3 layers	4.5
Method of images with substitutions, 4 layers	7.4
Method of images with substitutions, 14 layers	76.1
Roth's method, 1 harmonic	0.004
Roth's method, 3 harmonics	0.005
Roth's method, 4 harmonics	0.007
Roth's method, 14 harmonics	0.04
Roth's method, 110 harmonics	2.3
Classical approach	0.002
FEM 2-D ($\approx$ 165000 DoF)	$\approx$ 4 [h]

is depicted in Fig. 2.21, again for the calculation of $L_{sc}(1, 44)$ of the 360 MVA transformer. The performance of Roth's method is shown in Table 2.1.

It can be seen that at $M = 4$, the relative error and computational time of the new method are small. Hence, let us examine the relative error of each term of the short-circuit inductance matrix of the 360 MVA transformer, calculated with the new approach for 4 layers of images. The results are shown in Figs. 2.22 and 2.23.

For Roth's method, since the computational time is smaller, the number of space harmonics is increased to 110 (to achieve a similar error). The relative error of each term of the short-circuit inductance matrix of the 360 MVA transformer is illustrated in Fig. 2.24.

For the classical approach, since the coils have unequal heights, as explained earlier, one has to either use the average height of the coils for h in (2.11) or to use (2.12). For the studied transformers, because the thicknesses of the coils (d_1 and d_2) are small with respect to the thickness of the gap between them (d_g), the results of both approximations are very close. Hence, only the results of (2.12) are shown in Fig. 2.25 for the relative error of the terms in the short-circuit inductance matrix for the 360 MVA transformer. The computational time of this method is of course very small. These results will be discussed in § 2.8.

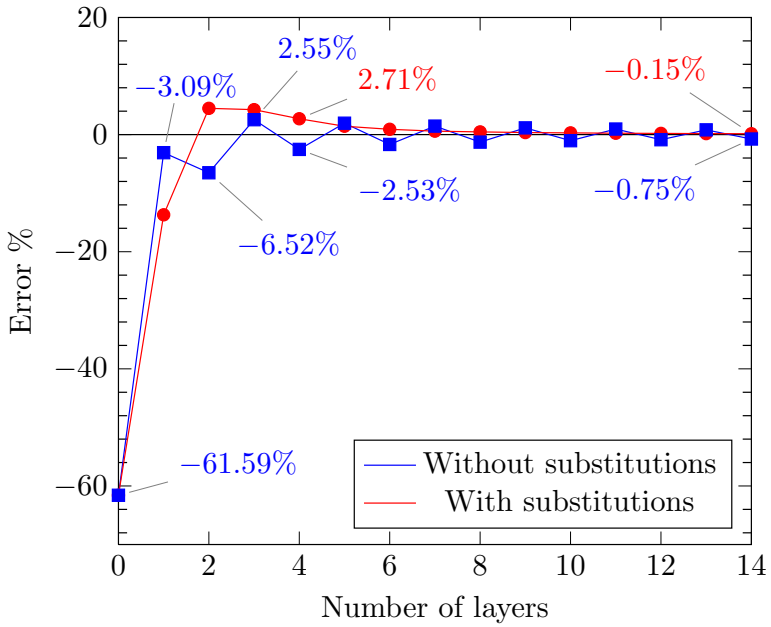

Figure 2.20 Relative error between the short-circuit inductance $L_{sc}(1, 44)$ of the 360 MVA transformer calculated with (2.80) (without and with substitutions) and the FEM in 2-D.

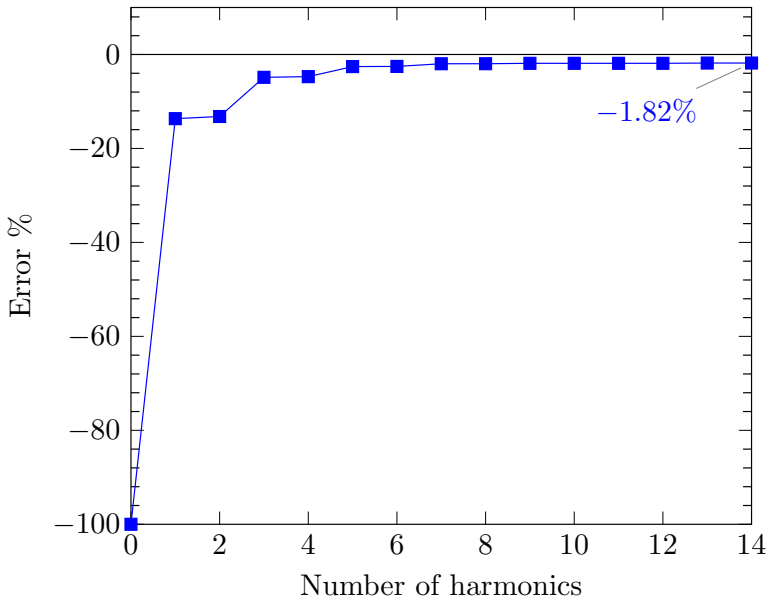

Figure 2.21 Relative error between the short-circuit inductance $L_{sc}(1, 44)$ of the 360 MVA transformer calculated with Roth's method and the FEM in 2-D.

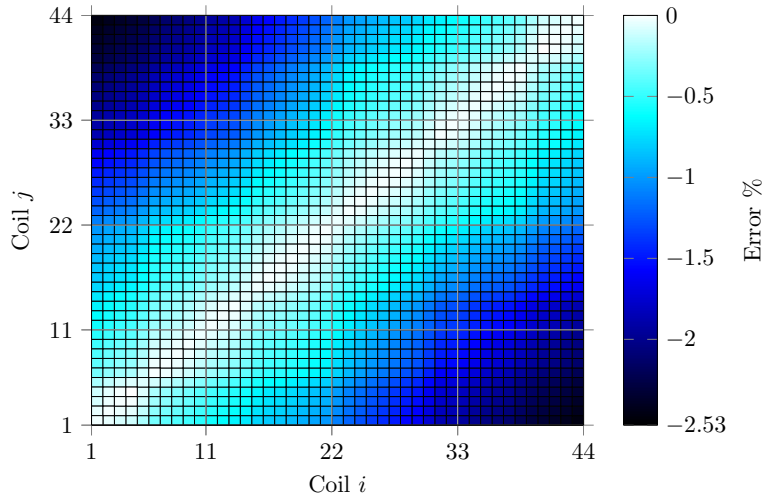

Figure 2.22 Error in the calculation of the short-circuit inductances $L_{sc}(i, j)$ of the 360 MVA transformer of the method of images (4 layers) with respect to the FEM in 2-D (Lambert *et al.*, 2013, Fig. 7), ©2013 IEEE.

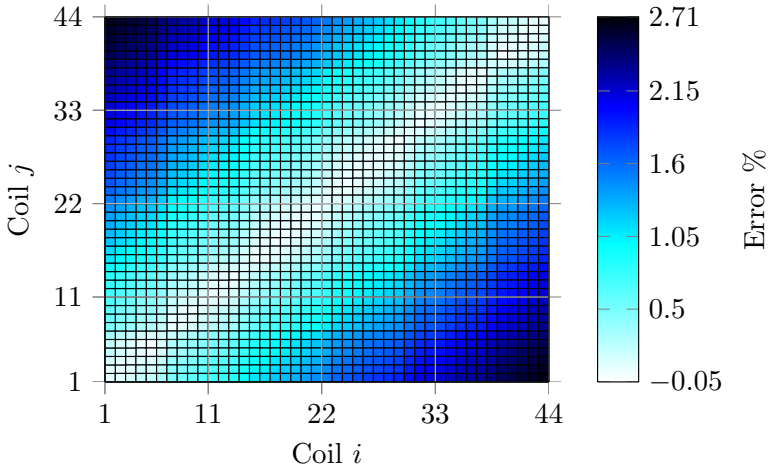

Figure 2.23 Error in the calculation of the short-circuit inductances $L_{sc}(i, j)$ of the 360 MVA transformer of the method of images (4 layers), with the substitutions, and with respect to the FEM in 2-D.

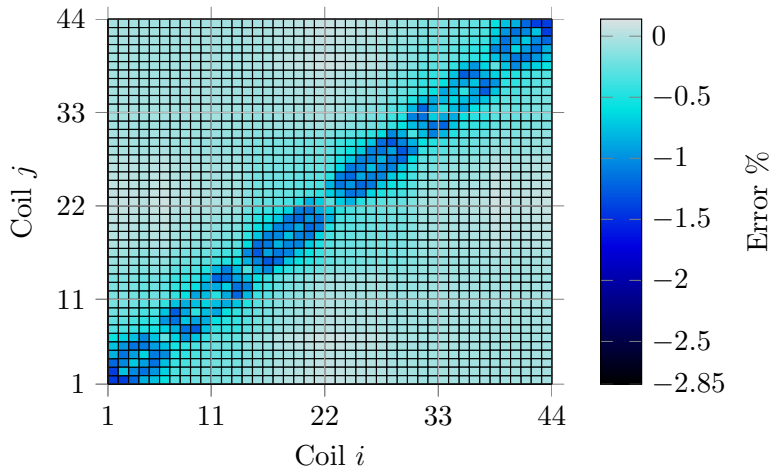

Figure 2.24 Error in the calculation of the short-circuit inductances $L_{sc}(i, j)$ of the 360 MVA transformer of Roth's method (110 harmonics) with respect to the FEM in 2-D.

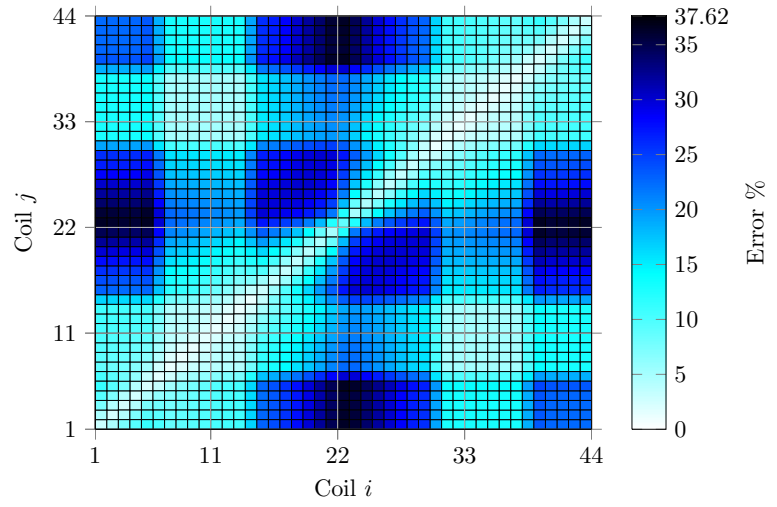

Figure 2.25 Error in the calculation of the short-circuit inductances $L_{sc}(i, j)$ of the 360 MVA transformer of the classical approach with respect to the FEM in 2-D (Lambert *et al.*, 2013, Fig. 8), ©2013 IEEE.

2.7.2 Results for the 570 MVA transformer

Another important aspect that is not studied in (Lambert *et al.*, 2013) is the effect of the 2-D approximation, with respect to the 3-D geometry. The 3-D geometrical data of the (magnetic) structure for the 570 MVA transformer was available, as seen in Fig. 2.16. Since the simulation time is longer in 3-D, only the short-circuit inductance between coils 1 and 44 is calculated. It is assumed that, since the distance between coils is maximal for this short-circuit, the error will also be maximal for this case. The calculated value is about 5.7% lower than the value calculated with the 2-D FEM. The number of degrees of freedom of the 3-D model is about 5 millions and the calculation took around 32 minutes. For illustrative purposes, the leakage flux is shown in Fig. 2.26 for this short-circuit.

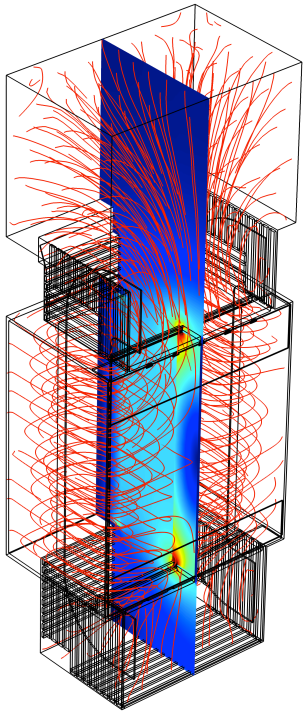

Figure 2.26 Leakage flux in the 570 MVA transformer during the short-circuit between coils 1 and 44, and flux density along the middle plane.

2.7.3 Results for the 96 MVA transformer

For the 96 MVA three-phase shell-type transformer, the results of the new approach are presented in Figs. 2.27 and 2.28, again for 4 layers of images and using the 2-D FEM as the reference. The results of Roth's method are shown in Fig. 2.29, using 110 harmonics, and the results of the classical formula are illustrated in Fig. 2.30.

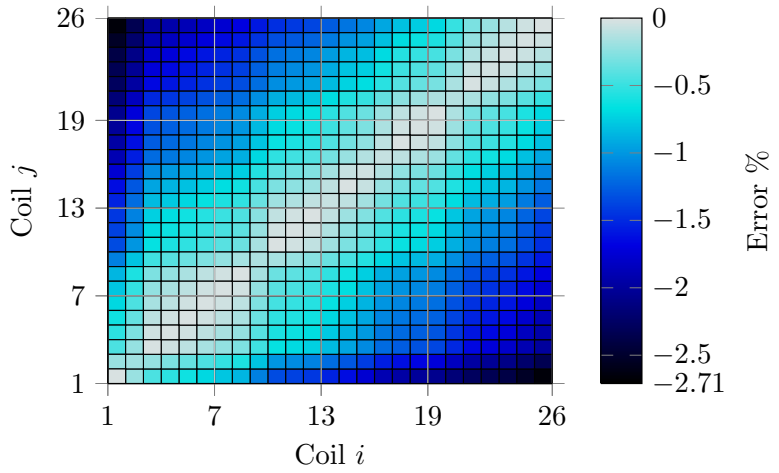

Figure 2.27 Error in the calculation of the short-circuit inductances $L_{sc}\,(i,j)$ of the 96 MVA transformer of the method of images (4 layers) with respect to the FEM in 2-D.

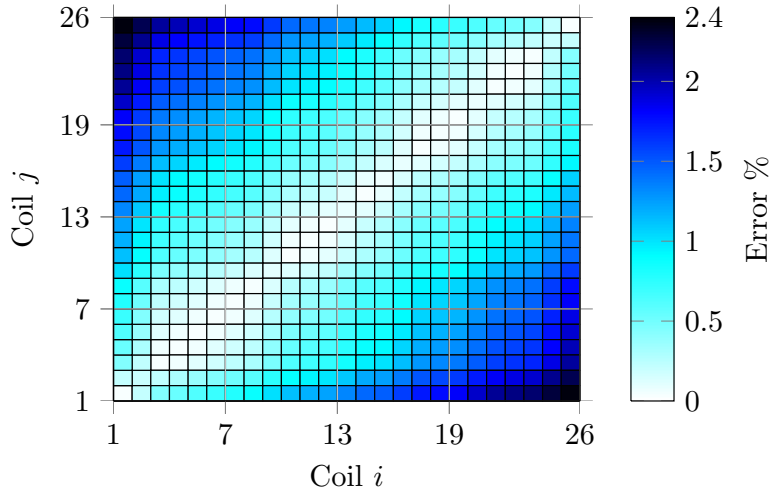

Figure 2.28 Error in the calculation of the short-circuit inductances $L_{sc}\,(i,j)$ of the 96 MVA transformer of the method of images (4 layers), with the substitutions, and with respect to the FEM in 2-D.

2.8 Discussion

It can be observed in Fig. 2.20 that the error of the method of images, without the substitutions, oscillates with respect to the number of layers. This phenomenon can also be noticed in (Gómez and de León, 2011, Fig. 6). This is caused by the way the terms are added in the double sum. Looking at Fig. 2.12 and assuming that $M = 2$ (2 layers of images), it can be seen that by summing for $j = -2$ to $j = 2$ and for $i = -2$ to $i = 2$, we include 4 images of the fourth order (i.e. the images in the corners, where we have k^4) and include 8

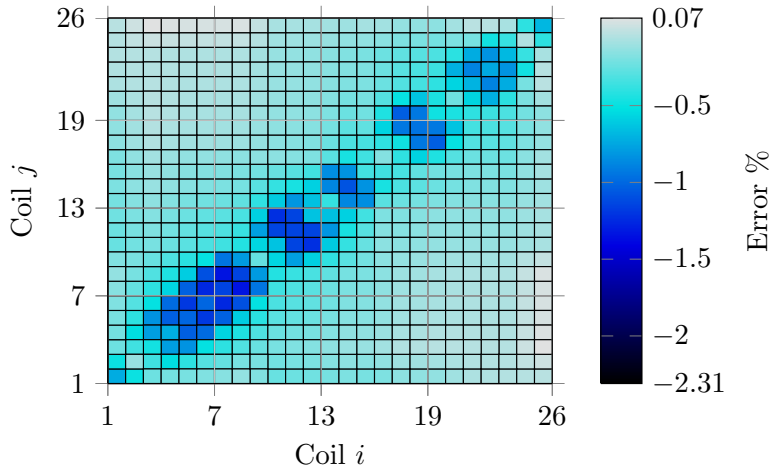

Figure 2.29 Error in the calculation of the short-circuit inductances $L_{sc}(i,j)$ of the 96 MVA transformer of Roth's method (110 harmonics) with respect to the FEM in 2-D.

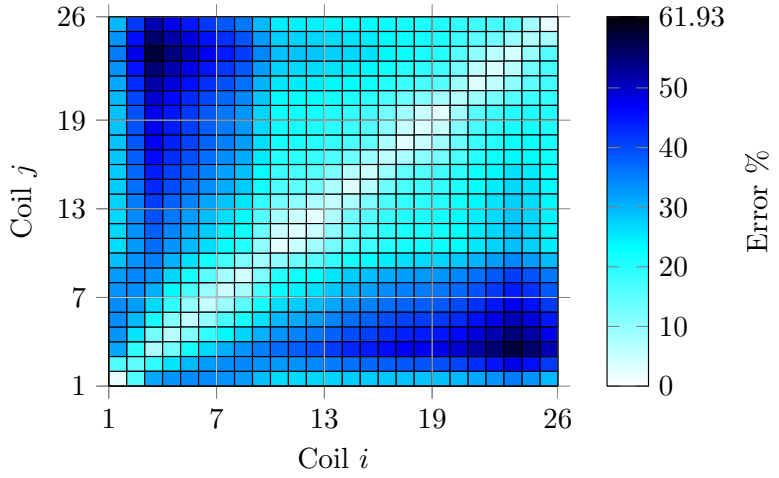

Figure 2.30 Error in the calculation of the short-circuit inductances $L_{sc}(i,j)$ of the 96 MVA transformer of the classical approach with respect to the FEM in 2-D.

images of the third order (i.e. the images in the corners, where we have k^3). This, in turn, will overestimate or underestimate the inductance, because of the alternating symmetry of the window, depending on the layer number. To solve this problem, it is proposed to rearrange the terms of the double sum using a taxicab circle, where its radius is equal to the layer number m. As illustrated in Fig. 2.20 in red, these substitutions remove the oscillatory behavior of the error. Since the taxicab circle's radius is equal to the layer number m, if we consider $M = 2$ (2 layers of images), it means that there is now twice as less images, which explains why the method is twice faster with the substitutions than without them, as observed in Table 2.1. It can also be seen from Fig. 2.20 that the assumption made in

(Margueron *et al.*, 2007, p. 888) that only the closest images are needed (first layer), is not necessarily correct. In this case, it would lead to a relative error of -13.7%, since considering only the first reflections is equivalent to the approach proposed here with substitutions, where $M = 1$.

From Fig. 2.21, it can be seen that Roth's method converges slowly (with respect to the number of harmonics), as previously mentioned in (Hammond, 1967, § 5.4). However, looking at Table 2.1, it is clear that it is much faster to calculate an additional space harmonic than it is to calculate an additional layer of images. Furthermore, by comparing Figs. 2.22, 2.23 and 2.24, it can be seen that the maximum error (in absolute value) of Roth's method is approximately the same than the new approach if 110 harmonics are used. Hence, from Table 2.1, it can be concluded that Roth's method is about 3 times faster than the new approach (with substitutions) to reach a comparable error. It is also apparent from Fig. 2.24 that for Roth's method, the error is higher for coils that are close to each other, as opposed to the new approach, where the error is maximal when the distance between coils is maximal, as seen in Figs. 2.22 and 2.23. This phenomenon can also be observed for the 96 MVA transformer in Fig. 2.29 for Roth's method, and in Figs. 2.27 and 2.28. Note that the error of the diagonal elements with Roth's method is zero (as with all other methods), but due to linear interpolation of the shaded plot with adjacent elements, the resulting color is different than zero on the color scale.

As previously discussed in § 2.2, one of the assumptions of the classical approach is that fringing flux is negligible. For the case where the windings are of equal heights and close to the yoke, as seen in Fig. 2.4a, the flux is essentially axial (vertical) and the approximation is correct. This can be observed in Fig. 2.25 for the 360 MVA transformer, where the errors for the short-circuits of low-voltage coils are small, since these coils are close to the yoke, as shown in Fig. 2.15. It is also seen in Table 2.1 that the classical approach, because of its simplicity, is very fast to calculate. However, for short-circuits involving coils farther from the yokes, e.g. coils 22 and 23, fringing flux is no longer negligible, as seen in Fig. 2.4b. This leads to appreciable errors in the evaluation of short-circuits involving high-voltage coils, as shown in Fig. 2.25, where the error reaches 37.62% for the 360 MVA transformer. A similar behavior is observed for the 96 MVA transformer in Fig. 2.30, where a maximum error of 61.93% occurs for the short-circuit between coils 3 and 24.

According to the results of the 570 MVA transformer, it can be reasonably concluded that the Cartesian 2-D model (rectangular cavity) is a good approximation for the shell-type transformer, since the leakage flux is mostly confined within the core window and the portion outside is similar due to the magnetic shunts and tank, as illustrated in Fig. 2.26. However, this conclusion does not necessarily applies to core-type transformers, because of

the significative portion of the coils outside the window. This aspect will need to be verified using a 3-D model of a core-type transformer.

2.9 Conclusion

In this chapter, a new method was proposed for the calculation of leakage inductances, which is based on the method of images and on the solution of Poisson's equation for the magnetic vector potential of a rectangular conductor in air. Furthermore, it was shown that the convergence of this new approach can be improved by reorganizing the terms of the double sum, using substitutions and taxicab trigonometry. The increase in the performance of the new method due to these substitutions is twofold.

It was demonstrated in this chapter that the 2-D approximation is acceptable for shell-type transformers of similar construction to Fig. 2.16, because leakage flux is mostly surrounded by the core (and outside the core, the magnetic shunts wrap the coils in a similar fashion), as mentioned earlier. However, more tests would be necessary to verify whether or not this assumption remains valid for core-type transformers.

By comparing the performance of Roth's method with respect to the new method, it could be seen that Roth's method is faster. However, the method of images is more general, since any permeability can be considered, using the image coefficient k, while Roth's method is limited to problems with boundaries of infinite permeability or zero permeability (Hammond, 1967, § 5.1). Roth's method is extended in (Roth, 1928a) to include the finite permeability of the core, but only for the wound leg. Nevertheless, for the calculation of short-circuit inductances, which is the purpose of this chapter, the assumption that the core's permeability is infinite is correct, as indicated previously (because the magnetomotive forces of each coil approximately cancel each other in short-circuit).

Another interesting method that is even more general is the finite element method. However, due to the complexity of its code, requiring a mesh generator and a magnetostatic solver, its implementation in EMT-type programs is impractical. Nevertheless, this method was useful to validate the analytical methods compared in this chapter, by using an overly large amount of degrees of freedom.

In addition, it was shown that the error of the classical approach can be large if the fringing flux is not negligible. Hence, unless the distance between the coils and the yoke is very small with respect to the window's height, it is preferable to avoid using the classical approach.

A possible extension of the new method could be the application of the method of images in 3-D for complex coil geometries. The magnetic vector potential in 3-D for conductors

of complex shapes can be calculated as the superposition of simpler shapes. The analytical solution of magnetic vector potential for circular and straight conductors in 3-D is given in Urankar's impressive work (Urankar, 1980, 1982a,b, 1984, 1990; Urankar and Henninger, 1991; Urankar *et al.*, 1994). However, these analytical solutions involve the numerical evaluation of elliptic integrals, which hinders the gain of performance of an analytical solution with respect to numerical methods in 3-D [18], such as the finite element method.

18. This is assuming that an iron boundary is present, such that superposition becomes necessary to take into account the boundary conditions.

CHAPTER 3

COUPLED LEAKAGE MODEL

After implementing a new method to calculate leakage inductances in shell-type transformers, the problem at hand is to connect those leakage inductances to other elements of a low-frequency transformer model, such as magnetizing branches and winding resistances. The connection of leakage inductances is the subject of this chapter. It is largely extracted from a previous paper by the author (Lambert *et al.*, 2014b), with additional explanations.

The most accurate transformer models for low-frequency electromagnetic transients (below the winding first resonance frequency, typically a few kHz (Martinez-Velasco and Mork, 2005, Sec. 1)) have a physical basis. In these models the magnetic flux is confined inside predefined paths called flux tubes, as seen in Chapter 1. Such models are termed *topological*, since each model element represents a part of the reluctance in the magnetic field physical path. These models are used in EMT-type programs instead of vectorial field models, because the computational cost involved with FEM simulations were prohibitive due to three facts: the transient nature of the phenomenon, which would require to compute a field solution for each time-step; the nonlinearities of transformer cores; the need to model not just one transformer but several of them (depending on the system configuration being studied). It will actually be demonstrated later in Chapter 5, that the generalization of magnetic circuit theory leads to discrete electromagnetism and more sophisticated 3-D models.

Even though the more recent models proposed in the literature are topological, thus physically-based, it can be seen that for a given transformer configuration, many different "topological" models exist. For instance, for the three-phase three-legged stacked-core transformer (with two and three windings), a shortened list of models is given by (Cho, 2002, Fig. 5.5), (Enright, 1996, Fig. 4.18), (Mork *et al.*, 2007a, Fig. 3), (Dijk, 1988, Fig. 2.15), (Chiesa *et al.*, 2010, Fig. 2), (Slemon, 1953, Fig. 6(b)) and (Yacamini and Bronzeado, 1994, Fig. 2). If the models are physically-based, why are there so many different topological models for the same transformer type? The answer is: because of leakage flux.

In theory, if magnetic insulators existed, the magnetic flux could be entirely confined within the magnetic "conductors", as it is the case for electric circuits at low frequencies. The key difference between electric and magnetic circuits is the difference in the relative values of magnetic permeability and conductivity between conductors and insulators. Because the ratio of permeabilities of oil (or air) and iron is in the range of 10^3–10^4, some of the magnetic flux leaks from the magnetic core, whereas the ratio of conductivities of pure air (or polymers)

and copper is in the order of 10^{22}–10^{28}. According to (Dept. Elect. Eng., Massachusetts Inst. Technology, 1943), finding an equivalent magnetic circuit with leakage flux is similar to deriving an equivalent electric circuit for a network of copper conductors immersed in an electrolyte solution[1]. Hence, the chosen paths (or flux tubes, to be more precise) and the points of connection of leaks to the circuit can vary from one model to another.

Despite the fact that discrepancies exist due to the particular choice of flux paths, another key difference comes from the fact that some models *divide* the leakage flux between a pair of windings into two fluxes, while others do not. This can be seen in (Saldaña and Calzolari, 1997, Figs. 7–8), where the leakage flux is divided, compared to (Chiesa *et al.*, 2010, Figs. 1–2), where it is not divided. The two types of models are shown in Figs. 3.1 and 3.2, respectively (the differences are highlighted in red). This difference in the modeling of leakage flux is highlighted in (Dijk, 1988, Chs. 1–2), where the two approaches were respectively termed *integral flux* approach and *divided flux* approach. Both approaches are explained in Section 3.1.

The main problem with those topological models is their failure to represent adequately short-circuit conditions for transformers with more than two windings (see (de León and Martinez-Velasco, 2009, Sec. III)). For topological models of N-winding transformers based on the integral flux approach, there are $N-1$ leakage inductances, and for those based on the divided flux approach, there are N leakage inductances. Since there are $N(N-1)/2$ different pairs of short-circuit combinations, it can be seen that these approaches will fail to represent all cases (they can work only for a given number of windings N).

To alleviate this problem, it was proposed in (Narang and Brierley, 1994; Mork *et al.*, 2007a; Chiesa, 2010) to use coupled inductors (or a mesh-equivalent network) to reproduce the $N(N-1)/2$ pairs of short-circuit conditions, where the indefinite admittance matrix can be calculated with the method proposed in (Brandwajn *et al.*, 1982) (BCTRAN). However, this representation of leakage inductances is no longer topological, it is just a solution for reproducing more accurately the terminal short-circuit measurements. This is highlighted in (Chiesa, 2010, p. 77). In order to connect a topological core model to the short-circuit admittance matrix, one or more fictitious windings are necessary, where a portion of the short-circuit admittance is divided with this approach. This approach was termed *hybrid model* in (Mork *et al.*, 2007a,b), to emphasize the fact that it uses a topological core model with a more appropriate representation of short-circuit admittances.

Even though the hybrid approach solves the problem of inadequacy between terminal short-circuit measurements and the values calculated with topological leakage models, it

1. This is the idea behind the Electrolytic Field Analyzer, presented for instance in (Farr and Wilson, 1951).

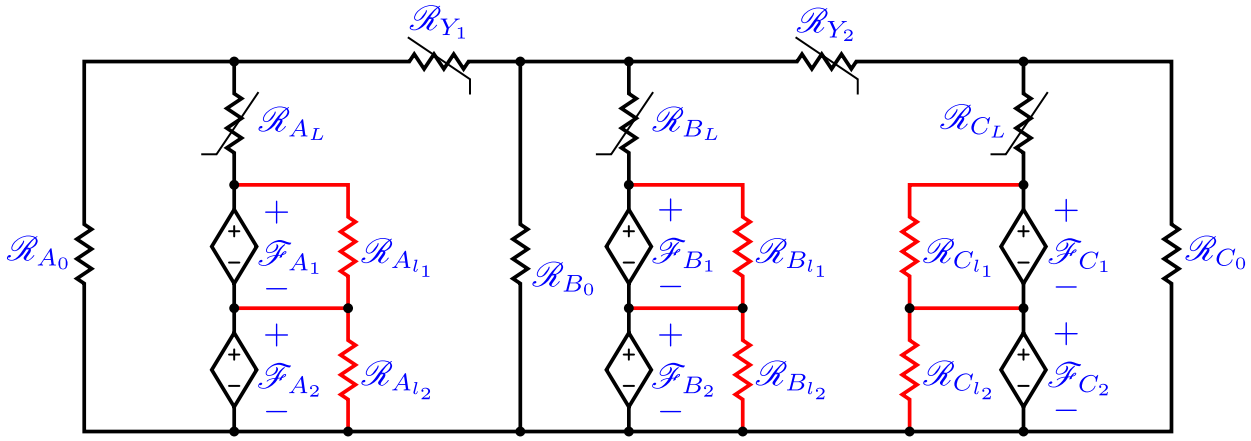

Figure 3.1 Equivalent magnetic circuits of a three-phase two-winding three-legged transformer, with divided leakage flux.

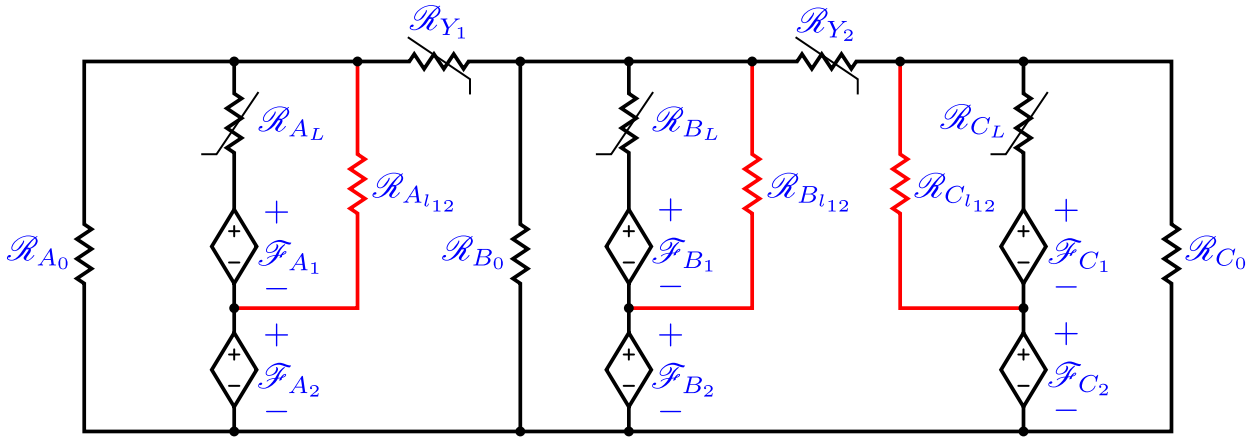

Figure 3.2 Equivalent magnetic circuits of a three-phase two-winding three-legged transformer, with integral leakage flux.

raises other issues. First, how many fictitious windings are required? According to (Narang and Brierley, 1994) and (de León, 1992), there are two fictitious windings (α and β), whereas there is only one in (Mork *et al.*, 2007a). Second, how to split the short-circuit admittance to account for these windings? The proportionality factor K of (Mork *et al.*, 2007a), to derive a "leakage inductance" between the inner winding and the fictitious winding, is proposed to be $K = 0.5$ in (Høidalen *et al.*, 2009). In (Chiesa *et al.*, 2010), a value of $K = 0.33$ is calculated from classical ampere-turn diagram formulas, assuming that the fictitious winding is infinitely thin. However, it was shown in (Lambert *et al.*, 2013) that these formulas can be inaccurate if the flux is not axial. Furthermore, in (Narang and Brierley, 1994), a coupling

factor $\delta = 10^3$ is used to couple the short-circuit admittance matrix to the fictitious winding. Third, it is mentioned in (Høidalen *et al.*, 2009) that: "*The artificial core winding is related to the leakage channel between the inner physical winding and the core*". However, which winding is the inner winding in the case of a sandwiched winding design? The issues raised here show the physical inconsistencies that exist with this approach.

Based on the above arguments, it can be concluded that a topological leakage model was needed. Such a model must reproduce the terminal short-circuit measurements without the use of fictitious windings.

This type of model was first presented in (de León and Martinez-Velasco, 2009), but the objective of the paper was to solve the numerical instability problems caused by the negative inductance in the star-equivalent circuit of a three-winding transformer, with the use of coupled leakage inductances. This principle was generalized to single-phase N-coil transformers in (Álvarez-Mariño *et al.*, 2012).

In this chapter, it is first demonstrated how this model is related to the integral flux approach and it is also explained why this approach is better. Afterwards, the mathematical equivalence between the divided and integral flux approaches is shown, for a single-phase two-winding transformer, assuming the core inductances are linear. Then, a new relationship is derived for the well-known T-network model (divided flux approach) to calculate the correct ratio on how to split the short-circuit inductance between the two leakage inductances, according to the core and windings' geometries. It is also demonstrated that when the core is considered nonlinear, for the T-network model to be mathematically equivalent, it requires nonlinear leakage inductances. Next, it is explained how to calculate the coupled leakage inductance matrix from the short-circuit inductance matrix. Finally, a new model is presented for a three-phase shell-type transformer that uses the coupled leakage approach.

3.1 Integral and divided fluxes

In order to understand the differences between the two methods, let us look at a simple example: the single-phase two-winding shell-type transformer with cylindrical windings. In the divided flux approach, the magnetic flux is split into three components: the leakage flux of winding 1 ϕ_{l_1}, the leakage flux of winding 2 ϕ_{l_2} and the common (or main) flux ϕ_c, as shown in Fig. 3.3a. For the integral flux approach, this division is not made and only one leakage flux can exist, namely the flux $\phi_{l_{12}}$ circulating between the windings, as seen in

Fig. 3.3b [2]. The equivalent magnetic circuits (after simplifications [3]) of both approaches are illustrated in Fig. 3.4, and the dual electric circuits are shown in Fig. 3.5. It can be seen that for this example, the divided flux approach leads to the well-known T-network, whereas the integral flux approach results into the Π-network [4]. Even though the two approaches are related through the star-delta transformation (if the nonlinear elements are assumed linear) and are equivalent for this example, it is not generally the case for all integral flux and divided flux magnetic circuits (e.g. with more than 2 windings). Thus, it is necessary to investigate which method is more appropriate and more generic, to model a transformer on a topological (physical) basis.

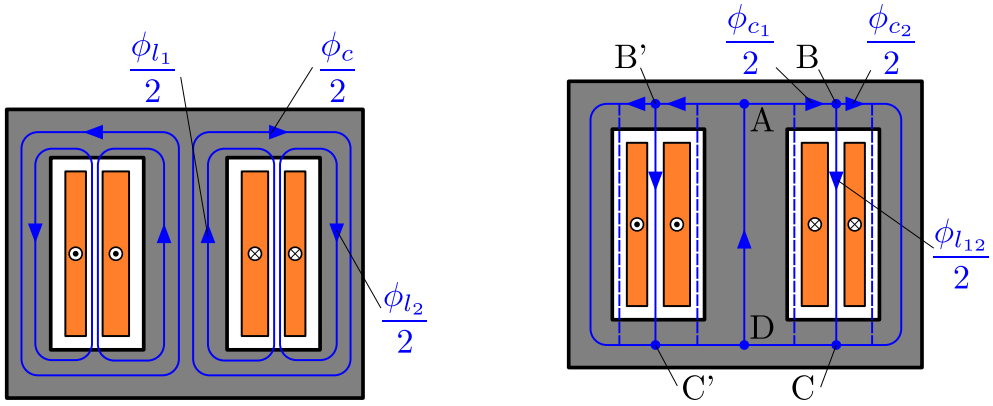

(a) Divided flux approach. (b) Integral flux approach.

Figure 3.3 Magnetic flux paths of a single-phase two-winding shell-type transformer, ©2014 IEEE.

This question was studied in (McEachron, 1922), (Bödefeld, 1931) and (Bödefeld and Sequenz, 1952) and later recalled in (Dijk, 1988). It was concluded that the T-network, hence the divided flux approach, is merely the result of mathematical manipulations, whereas the Π-network (integral flux approach) is physically-based. Furthermore, it is highlighted in (Dijk, 1988) that the star-delta transformation is only valid for linear elements. Thus, the integral flux approach should be privileged over the divided flux approach for the derivation of a topological transformer model, since the mathematical equivalence (existence and uniqueness of a solution) between the models is no longer guaranteed.

2. The shunt air paths (shown with dashed lines) are usually omitted, since they can be combined with the core's nonlinear reluctances $\mathscr{R}_{c_1}$ and $\mathscr{R}_{c_2}$.

3. Since the geometry is symmetric along the axis AD, both halves are in parallel (B and B' are virtually connected and so are C and C', because they have the same magnetic scalar potentials). Therefore, ϕ_{c_1} is the flux flowing in the path CC'-D-A-BB', ϕ_{c_2} is the flux flowing in the core from BB' to CC', and $\phi_{l_{12}}$ is the flux through the air from BB' to CC'.

4. For the core-type transformer, the same procedure can be followed and the dual circuit for the integral flux approach will be the same, as illustrated in (Martinez-Velasco, 2010, Fig. 4.8).

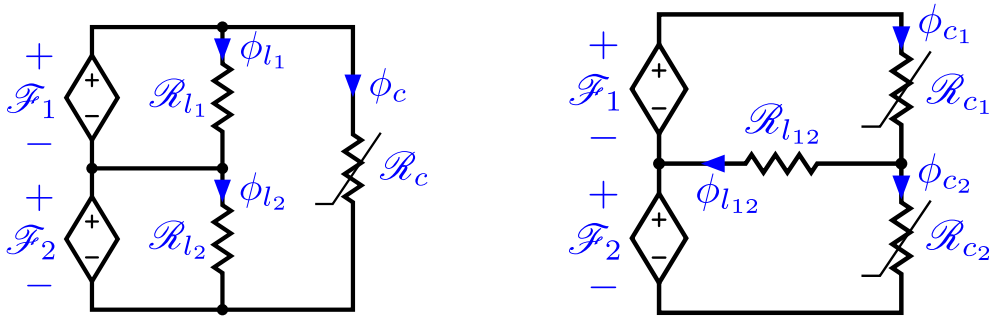

(a) Divided flux approach. (b) Integral flux approach.

Figure 3.4 Equivalent magnetic circuits of a single-phase two-winding shell-type transformer, ©2014 IEEE.

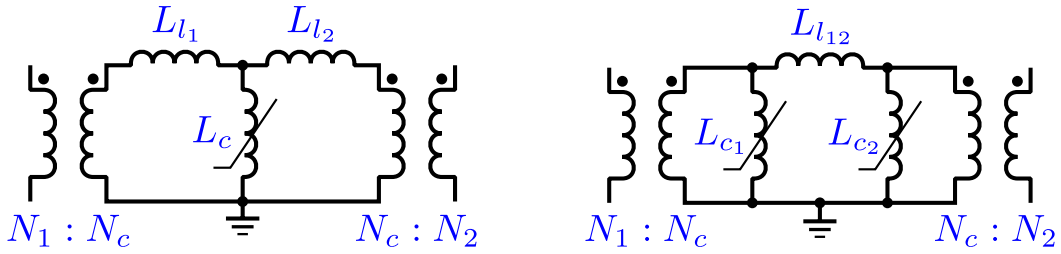

(a) Divided flux approach. (b) Integral flux approach.

Figure 3.5 Dual electric circuits of a single-phase two-winding shell-type transformer, ©2014 IEEE.

Despite the fact that the model mostly used for single-phase two-winding transformer is the T-network, a few authors also proposed the Π-network, see for instance (Arturi and Ubaldini, 1986), (Bossi *et al.*, 1979) and (Slemon, 1992, pp. 250–251). More recently, this model was also covered in (Martinez-Velasco, 2010, Sec. 4.4.2) and also in (Zirka *et al.*, 2012), where it is mentioned that the Π-network is the topological model for the single-phase transformer.

According to the star-delta transformation, the division factor between the leakage inductances L_{l_1} and L_{l_2} of the T-network (usually 0.5 or 0.75–0.9 (Martinez-Velasco *et al.*, 2005, p. 2053)) and the short-circuit inductance depends on the division of the core inductances of the Π-network (ratio of core lengths). This is detailed in the next section.

3.2 Star-delta transformation

Even though it was claimed that the star-delta transformation cannot be used for nonlinear elements in (Dijk, 1988), it is useful to demonstrate the relationship that exists between

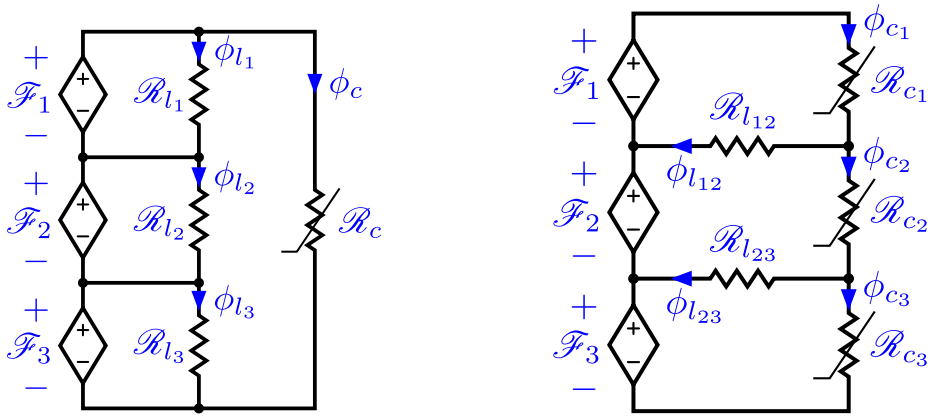

(a) Divided flux approach. (b) Integral flux approach.

Figure 3.6 Equivalent magnetic circuits for the three-winding single-phase shell-type transformer, ©2014 IEEE.

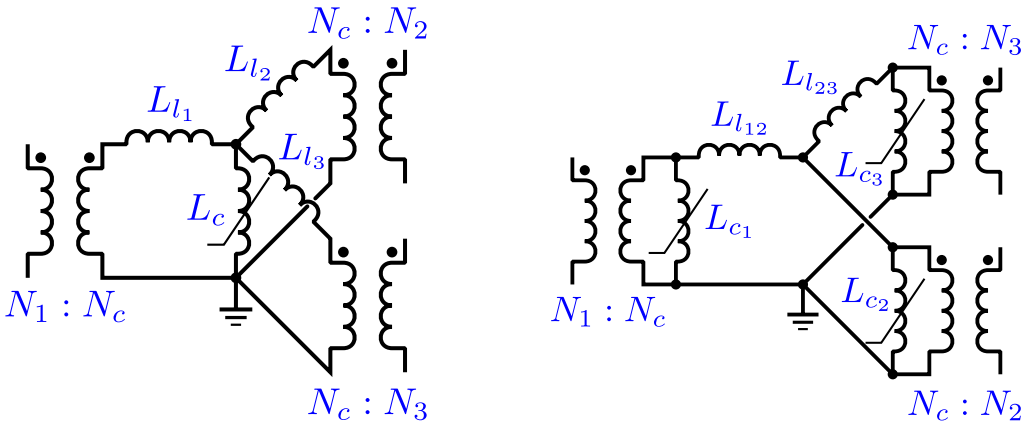

(a) Divided flux approach. (b) Integral flux approach.

Figure 3.7 Dual electric circuits for the three-winding single-phase shell-type transformer, ©2014 IEEE.

the integral flux and the divided flux approaches for single-phase transformers from a piecewise linear perspective. The inductances L_{l_1}, L_{l_2} and L_c in the divided flux approach are related to the inductances in the integral flux approach through the star-delta transformation

$$L_{l_1} = \frac{L_{c_1} L_{l_{12}}}{L_{c_1} + L_{c_2} + L_{l_{12}}} = K_1 L_{l_{12}} \tag{3.1}$$

$$L_{l_2} = \frac{L_{c_2} L_{l_{12}}}{L_{c_1} + L_{c_2} + L_{l_{12}}} = K_2 L_{l_{12}} \tag{3.2}$$

$$L_c = \frac{L_{c_1} L_{c_2}}{L_{c_1} + L_{c_2} + L_{l_{12}}} \tag{3.3}$$

Since $L_{c_1} + L_{c_2} \gg L_{l_{12}}$ if the core is unsaturated, it can be approximated that

$$L_c \approx (L_{c_1} L_{c_2})/(L_{c_1} + L_{c_2}) \tag{3.4}$$

$$K_1 \approx L_{c_1}/(L_{c_1} + L_{c_2}) \tag{3.5}$$

$$K_2 \approx L_{c_2}/(L_{c_1} + L_{c_2}) \tag{3.6}$$

so that $K_1 + K_2 \approx 1$ and L_c approximately equal to L_{c_1} in parallel with L_{c_2}. Considering from Fig. 3.5 that $N_c = 1$, the inductances can be rewritten in terms of the permeability μ, the core lengths l_{c_1}, l_{c_2} and the core cross-sections A_{c_1}, A_{c_2}

$$K_1 \approx \frac{\frac{\mu A_{c_1}}{l_{c_1}}}{\frac{\mu A_{c_1}}{l_{c_1}} + \frac{\mu A_{c_2}}{l_{c_2}}} \tag{3.7}$$

$$K_2 \approx \frac{\frac{\mu A_{c_2}}{l_{c_2}}}{\frac{\mu A_{c_1}}{l_{c_1}} + \frac{\mu A_{c_2}}{l_{c_2}}} \tag{3.8}$$

In the case of a core-type single-phase transformer, $A_{c_1} = A_{c_2}$. For a shell-type single-phase transformer, this is also the case if the outer leg cross-section is half the cross-section of the center leg [5]. Hence, in both cases, (3.7) and (3.8) become

$$K_1 \approx l_{c_2}/l_{tot} \tag{3.9}$$

$$K_2 \approx l_{c_1}/l_{tot} \tag{3.10}$$

where $l_{tot} = l_{c_1} + l_{c_2}$ is the total length.

An important conclusion is that in the linear case, the primary leakage inductance L_{l_1} is proportional to the ratio l_{c_2}/l_{tot} and the secondary leakage inductance L_{l_2} is proportional to the ratio l_{c_1}/l_{tot}. This claim was also made in (Blume *et al.*, 1951, p. 71), but without explanation. It is also mentioned that the two models are mathematically equivalent, which is true with linear (unsaturated) inductances.

If we consider that L_{c_1} and L_{c_2} are represented by the two-slope piecewise linear curve

5. Note that in practice, for shell-type power transformers, the outer legs (and yokes) cross-sections may be larger than half the cross-section of the center leg. In that case, the reluctance $\mathscr{R}_{c_1}$ that comes from the flux path CC'-D-A-BB' (as mentioned earlier) would need to be divided into 2 reluctances (in series). One for the center leg (path D-A) and one for the 2 yokes (paths CC'-D and A-BB').

presented in Fig. 3.8, in the case where the core is fully saturated we get

$$L_{l_1} = \frac{L_{c_1 sat} L_{l_{12}}}{L_{c_1 sat} + L_{c_2 sat} + L_{l_{12}}} = K_1 L_{l_{12}} \tag{3.11}$$

$$L_{l_2} = \frac{L_{c_2 sat} L_{l_{12}}}{L_{c_1 sat} + L_{c_2 sat} + L_{l_{12}}} = K_2 L_{l_{12}} \tag{3.12}$$

$$L_c = \frac{L_{c_1 sat} L_{c_2 sat}}{L_{c_1 sat} + L_{c_2 sat} + L_{l_{12}}} \tag{3.13}$$

where the saturation inductances $L_{c_1 sat}$ and $L_{c_2 sat}$ (represented by L_B in Fig. 3.8) are now in the order of magnitude of $L_{l_{12}}$ (since they all represent flux tubes with air permeability μ_0). Hence, it means that the leakage inductance split ratios K_1 and K_2 are not constants but functions of the saturation level of the core. Furthermore, if L_{c_1} starts to saturate, but L_{c_2} is not yet saturated, we have the intermediate case where $K_2 \approx 1$, and conversely, when L_{c_2} starts to saturate, but L_{c_1} is not yet saturated (again assuming two-slope saturation curves), then $K_1 \approx 1$. Note that the core inductance L_c in the divided flux approach is also dependent on the leakage inductance $L_{l_{12}}$, as the core starts to saturate.

The resulting curves for L_{l_1} and L_{l_2} are shown in Fig. 3.9 and for L_c in Fig. 3.10, for this particular case. As an example, consider the following numerical values for the Π-equivalent (it is assumed that $l_{c_1} = l_{c_2}$, but it is not mandatory):

— Π-equivalent: $L_A = 2$ H, $L_B = 2$ mH, $\lambda_{0_B} = 0.5994$ Wb, $L_{l_{12}} = 0.7$ mH.

Using the previous equations, we get for the T-equivalent:

— T-equivalent: $L_D = 0.3499$ mH, $L_E = 0.6991$ μH, $L_F = 0.2979$ mH, $\lambda_{0_E} = 0.2095$ mWb, $L_G = 0.9998$ H, $L_H = 1.9973$ mH, $L_I = 0.8511$ mH, $\lambda_{0_H} = 0.5986$ Wb, $\lambda_{0_I} = 0.5994$ Wb.

Thus, the two models are mathematically equivalent only if we consider nonlinear partial (divided) leakages for the T model. This partially explains the difference observed between both models in (de León *et al.*, 2012), where the divided leakage inductances were considered linear. In that case, if the parameters are made to fit measurements on one side for the T-equivalent model (with linear leakage inductances), the behavior of this model will be incorrect viewed from the other side. Hence, the T model will not be reversible [6] with linear leakage inductances. However, the reversibility of the Π-equivalent model was demonstrated in (Zirka *et al.*, 2012) and later in (Jazebi *et al.*, 2013).

Physically, it makes sense to have nonlinear divided leakages, because the divided leakage fluxes partially link the core, as shown in Fig. 3.3a. Furthermore, in the T-equivalent model theory, leakage inductances are defined as the difference between self and mutual inductances

6. By "not reversible" it is meant that if the parameters are calculated to fit with the nonlinear curve seen from one terminal, the nonlinear behavior will be incorrect seen from the other terminal.

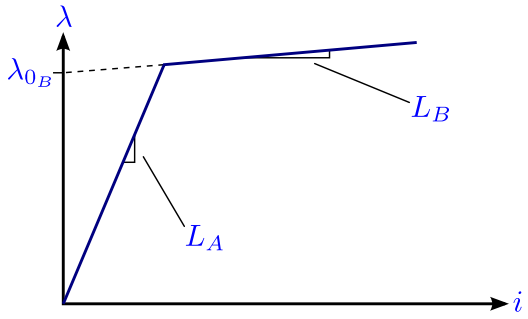

Figure 3.8 Two-slope piecewise-linear magnetizing curve for L_{c_1} and L_{c_2} of the Π equivalent, ©2014 IEEE.

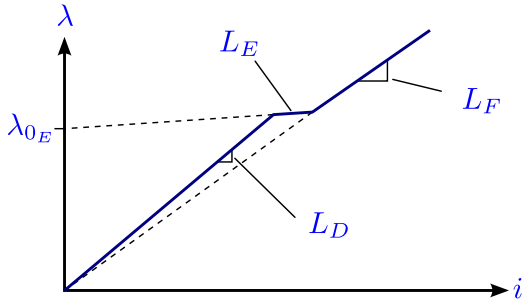

Figure 3.9 Resulting piecewise-linear leakage curve for L_{l_1} and L_{l_2} of the T equivalent, ©2014 IEEE.

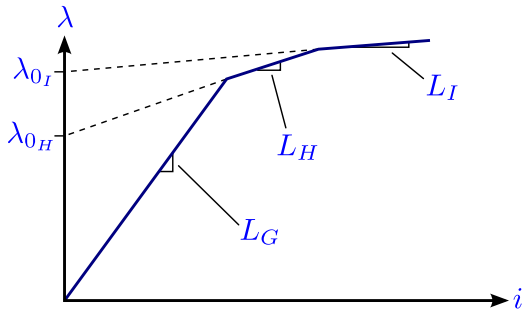

Figure 3.10 Resulting piecewise-linear magnetizing curve for L_c of the T equivalent, ©2014 IEEE.

(Dept. Elect. Eng., Massachusetts Inst. Technology, 1943, p. 314), where both are nonlinear. Since the correct representation of leakage in the divided flux approach is more complex than in the integral flux approach, it is preferable to use the later representation. The generalization to a N-winding transformer is also easier that way, as shown in the next section. The linearity of leakage inductances in the integral flux approach was demonstrated in (Inagaki *et al.*, 1988, pp. 1502–1503), where it is concluded that: “leakage inductance [...]

has little dependence on magnetizing conditions of the transformer core".

3.3 Coupled leakage approach

As mentioned at the beginning of this chapter, the problem with most topological models is their inability to reproduce the short-circuit measurements for more than 2 windings for the integral flux approach, and for more than 3 windings for the divided flux approach. This is explained in the following paragraphs.

By adding a third cylindrical winding to the transformer, the equivalent magnetic circuit of Fig. 3.4a becomes the one in Fig. 3.6a, and its dual electric circuit is shown in Fig. 3.7a, which is commonly referred to as the *star circuit* (Dommel, 1992). The fact that the star circuit is not valid for more than three windings in (Dommel, 1992, p. 14) can be observed from Fig. 3.7a, where a fourth winding would add a fourth branch connected to L_c: there would be only four leakage inductances, whereas there are six short-circuit conditions to satisfy ($L_{sc_{12}}$, $L_{sc_{13}}$, $L_{sc_{14}}$, $L_{sc_{23}}$, $L_{sc_{24}}$, $L_{sc_{34}}$).

Similarly, for the integral flux approach, let us add a third cylindrical winding to the transformer. The equivalent magnetic circuit of Fig. 3.4b is shown in Fig. 3.6b and its dual electric circuit is shown in Fig. 3.7b. Overall, for an N-winding transformer (or N-coil, if the windings are subdivided), there are $N\left(N-1\right)/2$ different short-circuit pairs. Hence, for a three-winding transformer, there are three short-circuit pairs: $L_{sc_{12}}$, $L_{sc_{13}}$ and $L_{sc_{23}}$. However, as it can be observed in Fig. 3.7b, there are only two leakage inductances and three short-circuit conditions to satisfy. For this reason, this approach is not valid for more than two windings.

The problem of finding an equivalent circuit for transformers with more than three windings is studied in (Blume *et al.*, 1951, pp. 112–124). For transformers with four windings, a star equivalent circuit is proposed in (Starr, 1933), as shown in Fig. 3.11, where the number of independent inductances is six (and the number of short-circuit conditions to satisfy is six, as mentioned earlier). The star equivalent circuit for the five-winding transformer is presented in (Aicher, 1943) and is generalized for the N-winding transformer in (Olivier and Gudefin, 1994). However, these models are not topological, as each inductance of the star equivalent circuit has no physical meaning. Hence, in that case, the indefinite admittance matrix method (BCTRAN) should be used instead, because of its simplicity.

A similar but simpler approach is to remove some of the inductances in the star equivalent circuit (for instance, short-circuit L_{l_e} or L_{l_f} from Fig. 3.11) to build a *simplified star equivalent circuit*, as illustrated in Fig. 3.12. This name comes from the fact that the model has only $2N-3$ inductances, whereas the number of different short-circuit pairs is $N\left(N-1\right)/2$. It is

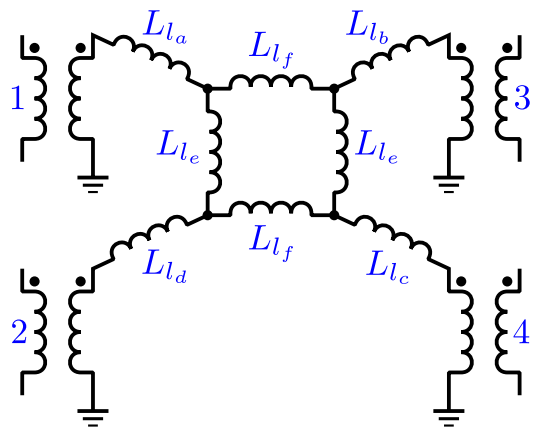

Figure 3.11 Star equivalent circuit for the single-phase four-winding transformer (core inductances not shown), ©2014 IEEE.

shown in (Bossi *et al.*, 1979) that some equations are not independent and must be removed, in order to calculate all the parameters. This type of model is presented for instance in (Henriksen, 2001, Fig. 4), (Cho, 2002, Fig. 6.2), (Arturi, 1994, Fig. 6) and (Chiesa, 2010, Fig. 4.10). It can also be explained by the addition of the inductances L_{l_2} to $L_{l_{N-1}}$ of Fig. 3.12 to the integral flux approach to match short-circuit measurements. It is said that these inductances compensate for the finite radial thickness of windings 2 to $N-1$ (Arturi, 1994).

It is proposed in (de León and Martinez-Velasco, 2009) to use coupled leakage inductances for the three-winding transformer case. The motivation of (de León and Martinez-Velasco, 2009) was to find an alternative to the star circuit, where there exists (for typical transformer designs) a negative leakage inductance that can lead to numerical instabilities during simulations. This method was generalized as a leakage model in (Álvarez-Mariño *et al.*, 2012), for a N-coil transformer, and is presented next. The addition of mutual leakage inductances in the integral flux approach allows to match short-circuit measurements.

From Figs. 3.5b and 3.7b, it can be seen that for the integral flux approach, there are $N-1$ leakage inductances for an N-coil transformer and the dual electric circuit for the single-phase transformer can be generalized for N cylindrical coils to the one presented in Fig. 3.13. In matrix form, it is shown in (Álvarez-Mariño *et al.*, 2012) that the elements of this new coupled leakage inductance matrix $[\mathscr{L}]$ in terms of the short-circuit inductances are given by

$$\mathscr{L}(i,j) = \frac{1}{2}\left[L_{sc}(i,j+1) + L_{sc}(i+1,j) - L_{sc}(i,j) - L_{sc}(i+1,j+1)\right] \tag{3.14}$$

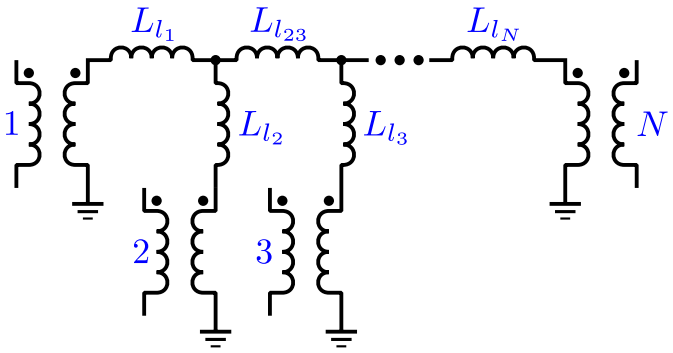

Figure 3.12 Simplified star equivalent circuit for the single-phase N-winding transformer (core inductances not shown), ©2014 IEEE.

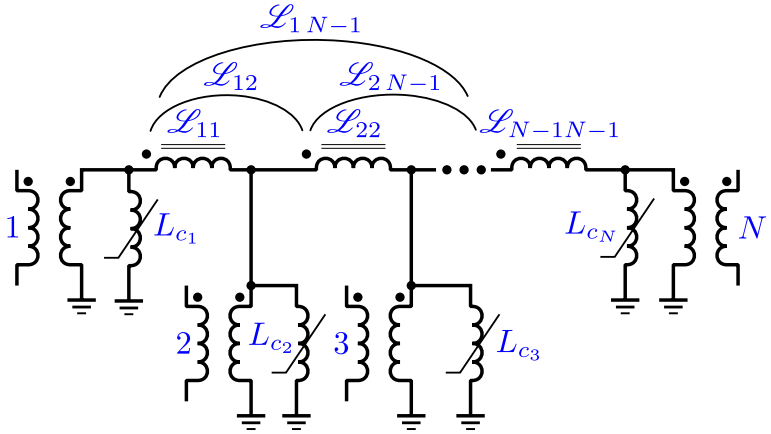

Figure 3.13 Coupled leakage model for the single-phase N-winding shell-type transformer with cylindrical windings (reciprocal mutual inductances $\mathscr{L}_{ji}$ are not shown), ©2014 IEEE.

For the particular case of the three-winding transformer, the short-circuit inductance matrix $[L_{sc}]$ is given by

$$[L_{sc}] = \begin{bmatrix} 0 & L_{sc_{12}} & L_{sc_{13}} \\ L_{sc_{12}} & 0 & L_{sc_{23}} \\ L_{sc_{13}} & L_{sc_{23}} & 0 \end{bmatrix} \tag{3.15}$$

and the coupled leakage inductance matrix $[\mathscr{L}]$ is

$$[\mathscr{L}] = \begin{bmatrix} L_{sc_{12}} & \dfrac{(L_{sc_{13}} - L_{sc_{12}} - L_{sc_{23}})}{2} \\ \dfrac{(L_{sc_{13}} - L_{sc_{12}} - L_{sc_{23}})}{2} & L_{sc_{23}} \end{bmatrix} \tag{3.16}$$

which is equivalent to (de León and Martinez-Velasco, 2009, eqs. 7–8). Note that the conclusion in (de León and Martinez-Velasco, 2009) that the mutual inductance is positive is

not necessarily true if the windings have different heights. This is the case for the two transformers presented next, for which some of the mutual inductances are negative.

It should be emphasized here that this method is different from the one presented in (Schultz, 2011), which was also termed the coupled leakage model. Indeed, by looking at its constitutive equation in (Schultz, 2011, eq. 4), it can be seen that this is the classic self/mutual inductances representation of the transformer (as presented for instance in (Brandwajn *et al.*, 1982, eq. 4)) and that it includes not only leakage inductances, but also core inductances.

3.4 Methods

As a verification for the new analytical method presented in Chapter 2, for the calculation of the short-circuit inductance matrix and also to test the new coupled leakage approach proposed by (Álvarez-Mariño *et al.*, 2012), short-circuits tests were performed on a single-phase, 360 MVA, $400/\sqrt{3}$ kV / 24 kV, 50 Hz, two-winding shell-type transformer with pancake coils and a three-phase 96 MVA, 400 kV / 3 x 6.8 kV, 50 Hz, four-winding shell-type transformer with pancake coils. The windings of the 360 MVA transformer are divided into 44 pancake coils and the four windings of the 96 MVA transformer are divided into 26 pancake coils per phase.

For single-phase shell-type transformers with pancake windings, it can be demonstrated that the dual electric circuit is the one shown in Fig. 3.13. For the three-phase shell-type transformer with pancake windings shown in Fig. 3.14, the magnetic equivalent circuit is illustrated in Fig. 3.15 [7], and its dual electric circuit is shown in Fig. 3.16.

Since the short-circuit measurements between coils are never available, the new analytical method presented in Chapter 2 was used to calculate the short-circuit inductance between each coil pair to fill up the short-circuit inductance matrix (2.85). With the short-circuit inductances known, the coupled leakage matrix (3.14) can be computed. The indefinite admittance matrix method presented in (Brandwajn *et al.*, 1982) (BCTRAN) was used to verify the results obtained with the approach presented in this paper. The commonly used short-circuit model of (Brandwajn *et al.*, 1982) is also used in hybrid topological models such as (Narang and Brierley, 1994) and (Mork *et al.*, 2007a), with modifications to account for the fictitious windings. The same short-circuit inductance matrix $[L_{sc}]$ was used for both methods.

Simulations were performed for both transformers with the two approaches and the short-circuit inductances between windings (coils are regrouped into windings) were calculated and

7. Note that in general, the magnetomotive forces of the center phase are reversed with respect to the outer phases. This is accounted for with the appropriate electrical connections to the sources (reversed source polarity for the center phase), outside the magnetic equivalent circuit.

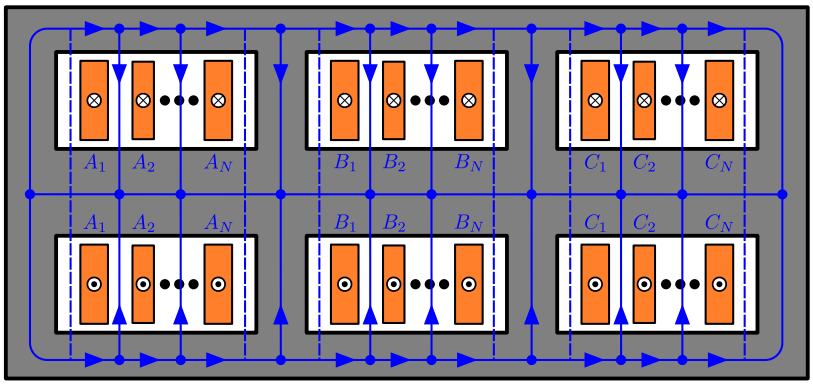

Figure 3.14 Magnetic flux paths for the three-phase N-winding shell-type transformer with pancake windings, ©2014 IEEE.

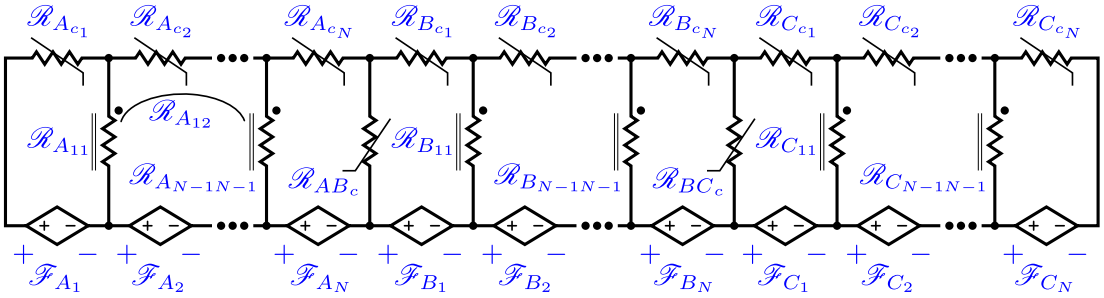

Figure 3.15 Equivalent magnetic circuit for the three-phase N-winding shell-type transformer with sandwiched windings (mutual reluctances $\mathscr{R}_{ij}$ are not shown, except for $\mathscr{R}_{A_{12}}$), ©2014 IEEE.

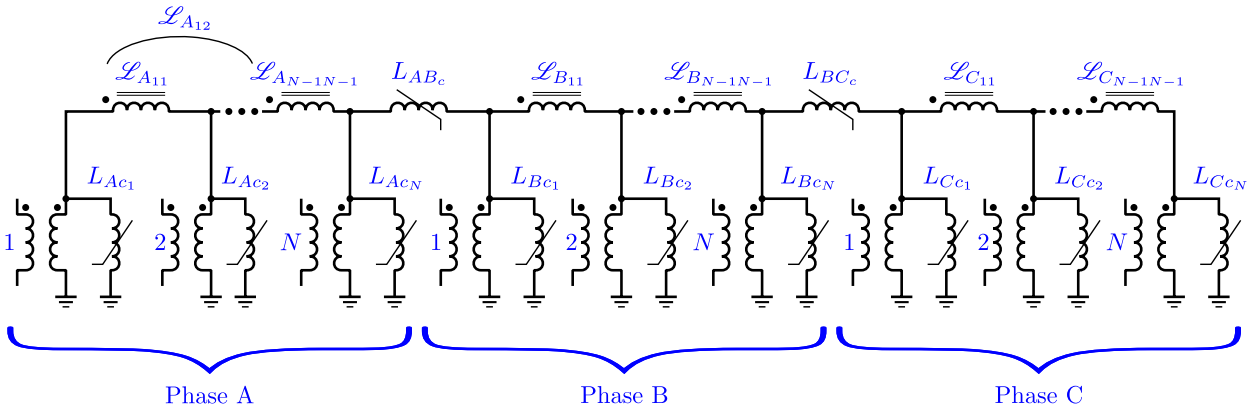

Figure 3.16 Coupled leakage model for the three-phase N-winding shell-type transformer with sandwiched windings (mutual inductances $\mathscr{L}_{ij}$ are not shown, except for $\mathscr{L}_{A_{12}}$), ©2014 IEEE.

compared with measurements. For the 96 MVA transformer, the positive-sequence short-circuit inductance was measured between the high-voltage winding (winding 1) and each of the low-voltage windings (2 to 4). In all simulation cases, the low-voltage winding is short-circuited and the high-voltage winding is energized with voltages corresponding to the measurements.

3.5 Results

The results for the short-circuit inductance of the 360 MVA transformer are presented in Table 3.1 between the high-voltage and the low-voltage windings. The difference between measurement and simulation is 0.04 %.

As for the 96 MVA transformer, the positive-sequence short-circuit inductances are shown in Tables 3.2–3.4. Each low-voltage winding is tested separately. The errors for the short-circuit inductances of each low-voltage winding are 6.02 %, 3.31 % and 7.93 %, respectively. Again, the error observed with BCTRAN comes from the fact that the method presented in Chapter 2 was used to calculate the short-circuit inductance between each coil pair to fill up the short-circuit inductance matrix, since short-circuit measurements between coils are never available.

3.6 Discussion

It can be seen in Tables 3.1–3.4 that there is no difference between the results of the coupled leakage method and the indefinite admittance matrix method (BCTRAN). Hence, from a short-circuit point of view, the two methods are equivalent. However, the coupled leakage model is topologically correct and can accommodate a topological core model without the use of fictitious windings, whereas one or more fictitious windings are necessary to connect the indefinite admittance matrix to the topological core in (Mork *et al.*, 2007a) and (Narang and Brierley, 1994). The establishment of such fictitious winding is arbitrary and is not supported by any physical basis. As such, the coupled leakage model proposed in (Álvarez-Mariño *et al.*, 2012), and generalized here for the three-phase shell-type transformer, appears to be a better and more intuitive approach for modeling leakage flux in topological transformer models.

Another interesting result observed from Tables 3.1–3.4 is that the method presented in Chapter 2 for the calculation of the short-circuit inductance matrix $[L_{sc}]$, was validated with experimental short-circuit measurements for two transformers. The higher differences observed in the three-phase case can be explained by the fact that the 2D approximation used in the analytical method of Chapter 2 used for evaluating the short-circuit inductances

Table 3.1 Short-circuit inductance for the 360 MVA transformer seen from the HV side, ©2014 IEEE

Method	**Short-circuit inductance [mH]**
Measurement	69.43
Coupled leakage model	69.4598
BCTRAN	69.4598

Table 3.2 Positive-sequence short-circuit inductance windings 1 and 2 for the 96 MVA transformer seen from the HV side, ©2014 IEEE

Method	**Short-circuit inductance [H]**
Measurement	1.22
Coupled leakage model	1.2934
BCTRAN	1.2934

Table 3.3 Positive-sequence short-circuit inductance windings 1 and 3 for the 96 MVA transformer seen from the HV side, ©2014 IEEE

Method	**Short-circuit inductance [H]**
Measurement	1.23
Coupled leakage model	1.2707
BCTRAN	1.2707

Table 3.4 Positive-sequence short-circuit inductance windings 1 and 4 for the 96 MVA transformer seen from the HV side, ©2014 IEEE

Method	**Short-circuit inductance [H]**
Measurement	1.27
Coupled leakage model	1.3707
BCTRAN	1.3707

is less accurate for that case. Nevertheless, the results obtained are acceptable.

3.7 Conclusion

In this chapter, the differences between topological transformer models were explained through the concepts of *divided* and *integral* fluxes. It was shown that the divided flux approach is the result of mathematical manipulations and that the integral flux approach

should be preferred, since it represents more closely the physical path of the flux lines in a transformer. Furthermore, a relationship was derived to calculate the split ratio of leakage inductances of the T-network model for the single-phase two-winding transformer, in the case where the core inductances are assumed linear. When the core inductances are nonlinear, it was demonstrated that nonlinear leakage inductances are necessary in the divided flux approach, in order for the models to be mathematically equivalent, whereas leakage inductances in the integral flux approach are linear by definition (flux tubes in air).

Also, a new model was proposed for the three-phase shell-type transformer that uses the coupled leakage model presented in (Álvarez-Mariño *et al.*, 2012). This new approach has the advantage of modeling all short-circuit conditions and works for transformers with more than two windings (or coils), whereas the uncoupled leakage inductances in topological models are limited to a very specific number of windings (two for the integral flux model and three for the divided flux model).

Furthermore, it was shown that the indefinite admittance matrix (BCTRAN) and the coupled leakage model give the same short-circuit results. However, since the coupled leakage model is topologically correct, no fictitious winding is required, and the coupled inductances can be connected directly to the topological core model. This represents an important improvement over existing hybrid topological models.

Finally, the analytical method presented in Chapter 2 to calculate the short-circuit inductance matrix was verified for two transformers and the results show good agreement between the measurements and the calculated short-circuit inductances.

CHAPTER 4

SHELL-TYPE TRANSFORMER CORE MODELING

In most cases, when core parameters are calculated (magnetizing branches), leakage fluxes are neglected. This is because in no-load (unsaturated) conditions, magnetic flux is mostly confined inside the ferromagnetic core. However, when increasing the no-load voltage, the core starts to saturate (and magnetic flux starts leaking outside the core). Therefore, it is necessary to take into account leakage inductances when calculating core parameters, unless it is to be modeled in a linear (unsaturated) way. This can explain the large difference observed in (de León *et al.*, 2012) between T and Π models, because as seen from (de León *et al.*, 2012, eq. 5), the magnetizing inductance L_m does not take into account the leakage inductance L_s, leading to wrong conclusions about the T (and Π) model. This situation was partially corrected in (Jazebi *et al.*, 2013), but only for the Π model and only the saturated inductances (final slopes) L_{1-sat} and L_{2-sat} were modified to take into account the leakage inductance L_s. Actually, not only we need to modify the final slopes (saturation inductances), but the whole curves. This explains the difference seen for the reversible model in (Jazebi *et al.*, 2013, Figs. 8 and 9) where the error in the second inrush current peak is higher.

The problem is related to what is called *reversibility* of the model, which is the ability of a model to correctly predict results if another winding is energized instead of the one from the no-load measurements. To understand reversibility, let us look at an example. If there were no leakage inductances in the single-phase transformer model of Fig. 3.13, all magnetizing branches would be in parallel. Therefore, regardless of which winding is energized, all magnetizing branches would share the same voltage (thus, the same magnetic flux), which means that the equivalent inductance would be the same for all windings (in per-unit). In reality, the equivalent magnetizing inductance should be different for each winding (in per-unit), because windings are different in size and/or position. Essentially, the difference comes from leakage inductances. This will be examined shortly.

4.1 Air-core inductance versus saturation inductance

There seems to be much confusion in the literature between the *air-core inductance* and the *saturation inductance*. Therefore, it is worthwhile to correctly distinguish the difference between both inductances. For instance, it is mentioned in (Dommel, 1992, § 6.6.2) that

"The slope in the saturated region above the knee is the air-core inductance, which

> is almost linear and fairly low compared with the slope in the unsaturated region [...] While it makes little difference to which terminal the unsaturated inductance is connected, it may make a difference for the saturated inductance, because of its low value."

which is not entirely correct.

On the one hand, the air-core inductance is the (self) inductance of a winding in air (with other windings opened). It is usually calculated from analytical formulas for the calculation of self inductance, such as that presented in (Grover, 2004), or from the Finite Element Method. Therefore, it can be said that the air-core inductance is the *slope in saturation viewed from a terminal* (outside) and when *every ferromagnetic parts of the transformer are saturated* so that their permeabilities are essentially that of vacuum, μ_0.

On the other hand, from a modeling perspective, the saturation inductance refers to the slope in saturation of nonlinear inductances in a particular transformer model. Therefore, as seen in (Chiesa *et al.*, 2011), its value depends on the model and there will be multiple saturation inductances if there are multiple magnetizing branches in the model, such as the one presented in Fig. 3.13.

It can be concluded that if there is only one nonlinear inductance in the model, and if it is placed across the terminals of a winding, then the saturation inductance will be equal in that case to the air-core inductance seen from that winding.

4.2 Parameter estimation from typical no-load tests

The major problem with transformer core modeling is the lack of data to properly describe core nonlinearities, which would require minor/major hysteresis loop measurements. Usually, only no-load measurements are available in test reports, which include RMS values of voltage and current, along with losses, for different levels of excitation (e.g. 90%, 100% and 110%).

It is unfortunate, since core nonlinearities are the most important aspect in low-frequency transformer transients. As an approximation, a method was proposed in (Neves and Dommel, 1993) to calculate the (instantaneous) curves of a piecewise linear inductance in parallel with a piecewise linear resistance that would draw the prescribed no-load RMS values of current and voltage (and losses), *assuming that measured voltages were sinusoidal during no-load tests*. The method is explained next, where additional results of integrals that were not provided in (Neves and Dommel, 1993) are also given.

4.2.1 From RMS to peak values

This method was first presented in (Prusty and Rao, 1980) and later extended in (Neves and Dommel, 1993) to include nonlinear losses. The model is that of Fig. 4.1, where the nonlinear resistor represents core losses, and the nonlinear inductor corresponds to core saturation. It is assumed that no-load voltage is sinusoidal and given by

$$v_k(\theta) = \hat{v}_k \sin\theta \tag{4.1}$$

where $\theta = \omega t$ is the angle, and $\hat{v}_k = \sqrt{2}V_k$ is the peak voltage for the given no-load RMS voltage V_k of each no-load point k. Since flux linkage is the time-integral of voltage, it is given by

$$\begin{aligned}\lambda_k(\theta) &= -\frac{\hat{v}_k}{\omega}\cos\theta \\ &= -\hat{\lambda}_k \cos\theta\end{aligned} \tag{4.2}$$

where $\hat{\lambda}_k = \frac{\sqrt{2}V_k}{\omega}$ is the peak flux linkage for the given no-load RMS voltage V_k of (no-load) point k.

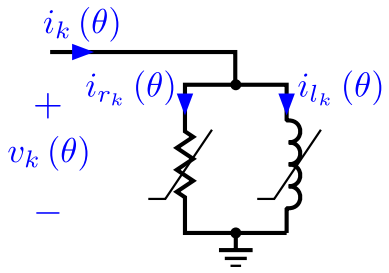

Figure 4.1 Piecewise linear magnetizing branch seen from a terminal.

Since the nonlinear curves are assumed to be antisymmetric (odd functions) there will only be odd current harmonics. Furthermore, the current harmonics of the nonlinear resistance will be in phase with voltage $v_k(\theta)$, while the current harmonics of the nonlinear inductance will be in phase with flux linkage $\lambda_k(\theta)$. Therefore, we can express these currents with Fourier series as

$$i_{r_k}(\theta) = \sum_{n=1,3,\cdots}^{\infty} a_n \sin n\theta \tag{4.3}$$

$$i_{l_k}(\theta) = \sum_{n=1,3,\cdots}^{\infty} b_n \cos n\theta \tag{4.4}$$

where i_{r_k} is the resistive current and i_{l_k} is the inductive current. The total (terminal) current $i_{t_k}(\theta)$ is the sum of both currents

$$i_{t_k}(\theta) = \sum_{n=1,3,\cdots}^{\infty} \sqrt{a_n^2 + b_n^2} \sin(n\theta + \gamma_n) \tag{4.5}$$

where $\gamma_n = \arctan\left(\frac{b_n}{a_n}\right)$. The RMS inductive current will be given by

$$I_{l_k} = \sqrt{I_{t_k}^2 - I_{r_k}^2} \tag{4.6}$$

where I_{t_k} is the measured (total) RMS no-load current for point k.

First, we have to calculate the nonlinear resistance, since we have P_k and V_k for each (no-load) point k, but we do not yet know how the current is divided between the resistance and the inductance. Again, because the nonlinear curves are assumed to be antisymmetric (odd functions), we only need to calculate the curves from a quarter of a cycle $\theta = \frac{\pi}{2}$. Hence, the average power is given by

$$P_k = \frac{2}{\pi} \int_0^{\frac{\pi}{2}} v_k(\theta)\, i_{r_k}(\theta)\, \mathrm{d}\theta \tag{4.7}$$

For a given no-load point k, there will be $k-1$ discontinuities in the current $i_{r_k}(\theta)$, called *break points* (since the characteristic is piecewise linear). From (4.1), each break point $j = 1, 2, \cdots, k-1$ will occur at an angle defined by [1]

$$\theta_j = \arcsin\left(\frac{\hat{v}_j}{\hat{v}_k}\right) \tag{4.8}$$

Furthermore, the incremental resistance R_j of each segment j of the piecewise-linear curve is defined as the slope between break points j and $j-1$

$$R_j = \frac{\hat{v}_j - \hat{v}_{j-1}}{\hat{i}_{r_j} - \hat{i}_{r_{j-1}}} \tag{4.9}$$

for $j = 1, 2, \cdots, k-1$. Note that for the first resistance, $\hat{i}_{r_0} = \hat{v}_0 = 0$. Alternatively, from (4.9) and (4.1), the value of resistive current $i_{r_k}(\theta)$ between break points j and $j-1$ will be

1. This comes from the fact that at θ_j, we have $v_k(\theta_j) = \hat{v}_j$. Therefore, according to (4.1), we have $\hat{v}_j = \hat{v}_k \sin\theta_j$.

given by

$$\begin{aligned} i_{r_k}(\theta) &= \hat{i}_{r_{j-1}} + \frac{v_k(\theta) - \hat{v}_{j-1}}{R_j} \\ &= \hat{i}_{r_{j-1}} + \frac{\hat{v}_k \sin\theta - \hat{v}_{j-1}}{R_j} \end{aligned} \tag{4.10}$$

With break points occuring at angles θ_j, the integral in (4.7) can be divided into $k-1$ integrals, corresponding to each segment of the piecewise-linear resistance between $\theta_0 = 0$ and $\theta_k = \frac{\pi}{2}$. Therefore, with this division, and using (4.10), we get

$$\begin{aligned} P_k = \frac{2}{\pi} \Bigg[& \int_{\theta_0}^{\theta_1} \hat{v}_k \sin\theta \frac{\hat{v}_k \sin\theta}{R_1} \mathrm{d}\theta \\ & + \int_{\theta_1}^{\theta_2} \hat{v}_k \sin\theta \left(\hat{i}_{r_1} + \frac{\hat{v}_k \sin\theta - \hat{v}_1}{R_2} \right) \mathrm{d}\theta + \cdots + \\ & + \int_{\theta_{k-1}}^{\theta_k} \hat{v}_k \sin\theta \left(\hat{i}_{r_{k-1}} + \frac{\hat{v}_k \sin\theta - \hat{v}_{k-1}}{R_k} \right) \mathrm{d}\theta \Bigg] \end{aligned} \tag{4.11}$$

where $\theta_0 = \hat{i}_{r_0} = \hat{v}_0 = 0$ and $\theta_k = \frac{\pi}{2}$. Solving the integrals in (4.11), we obtain

$$\begin{aligned} P_k = \frac{\hat{v}_k}{2\pi} \sum_{j=1}^{k} \frac{1}{R_j} \Big[& 4(\cos\theta_j - \cos\theta_{j-1}) \left(\hat{v}_{j-1} - \hat{i}_{r_{j-1}} R_j \right) \\ & + \hat{v}_k (2\theta_j - 2\theta_{j-1} + \sin 2\theta_{j-1} - \sin 2\theta_j) \Big] \end{aligned} \tag{4.12}$$

The only unknown in (4.12) is the last slope (resistance) R_k, since the other resistances are found *recursively* from previous $k-1$ no-load points. Therefore, it can be seen that the real power for point k can be expressed as

$$P_k = \frac{2\hat{v}_k}{\pi} \left[a_{r_k} + \frac{b_{r_k}}{R_k} \right] \tag{4.13}$$

where a_{r_k} and b_{r_k} are given by

$$a_{r_k} = \hat{i}_{r_{k-1}} \left[\cos\theta_{k-1} - \cos\theta_k\right] + \sum_{j=1}^{k-1} \hat{i}_{r_{j-1}} \left[\cos\theta_{j-1} - \cos\theta_j\right] + \frac{\hat{v}_{j-1}}{R_j} \left[\cos\theta_j - \cos\theta_{j-1}\right] + \frac{\hat{v}_k}{4R_j} \left[\sin 2\theta_{j-1} - \sin 2\theta_j + 2\theta_j - 2\theta_{j-1}\right] \tag{4.14}$$

$$b_{r_k} = \hat{v}_{k-1} \left[\cos\theta_k - \cos\theta_{k-1}\right] + \frac{\hat{v}_k}{4} \left[\sin 2\theta_{k-1} - \sin 2\theta_k + 2\theta_k - 2\theta_{k-1}\right] \tag{4.15}$$

Once the resistance R_k is known, the peak resistive current $\hat{i}_{r_k}$ at point k can be found using (4.9), which gives

$$\hat{i}_{r_k} = \hat{i}_{r_{k-1}} + \frac{\hat{v}_k - \hat{v}_{k-1}}{R_k} \tag{4.16}$$

Afterwards, we need to calculate the RMS value of the resistive current I_{r_k} for each point k. The squared RMS value of resistive current is given by the mean value (integral) of $i_r^2(\theta)$, where each $\hat{i}_{r_{j-1}}$ is found recursively from (4.16), giving

$$\begin{aligned}
I_{r_k}^2 &= \frac{2}{\pi} \int_0^{\frac{\pi}{2}} i_r^2(\theta)\, \mathrm{d}\theta \\
&= \frac{2}{\pi} \sum_{j=1}^{k} \int_{\theta_{j-1}}^{\theta_j} \left(\hat{i}_{r_{j-1}} + \frac{\hat{v}_k \sin\theta - \hat{v}_{j-1}}{R_j}\right)^2 \mathrm{d}\theta \\
&= \sum_{j=1}^{k} \frac{1}{\pi R_j^2} \Bigg[\left(2R_j^2 \hat{i}_{r_{j-1}}^2 - 4R_j \hat{i}_{r_{j-1}} \hat{v}_{j-1} + \hat{v}_k^2 + 2\hat{v}_{j-1}^2\right)(\theta_j - \theta_{j-1}) \\
&+4 \left(\hat{v}_{j-1}\hat{v}_k - \hat{i}_{r_{j-1}} \hat{v}_k R_j\right)(\cos\theta_j - \cos\theta_{j-1}) + \frac{\hat{v}_k^2}{2}(\sin 2\theta_{j-1} - \sin 2\theta_j) \Bigg]
\end{aligned} \tag{4.17}$$

and the RMS inductive current can be calculated from (4.6).

Similarly, we can calculate the squared RMS value of inductive current with

$$
\begin{aligned}
I_{l_k}^2 &= \frac{2}{\pi}\int_0^{\frac{\pi}{2}} i_l^2(\theta)\,\mathrm{d}\theta \\
&= \frac{2}{\pi}\sum_{j=1}^{k}\int_{\theta_{j-1}}^{\theta_j}\left(\hat{i}_{l_{j-1}} + \frac{-\hat{\lambda}_k\cos\theta - \hat{\lambda}_{j-1}}{L_j}\right)^2 \mathrm{d}\theta \\
&= \sum_{j=1}^{k}\frac{1}{\pi L_j^2}\Bigg[\left(2L_j^2\hat{i}_{l_{j-1}}^2 - 4L_j\hat{i}_{l_{j-1}}\hat{\lambda}_{j-1} + \hat{\lambda}_k^2 + 2\hat{\lambda}_{j-1}^2\right)(\theta_j - \theta_{j-1}) \\
&\quad +4\left(\hat{\lambda}_{j-1}\hat{\lambda}_k - \hat{i}_{l_{j-1}}\hat{\lambda}_k L_j\right)(\sin\theta_j - \sin\theta_{j-1}) + \frac{\hat{\lambda}_k^2}{2}(\sin 2\theta_j - \sin 2\theta_{j-1})\Bigg] \\
&= \sum_{j=1}^{k}\frac{1}{\pi L_j^2}\Bigg[\left(2L_j^2\hat{i}_{l_{j-1}}^2 - 4L_j\hat{i}_{l_{j-1}}\hat{\lambda}_{j-1} + \hat{\lambda}_k^2 + 2\hat{\lambda}_{j-1}^2\right)(\theta_j - \theta_{j-1}) \\
&\quad +4\left(\hat{\lambda}_{j-1}\hat{\lambda}_k - \hat{i}_{l_{j-1}}\hat{\lambda}_k L_j\right)(\cos\theta_j - \cos\theta_{j-1}) + \frac{\hat{\lambda}_k^2}{2}(\sin 2\theta_{j-1} - \sin 2\theta_j)\Bigg]
\end{aligned}
\tag{4.18}
$$

In this case, the only unknown in (4.18) is the last slope (inductance) L_k, since the other inductances are found *recursively* from previous $k-1$ no-load points. Therefore, it can be seen that (4.18) can be rewritten in the quadratic form

$$
a_{l_k}\left(\frac{1}{L_k}\right)^2 + b_{l_k}\left(\frac{1}{L_k}\right) + c_{l_k} = 0 \tag{4.19}
$$

where a_{l_k}, b_{l_k} and c_{l_k} are given by

$$
a_{l_k} = \left(\hat{\lambda}_k^2 + 2\hat{\lambda}_{k-1}^2\right)(\theta_k - \theta_{k-1}) + 4\hat{\lambda}_{k-1}\hat{\lambda}_k(\cos\theta_k - \cos\theta_{k-1}) + \frac{\hat{\lambda}_k^2}{2}(\sin 2\theta_{k-1} - \sin 2\theta_k) \tag{4.20}
$$

$$
b_{l_k} = 4\hat{i}_{l_{k-1}}\hat{\lambda}_{k-1}(\theta_{k-1} - \theta_k) + 4\hat{i}_{l_{k-1}}\hat{\lambda}_k(\cos\theta_{k-1} - \cos\theta_k) \tag{4.21}
$$

$$
\begin{aligned}
c_{l_k} &= -\pi I_{l_k}^2 + 2\hat{i}_{l_{k-1}}^2(\theta_k - \theta_{k-1}) + \sum_{j=1}^{k-1}\frac{1}{L_j^2}\Bigg[\left(2L_j^2\hat{i}_{l_{j-1}}^2 - 4L_j\hat{i}_{l_{j-1}}\hat{\lambda}_{j-1} + \hat{\lambda}_k^2 + 2\hat{\lambda}_{j-1}^2\right)(\theta_j - \theta_{j-1}) \\
&\quad +4\left(\hat{\lambda}_{j-1}\hat{\lambda}_k - \hat{i}_{l_{j-1}}\hat{\lambda}_k L_j\right)(\cos\theta_j - \cos\theta_{j-1}) + \frac{\hat{\lambda}_k^2}{2}(\sin 2\theta_{j-1} - \sin 2\theta_j)\Bigg]
\end{aligned}
\tag{4.22}
$$

The solution (positive inductance) is given by

$$L_k = \frac{2a_{l_k}}{-b_{l_k} + \sqrt{b_{l_k}^2 - 4a_{l_k}c_{l_k}}} \tag{4.23}$$

Finally, the peak inductive current $\hat{i}_{l_k}$ of point k can be computed from

$$\hat{i}_{l_k} = \hat{i}_{l_{k-1}} + \frac{\hat{\lambda}_k - \hat{\lambda}_{k-1}}{L_k} \tag{4.24}$$

For three-phase transformer, in the case where a delta winding is connected during no-load measurements, we have to take into account the cancellation that occurs for triplen harmonics in the RMS values of currents (seen from the terminals), with methods such as (Neves and Dommel, 1995; Chiesa and Høidalen, 2010).

4.2.2 Extension of the saturation curve beyond and between no-load points

After the conversion of RMS no-load measurements to instantaneous piecewise linear curves, the challenge is to properly extrapolate the curves, because in low-frequency transients such as inrush current, the excitation will increase beyond no-load measurements. For instance, it is proposed in (Martínez Duró *et al.*, 2013, § 5) to extend the piecewise linear inductance curve by adding the air-core inductance directly after the last point of the curve. However, this will lead to a lower y-intercept for the last slope (with respect to the real asymptote), which means that for a given flux linkage, the magnetizing current will be overestimated with this method.

Another method is to use curve fitting techniques to fit a curve to the previous instantaneous points, using the prescribed air-core inductance as an asymptote. This idea was employed for instance in (Høidalen *et al.*, 2011), where the fitted function is the modified Frölich equation of (Chiesa, 2005, p. 45)

$$\lambda = \frac{i}{a + b|i| + c\sqrt{|i|}} + L_\infty i \tag{4.25}$$

where a, b, c are fitting parameters and L_∞ is the saturation inductance (air-core inductance, since we are fitting terminal measurements).

Furthermore, if we assume that the major hysteresis loop has approximately a constant width [2], we can use the method presented in (Høidalen *et al.*, 2011, § 4) to calculate the major loop of the type-96 (static) hysteresis model presented in (Frame *et al.*, 1982).

2. Note that this is not quite correct, as seen in (Lambert *et al.*, 2009, Fig. 1).

The methods presented in this section are used to find the equivalent nonlinear curves *seen from the terminals* of the energized winding during no-load tests. We need to use this data to calculate magnetizing branches in transformer models. This is discussed next.

4.3 Calculation of magnetizing branches for single-phase transformers

The goal is to calculate the nonlinear inductances from no-load measurements and from the air-core inductance. First, let us neglect winding losses (copper and eddy current losses). This will enable us to generalize the method to any series/parallel combination of coils [3].

The single-phase shell-type transformer model is that of Fig. 3.13, which is shown in Fig. 4.2 with the different degrees of freedom in this problem. The previous model actually only illustrates the "magnetic side" (equivalent dual circuit), but without the *electrical* connections of the coils themselves, which is done by connecting the "electric side" of ideal transformers of the model in series/parallel to form windings. This is done deliberately, in order to take into account any possible combination of series/parallel connections of coils.

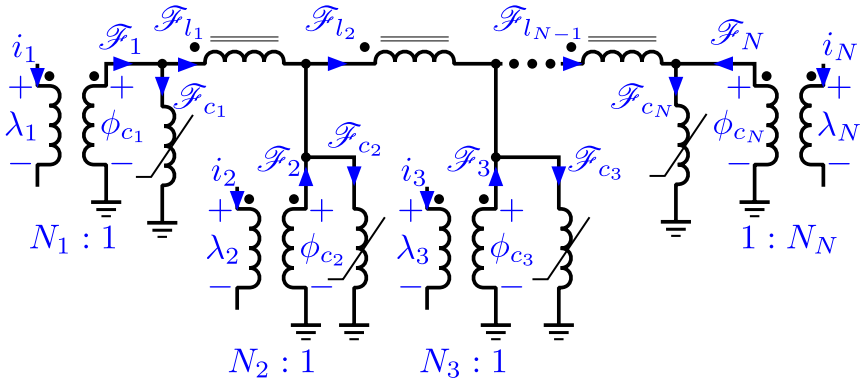

Figure 4.2 Degrees of freedom for the single-phase coupled leakage model without winding losses.

Since the coupled inductance matrix was computed with the method presented in Chapter 3, the degrees of freedom we are interested in are the magnetomotive forces $\mathscr{F}_{c_i}$ (equivalent to currents, since $N_c = 1$ on the magnetic side, as mentioned previously) and magnetic fluxes ϕ_{c_i} (equivalent to flux linkages for the previous reason) of magnetizing branches, in order to determine their nonlinear characteristics. However, the magnetomotive forces $\mathscr{F}_{l_i}$ in the coupled leakage inductances are also unknown, not to mention the magnetomotive forces $\mathscr{F}_i$ of each coil, and the degrees of freedom on the electric side (λ_i and i_i), as seen in Fig. 4.2.

3. Otherwise, because of time derivatives, a general analytical solution is not possible. The inclusion of winding losses in coils will be dealt with numerically in future work (the analytical method of Chapter 2 will also need to be modified to include winding losses).

Hence, for a transformer with N coils, the total number of unknowns is $6N-1$, which is grouped in an array

$$[x] = \left[\mathscr{F}_1 \cdots \mathscr{F}_N, \mathscr{F}_{c_1} \cdots \mathscr{F}_{c_N}, \mathscr{F}_{l_1} \cdots \mathscr{F}_{l_{N-1}}, \phi_{c_1} \cdots \phi_{c_N}, \lambda_1 \cdots \lambda_N, i_1 \cdots i_N\right]^{\mathrm{T}} \tag{4.26}$$

Applying Kirchhoff's Current Law for each node of the magnetic side, we get N equations of the form

$$\mathscr{F}_i - \mathscr{F}_{c_i} + \mathscr{F}_{l_{i-1}} - \mathscr{F}_{l_i} = 0 \tag{4.27}$$

for $i = 1, 2, \cdots, N$, and where we have $\mathscr{F}_{l_0} = 0$ and $\mathscr{F}_{l_N} = 0$.

If we add these N equations, we get

$$\sum_{i=1}^{N} \mathscr{F}_i = \sum_{i=1}^{N} \mathscr{F}_{c_i} \tag{4.28}$$

In other words, the sum of each coil's magnetomotive forces $\mathscr{F}_i$ (i.e. the *total* no-load MMF) is equal to the sum of magnetomotive forces of magnetizing branches $\mathscr{F}_{c_i}$.

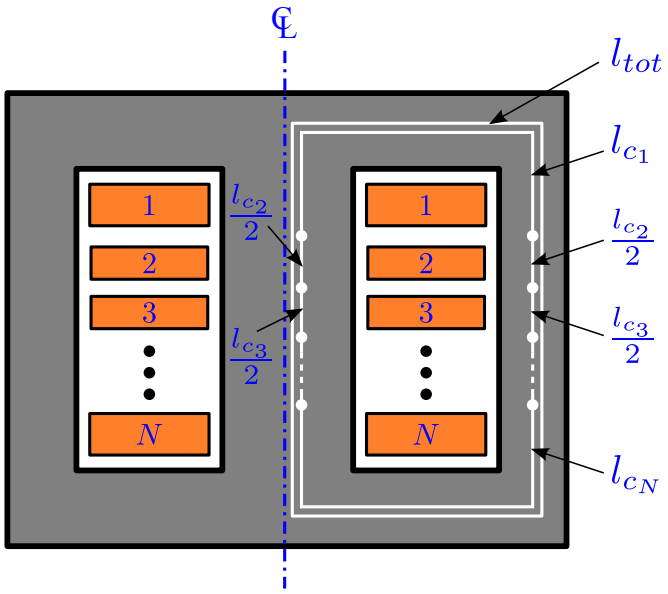

Figure 4.3 Length of each magnetizing branch for a single-phase shell-type transformer with N coils.

The idea behind the new method presented in this section lies in the division of the total no-load MMF along the total (mean) length l_{tot} of the core. The novel aspect of this new method is that flux linkages of magnetizing branches are calculated by taking into account leakage fluxes. Each magnetizing branch has a length of l_{c_i}, as seen in Fig. 4.3, and we can

express each $\mathscr{F}_{c_i}$ as a ratio K_{c_i} of the total no-load MMF [4], where K_{c_i} is given by

$$K_{c_i} = \frac{l_{c_i}}{l_{tot}} \tag{4.29}$$

Therefore, we have another $N-1$ equations for the magnetic side

$$\mathscr{F}_{c_i} = K_{c_i} \sum_{j=1}^{N} \mathscr{F}_j \tag{4.30}$$

for $i = 1, 2, \cdots, N-1$ (the last equation for $i = N$ is not independent, because if we add these N equations, we get (4.28)).

Applying Kirchhoff's Voltage Law for each mesh of the magnetic side, we have the following $N-1$ equations

$$\phi_{c_i} - \phi_{c_{i+1}} - \sum_{j=1}^{N-1} \mathscr{P}_{ij} \mathscr{F}_{l_j} = 0 \tag{4.31}$$

for $i = 1, 2, \cdots, N-1$ and where $\mathscr{P}_{ij} = \mathscr{L}(i,j)$, since $N_c = 1$. Each element of the coupled leakage inductance matrix $\mathscr{L}(i,j)$ is calculated according to (3.14). Actually, these are the equations that enables to remove the leakage fluxes, associated with $\mathscr{P}_{ij}\mathscr{F}_{l_j}$, from the fluxes of magnetizing branches ϕ_{c_i} and $\phi_{c_{i+1}}$.

The next $2N$ equations are those of the N ideal transformers (of turns ratio $N_i : 1$) of Fig. 4.2, given by

$$\lambda_i = N_i \phi_{c_i} \tag{4.32}$$

$$i_i = \frac{\mathscr{F}_i}{N_i} \tag{4.33}$$

for $i = 1, 2, \cdots, N$.

In order to solve this system, we need another $N+1$ equations that come from the electrical connections of each coil and that link with the flux linkage λ and current i measured from the terminals of a winding in a no-load test. Obviously, in a no-load test, not all coils of the transformer are energized. Therefore, if k coils are not energized, we will have k equations of the type $i_i = 0$. The remaining $N + 1 - k$ equations will be the m KCL equations (for m nodes) and n KVL equations (for n meshes). The terminal's current i will appear as a source in one of the m equations and the terminal's flux linkage λ will be a source in one of the n equations.

4. This is similar to the idea of length ratios presented in (Gonzalez-Molina *et al.*, 2004, § 5.5), except that the total length l_{tot} is used here to normalize, instead of leg length.

4.3.1 Simple example

In order to understand the previous method, let us apply it to a simple 4-coil fictitious transformer, where coils 1–3 are energized and coil 4 is left opened, as illustrated in Fig. 4.4 (only electric side shown, since the magnetic side is given by Fig. 4.2). Using the previous method, the system of equations for this problem will be given by

$$\begin{aligned}
\mathscr{F}_1 - \mathscr{F}_{c_1} - \mathscr{F}_{l_1} &= 0 \\
\mathscr{F}_2 - \mathscr{F}_{c_2} + \mathscr{F}_{l_1} - \mathscr{F}_{l_2} &= 0 \\
\mathscr{F}_3 - \mathscr{F}_{c_3} + \mathscr{F}_{l_2} - \mathscr{F}_{l_3} &= 0 \\
\mathscr{F}_4 - \mathscr{F}_{c_4} + \mathscr{F}_{l_3} &= 0
\end{aligned}$$

$$\begin{aligned}
\mathscr{F}_{c_1} - K_{c_1}\mathscr{F}_1 - K_{c_1}\mathscr{F}_2 - K_{c_1}\mathscr{F}_3 - K_{c_1}\mathscr{F}_4 &= 0 \\
\mathscr{F}_{c_2} - K_{c_2}\mathscr{F}_1 - K_{c_2}\mathscr{F}_2 - K_{c_2}\mathscr{F}_3 - K_{c_2}\mathscr{F}_4 &= 0 \\
\mathscr{F}_{c_3} - K_{c_3}\mathscr{F}_1 - K_{c_3}\mathscr{F}_2 - K_{c_3}\mathscr{F}_3 - K_{c_3}\mathscr{F}_4 &= 0
\end{aligned}$$

$$\begin{aligned}
\phi_{c_1} - \phi_{c_2} - \mathscr{P}_{11}\mathscr{F}_{l_1} - \mathscr{P}_{12}\mathscr{F}_{l_2} - \mathscr{P}_{13}\mathscr{F}_{l_3} &= 0 \\
\phi_{c_2} - \phi_{c_3} - \mathscr{P}_{21}\mathscr{F}_{l_1} - \mathscr{P}_{22}\mathscr{F}_{l_2} - \mathscr{P}_{23}\mathscr{F}_{l_3} &= 0 \\
\phi_{c_3} - \phi_{c_4} - \mathscr{P}_{31}\mathscr{F}_{l_1} - \mathscr{P}_{32}\mathscr{F}_{l_2} - \mathscr{P}_{33}\mathscr{F}_{l_3} &= 0
\end{aligned}$$

$$\begin{aligned}
\lambda_1 - N_1\phi_{c_1} &= 0 \\
\lambda_2 - N_2\phi_{c_2} &= 0 \\
\lambda_3 - N_3\phi_{c_3} &= 0 \\
\lambda_4 - N_4\phi_{c_4} &= 0 \\
i_1 - \frac{\mathscr{F}_1}{N_1} &= 0 \\
i_2 - \frac{\mathscr{F}_2}{N_2} &= 0 \\
i_3 - \frac{\mathscr{F}_3}{N_3} &= 0 \\
i_4 - \frac{\mathscr{F}_4}{N_4} &= 0
\end{aligned}$$

$$
\begin{aligned}
i_4 &= 0 \\
i_1 + i_3 &= i \\
-i_1 + i_2 &= 0 \\
\lambda_1 + \lambda_2 &= \lambda \\
-\lambda_1 - \lambda_2 + \lambda_3 &= 0
\end{aligned}
$$

In this case, we have $m = 2$ KCL equations, $n = 2$ KVL equations and $k = 1$ opened-coil equation. If we had considered other electrical connections for this 4-coil transformer, only the last 5 equations would have changed ($N + 1$ equations).

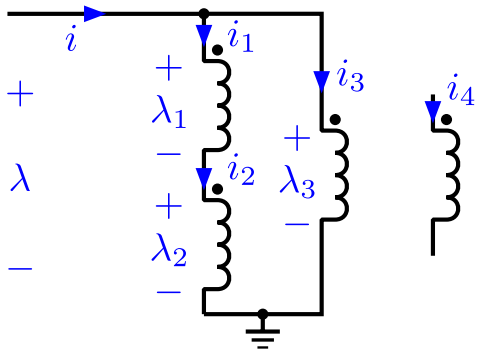

Figure 4.4 Simple example of a 4-coil transformer.

4.3.2 Application example and validation

The previous method was applied to calculate the magnetizing branches of the 360 MVA two-winding single-phase shell-type transformer presented in § 2.6, for the model shown in Fig. 4.2.

Four no-load measurements were available in the test report for the low-voltage winding, at excitation levels of 90%, 100%, 105% and 110%, as presented in Table 4.1. The air-core inductance was not available, but it was calculated with COMSOL in 3-D to be $L_{air} = 31.85$ mH for the low-voltage winding (same winding as the no-load tests). The coupled leakage inductance matrix was calculated previously for this transformer in Chapter 3.

The first step is to convert no-load RMS values to peak values with the method described in § 4.2. The result is shown in Fig. 4.5. Afterward, the peak values for the nonlinear inductance are fitted to the modified Frölich equation (4.25), along with the air-core inductance viewed from this winding (which is L_∞ of the modified Frölich equation). The results are shown in Fig. 4.6.

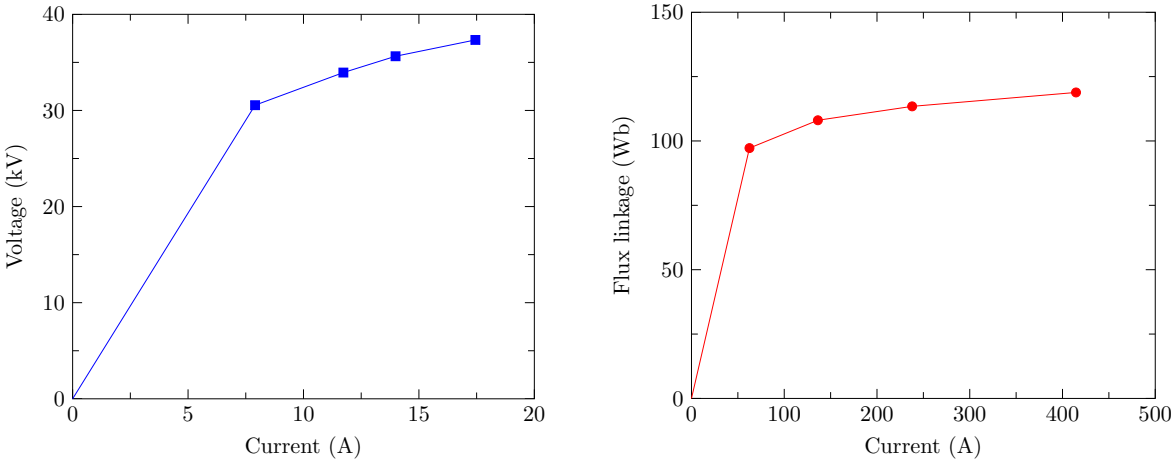

(a) Piecewise-linear resistance

(b) Piecewise-linear inductance

Figure 4.5 Resulting curves calculated from RMS no-load measurements.

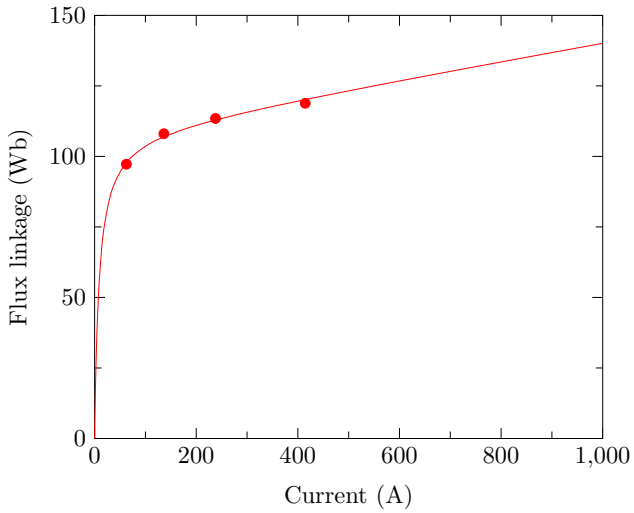

Figure 4.6 Modified Frölich equation fitted to the piecewise-linear inductance.

Table 4.1 No-load measurements (RMS) for the LV winding of the 360 MVA transformer

Voltage	**Current**	**Losses [kW]**
90%	0.297%	120.71
100%	0.464%	167.72
105%	0.700%	200.87
110%	1.157%	245.39

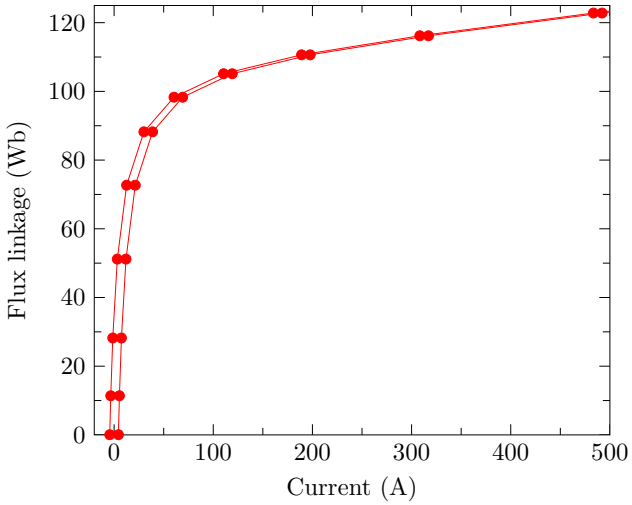

Figure 4.7 Type-96 hysteresis loop with constant width.

If we assume that the width of the major hysteresis loop is constant, we can calculate (with the method mentioned in § 4.2) the equivalent major loop for the Type-96 hysteresis model seen from the low-voltage terminals, which yields the loop of Fig. 4.7. Of course, all of this is an approximation to palliate the lack of proper hysteresis measurements. If no-load waveforms are available (that extend sufficiently into saturation), these can be used instead in the second step.

The second step is to properly divide the nonlinear characteristic $\lambda - i$, viewed from the terminals of a winding, within the model of Fig. 4.2. This is done using the method presented in § 4.3, taking into account the coupled leakage inductances.

In order to verify that the method of this last step properly divides the nonlinear characteric inside the model of Fig. 4.2, a simulation was made in EMTP-RV, where the low-voltage winding of the 360 MVA was connected to a 26.4 kV (RMS) voltage source through a 1 Ω resistor. The results are shown in Figs. 4.8 and 4.9, where *divided* refers to the quantities seen

from the terminals of the low-voltage winding for the model of Fig. 4.2, while *total* relates to the original terminal quantities calculated from the first step, before the division of the second step.

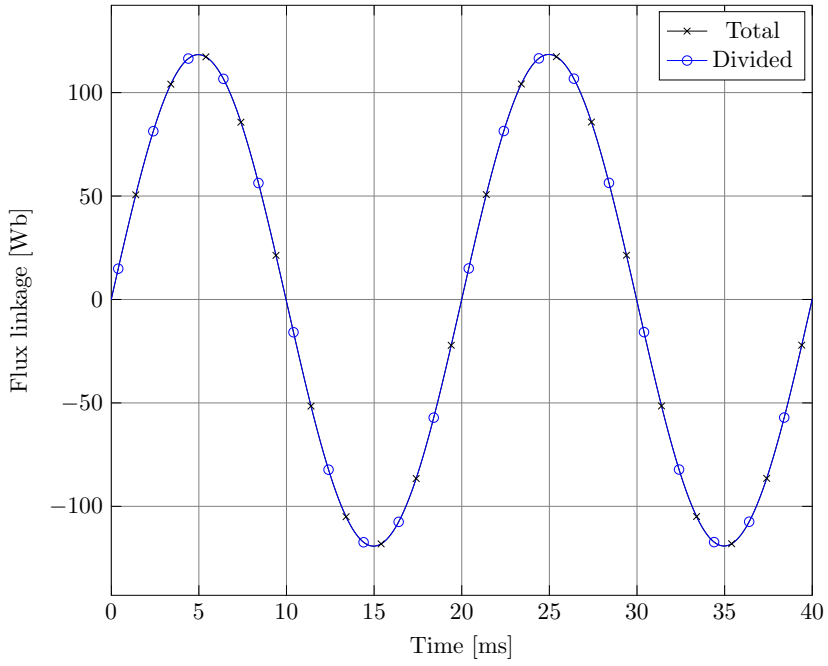

Figure 4.8 Flux linkages across the low-voltage terminals of the 360 MVA transformer.

From the previous results, it can be seen that the nonlinear characteristic $\lambda - i$, viewed from the terminals of a winding, is properly divided with this new method. However, as mentioned earlier, it must be emphasized that winding losses were neglected, since a general analytical solution does not exist for the core division with winding losses. The numerical solution with winding losses will be studied in future work.

4.4 Calculation of magnetizing branches for three-phase transformers

Similarly to the single-phase transformer we can write the equations for the coupled leakage model of the shell-type three-phase transformer presented in Fig. 3.16. Again, winding losses are neglected, in order to derive a general analytical solution. The numerical solution with winding losses will be considered in future work.

Applying Kirchhoff's Current Law for each node on the magnetic side, we get $N - 1$ equations of the form

$$\mathscr{F}_{A_i} - \mathscr{F}_{A_{c_i}} + \mathscr{F}_{A_{l_{i-1}}} - \mathscr{F}_{A_{l_i}} = 0 \tag{4.34}$$

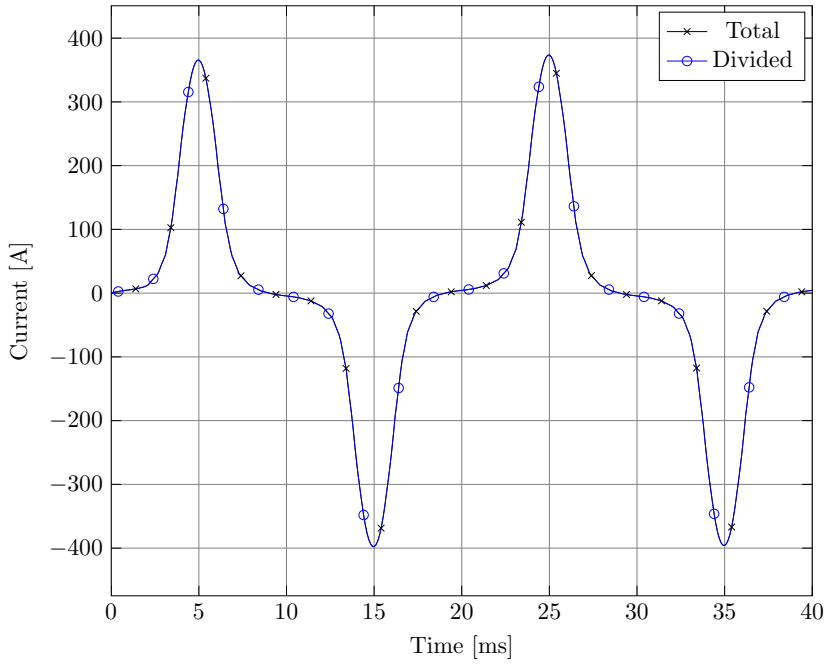

Figure 4.9 Currents in the low-voltage terminal of the 360 MVA transformer.

for $i = 1, 2, \cdots, N-1$, and where we have $\mathscr{F}_{A_{l_0}} = 0$, for phase A. To this, we add the N^{th} KCL equation of this phase

$$\mathscr{F}_{A_N} - \mathscr{F}_{A_{c_N}} + \mathscr{F}_{A_{l_{N-1}}} - \mathscr{F}_{AB_c} = 0 \tag{4.35}$$

For phase B, the first and last KCL equations are given by

$$\mathscr{F}_{B_1} - \mathscr{F}_{B_{c_1}} - \mathscr{F}_{B_{l_1}} + \mathscr{F}_{AB_c} = 0 \tag{4.36}$$

$$\mathscr{F}_{B_N} - \mathscr{F}_{B_{c_N}} + \mathscr{F}_{B_{l_{N-1}}} - \mathscr{F}_{BC_c} = 0 \tag{4.37}$$

and in between, there are $N-2$ KCL equations

$$\mathscr{F}_{B_i} - \mathscr{F}_{B_{c_i}} + \mathscr{F}_{B_{l_{i-1}}} - \mathscr{F}_{B_{l_i}} = 0 \tag{4.38}$$

for $i = 2, 3, \cdots, N-1$. For phase C, the first KCL equation is

$$\mathscr{F}_{C_1} - \mathscr{F}_{C_{c_1}} - \mathscr{F}_{C_{l_1}} + \mathscr{F}_{BC_c} = 0 \tag{4.39}$$

and the remaining $N-1$ KCL equations

$$\mathscr{F}_{C_i} - \mathscr{F}_{C_{c_i}} + \mathscr{F}_{C_{l_{i-1}}} - \mathscr{F}_{C_{l_i}} = 0 \tag{4.40}$$

for $i = 2, 3, \cdots, N$, and where we have $\mathscr{F}_{C_{l_N}} = 0$. This gives a total of $3N$ KCL equations for the magnetic side (N equations per phase).

If we add these N equations for each phase, we get

$$\sum_{i=1}^{N} \mathscr{F}_{A_i} = \sum_{i=1}^{N} \mathscr{F}_{A_{c_i}} + \mathscr{F}_{AB_c} \tag{4.41}$$

$$\sum_{i=1}^{N} \mathscr{F}_{B_i} = \sum_{i=1}^{N} \mathscr{F}_{B_{c_i}} - \mathscr{F}_{AB_c} + \mathscr{F}_{BC_c} \tag{4.42}$$

$$\sum_{i=1}^{N} \mathscr{F}_{C_i} = \sum_{i=1}^{N} \mathscr{F}_{C_{c_i}} - \mathscr{F}_{BC_c} \tag{4.43}$$

In other words, the sum of each coil's magnetomotive forces $\mathscr{F}_i$ of each phase (i.e. the *total* no-load MMF per phase) is equal to the sum of magnetomotive forces of magnetizing branches $\mathscr{F}_{c_i}$, plus or minus the magnetomotive forces of yokes.

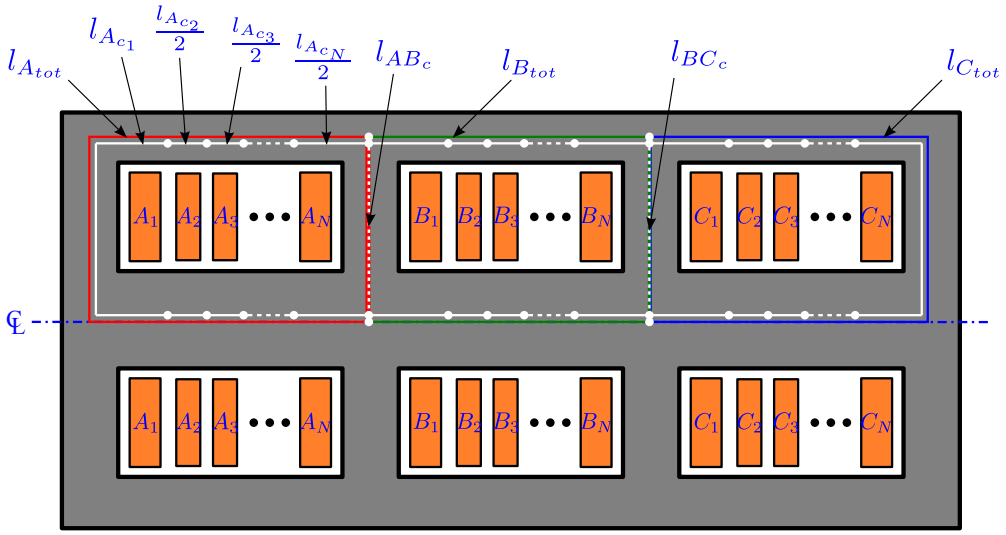

Figure 4.10 Length of each magnetizing branch for a Three-phase shell-type transformer with N coils.

Hence, the idea behind the new method for the three-phase shell-type transformer lies in the division of the total no-load MMF along the total (mean) length l_{tot} of the core for each phase. The difference with the single-phase shell-type transformer comes from the presence

of yokes, which can contribute additively or subtractively to the total no-load MMF of each phase. Therefore, in this case, the total lengths are given by (see Fig. 4.10)

$$l_{A_{tot}} = \sum_{i=1}^{N} l_{A_{c_i}} + l_{AB_c} \tag{4.44}$$

$$l_{B_{tot}} = \sum_{i=1}^{N} l_{B_{c_i}} - l_{AB_c} + l_{BC_c} \tag{4.45}$$

$$l_{C_{tot}} = \sum_{i=1}^{N} l_{C_{c_i}} - l_{BC_c} \tag{4.46}$$

and each magnetizing branch (represented in the model by a nonlinear inductance) has a length of $l_{j_{c_i}}$, where $j = A, B, C$. As done previously for the single-phase transformer, we can express each $\mathscr{F}_{c_i}$ as a ratio K_{c_i} of the total no-load MMF, where the K_{c_i} are given by (4.29). This gives another $3(N-1)$ equations for the magnetic side

$$\mathscr{F}_{A_{c_i}} = K_{A_{c_i}} \sum_{j=1}^{N} \mathscr{F}_{A_j} \tag{4.47}$$

$$\mathscr{F}_{B_{c_i}} = K_{B_{c_i}} \sum_{j=1}^{N} \mathscr{F}_{B_j} \tag{4.48}$$

$$\mathscr{F}_{C_{c_i}} = K_{C_{c_i}} \sum_{j=1}^{N} \mathscr{F}_{C_j} \tag{4.49}$$

$$\tag{4.50}$$

for $i = 2, 3, \cdots, N-1$. To this, we add the two equations for the yokes

$$\mathscr{F}_{AB_c} = K_{A_{AB_c}} \sum_{j=1}^{N} \mathscr{F}_{A_j} \tag{4.51}$$

$$\mathscr{F}_{BC_c} = K_{C_{BC_c}} \sum_{j=1}^{N} \mathscr{F}_{C_j} \tag{4.52}$$

where $K_{A_{AB_c}} = \frac{l_{AB_c}}{l_{A_{tot}}}$ and $K_{C_{BC_c}} = \frac{l_{BC_c}}{l_{C_{tot}}}$.

Afterward, applying Kirchhoff's Voltage Law for each mesh of the magnetic side, we have

the following $3(N-1)$ equations

$$\phi_{A_{c_i}} - \phi_{A_{c_{i+1}}} - \sum_{j=1}^{N-1} \mathscr{P}_{A_{ij}} \mathscr{F}_{A_{l_j}} = 0 \tag{4.53}$$

$$\phi_{B_{c_i}} - \phi_{B_{c_{i+1}}} - \sum_{j=1}^{N-1} \mathscr{P}_{B_{ij}} \mathscr{F}_{B_{l_j}} = 0 \tag{4.54}$$

$$\phi_{C_{c_i}} - \phi_{C_{c_{i+1}}} - \sum_{j=1}^{N-1} \mathscr{P}_{C_{ij}} \mathscr{F}_{C_{l_j}} = 0 \tag{4.55}$$

for $i = 1, 2, \cdots, N-1$ and where $\mathscr{P}_{ij} = \mathscr{L}(i,j)$, as mentioned previously. There are two additional KVL equations that include the yokes

$$\phi_{A_{c_N}} - \phi_{B_{c_1}} - \phi_{AB_c} = 0 \tag{4.56}$$

$$\phi_{B_{c_N}} - \phi_{C_{c_1}} - \phi_{BC_c} = 0 \tag{4.57}$$

The next $6N$ equations are those of the $3N$ ideal transformers (of turns ratio $N_i : 1$) of Fig. 3.16, given by

$$\lambda_{A_i} = N_i \phi_{A_{c_i}} \tag{4.58}$$

$$-\lambda_{B_i} = N_i \phi_{B_{c_i}} \tag{4.59}$$

$$\lambda_{C_i} = N_i \phi_{C_{c_i}} \tag{4.60}$$

$$i_{A_i} = \frac{\mathscr{F}_{A_i}}{N_i} \tag{4.61}$$

$$-i_{B_i} = \frac{\mathscr{F}_{B_i}}{N_i} \tag{4.62}$$

$$i_{C_i} = \frac{\mathscr{F}_{C_i}}{N_i} \tag{4.63}$$

for $i = 1, 2, \cdots, N$. Note that the negative signs in (4.59) and (4.62) take into account the fact that in general, the center phase (B) of a three-phase shell-type transformer is wound in the opposite direction to the outer phases (A and C), as mentioned in (Lambert *et al.*, 2014b, Footnote 7).

The remaining $3N-3$ equations are nodes KCL and meshes KVL on the electric side, linking with the measured no-load terminal currents (i_A, i_B and i_C) and flux linkages (λ_A, λ_B and λ_C). Just like the single-phase case, this takes into account series/parallel connections of coils, and the $3k$ unloaded coils contribute to the $3k$ equations $i_{A_i} = 0$, $i_{B_i} = 0$ and $i_{C_i} = 0$, for $i = 1, 2, \cdots, k$.

4.5 Conclusion

In this chapter, a new approach was proposed to properly divide terminal no-load measurements to calculate the magnetizing branch characteristics for shell-type transformers. This new method takes into account coupled leakage inductances, which proves to be important as the core saturates, as seen in (Jazebi *et al.*, 2013). However, in that paper, leakage inductances were only taken into account to calculate saturation inductances, instead of modifying the whole nonlinear curves of each magnetizing branch, as done in this chapter.

In order to find a general analytical solution, taking into account any possible series or parallel electrical connection of coils, winding losses were neglected in the derivation of this new method. The inclusion of winding losses will be considered in future work.

CHAPTER 5

DISCRETE ELECTROMAGNETISM

As seen in Chapters 1 and 3, even though a lot of transformer models are called "topological" models, there exist different variants of these models for a given transformer geometry. It was shown that this is caused by the way leakage "paths" are accounted for in divided and integral flux approaches, and that the divided flux approach is the result of mathematical manipulations, as opposed to the integral flux approach, which is more physically accurate. Another difference between those topological models comes from the place where these leakage paths are connected to the core, as seen previously.

The main problem with these topological models is the incorrect representation of leakage flux as the core saturates. It has been proposed in numerous models [1] to add shunt air reluctances to each core reluctances, to account for flux leakage in air as the core saturates. However, when we defined reluctances and flux tubes in Chapter 1, it was assumed that flux cannot leak from the side of the tube. Therefore, there is a fundamental problem with these topological transformer models, that comes from the classical definition of reluctances and flux tubes (flux tubes cannot be clearly defined for the core parts as they saturate). However, this does not mean that a saturable "topological" model cannot give satisfying results, provided that sufficient measurements are available to adequately characterize the core nonlinearities, which was the topic of the previous chapter.

The state of the art in transformer modeling (as well as other electromagnetic devices) is converging towards physically-based discrete electromagnetic models (e.g. finite element models), because computing power is ever increasing. For instance, today most commercial field simulators include interfaces to couple electric circuits to field models and there are a number of papers on this coupling with electric circuits (Tsukerman *et al.*, 1993; De Gersem *et al.*, 1998; Benderskaya *et al.*, 2004; Escarela-Perez *et al.*, 2009). Conversely, we could also imagine coupling field equations in circuit simulators, such as EMTP. According to recent litterature, this idea is gaining more interest (Schöps *et al.*, 2013, p. 2064). Another way to couple electric circuits with field models is to create an interface between the two programs, such as in (Dennetière *et al.*, 2007).

Since circuit elements are "lumped" elements (as opposed to the "distributed" behavior), therefore dependent on a particular discretization of space, one can rightfully ask what is the link between electric (or magnetic) circuits and discrete electromagnetics (such as finite

1. Such as (Zirka *et al.*, 2012, Fig. 3) or (Mork *et al.*, 2007a, Fig. 3).

elements, finite differences, finite integration, etc.)? Is there a better (more general) theoretical background than electric/magnetic flux tubes to discretize space into electric/magnetic circuits, so that the size of circuits would be related to mesh size in discrete electromagnetics?

The purpose of this chapter is to bridge the existing gap between electric/magnetic circuit theory and discrete electromagnetics, and to provide a better theoretical framework for what could be called *electromagnetic circuit theory*. This is particularly important to develop more sophisticated models, not only for transformers, but also for transmission lines or machines. However, the development of those models will have to be covered in future work.

First, it is shown that the concept of flux tube can be extended to allow for leakage through the sides of the tube. This leads to a more appropriate definition of magnetic circuit theory, derived from Maxwell's equations in magnetostatic.

Second, a similar extension is made for current tubes to allow leakage through the sides of the tube, which enables to give a more rigorous explanation of electric circuit theory. Furthermore, the coupling between electric and magnetic circuits is described, using Maxwell's equations in magnetoquasistatic. The circuits (and associated meshes) are shown to be dual and orthogonal to each other.

Third, this theory is generalized to the full set of Maxwell's equation in dynamics, in order to include capacitances, which leads to the electromagnetic circuit theory. It is also explained that this theory is very similar to other discrete (or finite) field formulations (such as finite element or finite difference), therefore bridging the gap between circuit theory and discrete electromagnetics.

Fourth, a more adequate definition of resistance, reluctance and capacitance is given, using what is called the *discrete Hodge operator*. It is also explained that the main difference between finite field formulations lies in the way these elements are calculated.

Fifth, two boundary conditions are described: the perfect electric boundary and the perfect magnetic boundary.

5.1 Magnetostatics

Since current is essentially confined inside conductors at low frequencies (that is for conductors surrounded by insulation), as mentioned in Chapter 3, leakages are essentially magnetic. This explains why one of the early attempts to discretize magnetic fields with equivalent magnetic circuits from Turowski, in what he calls the Reluctance Network Method (RNM), was concentrated in this direction (Turowski, 1989; Turowski *et al.*, 1990; Turowski, 1998; Rais *et al.*, 1988; Koppikar *et al.*, 2000). The goal of this method is essentially to model leakage flux to calculate stray losses. The Reluctance Network Method is still used today

by researchers and manufacturers, see (Soto *et al.*, 2008) and (López-Fernández *et al.*, 2012, Table 3.3). It is also used to calculate the leakage field in air-core reactors in (Santos Nunes *et al.*, 2013).

The Reluctance Network Method is based on an earlier paper by King, which uses finite differences (King, 1966) [2]. More information on this method can be found in (Turowski, 1995). Similar methods to the RNM were developped in (Iwahara and Miyazawa, 1981; Davey and King, 1981).

In the RNM, Instead of flux tubes (where magnetic flux enters from one end of the tube and exits from the other end, as seen in Fig. 1.1), space is discretized into a *primal mesh* containing cells (e.g. tetrahedra or hexahedra), such as that of Fig. 5.1. Comparing this cell with the flux tube of Fig. 1.1, one can see that magnetic flux is now allowed to leak from all sides (surfaces) of the cell. One can also see that each reluctance is actually shared between two adjacent cells, and that the magnetic circuit actually lies in the "middle" of the cells on what is called the *dual mesh*. We will come back to this later.

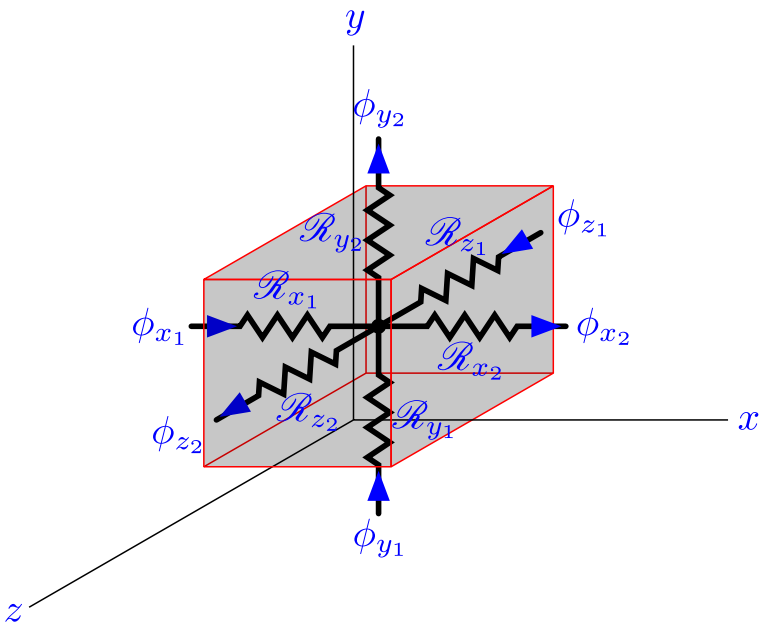

Figure 5.1 Magnetostatic cell without magnetomotive force sources.

Since magnetic induction is solenoidal (zero divergence), the sum of magnetic fluxes at the central magnetic node of Fig. 5.1 (using Gauss's theorem (1.18)) is

$$-\phi_{x_1} + \phi_{x_2} - \phi_{y_1} + \phi_{y_2} - \phi_{z_1} + \phi_{z_2} = 0 \tag{5.1}$$

2. Actually, this idea was also used earlier in (Roberts, 1960).

which is equivalent to Kirchhoff's current law (KCL) for magnetic circuits.

In the Reluctance Network Method, each reluctance $\mathscr{R}_i$ is calculated by (Turowski, 1995, p. 152)

$$\mathscr{R}_i = \frac{l_i}{\mu_0 S_i} \tag{5.2}$$

where l_i is the reluctance's "length" (between barycenters) and S_i is its cross-section, as shown in (Turowski, 1995, Fig. 4.7). Because this method is used to compute the leakage field in transformers, the permeability of each reluctance is that of vacuum μ_0. We can already anticipate a problem with this definition: how to calculate the reluctance at the interface of two materials (with different permeabilities)? We will come back to this, but first, let us talk about magnetomotive forces.

In Fig. 5.1, it was assumed that there was no current source, in order to compare with the previous definition of the flux tube of Fig. 1.1. Let us now look at 4 adjacent cells of some primal mesh (which has more than four cells, just to avoid discussing about boundary conditions now), as illustrated in Fig. 5.2 (again assuming magnetostatics). The primal (electric) mesh is illustrated in red and the dual (magnetic) mesh is shown in black. A current I_y is flowing across the surface $\tilde{S}$, formed by the edges $\tilde{L}_1$, $\tilde{L}_2$, $\tilde{L}_3$ and $\tilde{L}_4$ of the dual mesh (where $\tilde{}$ denotes entities on the dual mesh).

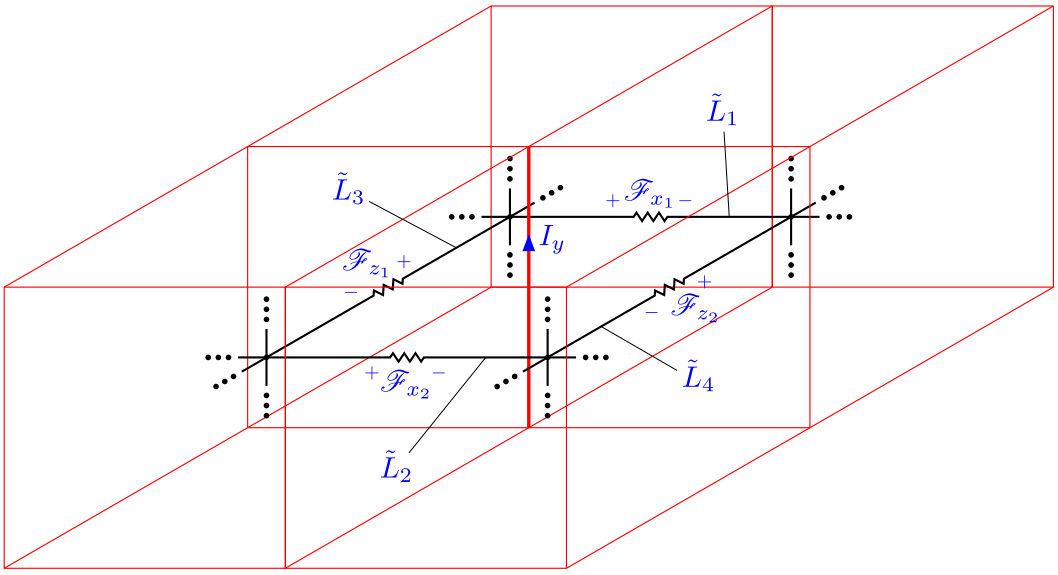

Figure 5.2 A loop of reluctances surrounding a current.

Using Stokes' theorem (1.31) with (1.2) along the closed loop $\tilde{L}$ in Fig. 5.2 (formed by the edges $\tilde{L}_1$, $\tilde{L}_2$, $\tilde{L}_3$ and $\tilde{L}_4$), along with the definition of current (1.10) and magnetomotive

force (1.14), we get

$$\mathscr{F}_{z_1} - \mathscr{F}_{z_2} - \mathscr{F}_{x_1} + \mathscr{F}_{x_2} = I_y \tag{5.3}$$

However, according to Kirchhoff's voltage law (KVL), the sum of magnetomotive forces around a loop must be zero (because in Hopkinsons' analogy, MMF is analog to EMF). Therefore, the current source I_y must be inserted as a magnetomotive force source in a cut and propagated along each branch of the cut, as discussed in § 1.1.7 or (Turowski, 1995, pp. 152–153).

Since Maxwell's equations in magnetostatic are fully respected with (5.1) and (5.3), one might rightfully ask where is the approximation in this discretization? The approximation is in fact in the discretization of the constitutive equation (1.5), i.e. in the way reluctances are calculated, such as with (1.21) and (5.2). We will come back to this later, but first, let us study the coupling between primal and dual meshes.

5.2 Magnetoquasistatics

The next step is to include the electric circuit and to couple it with the magnetic circuit. To do so, let us start by defining the (oriented) integral quantities corresponding to the vector potentials $\vec{A}$ and $\vec{T}$.

The path integral of the electric vector potential $\vec{T}$ along a curve $\tilde{L}$, given by

$$\mathscr{T} = \int_{\tilde{L}} \vec{T} \cdot \mathrm{d}\vec{l} \tag{5.4}$$

where $\mathrm{d}\vec{l}$ is the path's tangent vector. The integral quantity $\mathscr{T}$ is called *loop current* in (Demenko *et al.*, 2008, p. 718), and it is nameless in (Tonti, 2001, Table 2). For lack of a better name, $\mathscr{T}$ will be called loop current in this work.

Similarly, the path integral of the magnetic vector potential $\vec{A}$ along a curve L, given by

$$\mathscr{A} = \int_{L} \vec{A} \cdot \mathrm{d}\vec{l} \tag{5.5}$$

where $\mathrm{d}\vec{l}$ is the path's tangent vector. The integral quantity $\mathscr{A}$ is called *loop flux* in (Demenko *et al.*, 2008, p. 718), and *electrokinetic momentum* in (Tonti, 2001, Table 2). In order to be consistent, $\mathscr{A}$ will be called loop flux in this work.

Integrating on both sides of (1.29) on a surface $\tilde{S}$ (bounded by four edges $\tilde{L}_1$, $\tilde{L}_2$, $\tilde{L}_3$ and $\tilde{L}_4$) and using Stokes' theorem (1.31), along with the definitions of current (1.10) and loop

current (5.4), we get

$$\oint_{\tilde{L}} \vec{T} \cdot \mathrm{d}\vec{l} = \iint_{\tilde{S}} \vec{J} \cdot \mathrm{d}\vec{s}$$

$$\int_{\tilde{L}_1} \vec{T} \cdot \mathrm{d}\vec{l_1} + \int_{\tilde{L}_2} \vec{T} \cdot \mathrm{d}\vec{l_2} + \int_{\tilde{L}_3} \vec{T} \cdot \mathrm{d}\vec{l_3} + \int_{\tilde{L}_4} \vec{T} \cdot \mathrm{d}\vec{l_4} = I_y$$

$$\mathscr{T}_{z_1} - \mathscr{T}_{z_2} - \mathscr{T}_{x_1} + \mathscr{T}_{x_2} = I_y \tag{5.6}$$

Using (5.6) in (5.3), we get

$$\mathscr{F}_{z_1} - \mathscr{T}_{z_1} - \mathscr{F}_{z_2} + \mathscr{T}_{z_2} - \mathscr{F}_{x_1} + \mathscr{T}_{x_1} + \mathscr{F}_{x_2} - \mathscr{T}_{x_2} = 0 \tag{5.7}$$

Therefore, the currents of the electric circuit can be coupled to the magnetic circuit through controlled MMF sources, controlled by loop currents, as seen in Fig. 5.3.

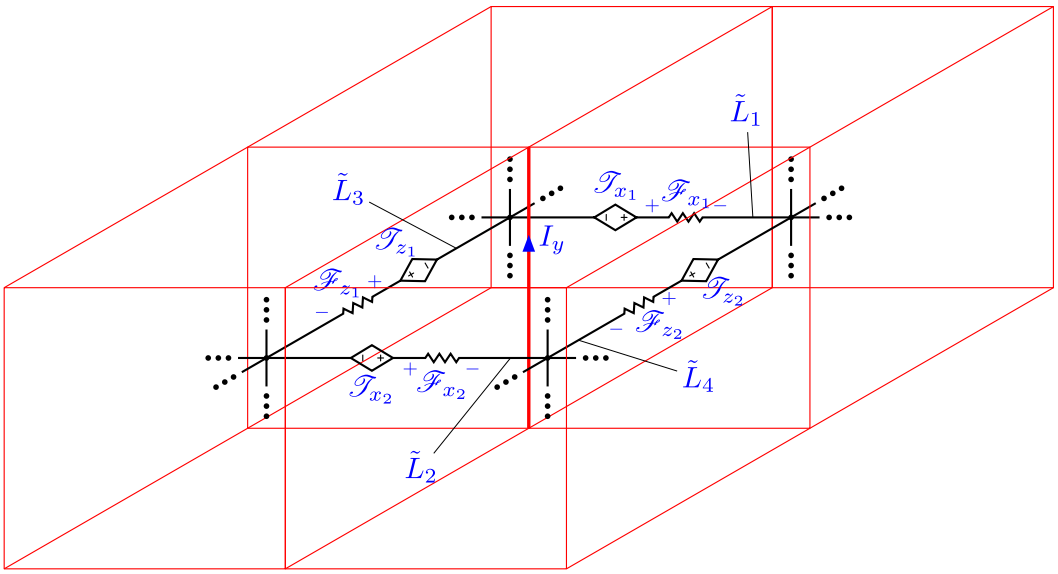

Figure 5.3 A loop of reluctances including couplings to the electric circuit.

Similarly to flux tubes, the concept of current tubes defined in § 1.1.4 can be generalized to allow for current leakages on the sides, which gives the hexahedral cell shown in Fig. 5.4 in magnetoquasistatics (magnetic induction is not included, yet). In this case, the cells of Fig. 5.4 are defined on the dual mesh and the electric circuit lies in the "middle", on the edges of the primal mesh.

Let us now look at 4 adjacent cells of some dual mesh (again to avoid discussing about boundary conditions now), as illustrated in Fig. 5.5 (assuming magnetoquasistatics). The

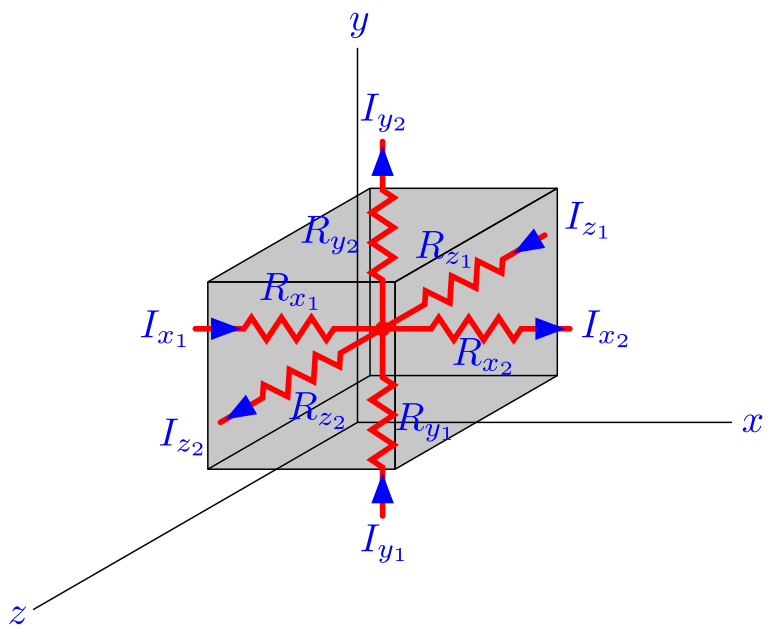

Figure 5.4 Resistive cell without electromotive force sources.

primal (electric) mesh is illustrated in red and the dual (magnetic) mesh is shown in black. A time-varying flux $\frac{\mathrm{d}\phi_z}{\mathrm{d}t}$ is flowing across the surface S, formed by the edges L_1, L_2, L_3 and L_4 of the primal mesh.

Using Stokes' theorem (1.31) with (1.1) along the closed loop L in Fig. 5.5 (formed by the edges L_1, L_2, L_3 and L_4), and using (5.5) and (1.26), we get

$$e_{x_1} + \frac{\mathrm{d}\mathscr{A}_{x_1}}{\mathrm{d}t} - e_{x_2} - \frac{\mathrm{d}\mathscr{A}_{x_2}}{\mathrm{d}t} + e_{y_2} + \frac{\mathrm{d}\mathscr{A}_{y_2}}{\mathrm{d}t} - e_{y_1} - \frac{\mathrm{d}\mathscr{A}_{y_1}}{\mathrm{d}t} = 0 \tag{5.8}$$

Therefore, the time-variations of magnetic fluxes in the magnetic circuit can be coupled to the electric circuit through controlled EMF sources, controlled by the time-variation of loop fluxes, as seen in Fig. 5.5.

Note: As mentioned in § 1.1.8, the assertion in (Turowski, 1995, p. 174) that Buntenbach's analogy (permeances are represented by capacitances in the magnetic circuit) is necessary to model time-dependent fields is incorrect. It can clearly be seen from the previous exemple that the time-dependence can be taken into account through proper coupling of magnetic and electric circuits. Therefore, eddy currents can be represented without the use of *transference* (Turowski, 1995, p. 176), from the time variation of loop fluxes in the electric circuit (induced electromotive forces, which will create currents in the electric circuit).

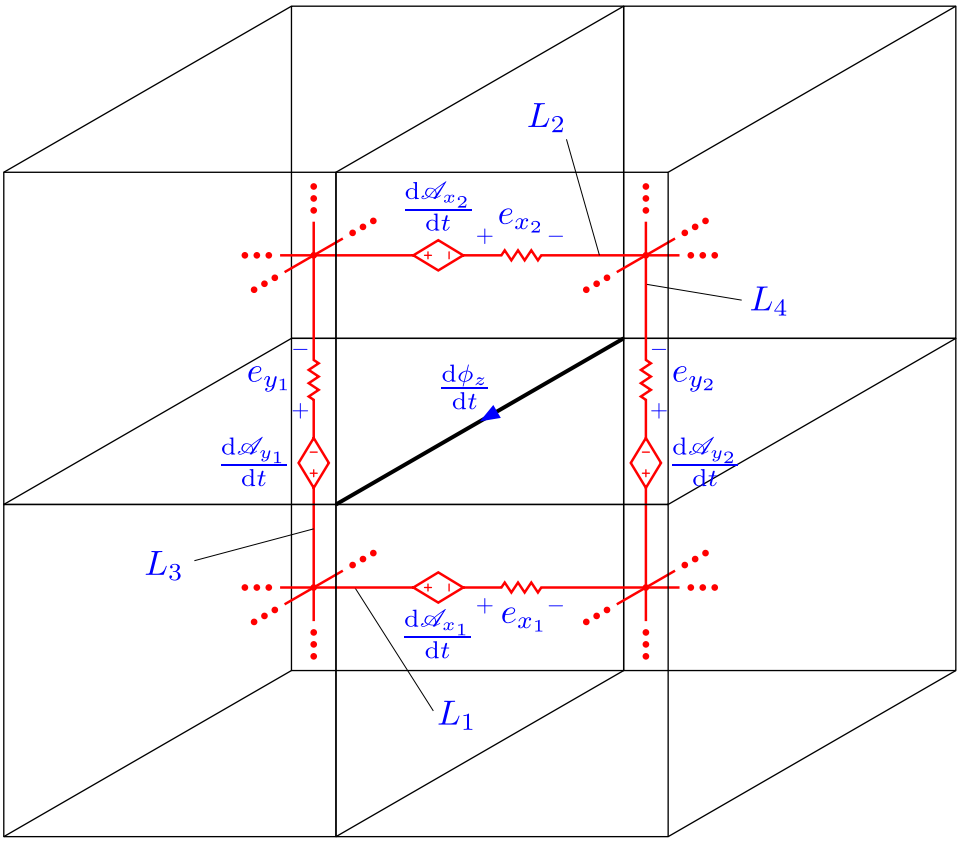

Figure 5.5 A loop of resistances surrounding a time-varying flux.

5.3 Dynamics

From the magnetoquasistatics approximation to the complete set of Maxwell's equation (1.1)–(1.4), the missing element is the electric displacement $\vec{D}$ and its time variation $\frac{\mathrm{d}\vec{D}}{\mathrm{d}t}$.

Using Gauss's theorem (1.18) in (1.9) with (1.4), we get

$$\vec{\nabla}\cdot\vec{J} = -\frac{\mathrm{d}\rho}{\mathrm{d}t}$$

$$\oiint_{\tilde{S}} \vec{J}\cdot\mathrm{d}\vec{s} = -\frac{\mathrm{d}}{\mathrm{d}t}\oiint_{\tilde{S}} \vec{D}\cdot\mathrm{d}\vec{s}$$

$$-I_{x_1} + I_{x_2} - I_{y_1} + I_{y_2} - I_{z_1} + I_{z_2} = \frac{\mathrm{d}\psi_{x_1}}{\mathrm{d}t} - \frac{\mathrm{d}\psi_{x_2}}{\mathrm{d}t} + \frac{\mathrm{d}\psi_{y_1}}{\mathrm{d}t} - \frac{\mathrm{d}\psi_{y_2}}{\mathrm{d}t} + \frac{\mathrm{d}\psi_{z_1}}{\mathrm{d}t} - \frac{\mathrm{d}\psi_{z_2}}{\mathrm{d}t} \tag{5.9}$$

where the time-variation of electric flux ψ is the displacement (capacitive) current. Therefore, (5.9) represents Kirchhoff's current law at the electric node in the center of a dual cell, where each branch is made of resistances in parallel with capacitances, as illustrated in Fig. 5.6.

As for the couplings between electric and magnetic circuits, the difference with the pre-

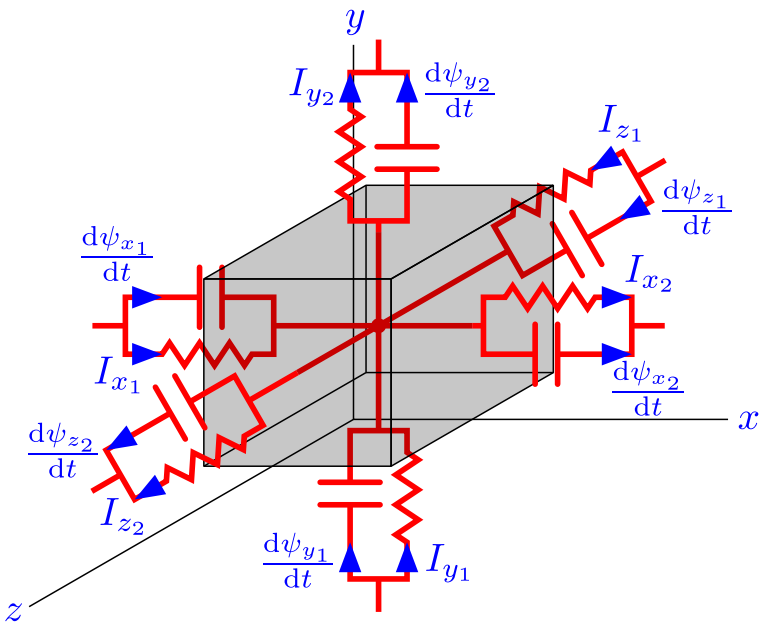

Figure 5.6 Resistive and capacitive cell without electromotive force sources.

vious couplings (controlled sources) presented in magnetoquasistatics is that the controlled MMF source in the magnetic circuit is now controlled by the *total loop current* $\mathscr{T}$ of this branch, which is given by

$$\mathscr{T} = \mathscr{T}_r + \mathscr{T}_c \tag{5.10}$$

where $\mathscr{T}_r$ is the resistive loop current (as used in MQS), and $\mathscr{T}_c$ is the capacitive loop current.

Following the discretization of vector potentials $\vec{T}$ and $\vec{A}$ into (total) loop current $\mathscr{T}$ and loop flux $\mathscr{A}$, respectively, the logical sequel is to discretize scalar potentials Ω and φ. Integrating along an edge $\tilde{L}_i$ (directed from node $\tilde{k}$ to node $\tilde{m}$ of the dual mesh) on both sides of (1.30), and with the definitions of magnetomotive force (1.14) and (total) loop current (5.4), we get

$$\int_{\tilde{L}_i} \vec{H} \cdot \mathrm{d}\vec{l} - \int_{\tilde{L}_i} \vec{T} \cdot \mathrm{d}\vec{l} = -\int_{\tilde{L}_i} \left(\vec{\nabla}\Omega\right) \cdot \mathrm{d}\vec{l}$$

$$\mathscr{F}_i - \mathscr{T}_i = \Omega_{\tilde{k}} - \Omega_{\tilde{m}} \tag{5.11}$$

It can be seen that the integral of the gradient is simply the difference in magnetic scalar potentials of the end nodes of $\tilde{L}_i$.

Similarly, integrating along an edge L_i (directed from node k to node m of the primal mesh) on both sides of (1.28), and with the definitions of electromotive force (1.13) and loop

flux (5.5), we get

$$\int_{L_i} \vec{E} \cdot \mathrm{d}\vec{l} + \frac{\mathrm{d}}{\mathrm{d}t} \int_{L_i} \vec{A} \cdot \mathrm{d}\vec{l} = -\int_{L_i} \left(\vec{\nabla}\varphi\right) \cdot \mathrm{d}\vec{l}$$

$$e_i + \frac{\mathrm{d}\mathscr{A}_i}{\mathrm{d}t} = \varphi_k - \varphi_m \tag{5.12}$$

Therefore, in the generalization of the Reluctance Network Method [3], each branch of the electric circuit (defined along the edges of the primal mesh) will be of the form presented in Fig. 5.7a. Similarly, each branch of the magnetic circuit (defined along the edges of the dual mesh) will be of the form shown in Fig. 5.7b. It is assumed that both meshes are dual and orthogonal to each other. Note that mutual reluctances, mutual resistances and mutual capacitances were not included in the previous development. This will be discussed in the next section.

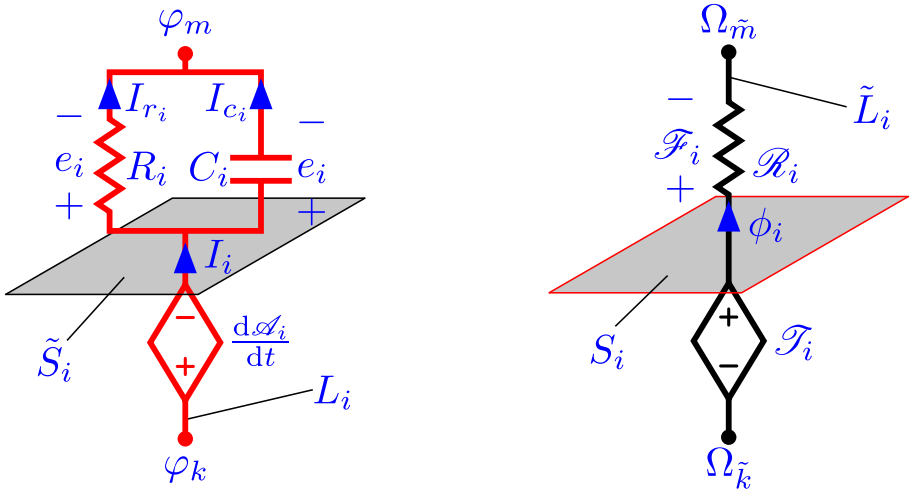

(a) Electric branch (b) Magnetic branch

Figure 5.7 Equivalent branches for electric and magnetic circuits.

The attentive reader will have noted the striking resemblance of the method presented in this section and the Finite Integration Technique (FIT) [4] (Weiland, 1977, 1996; Clemens and Weiland, 2001).

In fact, not only there is a resemblance of the method presented here and the Finite Integration Technique, but also with the Finite Element Method (FEM), as shown in (Demenko *et al.*, 1998; Demenko, 2000; Demenko and Sykulski, 2002, 2006; Demenko *et al.*,

3. Again, the Reluctance Network Method is used only to calculate the leakage field in magnetostatics.
4. For an historical review of this method, see (Weiland, 2003).

2008; Demenko and Hameyer, 2010) [5]. There are also some similarities with Tonti's Finite Formulation (Tonti, 2001) and Yee's Finite Difference Time Domain (FDTD) (Yee, 1966).

Actually, it was shown by Bossavit *et al.* that all these methods are equivalent to what he calls *Generalized Finite Differences* [6], and that they mainly differ in their specific calculation of the *discrete Hodge operator* (Bossavit and Kettunen, 2000; Bossavit, 2001; Tarhasaari *et al.*, 1999). In other words, the main difference between those methods lies in the way reluctances, resistances and capacitances are calculated. Also, as with circuit analysis, where there are different methods to solve a circuit (e.g. nodal analysis, loop analysis, hybrid analysis, etc.), another difference comes from the particular choice of *formulation* or *scheme* (Bossavit, 2001, § 5), depending on the chosen degrees of freedom (e.g. $\vec{T}$-Ω formulation, $\vec{A}$-φ formulation, etc.).

Finally, looking at (Kron, 1944), it can be seen that using "spherical inductances" (containing ideal transformers), it is possible to find an equivalent all-electric 3-D circuit for discrete electromagnetics.

5.4 Resistance, reluctance and capacitance

Up until now, only the *topological relationships* were given, since we have only used Maxwell's equations (1.1)–(1.4). These are the so-called *fundamental equations of electromagnetism* in (van Dantzig, 1934), which are independent of metrics. It is the remaining constitutive equations (1.5)–(1.7) which contain this information, as seen in our previous definitions of resistance (1.23) and reluctance (1.21).

Let us first have a look at (1.5), since our discussion began in magnetostatics. From the definitions of magnetic flux (1.11) and magnetomotive force (1.14), we can see from Fig. 5.1 that reluctance $\mathscr{R}$ is an *operator* mapping a surface integral quantity to a path integral quantity on its dual (orthogonal) edge. In terms of differential geometry, the quantity (form) $\vec{B} \cdot \mathrm{d}\vec{s}$ integrated on a face S of the primal mesh is called a *2-form*, and the quantity (form) $\vec{H} \cdot \mathrm{d}\vec{l}$ integrated along its dual edge is called a *1-form*. The operator mapping a 2-form to a dual 1-form is called the *Hodge operator*. Similarly, the operator mapping the *integrals* of the 2-forms and the dual 1-forms is called the *discrete Hodge operator* (Tarhasaari *et al.*, 1999; Bossavit and Kettunen, 2000), which is a square matrix. This matrix is also called mass matrix (Bossavit and Kettunen, 2000, p. 864).

Therefore, the discretization of the constitutive equation (1.5), as done similarly for (1.24),

5. It is mentioned in (Demenko, 2000, p. 741) that the coupling between the electric and magnetic networks originate from (Davidson and Balchin, 1983), which neglects earlier work on the subject by (Carpenter, 1975a,b; Roberts, 1960), for instance.

6. This type of methods is also called *Finite Formulation* in (Repetto and Trevisan, 2003; Tonti, 2002).

translates to

$$[\phi] = [\mathscr{P}]\,[\mathscr{F}] \tag{5.13}$$

which is the inverse of Hopkinsons' law (1.20) in matrix form, where $[\mathscr{P}]$ (permeance matrix) is the discrete Hodge operator mapping magnetic fluxes $[\phi]$ to dual magnetomotive forces $[\mathscr{F}]$.

In the same fashion, we can discretize the constitutive equation (1.6), as in (1.25), which gives

$$[\psi] = [C]\,[e] \tag{5.14}$$

where $[C]$ (capacitance matrix) is the discrete Hodge operator mapping electric fluxes $[\psi]$ to electromotive forces $[e]$.

The discretization of the last constitutive equation (1.7) is basically the inverse of Ohm's law (1.22) in matrix form

$$[I_r] = [G]\,[e] \tag{5.15}$$

where $[G]$ (conductance matrix) is the discrete Hodge operator mapping conduction currents $[I_r]$ to electromotive forces $[e]$.

In fact, it is surprising that the link of the discrete Hodge operator with (self and mutual) resistances, capacitances and reluctances was not recognized in (Tarhasaari *et al.*, 1999):

> In this light the matrix $\mathbf{H}_2$—including all metric data—is like the impedance matrix $\mathbf{Z}$ in circuit theory, with the exception that the metric of space is encoded into $\mathbf{H}_2$ but not $\mathbf{Z}$.

From (Tarhasaari *et al.*, 1999, eq. 5) and the definitions of arrays $\bar{b}$ (magnetic fluxes embraced by surfaces of the primal mesh) and $\bar{h}$ (magnetomotive forces along the edges of the dual mesh), it is obvious that the matrix $\star$ is the permeance matrix (deduced from Hopkinsons' law). Therefore, its inverse $\mathbf{H}_2$ is equivalent to the reluctance matrix, so that the metric of space in $\mathbf{H}_2$ is also included in the inductive part of $\mathbf{Z}$.

It can be seen from the previous equations that there can be mutual permeances, mutual capacitances and mutual conductances between each branch of electric and magnetic circuits, which are not shown in the previous figures (with the FIT or the RNM, the mutual terms are zero). As mentioned earlier, the main difference between the different methods lies in the calculation of the discrete Hodge operators.

Let us first examine how these matrices are calculated in the Finite Integration Technique. In this method, the matrices are diagonal (no mutuals). Each (self) permeance $\mathscr{P}_{ii}$ (for a given face S_i and its dual edge $\tilde{L}_i$) of the matrix $[\mathscr{P}]$ is given using the lengthwise average

of permeability $\bar{\mu}_i$

$$\mathscr{P}_{ii} = \frac{\bar{\mu}_i s_i}{\tilde{l}_i} \tag{5.16}$$

As illustrated in Fig. 5.8, we can see that the face S_i (of area s_i) is shared between two cells of the primal mesh (red). It is assumed that permeability is uniform in each cell, but with different values μ_1 and μ_2, so that the edge $\tilde{L}_i$ (of length $\tilde{l}_i$) is divided into two parts of lengths $\tilde{l}_1$ and $\tilde{l}_2$, where $\tilde{l}_1$ is actually half the length of the first (primal) cell $\tilde{l}_1 = l_1/2$, and that the length $\tilde{l}_2$ is half the length of the second (primal) cell $\tilde{l}_2 = l_2/2$[7]. Therefore, the lengthwise average of permeability is given by

$$\bar{\mu}_i = \frac{\mu_1 l_1 + \mu_2 l_2}{2\tilde{l}_i} \tag{5.17}$$

In the special case where $\mu_1 = \mu_2 = \mu_0$, the reluctance is that of the Reluctance Network Method (5.2).

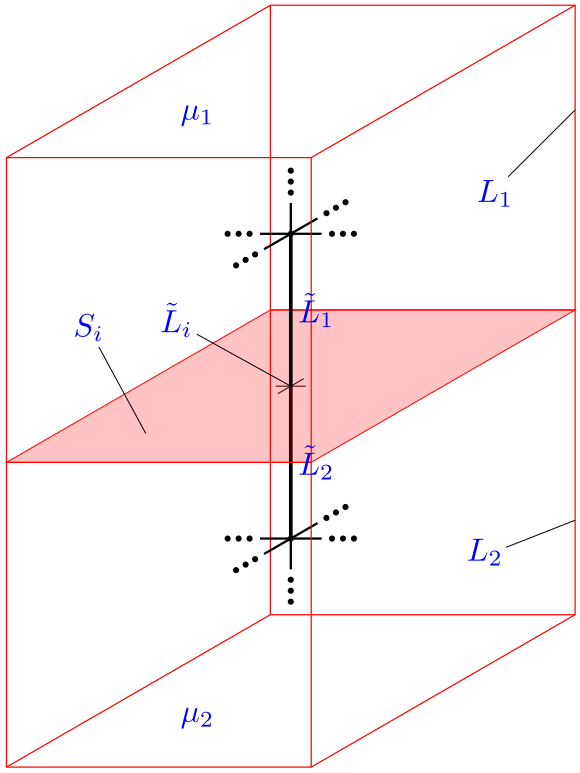

Figure 5.8 Lengthwise average for the calculation of (self) permeance.

One can see that there is another approximation not only in the calculation of the reluc-

7. Note that this is true because we have dual orthogonal and hexahedral meshes. Otherwise, we would need to calculate lengths $\tilde{l}_1$ and $\tilde{l}_2$ from the intersection point of edge $\tilde{L}_i$ with face S_i.

tances themselves, but also in the calculation of μ_1 or μ_2 if the boundary between materials does not coincide with the faces of the cells. A *pixelization* will occur at the interface of different materials located inside cells, also called the *staircase approximation* of complex boundaries in (Weiland, 2003). Different solutions to that problem exist, such as the *perfect boundary approximation technique* (Krietenstein *et al.*, 1998).

Similarly, the (self) capacitance C_{ii} and the (self) conductance G_{ii} for a given edge L_i and its dual face $\tilde{S}_i$ are given by using the areawise average of permittivity $\bar{\varepsilon}_i$ and conductivity $\bar{\sigma}_i$, respectively

$$C_{ii} = \frac{\bar{\varepsilon}_i \tilde{s}_i}{l_i} \tag{5.18}$$

$$G_{ii} = \frac{\bar{\sigma}_i \tilde{s}_i}{l_i} \tag{5.19}$$

As shown in Fig. 5.9, the edge L_i (of length l_i) is shared between four cells of the primal mesh (red) with different values of permeabilities and conductivities (uniform in each cell), whereas the dual face $\tilde{S}_i$ (of area $\tilde{s}_i$) is divided into four parts of areas $\tilde{s}_1$, $\tilde{s}_2$, $\tilde{s}_3$ and $\tilde{s}_4$. Those four areas are actually a quarter of the area of faces on the primal grid (s_1, s_2, s_3 and s_4)[8]. Hence, the areawise average of permittivity and conductivity are given by

$$\bar{\varepsilon}_i = \frac{\varepsilon_1 s_1 + \varepsilon_2 s_2 + \varepsilon_3 s_3 + \varepsilon_4 s_4}{4\tilde{s}_i} \tag{5.20}$$

$$\bar{\sigma}_i = \frac{\sigma_1 s_1 + \sigma_2 s_2 + \sigma_3 s_3 + \sigma_4 s_4}{4\tilde{s}_i} \tag{5.21}$$

Another way to calculate permeances, conductances and capacitances, is with the use of interpolation functions $\vec{w}_L$ over primal edges and $\vec{w}_{\tilde{S}}$ over dual faces, or conversely, $\vec{w}_{\tilde{L}}$ over dual edges and $\vec{w}_S$ over primal faces. This results in a "smoothing" of circuit elements with neighboring cells, therefore including mutual effects, and the discrete Hodge operators will no longer be diagonal (but symmetric and positive-definite). Diagonal matrices can be obtained afterward through the use of "lumping" techniques, such as presented in (Bossavit and Kettunen, 1999).

5.5 Boundary conditions

One of the questions that arises when defining primal and dual meshes is what happens to the dual mesh at the boundaries of the domain? For instance, suppose we have only one cell on the primal mesh, like the one illustrated in Fig. 5.1. It can be seen that a part of

8. Again, note that this is true because we have dual orthogonal and hexahedral meshes. Otherwise, we would need to calculate areas $\tilde{s}_1$, $\tilde{s}_2$, $\tilde{s}_3$ and $\tilde{s}_4$ from the intersection points.

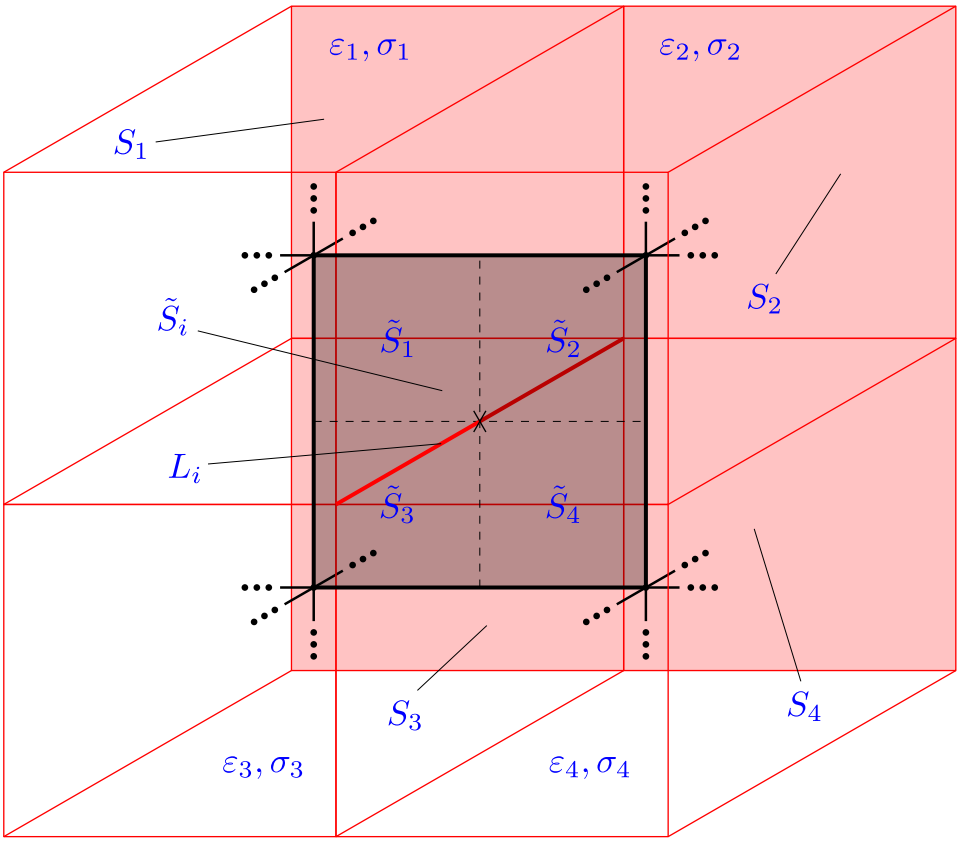

Figure 5.9 Areawise average for the calculation of (self) capacitance and (self) conductance.

each dual edge actually lies outside the boundary. Therefore, how do we calculate the values of these reluctances? Similarly, for each edge of the domain (in red), part of their dual faces will be outside the boundary. Hence, how are the resistances and capacitances calculated on these edges? These questions are actually related to the boundary conditions.

Two boundary conditions will be considered here [9]: the perfect electric conductor and the perfect magnetic conductor.

In the perfect electric conductor boundary, all magnetic fluxes embraced by the boundary's faces are zero and all electromotive forces along the boundary's edges are zero. In this case, because the magnetic fluxes of reluctances that cross the boundary are zero, these magnetic branches are open-circuited (no need to calculate them). In a similar fashion, because the electromotive forces of electric branches on the boundary's edges, these electric branches are short-circuited (again, no need to calculate them). Therefore, the aforementioned problem of calculating permeances, conductances or capacitances for branches at the boundary is avoided.

9. There are also other boundary conditions, such as Perfectly Matched Layers (absorbing boundary) (Bérenger, 1994), or periodic.

For the perfect magnetic conductor boundary, all currents (conduction and displacement) through the boundary's faces are zero and all magnetomotive forces along the boundary's edges are zero. There are two ways to implement this. Since magnetomotive forces and currents are defined as integrals of differential forms on the dual mesh, we can truncate the primal mesh to the dual mesh on this boundary (so that faces and edges of the boundary are those of the dual mesh). In this case, we treat the boundary condition similarly to the perfect electric conductor: tangential reluctances are short-circuited (zero magnetomotive force) and normal resistances/capacitances are open-circuited (zero current). However, this solution involves modifying the mesh, which is not desirable if the boundary conditions of the problem are to be changed. Another solution is to extend the dual mesh and realize that the zero tangential magnetomotive force at the boundary can be reproduced through tangential image magnetomotive forces (of opposite directions).

5.6 Conclusion

A simple example of "electromagnetic" circuit is illustrated in Fig. 5.10, where two conductors are surrounded by air (here assumed to have an infinite resistance). The primal (electric) mesh is illustrated in black, while the dual (magnetic) mesh is shown in white. It is assumed that the discrete Hodge operators are diagonal matrices, such as in the Finite Integration Technique, so that there are no mutual resistances, capacitances or reluctances. Coupling sources between electric and magnetic circuits are not shown, and red rectangles represent a resistance in parallel with a capacitance (only capacitances remain in air, since it is assumed to have an infinite resistance). The boundary conditions are of the Perfect Electric Conductor type on all outside faces of the primal mesh.

The theoretical framework presented in this chapter is necessary to properly develop real topological models and paves the way for more sophisticated models, not only for transformers, but also for machines (Roberts, 1960; Davey and King, 1981; Funieru, 2007; Demenko and Hameyer, 2010) or transmission lines. The link of "electromagnetic" circuits with other finite formulations is useful, because it gives access to specialized literature on similar problems, such as coupling with thermal circuits (Hsu and Vu-Quoc, 1996; Clemens *et al.*, 2000), field coupling with electric circuits (Tsukerman *et al.*, 1993; De Gersem *et al.*, 1998; De Gersem and Weiland, 2004; Benderskaya, 2007; Schöps *et al.*, 2013), mesh solutions to represent movement in machines (Rodger *et al.*, 1990; Sadowski *et al.*, 1992; Perrin-Bit and Coulomb, 1995), convergence (Bossavit, 2001; Munteanu and Hirtenfelder, 2005), mesh subgridding (Thoma and Weiland, 1996; Podebrad *et al.*, 2003), etc.

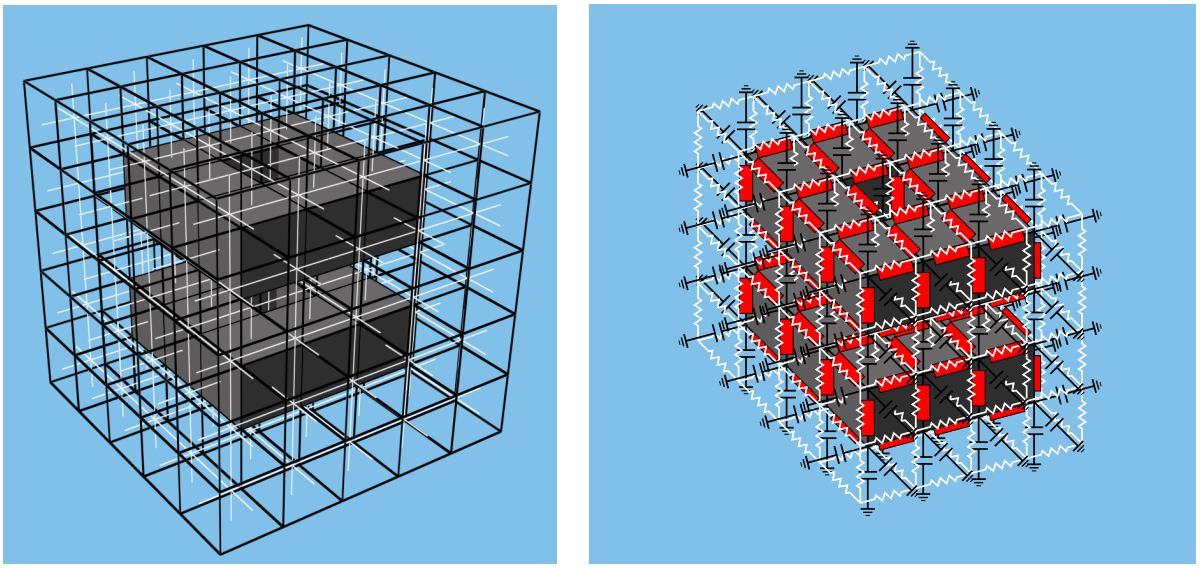

(a) Primal and dual meshes

(b) Electromagnetic circuit

Figure 5.10 Two conductors in air with Perfect Electric Conductor boundary conditions.

CHAPTER 6

CONCLUSION

6.1 Summary

The main objective of this work was to develop new shell-type (single-phase and three-phase) transformer models for the simulation of low- and mid-frequency electromagnetic transients. Similarly to previous works on low-frequency transformer modeling, the problems associated with low-frequency transients are essentially related to the proper modeling of the flux leakages and of the nonlinear core.

To improve the model capabilities and accuracy, it was proposed to discretize windings into coils, and to divide yokes to include leakage "paths" (so that leakages are represented more finely). Unfortunately, short-circuit measurements are never available between coils. This is associated with Problem 1 of § 1.3. To compensate for this difficulty, it was necessary to find a method to calculate leakage inductances from geometrical data. For this purpose, a new 2-D analytical method was implemented in this work, which is based on the method of images, which allows the calculation of short-circuit inductances between coils. The new method was verified against numerical results of the FEM in 2-D. More than that, it was demonstrated that the 2-D approximation is good, at least for the shell-type transformer, since the results were reasonably close to those obtained from a more complete 3-D model. Furthermore, it was shown that the classical formula to calculate the short-circuit inductance can lead to a large error if fringing flux is not negligible. The new method was also compared to Roth's method and it was shown that Roth's method is faster. However, the new method is believed to be more general, since the method of images can also be applied if the boundary's permeability is not infinite, which could prove to be useful to extend the method to complex coil geometries in 3-D. Also, this method was used to calculate short-circuit inductances between coils for the coupled leakage model, and it was validated using experimental measurements.

Over the years, several more "physical" low-frequency transformer models were proposed, called "topological" models (which are derived from equivalent magnetic circuits). Even though these models are physically-based (derived from flux paths), several models exist for the same transformer geometry. This was identified in Problem 2 of § 1.3. The differences between these models were explained in this work through the concepts of divided and integral fluxes, where the divided flux approach is the result of mathematical manipulations, whereas the integral flux approach is more physically related to the average flux in each part of the

transformer. For the case of the two-winding single-phase transformer, it was shown that the divided flux approach yields the T-network model, whereas the integral flux approach gives the Π-network model. Furthermore, it was demonstrated that for this simple model, the leakage split ratio of the T-network model is actually related to the lengths of core reluctances, in the unsaturated case. Otherwise, it was demonstrated that for both models to be equivalent, the leakage inductances of the T-network model need to be nonlinear.

The second part of the problem (that was described in Problem 2 of § 1.3) with those "topological" models is the connection of the short-circuit inductance model to the core through fictitious windings. To avoid this, it was demonstrated in this work that the existing coupled leakage model is able to correctly represent the short-circuit behavior of the transformer, while providing more physically-acceptable connections to the core, without the use of fictitious windings. Furthermore, a new low-frequency three-phase shell-type transformer model was presented, which uses this coupled leakage model.

The main challenge of parameter determination for low-frequency transformer models is to properly calculate the magnetizing branches, so that the model is reversible. This was described as Problem 3 in § 1.3. To do so, a new method was proposed in this work to properly take into account leakage inductances while the core starts to saturate (leakage inductances are neglected in other methods, or only taken into account for the calculation of saturation inductances from air-core inductances), in order to calculate each magnetizing branch from no-load measurements. This method was also generalized in this work, in order to include all possible connections (series/parallel) of coils.

Finally, the fourth problem highlighted in § 1.3 was that classical magnetic circuit theory is incorrect when the core starts to saturate, since the problem is discretized into flux tubes and flux cannot leak from their sides. In this dissertation, a general theoretic development of electromagnetic circuits was provided, in hope to bridge the existing gap between "topological" models and discrete field models. It also serves as a coherent synthesis between existing discrete electromagnetic methods, and explained from a circuit point of view, starting from statics to dynamics. This could enable not only to have more sophisticated 3-D transformer models, but could also prove useful for machines and transmission lines models, not to mention coupling with thermal or mechanical equations, for instance.

6.2 Limitations of the new methods

It is important to understand that where there are assumptions and approximations, there are also limitations.

For instance, in order to calculate leakage inductances, it was assumed that the leakage

field is approximately 2-D. While this assumption was shown to be reasonably accurate for shell-type transformer, since most of the windings are surrounded by the core, it would perhaps be incorrect for core-type transformers. Furthermore, eddy current in coils were neglected for the calculation of the leakage field (and inductance).

In the coupled leakage model, eddy-current losses in windings were also neglected. If we were to match the coils series resistances to short-circuit losses, this gives rise to the same problem there was with the star-equivalent circuit to calculate leakage inductances from short-circuit inductances: being unable to comply with all the short-circuit measurements, except for the special case of a three-winding transformer (three parameters, three measurements). Again, this is caused by the fact that there are N series resistances (for N coils) and $N(N-1)/2$ different pairs of short-circuit combinations.

For the calculation of core parameters, the winding losses (copper and eddy) were neglected. In reality, for the model to be truly reversible, winding (eddy) losses must be included in the coupled leakage model [1] and magnetizing branches should be divided accordingly. Also, the correct extrapolation of no-load measurements is dependent on the fitting to a particular function and whether or not this function is close to the physical behavior of the core (and if the calculated/estimated air-core inductance is close to reality).

It must be emphasized that the proposed single-phase and three-phase shell-type transformer were developed for low-frequency transients simulation. They do not include capacitances, which becomes increasingly important as frequency increases.

As for the discrete electric and magnetic 3-D circuits approach, it is more complicated to implement a model with this method, because it is a device-specific model. Furthermore, because of the higher number of degrees of freedom (possibly including nonlinear branches), this method will be more computationally expensive.

6.3 Future work

On the few opportunities to continue and improve on this work, first there is the development of a new analytical method to calculate both short-circuit inductance and resistance between coils, since short-circuit resistances between coils are also never available.

Second, resistances must be included in the coupled leakage model, in order to account for all possible short-circuit combination of coils. The goal is of course to increase the reversibility of the model.

Third, a general numerical method will need to be implemented to calculate magnetizing branches, in order to properly divide no-load measurements while taking into account both

1. This could be explained by the fact that series resistances create a voltage drop that translates into a drop of flux linkage, but this hypothesis remains to be proved.

leakage inductance and resistance.

Fourth, the methods developed in this work will have to be extended to core-type transformers.

Finally, a generalized finite differences module could be implemented in EMTP-RV. This would enable to couple discrete electromagnetic models to EMT-type programs, while maintaining all power system modeling capabilities (controls, load flow, etc.), as opposed to rudimentary circuit modeling capabilities of modern field simulators.

REFERENCES

AICHER, L. C. (1943). A useful equivalent circuit for a five-winding transformer. *Trans. AIEE, 62*(2), 66–70.

AKÇA, Z., & KAYA, R. (1997). On the taxicab trigonometry. *Jour. Inst. Math. Comp. Sci., 10*(3), 151–159.

ÁLVAREZ-MARIÑO, C., DE LEÓN, F., & LÓPEZ-FERNÁNDEZ, X. M. (2012). Equivalent circuit for the leakage inductance of multiwinding transformers: unification of terminal and duality models. *IEEE Trans. Power Del., 27*(1), 353–361.

AMOIRALIS, E. I., TSILI, M. A., & KLADAS, A. G. (2009). Transformer design and optimization: a literature survey. *IEEE Trans. Power Del., 24*(4), 1999–2024.

ANDERSEN, O. W. (1973). Transformer leakage flux program based on the finite element method. *IEEE Trans. Power App. Syst., 92*(2), 682–689.

APOLÔNIO, R., DE OLIVEIRA, J. C., BRONZEADO, H. S., & DE VASCONCELLOS, A. B. (2004). Transformer controlled switching for minimization of magnetization transient currents: strategy proposal and laboratory validation. In *IEEE/PES Transmission and Distribution Conference and Exposition: Latin America*, 505–510.

ARNOLD, E., & LA COUR, J. L. (1904). Die Gleichungen und Konstanten eines Einphasentransformators. In Arnold, E. (Ed.), *Die Wechselstromtechnik, vol. 2: die Transformatoren* (pp. 16–35). Berlin, Germany: Springer.

ARTURI, C. M. (1991). Transient simulation and analysis of a three-phase five-limb step-up transformer following an out-of-phase synchronization. *IEEE Trans. Power Del., 6*(1), 196–207.

ARTURI, C. M. (1994). Model of a highly saturated three-phase autotransformer with tertiary winding and five-limb core and analysis of a time-varying short-circuit transient. *Euro. Trans. Elect. Power, 4*(6), 513–524.

ARTURI, C. M., & UBALDINI, M. (1986). *Equivalent networks of heavily saturated static electromagnetic devices.* Presented at the International Conference on Electrical Machines, Munich, Germany.

AVENDAÑO CECEÑA, A. (2011). *Transformer modeling in ATP: internal faults & high-frequency discretization.* (Ph.D. dissertation, Michigan Technological University, Houghton, MI).

BARRET, P. (1976). *Cours d'électrotechnique, transformateurs, tome I.* École Supérieure d'Électricité.

BASTARD, P., BERTRAND, P. and MEUNIER, M. (1994). A transformer model for winding fault studies. *IEEE Trans. Power Del., 9*(2), 690–699.

BENDERSKAYA, G. (2007). *Numerical Methods for Transient Field-Circuit Coupled Simulations Based on the Finite Integration Technique and a Mixed Circuit Formulation.* (Ph.D. dissertation, Technischen Universität Darmstadt, Darmstadt, Germany).

BENDERSKAYA, G., DE GERSEM, H., WEILAND, T., & CLEMENS, M. (2004). Transient field-circuit coupled formulation based on the finite integration technique and a mixed circuit formulation. *COMPEL, 23*(4), 968–976.

BÉRENGER, J.-P. (1994). A perfectly matched layer for the absorption of electromagnetic waves. *J. Comput. Phys., 114*(2), 185–200.

BETHENOD, I. (1939). Édouard Roth. *Rev. Gén. Élect., 46*(5), 131–134.

BILLIG, E. (1951). The calculation of the magnetic field of rectangular conductors in a closed slot, and its application to the reactance of transformer windings. *Proc. IEE—Part IV: Institution Monographs, 98*(1), 55–64.

BINNS, K. J., LAWRENSON, P. J., & TROWBRIDGE, C. W. (1992). *The analytical and numerical solution of electric and magnetic fields.* Chichester, England: Wiley.

BLANKEN, P. G. (2001). A lumped winding model for use in transformer models for circuit simulation. *IEEE Trans. Power Electron., 16*(3), 445–460.

BLANKEN, P. G., & VAN VLERKEN, J. J. L. M. (1991). Modeling of electromagnetic systems. *IEEE Trans. Magn., 27*(6), 4509–4515.

BLOCH, A. (1946). On methods for the construction of networks dual to non-planar networks. *Proc. Phys. Soc., 58*(6), 677–694.

BLUME, L. F., CAMILLI, G., BOYAJIAN, A., & MONTSINGER, V. M. (1951). *Transformer engineering* (2nd ed.). New York, NY: Wiley.

BÖDEFELD, T. (1931). Streuung und Feldbild in der Elektrotechnik. *Elektrotechnische Zeitschrift, 52*(24), 763–768.

BÖDEFELD, T., & SEQUENZ, H. (1952). *Elektrische Maschinen.* Vienna, Austria: Springer.

BOSSAVIT, A. (2001). 'Generalized finite differences' in computational electromagnetics. *Progress In Electromagnetics Research, 32*, 45–64.

BOSSAVIT, A., & KETTUNEN, L. (1999). Yee-like schemes on a tetrahedral mesh, with diagonal lumping. *Int. J. Numer. Model. El., 12*(1–2), 129–142.

BOSSAVIT, A., & KETTUNEN, L. (2000). Yee-like schemes on staggered cellular grids: a synthesis between FIT and FEM approaches. *IEEE Trans. Magn., 36*(4), 861–867.

BOSSI, A., CAPRIO, G., CREPAZ, S., PESCÙ, G., & UBALDINI, M. (1979). Reti equivalenti di trasformatori a più avvolgimenti. *L'Elettrotecnica, 66*(4), 321–336.

BOYAJIAN, A. (1954). Leakage reactance of irregular distributions of transformer windings by the method of double Fourier series. *AIEE Trans. Power App. Syst., Part III, 73*(2), 1078–1086.

BRANDWAJN, V., DOMMEL, H. W., & DOMMEL, I. I. (1982). Matrix representation of three-phase N-winding transformers for steady-state and transient studies. *IEEE Trans. Power App. Syst., 101*(6), 1369–1378.

BUNTENBACH, R. W. (1968). Improved circuit models for inductors wound on dissipative magnetic cores. In *Asilomar Conf. on Circuits & Systems*, 229–236.

CARPENTER, C. J. (1960). The application of the method of images to machine end-winding fields. *Proc. IEE—Part A: Power Engineering, 107*(35), 487–500.

CARPENTER, C. J. (1968). Magnetic equivalent circuits. *Proc. IEE, 115*(10), 1503–1511.

CARPENTER, C. J. (1975a). Finite-element network models and their application to eddy-current problems. *Proc. IEE, 122*(4), 455–462.

CARPENTER, C. J. (1975b). A network approach to the numerical solution of eddy-current problems. *IEEE Trans. Magn., 11*(5), 1517–1522.

CHEN, X. (1996). A three-phase multi-legged transformer model in ATP using the directly-formed inverse inductance matrix. *IEEE Trans. Power Del., 11*(3), 1554–1562.

CHEN, X. S., & NEUDORFER, P. (1992). Digital model for transient studies of a three-phase five-legged transformer. *Proc. IEE—Part C: Generation, Transmission and Distribution, 139*(4), 351–358.

CHEN, X. S., & NEUDORFER, P. (1993). *The development of a three-phase multi-legged transformer model for use with EMTP.* (Tech. report, DOE contract DE-AC79-92BP26702). USA: Bonneville Power Administration.

CHENG, D. K.-W., WONG, L.-P., & LEE, Y.-S. (2000). Design, modeling, and analysis of integrated magnetics for power converters. *IEEE Power Electronics Specialists Conference, 1*, 320–325.

CHERRY, E. C. (1949). The duality between interlinked electric and magnetic circuits and the formation of transformer equivalent circuits. *Proc. Phys. Soc., 62*(2), 101–111.

CHIESA, N. (2005). *Power transformer modelling: advanced core model.* (Master's thesis, Politecnico di Milano, Milan, Italy).

CHIESA, N. (2010). *Power transformer modeling for inrush current calculation.* (Ph.D. dissertation, Norwegian Univ. Sci. Technology, Trondheim, Norway).

CHIESA, N., & HØIDALEN, H. K. (2010). Analytical algorithm for the calculation of magnetization and loss curves of delta-connected transformers. *IEEE Trans. Power Del., 25*(3), 1620–1628.

CHIESA, N., HØIDALEN, H. K., LAMBERT, M., & MARTÍNEZ DURÓ, M. (2011). *Calculation of inrush currents–benchmarking of transformer models.* Presented at the Int. Conf. Power System Transients, Delft, the Netherlands.

CHIESA, N., MORK, B. A., & HØIDALEN, H. K. (2010). Transformer model for inrush current calculations: simulations, measurements and sensitivity analysis. *IEEE Trans. Power Del., 25*(4), 2599–2608.

CHO, S. D. (2002). *Parameter Estimation for Transformer Modeling.* (Ph.D. dissertation, Michigan Technological University, Houghton, MI).

CHUA, L. O. (1968). Synthesis of new nonlinear network elements. *Proc. IEEE, 56*(8), 1325–1340.

CHUA, L. O. (1971). Memristor-the missing circuit element. *IEEE T. Circuits. Syst., 18*(5), 507–519.

CHUA, L. O., & CHEN, L. K. (1976). Diakoptic and generalized hybrid analysis. *IEEE Trans. Circuits and Systems, 23*(12), 694–705.

CHUA, L. O., DESOER, C. A., & KUH, E. S. (1987). *Linear and nonlinear circuits.* McGraw-Hill.

CHUA, L. O., & LIN, P.-M. (1975). *Computer-aided analysis of electronic circuits: algorithms & computational techniques.* Prentice-Hall.

CIGRÉ (1997). *Guidelines for representation of network elements when calculating transients.* (Tech. report, WG 02, SC 33). Paris, France: CIGRÉ.

CLEMENS, M., GJONAJ, E., PINDER, P., & WEILAND, T. (2000). Numerical simulation of coupled transient thermal and electromagnetic fields with the finite integration method. *IEEE Trans. Magn., 36*(4), 1448–1452.

CLEMENS, M., & WEILAND, T. (2001). Discrete electromagnetism with the finite integration technique. *Progress In Electromagnetics Research, 32*, 65–87.

DAVEY, K. R., & KING, E. I. (1981). A three dimensional scalar potential field solution and its application to the turbine generator end region. *IEEE Trans. Power App. Syst., 100*(5), 2302–2310.

DAVIDSON, J. A. M., & BALCHIN, M. J. (1983). Three dimensional eddy current calculation using a network method. *IEEE Trans. Magn., 19*(6), 2325–2328.

DE AZEVEDO, A. C., DELAIBA, A. C., DE OLIVEIRA, J. C., CARVALHO, B. C., & BRONZEADO, H. S. (2007). *Transformer mechanical stress caused by external short-circuit: a time domain approach.* Presented at the Int. Conf. Power System Transients, Lyon, France.

DE GERSEM, H., MERTENS, R., PAHNER, U., BELMANS, R., & HAMEYER, K. (1998). A topological method used for field-circuit coupling. *IEEE Trans. Magn., 34*(5), 3190–3193.

DE GERSEM, H., & WEILAND, T. (2004). Field-circuit coupling for time-harmonic models discretized by the finite integration technique. *IEEE Trans. Magn., 40*(2), 1334–1337.

DE KUIJPER, C. E. M. (1949). *Bijdrage tot de berekening van de spreidingsreactantie van transformatoren en van de krachten, welke op de wikkelingen van transformatoren werken.* (Ph.D. dissertation, Technische Hogeschool, Delft, the Netherlands).

DE LEÓN, F. (1992). *Transformer model for the study of electromagnetic transients.* (Ph.D. dissertation, Univ. Toronto, Toronto, ON).

DE LEÓN, F., FARAZMAND, A., & JOSEPH, P. (2012). Comparing the T and π equivalent circuits for the calculation of transformer inrush currents. *IEEE Trans. Power Del., 27*(4), 2390–2398.

DE LEÓN, F., & MARTINEZ-VELASCO, J. A. (2009). Dual three-winding transformer equivalent circuit matching leakage measurements. *IEEE Trans. Power Del., 24*(1), 160–168.

DE LEÓN, F., & SEMLYEN, A. (1992a). Efficient calculation of elementary parameters of transformers. *IEEE Trans. Power Del., 7*(1), 376–383.

DE LEÓN, F., & SEMLYEN, A. (1992b). Reduced order model for transformer transients. *IEEE Trans. Power Del., 7*(1), 361–369.

DE LEÓN, F., & SEMLYEN, A. (1993). Time domain modeling of eddy current effects for transformer transients. *IEEE Trans. Power Del., 8*(1), 271–280.

DE LEÓN, F., & SEMLYEN, A. (1994). Complete transformer model for electromagnetic transients. *IEEE Trans. Power Del., 9*(1), 231–239.

DEL VECCHIO, R. M., POULIN, B., FEGHALI, P. T., SHAH, D. M., & AHUJA, R. (2010). *Transformer design principles: with applications to core-form power transformers* (2nd ed.). Boca Raton, FL: CRC Press.

DEMENKO, A. (2000). Three dimensional eddy current calculation using reluctance-conductance network formed by means of FE method. *IEEE Trans. Magn., 36*(4), 741–745.

DEMENKO, A., & HAMEYER, K. (2010). Field and field-circuit models of electrical machines. *COMPEL, 29*(1), 8–22.

DEMENKO, A., NOWAK, L., & SZELAG, W. (1998). Reluctance network formed by means of edge element method. *IEEE Trans. Magn., 34*(5), 2485–2488.

DEMENKO, A., & SYKULSKI, J. K. (2002). Network equivalents of nodal and edge elements in electromagnetics. *IEEE Trans. Magn., 38*(2), 1305–1308.

DEMENKO, A., & SYKULSKI, J. K. (2006). Magneto-electric network models in electromagnetism. *COMPEL, 25*(3), 581–588.

DEMENKO, A., SYKULSKI, J. K., & WOJCIECHOWSKI, R. (2008). Network representation of conducting regions in 3-D finite-element description of electrical machines. *IEEE Trans. Magn., 44*(6), 714–717.

DENNETIÈRE, S., GUILLOT, Y., MAHSEREDJIAN, J., & RIOUAL, M. (2007). *A link between EMTP-RV and FLUX3D for transformer energization studies.* Presented at the Int. Conf. Power System Transients, Lyon, France.

DEPT. ELECT. ENG., MASSACHUSETTS INST. TECHNOLOGY (Ed.). (1943). *Magnetic circuits and transformers.* New York, NY: Wiley.

DICK, E. P., & WATSON, W. (1981). Transformer models for transient studies based on field measurements. *IEEE Trans. Power App. Syst., 100*(1), 409–419.

DIJK, H. E. (1988). *On transformer modelling: a physically based three-phase transformer model for the study of low frequency phenomena in electrical power systems.* (Ph.D. dissertation, Technische Universiteit Delft, Delft, The Netherlands).

DOEBBELIN, R., TEICHERT, C., BENECKE, M., & LINDEMANN, A. (2009). Computerized calculation of leakage inductance values of transformers. *PIERS Online, 5*(8), 721–726.

DOHERTY, R. E., & KELLER, E. G. (1936). *Mathematics of modern engineering*, vol. 1. New York, NY: Wiley.

DOMMEL, H. W. (1992). Transformers. In *EMTP Theory Book* (2nd ed., chap. 6). Vancouver, Canada: Microtran Power System Analysis Corporation.

EATON, M. E. (1994). Modeling magnetic devices using the gyrator re-cap core model. In *Northcon Conference.* pp. 60–66.

EATON, M. E. (1998). Adding flux paths to SPICE's analytical capability improves the ease and accuracy of simulating power circuits. In *Applied Power Electronics Conference and Exposition.* vol. 1, pp. 386–392.

EKMAN, J. (2003). *Electromagnetic modeling using the partial element equivalent circuit method.* (Ph.D. dissertation, Luleå Univ. Tech., Luleå, Sweden).

EL-HAMAMSY, S. A., & CHANG, E. I. (1989). Magnetics modeling for computer-aided design of power electronics circuits. In *IEEE Power Electronics Specialists Conference*. vol. 2, pp. 635–645.

ENRIGHT, W. G. (1996). *Transformer models for electromagnetic transient studies with particular reference to HVdc transmission*. (Ph.D. dissertation, Univ. Canterbury, Christchurch, New Zealand).

ENRIGHT, W. G., ARRILLAGA, J., WATSON, N. R., & ZAVAHIR, J. (1998). Modelling multi-limb transformers with an electromagnetic transient program. *Mathematics and Computers in Simulation, 46*, 213–223.

ENRIGHT, W. G., NAYAK, O. B., IRWIN, G. D., & ARRILLAGA, J. (1997). An electromagnetic transients model of multi-limb transformer using normalized core concept. In *Int. Conf. Power System Transients, Seattle, WA*. pp. 93–98.

ENRIGHT, W. G., WATSON, N., & NAYAK, O. (1999). Three-phase five-limb unified magnetic equivalent circuit transformer models for PSCAD V3. In *Int. Conf. Power System Transients, Budapest, Hungary*. pp. 462–467.

ERDEI, M. (1962). Duality of non-planar electric circuits without the use of ideal transformers. *Proc. Phys. Soc., 79*(3), 599–604.

ESCARELA-PEREZ, R., MELGOZA, E., & ALVAREZ-RAMIREZ, J. (2009). Coupling circuit systems and finite element models: a 2-D time-harmonic modified nodal analysis framework. *IEEE Trans. Magn., 45*(2), 707–715.

ESLAMIAN, M., & VAHIDI, B. (2012). New methods for computation of the inductance matrix of transformer windings for very fast transients studies. *IEEE Trans. Power Del., 27*(4), 2326–2333.

FARR, H. K., & WILSON, W. R. (1951). Some engineering applications of the electrolytic field analyzer. *Trans. AIEE, 70*(2), 1301–1309.

FERGESTAD, P. I., & HENRIKSEN, T. (1974). Inductances for the calculation of transient oscillations in transformers. *IEEE Trans. Power App. Syst., 93*(2), 510–517.

FRAME, J. G., MOHAN, N., & LIU, T.-H. (1982). Hysteresis modeling in an electromagnetic transients program. *IEEE Trans. Power App. Syst., 101*(9), 3403–3412.

FUNIERU, M. (2007). *Simulation of electromechanical actuators using the finite integration technique*. (Ph.D. dissertation, Technischen Universität Darmstadt, Darmstadt, Germany).

GÉRIN-LAJOIE, L., GUILLON, S., MAHSEREDJIAN, J., & SAAD, O. (2013). *Impact of transformer saturation from GIC on power system voltage regulation*. Presented at the Int. Conf. Power System Transients, Vancouver, Canada.

GÓMEZ, P., & DE LEÓN, F. (2011). Accurate and efficient computation of the inductance matrix of transformer windings for the simulation of very fast transients. *IEEE Trans. Power Del., 26*(3), 1423–1431.

GONZALEZ-MOLINA, F., ISHCHENKO, D., & MORK, B. A. (2003a). *Parameter estimation and advancements in transformer models for EMTP simulations.* (Tech. report, task/activity MTU-6: Parameter estimation). USA: Bonneville Power Administration.

GONZALEZ-MOLINA, F., MITRA, J., & MORK, B. A. (2003b). *Parameter estimation and advancements in transformer models for EMTP simulations.* (Tech. report, task/activity MTU-4/NDSU-2: Develop library of model topologies). USA: Bonneville Power Administration.

GONZALEZ-MOLINA, F., MITRA, J., & MORK, B. A. (2004). *Parameter estimation and advancements in transformer models for EMTP simulations.* (Tech. report, task/activity MTU-7: Model performance and sensitivity analysis). USA: Bonneville Power Administration.

GONZALEZ-MOLINA, F., & MORK, B. A. (2002). *Parameter estimation and advancements in transformer models for EMTP simulations.* (Tech. report, task/activity MTU-1: Develop prototype software interface & preprocessor). USA: Bonneville Power Administration.

GROVER, F. W. (2004). *Inductance calculations.* Mineola, NY: Dover Publications.

HAMILL, D. C. (1993). Lumped equivalent circuits of magnetic components: the gyrator-capacitor approach. *IEEE Trans. Power Electron., 8*(2), 97–103.

HAMILL, D. C. (1994). Gyrator-capacitor modeling: a better way of understanding magnetic components. In *Proc. Applied Power Electronics Conference and Exposition.* vol. 1, pp. 326–332.

HAMMOND, P. (1960). Electric and magnetic images. *Proc. IEE—Part C: Monographs, 107*(12), 306–313.

HAMMOND, P. (1967). Roth's method for the solution of boundary-value problems in electrical engineering. *Proc. IEE, 114*(12), 1969–1976.

HAYDOCK, L. (1985). *Systematic development of equivalent circuits for synchronous machines.* (Ph.D. dissertation, Imperial College of Science and Technology, University of London, London, England).

HAYDOCK, L., & HOLLAND, S. A. (1994). Transient analysis of power transformers using magnetic and electric equivalent circuits. *IEEE Trans. Magn., 30*(5), 2996–2999.

HEILES, F. (1932). Über zusätzliche Verluste in Transformatoren. *Elektrotechnische Zeitschrift, 37*, 883–885.

HENRIKSEN, T. (2001). *Transformer leakage flux modeling.* Presented at the Int. Conf. Power System Transients, Rio de Janeiro, Brazil.

HØIDALEN, H. K., CHIESA, N., AVENDAÑO, A., & MORK, B. A. (2011). *Developments in the hybrid transformer model–core modeling and optimization.* Presented at the Int. Conf. Power System Transients, Delft, the Netherlands.

HØIDALEN, H. K., MORK, B. A., GONZALEZ-MOLINA, F., ISHCHENKO, D., & CHIESA, N. (2007). *Implementation and verification of the hybrid transformer in ATP-Draw.* Presented at the Int. Conf. Power System Transients, Lyon, France.

HØIDALEN, H. K., MORK, B. A., GONZALEZ-MOLINA, F., ISHCHENKO, D., & CHIESA, N. (2009). Implementation and verification of the hybrid transformer model in ATPDraw. *Elect. Pow. Syst. Res., 79*(3), 454–459.

HOPKINSON, J. (1885). Magnetisation of iron. *Phil. Trans. R. Soc., 176*, 455–469.

HOPKINSON, J., & HOPKINSON, E. (1886). Dynamo-electric machinery. *Phil. Trans. R. Soc., 177*, 331–358.

HSU, J. T., & VU-QUOC, L. (1996). A rational formulation of thermal circuit models for electrothermal simulation—part I: finite element method. *IEEE Trans. Circuits Syst. I, Fundam. Theory Appl., 43*(9), 721–732.

IEC (2004). *Insulation co-ordination—part IV: computational guide to insulation co-ordination and modelling of electrical networks.* (Tech. report, ref. IEC/TR 60071-4:2004(E)). Geneva, Switzerland: IEC.

INAGAKI, K., HIGAKI, M., MATSUI, Y., KURITA, K., SUZUKI, M., YOSHIDA, K., & MAEDA, T. (1988). Digital protection method for power transformers based on an equivalent circuit composed of inverse inductance. *IEEE Trans. Power Del., 3*(4), 1501–1510.

ISHIBASHI, K., & SAWADO, E. (1990). Three-dimensional analysis of electromagnetic fields in rectangular waveguides by the boundary integral equation method. *IEEE Trans. Microw. Theory Techn., 38*(9), 1300–1308.

IWAHARA, M., & MIYAZAWA, E. (1981). Finite magnetic circuits method and its application. *IEEE Trans. Magn., 17*(6), 3405–3407.

JAZEBI, S., DE LEÓN, F., FARAZMAND, A., & DESWAL, D. (2013). Dual reversible transformer model for the calculation of low-frequency transients. *IEEE Trans. Power Del., 28*(4), 2509–2517.

JONNES, J. (2004). *Empires of light.* New York, NY: Random House.

JULIA, R. (1939). Contribution à l'étude des réseaux réciproques. *Bull. Soc. Franc. Élect., 9*(99), 281–302.

KAPP, G. (1898). Ein Beiträge zur Vorausberechnung der Streuung in Transformatoren. *Elektrotechnische Zeitschrift, 19*, 244–246.

KAPP, G. (1908). *Transformers for single and multiphase currents* (2nd ed., pp. 176–197). London, England: Whittaker.

KARSAI, K., KERÉNYI, D., & KISS, L. (1987). *Large power transformers*. Elsevier.

KING, E. I. (1966). Equivalent circuits for two-dimensional magnetic fields: I—the static field. *IEEE Trans. Power App. Syst., 85*(9), 927–935.

KOPPIKAR, D. A., KULKARNI, V., & TUROWSKI, J. (2000). Fast 3-dimensional interactive computation of stray field and losses in asymmetric transformers. *IEE Proc.-Gener. Transm. Distrib., 147*(4), 197–201.

KRIETENSTEIN, B., SCHUHMANN, R., THOMA, P., & WEILAND, T. (1998). The perfect boundary approximation technique facing the big challenge of high precision field calculation. In *Int. Linear Accelerator Conference*, pp. 860–862.

KRON, G. (1944). Equivalent circuit of the field equations of Maxwell—I. *Proc. IRE, 32*(5), 289–299.

KULKARNI, S. V., & KHAPARDE, S. A. (2004). *Transformer engineering: design and practice*. New York, NY: Marcel Dekker.

LAITHWAITE, E. R. (1967). Magnetic equivalent circuits for electrical machines. *Proc. IEE, 114*(11), 1805–1809.

LAMBERT, M., & MAHSEREDJIAN, J. (2013). *EMT-type transformer models for GIC studies*. (Tech. report, ref. 3002000832). Palo Alto, CA: EPRI.

LAMBERT, M., MAHSEREDJIAN, J., DESSAINT, L.-A., & GAUDREAU, A. (2009). *Implementation of a new magnetizing branch in EMTP-RV using the A(x) model*. Presented at the Int. Conf. Power System Transients, Kyoto, Japan.

LAMBERT, M., MAHSEREDJIAN, J., MARTÍNEZ DURÓ, M., & SIROIS, F. (2014a). Magnetic circuits within electric circuits: critical review of existing methods and new mutator implementation. Submitted to the *IEEE Trans. Power Del.*

LAMBERT, M., MARTÍNEZ DURÓ, M., MAHSEREDJIAN, J., DE LEÓN, F., & SIROIS, F. (2014b). Transformer leakage flux models for electromagnetic transients: critical review and validation of a new model. Accepted for publication in *IEEE Trans. Power Del.*

LAMBERT, M., SIROIS, F., MARTÍNEZ DURÓ, M., & MAHSEREDJIAN, J. (2013). Analytical calculation of leakage inductance for low-frequency transformer modeling. *IEEE Trans. Power Del., 28*(1), 507–515.

LANGLEY MORRIS, A. (1940). The influence of various factors upon the leakage reactance of transformers. *Journal IEE, 86*(521), 485–495.

LAWRENSON, P. J. (1962). A note on the analysis of the fields of line currents and charges. *Proc. IEE—Part C: Monographs, 109*(15), 86–90.

LÓPEZ-FERNÁNDEZ, X. M., BÜLLENT ERTAN, H., & TUROWSKI, J., editors (2012). *Transformers: analysis, design, and measurement*. Boca Raton, FL: CRC Press.

MAGDZIARZ, A., & ŻAGAŃ, Z. (1986). Mathematical simulation model of power transformer for electrical power system protective schemes. In *Proc. IFIP Conference, Budapest, Hungary*. vol. 84 of *Lecture Notes in Control and Information Sciences*.

MAHSEREDJIAN, J. (2008). Régimes transitoires électromagnétiques: simulation. *Édition Les Techniques de l'Ingénieur*, D 4 130.

MAHSEREDJIAN, J. (2012). *Literature survey on transformer models for the simulation of electromagnetic transients with emphasis on GIC applications*. (Tech. report, ref. 1025844, Technical Update). Palo Alto, CA: EPRI.

MAHSEREDJIAN, J., DENNETIÈRE, S., DUBÉ, L., KHODABAKHCHIAN, B., & GÉRIN-LAJOIE, L. (2007). On a new approach for the simulation of transients in power systems. *Elect. Pow. Syst. Res., 77*(11), 1514–1520.

MARGUERON, X., KERADEC, J.-P., & MAGOT, D. (2007). Analytical calculation of static leakage inductances of HF transformers using PEEC formulas. *IEEE Trans. Ind. Appl., 43*(4), 884–892.

MARTÍNEZ DURÓ, M., ZGAINSKI, F.-X., & CAILLAULT, B. (2013). *Transformer energization studies with uncertain power system configurations*. Presented at the Int. Conf. Power System Transients, Vancouver, Canada.

MARTINEZ-VELASCO, J. A., editor (2010). *Power System Transients: Parameter Determination*. Boca Raton, FL: CRC.

MARTINEZ-VELASCO, J. A., GONZALEZ-MOLINA, F., & MORK, B. A. (1999). *Preprocessor for EMTP power transformer models*. Presented at the Int. Conf. Power System Transients, Budapest, Hungary.

MARTINEZ-VELASCO, J. A., & MORK, B. A. (2005). Transformer modeling for low- and mid-frequency transients—a review. *IEEE Trans. Power Del., 20*(2), 1625–1632.

MARTINEZ-VELASCO, J. A., WALLING, R., MORK, B. A., MARTIN-ARNEDO, J., & DURBAK, D. (2005). Parameter determination for modeling system transients—part III: transformers. *IEEE Trans. Power Del., 20*(3), 2051–2062.

MCEACHRON, K. B. (1922). Magnetic flux distribution in transformers. *Trans. AIEE, 41*, 247–261.

MITRA, J. (2002). *Advanced transformer modeling for transients simulation.* (Tech. report, task/activity NDSU-1: laboratory testing of 3-leg and 5-leg distribution transformers). USA: Bonneville Power Administration.

MITRA, J. (2003). *Advanced transformer modeling for transients simulation.* (Tech. report, task/activity NDSU-4, 5 and 6: additional laboratory testing of 3-leg and 5-leg distribution transformers for parameter refinement). USA: Bonneville Power Administration.

MITRA, J., MASCARENHAS, R. D., & JAYACHANDRAN, M. A. (2003). *Advanced transformer modeling for transients simulation.* (Tech. report, task/activity NDSU-3: Frequency dependence of parameters of 3-leg and 5-leg distribution transformers). USA: Bonneville Power Administration.

MORK, B. A. (1999). Five-legged wound-core transformer model: derivation, parameters, implementation and evaluation. *IEEE Trans. Power Del., 14*(4), 1519–1526.

MORK, B. A., GONZALEZ-MOLINA, F., ISHCHENKO, D., STUEHM, D. L., & MITRA, J. (2007a). Hybrid transformer model for transient simulation—part I: development and parameters. *IEEE Trans. Power Del., 22*(1), 248–255.

MORK, B. A., GONZALEZ-MOLINA, F., ISHCHENKO, D., STUEHM, D. L., & MITRA, J. (2007b). Hybrid transformer model for transient simulation—part II: laboratory measurements and benchmarking. *IEEE Trans. Power Del., 22*(1), 256–262.

MORRIS, D. (1951). Some practical equivalent circuits for multi-circuit transformers. *Proc. IEE—Part II: Power Engineering, 98*(62), 256–261.

MULLINEUX, N., REED, J. R., DE KUIJPER, C., & HAMMOND, P. (1969). Roth's method for solution of boundary-value problems. *Proc. IEE, 116*(2), 291–293.

MUNTEANU, I., & HIRTENFELDER, F. (2005). *Convergence of the finite integration technique on various mesh types.* Presented at the German Microwave Conference, Ulm, Germany.

MYINT-U, T., & DEBNATH, L. (2007). *Linear partial differential equations for scientists and engineers.* Boston, MA: Birkhäuser.

NADERIAN-JAHROMI, A., FAIZ, J., & MOHSENI, H. (2002). Calculation of distribution transformer reactance using energy technique. In *Australasian Universities Power Engineering Conference.* pp. 1–5.

NARANG, A., & BRIERLEY, R. H. (1994). Topology based magnetic model for steady-state and transient studies for three-phase core type transformers. *IEEE Trans. Power Syst., 9*(3), 1337–1349.

NARANG, A., DICK, E. P., & CHEUNG, R. C. (1997). *Transformer model for electromagnetic transient studies.* (Tech. report No. 175 T 331G). Montréal, QC: Canadian Electricity Association.

NEVES, W. L. A., & DOMMEL, H. W. (1993). On modelling iron core nonlinearities. *IEEE Trans. Power Syst., 8*(2), 417–425.

NEVES, W. L. A., & DOMMEL, H. W. (1995). Saturation curves of delta-connected transformers from measurements. *IEEE Trans. Power Del., 10*(3), 1432–1437.

OKABE, M., & KIKUCHI, N. (1983). Analytical solutions of some steady-state electrical problems in the rectangular domain. *Computer Methods in Applied Mechanics and Engineering, 36*(2), 167–189.

OLIVEIRA, J. C., APOLONIO, R., & VASCONCELLOS, A. B. (2003). The use of Saber simulator for non-linear magnetic devices simulation: analysis and improvements. In *IEEE Int. Symposium on Industrial Electronics*. vol. 1, pp. 511–515.

OLIVIER, G., & GUDEFIN, E. J. (1994). Modelling of multiple-winding transformers. In *IMACS World Congress on Computational and Applied Mathematics*. pp. 858–863.

PALMER-BUCKLE, P., BUTLER, K. L., & SARMA, N. D. R. (1999). Characteristics of transformer parameters during internal winding faults based on experimental measurements. In *IEEE Transmission and Distribution Conference*. vol. 2, pp. 882–887.

PERRIN-BIT, R., & COULOMB, J.-L. (1995). A three dimensional finite element mesh connection for problems involving movement. *IEEE Trans. Magn., 31*(3), 1920–1923.

PODEBRAD, O., CLEMENS, M., & WEILAND, T. (2003). New flexible subgridding scheme for the finite integration technique. *IEEE Trans. Magn., 39*(3), 1662–1665.

PRAMANIK, A. (1969). Extension of Roth's method to 2-dimensional rectangular regions containing conductors of any cross-section. *Proc. IEE, 116*(7), 1286–1288.

PRAMANIK, A. (1975). Extension of Roth's method to three-dimensional multi-region eddy current problems. *IEEE Trans. Magn., 11*(5), 1526–1528.

PRUSTY, S., & RAO, M. (1980). A direct piecewise linearized approach to convert rms saturation characteristic to instantaneous saturation curve. *IEEE Trans. Magn., 16*(1), 156–160.

RABINS, L. (1956). Transformer reactance calculations with digital computers. *AIEE Trans., 75*, 261–267.

RAIS, V. R., TUROWSKI, J., & TUROWSKI, M. (1988). Reluctance network analysis of coupled fields in a reversible electromagnetic motor. In *Proc. ISEF' 87*, pp. 279–283. New York, NY: Plenum Press.

REPETTO, M., & TREVISAN, F. (2003). 3-D magnetostatic with the finite formulation. *IEEE Trans. Magn., 39*(3), 1135–1138.

ROBERTS, J. (1960). Analogue treatment of eddy-current problems involving two-dimensional fields. *Proc. IEE—Part C: Monographs, 107*(11), 11–18.

ROBERTSON, B. L., & TERRY, I. A. (1929). Analytical determination of magnetic fields—simple cases of conductors in slots. *AIEE Trans., 48*(4), 1242–1259.

RODGER, D., LAI, H. C., & LEONARD, P. J. (1990). Coupled elements for problems involving movement. *IEEE Trans. Magn., 26*(2), 548–550.

ROGOWSKI, W. (1908). *Ueber das Streufeld und den Streuinduktionskoeffizienten eines Transformators mit Scheibenwicklung und geteilten Endspulen.* (Ph.D. dissertation, Technischen Hochschule zu Danzig, Gdańsk, Poland).

ROGUIN, J., & RANJAMINA, V. (1984). *Modélisation de circuits magnétiques avec l'EMTP.* (Tech. report, ref. HM/72-5146 JE-VR/Ext. PS.). Clamart, France: EDF R&D.

ROSHEN, W. A. (1990). Analysis of planar sandwich inductors by current images. *IEEE Trans. Magn., 26*(5), 2880–2887.

ROTH, E. (1927a). Introduction à l'étude analytique de l'échauffement des machines électriques. *Bull. Soc. Franc. Élect., 7*, 840–965.

ROTH, E. (1927b). Étude analytique du champ propre d'une encoche. *Rev. Gén. Élect., 22*, 417–424.

ROTH, E. (1928a). Étude analytique des champs thermique et magnétique lorsque la conductibilité thermique ou la perméabilité n'est pas la même dans toute l'étendue du domaine considéré. *Rev. Gén. Élect., 24*, 137–148 and 179–187.

ROTH, E. (1928b). Étude analytique du champ de fuites des transformateurs et des efforts mécaniques exercés sur les enroulements. *Rev. Gén. Élect., 23*, 773–787.

ROTH, E. (1932). Étude analytique du champ résultant d'une encoche de machine électrique. *Rev. Gén. Élect., 32*, 761–768.

ROTH, E. (1936). Inductance due aux fuites magnétiques dans les transformateurs à bobines cylindriques et efforts exercés sur les enroulements. *Rev. Gén. Élect., 40*, 259–268, 291–303 and 323–336.

ROTH, E. (1938). Champ magnétique et inductance d'un système de barres rectangulaires parallèles. *Rev. Gén. Élect., 44*, 275–283.

ROTH, E., & KOUSKOFF, G. (1928). Sur une méthode de sommation de certaines séries de Fourier. *Rev. Gén. Élect., 23*, 1061–1073.

RUEHLI, A. E. (1972). Inductance calculations in a complex integrated circuit environment. *IBM J. Res. Develop., 16*, 470–481.

RUEHLI, A. E. (1974). Equivalent circuit models for three-dimensional multiconductor systems. *IEEE Trans. Microw. Theory Techn., 22*(3), 216–221.

SADOWSKI, N., LEFÈVRE, Y., LAJOIE-MAZENC, M., & CROS, J. (1992). Finite element torque calculation in electrical machines while considering the movement. *IEEE Trans. Magn., 28*(2), 1410–1413.

SALDAÑA, C., & CALZOLARI, G. (1997). *Analysis of core type transformer models based on the principle of duality in electromagnetic transients studies*. Presented at the Int. Conf. Power System Transients, Seattle, WA.

SALIMI, M., GOLE, A. M., & JAYASINGHE, R. P. (2013). *Improvement of transformer saturation modeling for electromagnetic transient programs*. Presented at the Int. Conf. Power System Transients, Vancouver, Canada.

SANTOS NUNES, A., KUO-PENG, P., & GRAFULHA VANTI, M. (2013). *Air core reactor analysis based on RNM method*. Presented at COMPUMAG, Budapest, Hungary.

SAWHNEY, A. K. (1997). *A course in electrical machine design*. Delhi: Dhanpat Rai.

SCHÖPS, S., DE GERSEM, H., & WEILAND, T. (2013). Winding functions in transient magnetoquasistatic field-circuit coupled simulations. *COMPEL, 32*(6), 2063–2083.

SCHULTZ, C. P. (2011). The coupled leakage model of a multiple winding transformer. In *IEEE Proc. Southeastcon*. pp. 6–11.

SILVESTER, P., & KONRAD, A. (1973). Analysis of transformer leakage phenomena by high-order finite elements. *IEEE Trans. Power App. Syst., 92*(6), 1843–1855.

SIROIS, F. (2002). *Modélisation de la caractéristique $E - J$ des supraconducteurs à haute température critique*. (Ph.D. dissertation, École Polytechnique de Montréal, Montréal, Canada).

SLEMON, G. R. (1953). Equivalent circuits for transformers and machines including nonlinear effects. *Proc. IEE—Part IV: Institution Monographs, 100*(5), 129–143.

SLEMON, G. R. (1992). *Electric Machines and Drives*. Reading, MA: Addison-Wesley.

SMYTHE, W. R. (1950). *Static and Dynamic Electricity* (2nd ed.). New York, NY: McGraw-Hill.

SOTO, A., SOUTO, D., TUROWSKI, J., LÓPEZ-FERNÁNDEZ, X. M., & COUTO, D. (2008). *Software for fast interactive three-dimensional modeling of electromagnetic leakage*

field and magnetic shunts design in shell type transformers. Presented at the International Conference on Electrical Machines, Vilamoura, Portugal.

STARR, F. M. (1933). An equivalent circuit for the four-winding transformer. *General Electric Review, 36*(3), 150–152.

STEINMETZ, C. P. (1897). The alternating-current transformer. In *Theory and calculation of alternating current phenomena* (pp. 167–192). New York, NY: W. J. Johnston.

STEVENSON, A. R., & PARK, R. H. (1927). Graphical determination of magnetic fields theoretical considerations. *AIEE Trans., 46*, 112–135.

STRÜTT, M. (1926). Das magnetische Feld eines rechteckigen, von Gleichstrom durchflossenen Leiters. *Archiv für Elektrotechnik, 17*, 533–535.

STUEHM, D. L. (1993). *Three-phase transformer core modeling.* (Tech. report, ref. DE-BI79-92BP26700). USA: Bonneville Power Administration.

TARHASAARI, T., KETTUNEN, L., & BOSSAVIT, A. (1999). Some realizations of a discrete Hodge operator: a reinterpretation of finite element techniques. *IEEE Trans. Magn., 35*(3), 1494–1497.

TELLEGEN, B. D. H. (1948). The gyrator, a new eletric network element. *Philips Res. Rept., 3*, 81–101.

THOMA, P., & WEILAND, T. (1996). A consistent subgridding scheme for the finite difference time domain method. *Int. J. Numer. Model., 9*(5), 359–374.

THOMSON, W. (1845). Extrait d'une lettre de M. William Thomson à M. Liouville. *J. Math. Pure Appl., 10*, 364–367.

TONTI, E. (2001). Finite formulation of the electromagnetic field. *Progress In Electromagnetics Research, 32*, 1–44.

TONTI, E. (2002). Finite formulation of electromagnetic field. *IEEE Trans. Magn., 38*(2), 333–336.

TSUKERMAN, I. A., KONRAD, A., MEUNIER, G., & SABONNADIÈRE, J.-C. (1993). Coupled field-circuit problems: trends and accomplishments. *IEEE Trans. Magn., 29*(2), 1701–1704.

TUROWSKI, J. (1989). Modelling and simulation of electromagnetic field in electrical machines and transformers with the help of equivalent reluctance network. In J. Robert & W. Midvidy (Eds.), *IMACS transactions on scientific computing'88* (vol. 6, pp. 109–112). Bassel, Switzerland: J. C. Baltzer AG.

TUROWSKI, J. (1995). Reluctance networks. In J. K. Sykulski (Ed.), *Computational Magnetics* (pp. 145–178). London, England: Chapman & Hall.

TUROWSKI, J. (1998). Fast computation of coupled fields in complex, 3-D, industrial electromagnetic structures. *COMPEL, 17*(4), 489–505.

TUROWSKI, J., TUROWSKI, M., & KOPEC, M. (1990). Method of three-dimensional network solution of leakage field of three-phase transformers. *IEEE Trans. Magn., 26*(5), 2911–2919.

UPPENBORN, F. (1889). *History of the transformer*. London, England: E. & F. N. Spon.

URANKAR, L. K. (1980). Vector potential and magnetic field of current-carrying finite arc segment in analytical form, part I: filament approximation. *IEEE Trans. Magn., 16*(5), 1283–1288.

URANKAR, L. K. (1982a). Vector potential and magnetic field of current-carrying finite arc segment in analytical form, part II: thin sheet approximation. *IEEE Trans. Magn., 18*(3), 911–917.

URANKAR, L. K. (1982b). Vector potential and magnetic field of current-carrying finite arc segment in analytical form, part III: exact computation for rectangular cross section. *IEEE Trans. Magn., 18*(6), 1860–1867.

URANKAR, L. K. (1984). Vector potential and magnetic field of current-carrying finite arc segment in analytical form, part IV: general three-dimensional current density. *IEEE Trans. Magn., 20*(6), 2145–2150.

URANKAR, L. K. (1990). Vector potential and magnetic field of current-carrying circular finite arc segment in analytical form–part V: polygon cross section. *IEEE Trans. Magn., 26*(3), 1171–1180.

URANKAR, L. K., & HENNINGER, P. (1991). Compact extended algorithms for elliptic integrals in electromagnetic field and potential computations part I: elliptic integrals of the first and second kind with extended integration range. *IEEE Trans. Magn., 27*(5), 4338–4342.

URANKAR, L. K., HENNINGER, P., & NESTEL, F. S. (1994). Compact extended algorithms for elliptic integrals in electromagnetic field and potential computations part II: elliptic integral of third kind with extended integration range. *IEEE Trans. Magn., 30*(3), 1236–1241.

VAN DANTZIG, D. (1934). The fundamental equations of electromagnetism, independent of metrical geometry. *Math. Proc. Camb. Phil. Soc., 30*, 421–427.

WEILAND, T. (1977). Eine Methode zur Lösung der Maxwellschen Gleichungen für sechskomponentige Felder auf diskreter Basis. *AEÜ—International Journal of Electronics and Communications, 31*(3), 116–120.

WEILAND, T. (1996). Time domain electromagnetic field computation with finite difference methods. *Int. J. Numer. Model., 9*(4), 295–319.

WEILAND, T. (2003). RF & microwave simulators—from component to system design. In *European Microwave Conference*. vol. 2, pp. 591–596.

WHITNEY, H. (1932). Non-separable and planar graphs. *Trans. Amer. Math. Soc., 34*, 339–362.

WILCOX, D. J., CONLON, M., & HURLEY, W. G. (1988). Calculation of self and mutual impedances for coils on ferromagnetic cores. *Proc. IEE—Part A, 135*(7), 470–476.

WOODFORD, D. A., GOLE, A. M., & MENZIES, R. W. (1983). Digital simulation of DC links and AC machines. *IEEE Trans. Power App. Syst., 102*(6), 1616–1623.

YACAMINI, R., & BRONZEADO, H. S. (1994). Transformer inrush calculations using a coupled electromagnetic model. *IEE Proc.-Sci. Meas. Techol., 141*(6), 491–498.

YAN, L., & LEHMAN, B. (2005). A capacitor modeling method for integrated magnetic components in DC/DC converters. *IEEE Trans. Power Electron., 20*(5), 987–996.

YEE, K. (1966). Numerical solution of initial boundary value problems involving Maxwell's equations in isotropic media. *IEEE Trans. Antennas Propag., 14*(3), 302–307.

ZHALEFAR, F., & SANAYE-PASAND, M. (2006). *Transformer core modeling as applied to slow transients and protective studies*. Presented at the IEEE Power India Conference.

ZIRKA, S. E., MOROZ, Y. I., ARTURI, C. M., CHIESA, N., & HØIDALEN, H. K. (2012). Topology-correct reversible transformer model. *IEEE Trans. Power Del., 27*(4), 2037–2045.

ZISSERMAN, A., SAUNDERS, R., & CALDWELL, J. (1987). Analytic solutions for axisymmetric magnetostatic systems involving iron. *IEEE Trans. Magn., 23*(6), 3895–3902.